Quantum Chemistry of Small Clusters of Elements of Groups Ia, Ib, and IIa: Fundamental Concepts, Predictions, and Interpretation of Experiments

VLASTA BONAČIĆ-KOUTECKÝ,*,† PIERCARLO FANTUCCI,‡ and JAROSLAV KOUTECKÝ†

Institut für Physikalische und Theoretische Chemie, Freie Universität Berlin, Takustr. 3, 1000 Berlin 33, Germany, and Dipartimento di Chimica Inorganica e Metallorganica, Centro CNR, Universita di Milano, Via Venezian 21, I-20133 Milano, Italy

Received March 26, 1991 (Revised Manuscript Received May 10, 1991)

Contents

Abbreviations

AE	all electron
AO	atomic orbital
BO	Born–Oppenheimer
CAS	complete active space
CAS-SCF	complete active space self-consistent field
CCSD	coupled cluster-single-double
CIPSI	configuration interaction by perturbation of multiconfigurational wave function selected iteratively
CI	configuration interaction
CPF	coupled pair functional
CPP	core polarization potential
CVC	core–valence correlation

† Freie Universität Berlin.
‡ Universita di Milano.

0009-2665/91/0791-1035$09.50/0

Vlasta Bonačić-Koutecký received her B.Sc. (1967) and M.Sc. (1969) in theoretical physics and theoretical chemistry from University of Zagreb, Yugoslavia. Her Ph.D. (1968–1971) studies were performed under R. G. Parr at the Johns Hopkins University. After a postdoctoral fellowship with J. Musher at Belfer Graduate School of Science, Yeshiva University, New York, she became Assistent Professor in Institut für Physikalsiche und Theoretische Chemie, Freie Universität Berlin (1973), were she habilitated in theoretical chemistry (1977). Since 1982 she has been apl. Professor at the Freie Universität of Berlin. Her research direction is applied quantum chemistry in broad sense and some aspects of molecular dynamics. Her main research interest has been electronic aspects of theoretical photochemistry. Her recent research activities include electronic structure of elemental clusters and their reactivity.

Piercarlo Fantucci graduated in chemistry from the University of Milano, Italy, in 1969 and developed a strong interest in spectroscopy and bonding theory of inorganic complexes. From 1973 to 1981 he was appointed as a lecturer of inorganic chemistry at the University of Milano. At the same time he was associated with the department of Computational Chemistry led by E. Clementi at Donegani Institute, Novara, Italy. Since 1973 he has been Associate Professor of Inorganic Chemistry at the University of Milano. For several years, his interest has mainly focused on the theoretical aspects of the electronic structure of metallic clusters and on simple cluster models for the chemisorption processes.

Jaroslav Koutecký received his RNDr degree in theoretical physics at Charles University in Prague in 1951. He worked in various industrial institutions from 1941 to 1945 and from 1949 to 1952. He was scientific co-worker and later leader of the department of quantum chemistry in the Institute of Physical Chemistry, Czechoslovakian Academy of Sciences, Prague, from 1953 to 1969. He was awarded with a State Prize in 1954 for the solution of the problem of polarographic kinetic currents (together with Prof. R. Brdička) and in 1963 with a State prize for establishing research in quantum chemistry in Czechoslovakia. He was a corresponding member of the Czechoslovakian Academy of Sciences from 1962 to 1971. In the year 1969 he was elected in the International Academy of Quantum Molecular Sciences. He was professor of physical chemistry at Belfer Graduate School of Science, Yeshiva University, New York, in 1970–1973. In 1973 he moved to the Freie Universität of Berlin. In 1989 he was rehabilitated as a member of the Czechoslovakian Academy of Sciences. He was interested in the theory of electrode processes, in the semiempirical quantum theory of conjugated compounds, and the general properties of the solutions of Hartree–Fock equations. His recent research activities cover a broad range of the theoretical chemistry field, including purely theoretical aspects, and applications of quantum chemistry methods of electronic structure of metallic clusters, to surface phenomena and to models for catalytic processes, as well as on molecular excited states.

DF	density functional
EA	electron affinity
ECP	*effective core potential*
ESM	ellipsoidal shell model
ESR	electron-spin resonance
GF	Green's function
GVB	generalized valence bond
HF	Hatree–Fock
HOMO	highest occupied molecular orbital
JT	Jahn–Teller
KKR	Korringa–Kohn–Rostocker
LCAO	linear combination of atomic orbitals
LD	local density
LIF	laser-induced fluorescence
LSD	local spin density
LUMO	lowest unoccupied molecular orbital
MC-SCF	multiconfiguration SCF
MO	molecular orbital
MP	Möller–Plesset
MPI	multiphoton ionization
MRCI	multireference–configuration interaction
MR-DCI	multireference diexcitation configuration interaction
MR-SDCI	multireference single–double configuration interaction
PPP	Pariser–Parr–Pople
QMD	quantum molecular dynamics
RECP	relativistic effective core potential
RPA	random phase approximation
RSW	relativistic scattered wave
SCF	*self-consistent field*
SD-CI	single–double configuration interaction
SDTQ	single–double–triple–quadruple
TDA	Tamm–Dancoff approximation
TDHF	time-dependent Hartree–Fock
TD-LDA	time-dependent local density approximation
TPI	two-photon ionization
UHF	unrestricted Hartree–Fock
UPS	ultraviolet photoemission spectroscopy
VDE	vertical detachment energy

I. Introduction

A. Specific Features of Elemental Clusters

Common physical laws valid for atoms, molecules, and solids—as well as other physical systems—govern the nature of clusters under quite specific conditions. Consequently, we can expect them to lead to effects uncommon for other more stable electronic systems, such as molecules or solids. In other words, clusters do not only represent a transition—a bridge—between atoms and solids but they exhibit several of their own specific features as well. Formal similarities due to common physical laws might be present for systems which possess a number of substantially different basic physical properties. In such cases, it is important to analyze carefully the reasons for such similarities in order to avoid erroneous conclusions about the physical nature of these parallels. For example, very specific conditions under which the physical laws act in small elemental clusters may give rise to regularities similar to those characteristic for the physical behavior of atomic nuclei, in spite of the fact that the constituent particles and forces acting among them are basically different.

Similarly caution is advised in interpreting the results when an attempt is made to answer the question often raised: at which cluster size does metallic character appear? Individual cluster properties can easily resemble metallic characteristics, but at the same time other properties can be still very far from those which are typical for the metallic state.

Since cluster physics opens new aspects which are not usually met in the molecular or solid-state physics, the theory of the electronic structure of clusters can be useful in finding the basic reasons for their appearance.

B. Methodological Requirements

Many theoretical concepts and methods employed customarily in molecular physics and solid-state theory have some features tailored to the specific properties of the given class of investigated systems. Such an adjustment using appropriate concepts, treatable models, and mathematical approximations is necessary and useful, since the complexity of the quantum mechanical laws makes it necessary to simplify the employed procedures. The interplay of adequate assumptions justifiable in the given scientific domain and of the simplified physical laws builds the basis of the techniques which are used for determining the properties of interest.

However, such an approach is not always applicable in cluster physics, since our knowledge of the basic facts about clusters is not sufficient for this purpose. Therefore, it is risky to employ quantum chemical semiempirical and empirical methods for the description of cluster properties without obtaining and comparing results from more sophisticated methods. Similarly, the customary, considerably simplified methodology of solid-state quantum theory must be carefully verified before it is applied in this field.

The most frequently experimentally studied clusters have so many electrons that very sophisticated quantum chemical methods, relatively free from ad hoc assumptions, are hardly applicable. For example, it is difficult to routinely use the "ab initio" quantum chemical methods for transition-metal clusters that are particularly interesting for various practical reasons and, therefore, intensively investigated experimentally.

Therefore, it is necessary to begin by applying ab initio quantum chemical methods to relatively simple systems with a small number of electrons, and then use that knowledge to understand complicated systems. Since studies of medium-size clusters are the primary goal of such investigations, the methodological details must be chosen so that the largest possible simplifications are combined with care so as not to neglect some relevant methodological features allowing for the description of the essential physical features governing the interactions inside clusters.

Such compromises require physical feeling and sufficient experience. They can be sometimes considered as not sufficiently cautious from the standpoint of ab initio quantum chemists and not reduced sufficiently to the basic essentials for those who are used to dealing with simple models, but they are unavoidable for obtaining basic knowledge about the physical properties of the electronic structure of clusters.

C. The Task of Quantum Chemistry in Cluster Research

When applied to small molecules, including those that are not stable under usual conditions or are involved, e.g., in photophysical and photochemical processes, the quantum chemical methods at high level of accuracy yielded novel insights. The same type of methods are, in principle, useful also for the investigation of clusters. Unfortunately, the application of these procedures are limited to relatively small clusters with a small number of explicitly considered electrons.

At first glance, these obvious limitations are quite discouraging if one considers the importance of the interpretation of size-dependent cluster properties, which are experimentally investigated in a wide range, as well as the practical importance of larger clusters, mainly of heavier atoms. However, recent methodological developments in ab initio quantum chemistry and the availability of powerful computers make it possible to study a wide range of cluster sizes at least for simple elements such as those of the Ia and Ib columns. Apart from their predictive power, they can serve as guides for designing acceptable simplifications. For example, it is a challenging task to distinguish those cluster properties arising from the specific nature of the constituent atoms and their ability to participate in bonding from those which are caused solely by the symmetry or topology. Further, the analysis of the results obtained from the advanced quantum chemical procedures can be used to determine the essential ingredients which should not be omitted in any simplified theoretical treatment of clusters. This might also be useful for proposing "semiempirical" approaches specifically adopted to the study of larger clusters.

D. Limitations and Scope of the Review

Recently, numerous reviews[1-18] as well as compendia[19-25] have been published concerning theoretical and experimental work on elemental clusters. For this reason, the present review does not seek to give a bal-

anced survey of the research on all properties of all interesting classes of clusters or to give a comprehensive summary of the explosively growing literature of cluster research. Instead, this review focuses on problems in which the application of quantum chemical methods can yield a deeper insight into the fundamental laws governing the structure of clusters. Section II.A briefly describes approaches commonly applied in quantum chemistry. Section II.B and the Appendixes analyze and compare the concepts of solid-state theory and nuclear physics frequently applied for the description of cluster properties. We have emphasized the latter aspect because a number of problems at the borderline of these cluster research disciplines can open new fields for applied quantum chemistry. For this reasons we have treated extensively the theory of excited states of clusters and its application to the spectroscopy of clusters (section IV). The selected ground-state properties have been analyzed as well, in order to demonstrate how some general laws manifest themselves in cluster physics (section III). The Green's function technique can serve as a link among various methods employed to investigate perturbations to which a cluster is subjected. For this reason the Green's operator, Green's functions, and some illustrative examples of their application are described in section II.B.2. Several general connections among Green's function technique and various concepts, useful in cluster theory, are sketched in the Appendixes. This analysis serves also for establishing common features among different response theories given in sections II.B.4, II.B.5, and II.B.7. (Readers interested only in the application of quantum chemistry to clusters can omit the section II.B and the Appendixes.)

A clear and lucid understanding of the ground- and excited-states phenomena is possible only for relatively simple cluster classes. For this reason, no attempt has been made to extend the present review to clusters of transition-metal atoms as well as to clusters for which the conventional valence rules are applicable (e.g. sulfur clusters).

The conclusions drawn from theoretical and experimental investigation of small clusters do not completely refer to very large cluster sizes for which a number of other phenomena might occur.

The main part of this review deals with alkali-metal clusters, since in this case the theory can be applied at a relatively high level of accuracy. The next simplest systems are Ib clusters, and their properties are also addressed. Other clusters with atoms from groups II–IV of the periodic table are considered only when a comparison with the Ia and Ib clusters is illustrative.

II. Comparison of Quantum Chemical and Solid-State Theoretical Concepts and Methods

In the last two decades, methods and notions developed in a particular scientific field have been frequently adopted in other disciplines. The introduction of such new ideas and procedures is very often useful and successful. The use of second quantization and of related methods in molecular physics is only one of many similar examples. The tight binding methods, particularly the Koster–Slater semiempirical approach, can be considered parallel to the Mulliken LCAO (linear combination of atomic orbitals) methods of quantum chemistry.

Elemental clusters represent a transition domain between solids and individual atoms. They also exhibit some properties resembling those found in nuclear physics. Small clusters have, in general, sizes of molecules investigated in organic chemistry and biochemistry. Therefore, cluster theory is a field of science where the advantages of quantum chemical approaches, solid-state theory, and models and methods of nuclear physics can be compared, tested, and analyzed. A better understanding of connections between corresponding scientific concepts and attitudes can result from such studies. This is important for cluster theory and is also of general interest for applied quantum mechanics.

Only those aspects of the scientific fields relevant for the theoretical interpretation of properties of elemental clusters will be addressed in this section. A partly simplified presentation of the topic should help to emphasize the similarities and differences among approaches customary in quantum chemistry, solid-state theory, and nuclear physics.

A. Concepts of Quantum Chemistry

A very important and frequently used class of quantum chemical methods derives molecular properties from those of the constituent atoms. For example, this can be achieved by using one-electron functions which have the form of linear combinations of the basis functions centered at the positions of atomic nuclei in the molecular system (atomic orbitals, LCAO approximation). The characteristic parameters of these localized functions allow a derivation of molecular and atomic properties within the framework of the chosen quantum chemical method. It is not within the scope of this review to analyze the advantages and deficiencies met in the applications of the LCAO type of methods.

Tight-binding procedures represent a class of methods used in solid-state theory which are closely related to a philosophy typical of quantum chemical approaches. However, due to a number of simplifications introduced, the majority of methods used in solid-state theory try to avoid the large difficulties that arise when quantum chemical methods are applied to large systems, by introducing a number of simplifications.

1. One-Electron Approximations: Hartree–Fock and Density Functional Theories

The simplest many-electron wave function obeying the antisymmetry principle is the Slater determinant of one-electron functions $\varphi_i(\mathbf{x}_i)$ (or spin orbitals):[26-28]

$$\phi(\mathbf{x}_1\mathbf{x}_2...\mathbf{x}_N) = \mathcal{A}[\varphi_1(\mathbf{x}_1)\varphi_2(\mathbf{x}_2)...\varphi_N(\mathbf{x}_N)] \qquad \text{(IIA1.1)}$$

where $\mathcal{A}$ is the antisymmetrizer, $\mathbf{x}_i$ is the set of space ($\mathbf{r}_i$) and spin ($\eta_i = \alpha, \beta$) coordinates, and N is the number of electrons.

For the pure electrostatic Hamiltonian $\hat{H}_0$ in the Born–Oppenheimer approximation (BO), assuming orthogonal basis in (IIA1.1), the total energy can be computed according to

$$E = \langle\phi|\hat{H}_0|\phi\rangle = \sum_i^{n_o}\langle\varphi_i(1)|\hat{h}(1)|\varphi_i(1)\rangle + (1/2)\sum_{i,j}^{n_o}\{[ij|ij] - [ij|ji]\} + V_n \quad \text{(IIA1.2)}$$

where the following shorthand notations have been used:

$$[ij|kl] = [i(1)j(2)|k(1)l(2)] = \int\int \varphi_i^*(\mathbf{x}_1)\varphi_j^*(\mathbf{x}_2)(1/r_{12})\varphi_k(\mathbf{x}_1)\varphi_l(\mathbf{x}_2)\, d\mathbf{x}_1 d\mathbf{x}_2$$

$$\hat{h}(1) = (-1/2)\nabla^2(1) - \sum_A(Z_A/r_{1A}) \quad \text{(IIA1.3)}$$

and

$$V_n = \sum_{A<B}(Z_A Z_B/R_{AB}) \quad \text{(IIA1.4)}$$

The summations in (IIA1.2) run over the set of n_o (occupied) spin orbitals contained in ϕ.

The spin orbitals minimizing the expectation value E are eigenfunctions of the Hartree–Fock (HF) operator:

$$\hat{F}(1)|\varphi_i\rangle = [\hat{h}(1) + \hat{J}(1) - \hat{K}(1)]|\varphi_i\rangle = \epsilon_i|\varphi_i\rangle \quad \text{(IIA1.5)}$$

where $\hat{h}(1)$ collects all the one-electron contributions while the Coulomb $\hat{J}(1)$ and exchange $\hat{K}(1)$ operators define the electron–electron potential experienced by a single electron:

$$J(i) - K(i) = \langle\varphi_i(1)|\hat{J}(1) - \hat{K}(1)|\varphi_i(1)\rangle = \sum_j^{n_o}([ij|ij] - [ij|ji]) \quad \text{(IIA1.6)}$$

It is useful to introduce the definition of the one-electron density which plays a fundamental role in all the independent particle methods:

$$\rho(\mathbf{x}_1) = N\int \phi(\mathbf{x}_1,\mathbf{x}_2,\ldots\mathbf{x}_N)\phi^*(\mathbf{x}_1,\mathbf{x}_2,\ldots\mathbf{x}_N)\, d\mathbf{x}_2\ldots d\mathbf{x}_N \quad \text{(IIA1.7)}$$

or its "spin-free" form $\rho(\mathbf{r}_1)$, obtained by integrating over the spin variables. When the HF spin orbitals are expanded in a fixed set of (real) basis functions $\{\chi_\lambda\}$ (Roothaan method) according to

$$|\varphi_i(\mathbf{x})\rangle = |\bar{\varphi}_i(\mathbf{r})\rangle|\eta_i\rangle = \sum_\lambda C_{\lambda i}|\chi_\lambda(\mathbf{r})\rangle|\eta_i\rangle \quad \text{(IIA1.8)}$$

in terms of spatial orbitals $\bar{\varphi}_i(\mathbf{r})$ and fixed real basis functions $\{\chi_\lambda\}$, $\rho(\mathbf{r})$ assumes the form

$$\rho(r) = \sum_i^{n_o}\sum_{\lambda\mu} n_i C_{\lambda i}C_{\mu i}\chi_\lambda(\mathbf{r})\chi_\mu(\mathbf{r}) = \sum_i^{n_o}\sum_{\lambda\mu} R_{\lambda\mu}^i\chi_\lambda(\mathbf{r})\chi_\mu(\mathbf{r}) = \sum_{\lambda\mu} R_{\lambda\mu}\chi_\lambda(\mathbf{r})\chi_\mu(\mathbf{r}) \quad \text{(IIA1.9)}$$

where n_i is the orbital occupation number ($n_i = 1, 2$). $\mathbf{R} = [R_{\lambda\mu}] = \sum_i^{n_o}\mathbf{R}^i$ is the matrix representation of the density $\rho(\mathbf{r})$ in the basis $\{\chi_\lambda\}$. Coulomb and exchange integrals can be written in terms of quantities defined over the basis $\{\chi_\lambda\}$ according to

$$\mathbf{J}_i = \sum_{\lambda\mu} R_{\lambda\mu}^i\{\sum_j^{n_o}\sum_{\nu\sigma} n_j R_{\nu\sigma}^j[\lambda\nu|\mu\sigma]\} = \sum_{\lambda\mu} R_{\lambda\mu}^i J_{\lambda\mu}$$

$$K_i = \sum_{\lambda\mu} R_{\lambda\mu}^i\{\sum_j^{n_o}\sum_{\nu\sigma} n_j R_{\nu\sigma}^j[\lambda\nu|\sigma\mu]\} = \sum_{\lambda\mu} R_{\lambda\mu}^i K_{\lambda\mu} \quad \text{(IIA1.10)}$$

For a multielectron system it is always possible to identify groups of electrons which share the same Fock operator (shells). In particular, for a closed-shell system ($n_i = 2$, $\forall i$) all the pairs of electrons with opposite spin occupy the same spatial orbitals. Systems with unpaired electrons can be also considered as composed by a closed shell and one or more open shells. In general, for n_s shells, one can define the matrix elements for each Fock operator in the form

$$F_{\lambda\mu}^s = h_{\lambda\mu} + \sum_{s'}\sum_{\nu\sigma} R_{\nu\sigma}^{s'}(a_{ss'}[\lambda\nu|\mu\sigma] - b_{ss'}[\lambda\nu|\sigma\mu])$$

$$h_{\lambda\mu} = \langle\chi_\lambda|\hat{h}(1)|\chi_\mu\rangle \quad \text{(IIA1.11)}$$

where $s,s' = 1, 2, \ldots n_s$. The constants $a_{ss'}$ and $b_{ss'}$ depend upon the spin coupling which is characteristic of the electronic state under consideration and depend upon the occupation number of the shell s.

When the constraint that pairs of electrons must be described by the same spatial orbitals is removed, that is when $n_{o\alpha}$ spin α and $n_{o\beta}$ spin β electrons are described by two sets of nonorthogonal orbitals with coefficients $\{C_{\lambda i}^\alpha\}$, $\{C_{\lambda i}^\beta\}$, one has

$$R_{\lambda\mu}^{\tau i} = C_{\lambda i}^\tau C_{\mu i}^\tau \qquad \mathbf{R}^\tau = \sum_i^{n_{o\tau}}\mathbf{R}^{\tau i}\ (\tau = \alpha,\beta) \qquad \mathbf{R} = \mathbf{R}^\alpha + \mathbf{R}^\beta \quad \text{(IIA1.12)}$$

and the corresponding matrix elements of the Fock operator obey the definition

$$F_{\lambda\mu}^\tau = h_{\lambda\mu} + \sum_{\nu\sigma}\{R_{\nu\sigma}[\lambda\nu|\mu\sigma] - R_{\nu\sigma}^\tau[\lambda\nu|\sigma\mu]\} \quad (\tau = \alpha,\beta) \quad \text{(IIA1.13)}$$

The above equation forms the basis of the "unrestricted Hartree–Fock" (UHF) method, also called "spin-polarized" method, often used in quantum chemical studies of clusters. It must be pointed out, however, that the wave function ϕ_0 constructed with unrestricted spin orbitals $\{\varphi_i^\alpha\}$ and $\{\varphi_j^\beta\}$ is not an eigenfunction of the spin operator, $\hat{S}^2$, that is, in general it does not represent a pure spin state. This fact does not seem to be carefully considered in cluster studies, especially when the UHF method is used to investigate large portions of the Born–Oppenheimer surfaces. The $\langle\hat{S}^2\rangle$ expectation value can vary from point to point along with the degree of "spin-contamination" of the wave function.

It is important to note that the exchange term of (IIA1.13) is essentially a nonlocal contribution, while the Coulomb term has the classical meaning of interaction between electronic clouds and can be represented in terms of local values of the one-electron density. For instance, for a single closed-shell wave function the HF electron energy can be written, as the sum of traces of matrix products, in the form

$$E_{el} = \text{tr}\,\mathbf{Rh} + \text{tr}\,\mathbf{RJ}(\mathbf{R}) - (1/2)\,\text{tr}\,\mathbf{RK}(\mathbf{R}) \quad \text{(IIA1.14)}$$

or equivalently in terms of integrals over the electron coordinate $\mathbf{r}$:

$$E_{el} = \int \rho(\mathbf{r})h(\mathbf{r})\, d\mathbf{r} + (1/2)\int\int \frac{\rho(\mathbf{r})\rho(\mathbf{r}')}{|\mathbf{r} - \mathbf{r}'|}\, d\mathbf{r}d\mathbf{r}' - E_x[\rho(\mathbf{r})] \quad \text{(IIA1.15)}$$

Equation IIA1.15 is a basic relation used to express the electronic energy in terms of the electron density only.

The density functional (DF) formalism of Hohenberg and Kohn[29] is based on the theorem stating that for a system of N interacting electrons the ground-state energy E_{gs} is determined uniquely by $\rho(\mathbf{r})$, that is $E_{gs} = E[\rho(\mathbf{r})]$. Furthermore, the exact ground-state energy E_{gs} can be found only for the exact ground-state density $\rho_0(\mathbf{r})$. The connection between the formulation based on the exact one-electron density and that based on the exact many-electron wave function ϕ_0 ($\rho_0(\mathbf{r}_1) = N\int \phi_0(\mathbf{x}_1,\mathbf{x}_2,...\mathbf{x}_N)\phi_0^*(\mathbf{x}_1,\mathbf{x}_2,...\mathbf{x}_N)\, d\eta_1 d\mathbf{x}_2...d\mathbf{x}_N$) has been established by Levy.[30] According to the variational principle, the function ϕ_0^{min} which minimizes the functional

$$\langle\phi_0^{min}| - (1/2)\sum_i\nabla^2(i) + \hat{H}_{ne} + \hat{H}_{ee}|\phi_0^{min}\rangle \geq E_{gs} \quad \text{(IIA1.16)}$$

can be found, in principle, through a search of "all" possible trial functions ϕ_0. Correspondingly, the functional

$$Q[\rho(\mathbf{r})] + \int \rho(\mathbf{r})\hat{H}_{ne}(\mathbf{r})\, d\mathbf{r} \geq E_{gs} \quad \text{(IIA1.17)}$$

must be in principle searched for all the N representable densities. Note that $Q[\rho(\mathbf{r})]$ contains all the terms (kinetic, Coulomb, exchange, and correlation energy) for interacting electrons.

A practical solution of (IIA1.17) has been proposed by Kohn and Sham,[31] based on the use of the functional

$$E[\rho(\mathbf{r})] = T_0[\rho(\mathbf{r})] + \int \rho(\mathbf{r})[\hat{H}_{ne}(\mathbf{r}) + \hat{H}_{Cee}(\mathbf{r})]\, d\mathbf{r} + E_{xc}[\rho(\mathbf{r})] \quad \text{(IIA1.18)}$$

where T_0 is the kinetic energy which the system would have in absence of electron–electron interactions. The contributions due to the operator $\hat{H}_{ee}$ have been separated into Coulomb ($\hat{H}_{Cee}$) contribution which can be easily evaluated in a classical way, and an exchange and correlation term E_{xc} which is a typical feature of all DF methods.

In the DF theories, one usually defines "intermediate" one-electron functions (Kohn–Sham orbitals)[31,32] which are solutions of the equation

$$\hat{H}_0|\varphi_i\rangle = \epsilon_i|\varphi_i\rangle \qquad \rho(\mathbf{r}) = \sum_i|\varphi_i(\mathbf{r})|^2 \quad \text{(IIA1.19)}$$

with

$$\hat{H}_0(1) = (-1/2)\nabla^2(1) - \sum_A\frac{Z_A}{\mathbf{r}_{1A}} + \int\frac{\rho(\mathbf{r}')\, d\mathbf{r}'}{|\mathbf{r}_1 - \mathbf{r}'|} - \frac{\partial E_{xc}[\rho(\mathbf{r}_1)]}{\partial\rho(\mathbf{r}_1)} \quad \text{(IIA1.20)}$$

The modern literature of the DF methods (see ref 33 and references therein) is rich in suggestions for analytical expressions of the $E_{xc}[\rho(\mathbf{r})]$ functional, based on simple local values of $\rho(\mathbf{r})$ or including corrections for nonlocal effects. The most general form of E_{xc} is $E_{xc}[\rho(\mathbf{r})] = f[\rho(\mathbf{r}), \nabla\rho(\mathbf{r}), \nabla^2\rho(\mathbf{r}), ...]$. However, in order to reduce the computational difficulties, simple dependencies on the local values of the density or its spin components $\rho^\alpha(\mathbf{r})$ and $\rho^\beta(\mathbf{r})$ are assigned to E_{xc}: these approximations are known as local density (LD) or local spin density (LSD) approach.

In the framework of the HF and LD theories, effective core potential (ECP) methods[34,35] have been developed with the aim of representing in a simple way the Coulomb and exchange potential generated by the core electrons and acting on the valence ones. ECP methods allow us to carry out calculations only on valence electrons, thus drastically reducing the computational time, especially in the case of large molecular systems composed of atoms of heavy elements. The most reliable forms of the ECP operator include nonlocal contributions expressed in terms of projectors on the space spanned by the angular momentum functions centered on a given nucleus. This gives us the ability to consider in a proper way the nonlocal character of the exchange potential. Short range terms in the ECP operators must be repulsive, in order to avoid the variational collapse of the valence electrons into the core region. Long range terms are attractive in order to take into account for the fact that the core electrons do not completely screen the nuclear charges.

Usually the ECP operators are determined in such a way that the atomic pseudoorbitals and their energies match the corresponding results obtained from all-electron (AE) calculation. When AE wave functions determined according to relativistic Dirac–Fock calculations are used as reference functions for deriving the effective valence-only operators, the resulting relativistic ECP's (RECP) automatically include the most important relativistic corrections.[35,36] For example, pseudoorbitals of s symmetry that are eigenfunctions of RECP operators show a characteristic contraction with respect to the corresponding functions obtained from nonrelativistic ECP calculations.

Tabulations of ECP or RECP operators and the associated atomic basis sets have been reported for a large number of chemical elements, both in connection with HF[37-44] (see also ref 35 and references therein) and LSD[41,42] methods.

Several test calculations in which a comparison has been made between ECP and AE results have confirmed the validity and reliability of the valence-only approaches, which are now also routinely applied to elemental clusters, especially those of larger dimensions and composed of heavy atoms (see sections III and IV).

2. Correlation Effects

As is well known, all one-electron properties can be expressed in terms of the one-electron density matrix. In particular, as shown in the previous section, this is true for the electronic energy of the HF and other independent-particle methods. A single-determinant wave function $|\phi\rangle$ does not describe correlation of electrons with different spin. Electrons of equal spin are correlated due to the antisymmetric character of $|\phi\rangle$. Therefore, the independent electron models give energy values higher than the true ones by an amount called the correlation energy, which is formally defined as the difference between the exact nonrelativistic value and the HF energy associated with a complete HF space. When working with truncated basis sets $\{\chi_\lambda\}$, both the HF and correlation energy become basis set dependent quantities. In particular, the calculated correlation energy is underestimated in the case of large systems with many electrons, for which relatively small basis sets have to be adopted.

Wave functions which approximate the exact wave function better than ϕ and which automatically include part (or all) of the correlation effects can be expanded in terms of configuration functions (CF) according to[45]

$$|\Psi\rangle = |\phi_0\rangle + \sum_{ip} A_i^p|\phi_i^p\rangle + \sum_{\substack{i<j \\ p<q}} A_{ij}^{pq}|\phi_{ij}^{pq}\rangle + \ldots =$$
$$(1 + \sum_{ip} A_i^p \hat{a}_p^\dagger \hat{a}_i + \sum_{\substack{i<j \\ p<q}} A_{ij}^{pq} \hat{a}_p^\dagger \hat{a}_q^\dagger \hat{a}_j \hat{a}_i + \ldots)|\phi_0\rangle \quad \text{(IIA2.1)}$$

where $|\phi_0\rangle$ is the HF single determinant wave function in which the spin orbitals i, j, k, etc. are occupied. The spin orbitals p, q, r, etc. are solution of the complete HF problem but do not enter the definition of $|\phi_0\rangle$ (virtual orbitals). $|\phi_i^p\rangle$, $|\phi_{ij}^{pq}\rangle$, etc. are called singly, doubly, etc. excited configurations with respect to $|\phi_0\rangle$ and can be formally generated by using annihilation $\hat{a}_i$ and creation $\hat{a}_p^\dagger$ operators.[46]

It is convenient to introduce the excitation or "replacement" operators $\hat{E}_{pi}$ and the spinless operators $\hat{\mathcal{E}}_{pi}$:[47]

$$\hat{E}_{pi} = \hat{a}_p^\dagger \hat{a}_i$$

$$\hat{\mathcal{E}}_{pi} = \hat{a}_{p\alpha}^\dagger \hat{a}_{i\alpha} + \hat{a}_{p\beta}^\dagger \hat{a}_{i\beta} \quad \text{(IIA2.2)}$$

$$\hat{\Gamma}_{pq,ij} = \hat{\mathcal{E}}_{pi}\hat{\mathcal{E}}_{qj} - \delta_{iq}\hat{\mathcal{E}}_{pj} = \hat{\mathcal{E}}_{qj}\hat{\mathcal{E}}_{pi} - \delta_{jp}\hat{\mathcal{E}}_{qi} \quad \text{(IIA2.3)}$$

The operators E_{pi} and $\hat{\mathcal{E}}_{pi}$ are generators of Lie algebra. These operators are often used in modern theory of correlated wave functions and are very useful to express, for instance, the electronic Hamiltonian in a general form

$$\hat{H}_0 = \sum_{ip} h_{pi}\hat{\mathcal{E}}_{pi} + (1/2)\sum_{ij,pq}\hat{\Gamma}_{pq,ij}[ij|pq] \quad \text{(IIA2.4)}$$

where the coefficients h_{pi} and $[ij|pq]$ are quantities defined in the basis of the orbitals $\{\bar{\varphi}_i\}$ (cf. IIA1.3 and IIA1.8).

Equation IIA2.4 is the form of the time-independent Hamiltonian most suitable for the computation of elements of the matrix **H** among the configurations $|\phi_{ijk\ldots}^{pqr\ldots}\rangle$. **H** is the matrix of the secular or configuration interaction (CI) problem

$$\mathbf{H}\mathbf{a}_s = E_s\mathbf{a}_s \quad \text{(IIA2.5)}$$

The vector $\mathbf{a}_s$ collects the coefficients of (IIA2.1) for a specific electronic state s, while different roots of the secular determinant eqution $|\mathbf{H} - \mathbf{E}| \equiv 0$ give the energies of the ground and excited states.

When the sets of configurations $\{\phi_i^p\}$ and $\{\phi_{ij}^{pq}\}$ are generated from a single reference configuration (usually $|\phi_0\rangle$), one obtains the so called "single and double CI" (SD-CI) method. When single and double excitations are generated with respect to several reference configurations, the CI expansion is of the multireference type (MR-CI) and includes higher order excitations with respect to $|\phi_0\rangle$.

As the number of electrons increases, the number of multiple-excited configurations increases dramatically and the required computational effort may be so large that a truncation of the expansion must be accepted. There are two ways to reduce the number of configurations to be inserted in the CI expansion. The first is to reduce the space of the virtual orbitals to which specific excitations are allowed and the other way is to retain only those configurations which according to some "energy lowering" criterion are expected to contribute significantly to the final correlation energy. The latter approach forms the basis of the MRDCI method,[48,49] which offers several advantages especially in connection with the determination of multiple roots of the secular equation (cf. section IV.B).

It is important to recall that CI expansions including only low-order excitations may be affected by large errors due to size inconsistency. This is an intrinsic bias of the CI method because for a fixed order of excitations the corresponding expansion is close to the full CI limit for systems with a few electrons and far from the full CI limit for larger systems. The coupled pair functional (CPF) approach and other related methods[50,51] aim to overcome the size-inconsistency effects.

A bottleneck of the CI calculations is represented by the high number of configurations to be generated (and selected), which is a consequence of the slow convergence of the method especially if the basis of spin orbitals is not well chosen. Accurate calculations may include up to 10^6 configurations and the corresponding matrix elements cannot be stored in computer memory or retrieved in an efficient way. These difficulties can be overcome since the matrix elements between configuration ϕ_K and ϕ_L have the form

$$H_{KL} = \sum_{ip} h_{ip}\langle\phi_K|\hat{\mathcal{E}}_{pi}|\phi_L\rangle + (1/2)\sum_{ij,pq}[ij|pq]\langle\phi_K|\hat{\Gamma}_{pq,ij}|\phi_L\rangle \quad \text{(IIA2.6)}$$

and the matrix elements of the excitation operators act just as coefficients of the one- and two-electron integrals.[52] Conversely, each integral can be associated with the labels of the matrix elements to which it contributes and with corresponding factors. In this way, the construction (and storage) of the matrix **H** is avoided and the determination of the energy E_s and the associated vector $\mathbf{a}_s$ can be carried out iteratively with an "integral driven" algorithm. The method is known as "direct-CI"[53a] and is well suited for large-scale calculations.

Other approaches for evaluating the correlation energy which are frequently used in cluster studies are based on Möller–Plesset perturbational tretment (MP) at different orders.[27] The second order expansion (MP2) is the most commonly used because it requires a computational work drastically reduced with respect to the variational CI. MP4 expansion can efficiently handle all the excitations up to the quadruple ones due to the fact that the **H** matrix does not need to be explicitely constructed and diagonalized. Other efficient approaches, like the CIPSI[54,55] method, combine a variational CI step carried out in order to define a relatively small intermediate space of configurations from which higher excited configurations are generated and treated in a perturbative way.

3. Born–Oppenheimer Surfaces, Local and Absolute Minima, Vibrations, and Molecular Dynamics

The time-independent Hamiltonian $\hat{H}_0$ that obeys the Born–Oppenheimer assumption allows the computation of the total molecular energy for a fixed nuclear configuration as a parametric function of the $3n - 6$ ($3n - 5$ for linear systems) internal degrees of freedom.

In the simple case of a closed-shell molecules the total HF energy (IIA1.2) can be written in the form

$$E_{HF} = \sum_{\lambda\mu} R_{\lambda\mu} h_{\lambda\mu} + (1/2)\sum_{\lambda\mu\nu\sigma} R_{\lambda\mu} R_{\nu\sigma}([\lambda\nu|\mu\sigma] - 1/2[\lambda\nu|\sigma\mu]) + V_n \quad \text{(IIA3.1)}$$

If the nuclear displacements from the minimum (equilibrium) geometry are expressed in terms of nu-

clear coordinates q, the derivative of the energy E_{HF} has the form[56]

$$\frac{\partial E_{HF}}{\partial q} = \sum_{\lambda\mu} R_{\lambda\mu} \frac{\partial h_{\lambda\mu}}{\partial q} + (1/2)\sum_{\lambda\mu\nu\sigma} R_{\lambda\mu} R_{\nu\sigma} \frac{\partial}{\partial q}([\lambda\nu|\mu\sigma] - (1/2)[\lambda\nu|\sigma\mu]) + (\partial V_n/\partial q) - \sum_{\lambda\mu} W_{\lambda\mu} \frac{\partial S_{\lambda\mu}}{\partial q} \quad \text{(IIA3.2)}$$

where $W_{\lambda\mu} = \sum_i^n \epsilon_i R_{\lambda\mu}^i$, ϵ_i is the orbital energy and $S_{\lambda\mu} = \langle \chi_\lambda | \chi_\mu \rangle$ is an overlap matrix element.

As is well known, the most computationally demanding part of (IIA3.2) is the evaluation of the derivative of the two-electron integrals which, in principle, cannot be neglected because the wave function associated with E_{HF} is usually far from being exact. In fact, only for exact wave functions the forces acting on the nuclei depend only on the derivatives of one-electron integrals and on V_n (Hellman–Feynman theorem). The assumption that gradient components can be represented by one-electron terms only is present in some studies on clusters carried out in the framework of the LDA methods. This probably was a necessary approximation because the two-electron part of the LDA energy (E_{xc}) cannot be put in a simple analytical form and its derivatives cannot be easily computed. Only recently, in fact, the theory has been developed in order to work out analytical forms of the orbital forces.[57,58]

In searching for the minimum energy conformations of clusters, quasi-Newton algorithms have to be adopted if only first derivatives are available: the Hessian matrix is evaluated only in an approximate way and updated at each iterative step.[59]

The two-electron integral derivatives are clearly even more computationally demanding when working with minimization algorithms based on exact second derivatives (Newton methods). However, such procedures are expected to be much faster in convergence than the quasi-Newton approaches based only on gradients. The exact second derivative methods have been seldom adopted in cluster studies despite the fact that this is certainly an ideal field of application. In fact, it is now well established that the BO surfaces of elemental clusters (in particular those composed of metal atoms) are characterized by low curvatures also in points far from the stationary ones. Experience has shown that quasi-Newton methods may present difficulties because the approximate Hessian matrix is sometimes not positively definite due to numerical inaccuracies.

In cluster studies, one of the most challenging problems is to answer the question of how many stable conformers exist and how large is the energy separation among them. This is a basic problem since the experiments on clusters are usually carried out at such high temperature that a statistical population of isomers has to be taken into account. However, the identification of different isomers by means of gradient-based theoretical calcualtions can be a very difficult task because such methods are able to locate only the minimum point nearest to the starting point. Other minima can be identified by repeated runs of geometry optimization by starting from different (e.g., randomly generated) initial configurations.

As for normal molecules, once the minimum geometry of a cluster has been identified, it would be interesting to carry out a full vibrational analysis. This would not only give information on the lowest energy distortions that the cluster can undergo but would also help in interpreting experimental data. This has been done only for very small species.[60-63] However, in carrying out a theoretical vibrational analysis the same computational difficulties mentioned for the geometry optimizations can arise if exact (analytical) second derivatives are not available. The numerical accuracy of the approximate second derivatives can be unsatisfactory, especially for normal modes characterized by small force constants and frequencies. This can further increase the inadequacy of the HF approach in predicting vibrational properties. As a consequence, the computed vibrational frequencies can be ultimately unreliable from a quantitative point of view. However, even an approximate analysis can be useful in order to confirm the character of minima of the stationary points which are often reached with an optimum geometry search carried out with symmetry constraints.

Recent developments of the quantum molecular dynamics (QMD) method proposed by Car and Parrinello[64,65] open new a horizon for studying large portions of BO surfaces and for identifying local and absolute minima.

In the QMD method the total molecular energy is considered simultaneously as a function of spin orbitals φ_i and of nuclear coordinates

$$E = E[\{\varphi_i\}, \{\mathbf{r}_A\}] \qquad (i = 1,...N;\ A = 1,...n) \quad \text{(IIA3.3)}$$

E is the expectation value of a DF Hamiltonian including a LSD exchange–correlation functional

$$\hat{H}_0 = \hat{H}_{en} - (1/2)\sum_i \nabla^2(i) + \hat{V}_c + \hat{V}_{xc} + \hat{H}_n \quad \text{(IIA3.4)}$$

For computational convenience the orbitals $\varphi_i(\mathbf{r})$ are expanded in a (truncated) set of plane waves, according to

$$\varphi_i(\mathbf{r}) = \sum_{\mathbf{g}} C_{\mathbf{g}i} \exp(i\mathbf{g}\cdot\mathbf{r}) \quad \text{(IIA3.5)}$$

The minimum electronic energy for a fixed nuclear configuration can be found without building and diagonalizing a Kohn–Sham type one-electron operator matrix, by means of quasidynamical treatment. In fact, introducing a fictitious time variable t for the "motion" of the electrons, the following equation can be written:

$$(\partial\varphi_i(\mathbf{r},t)/\partial t) = (-1/2)[\partial E/\partial\varphi_i^*(\mathbf{r},t)] = \hat{H}_0\varphi_i(\mathbf{r},t) \quad \text{(IIA3.6)}$$

Let Δt be the elementary time step: it controls implicitly the convergence rate of the optimization which, when carried out according to a simple steepest descent scheme leads to a variation of φ_i defined by

$$\varphi_i(\mathbf{r},t + \Delta t) = \varphi_i(\mathbf{r},t) - \Delta t\, \hat{H}_0\varphi_i(\mathbf{r},t) + (\text{constraints}) \quad \text{(IIA3.7)}$$

where the constraints collect all the contributions derived from the orthonormality conditions

$$\int \varphi_i^*(\mathbf{r})\varphi_j(\mathbf{r})\, d\mathbf{r} = \delta_{ij} \quad \text{(IIA3.8)}$$

The "dynamics" for the electrons can be combined with dynamics involving the nuclear centers by using the set of equations

$$\mu_i \frac{\partial^2\varphi_i(\mathbf{r},t)}{\partial t^2} = (-1/2)\frac{\partial E}{\partial\varphi_i^*(\mathbf{r},t)} + \sum_j \Delta_{ij}\varphi_i(\mathbf{r},t) \quad \text{(IIA3.9)}$$

$$M_A \frac{\partial^2\mathbf{r}_A(t)}{\partial t^2} = -\frac{\partial E}{\partial r_A(t)} - \sum_c \frac{\partial}{\partial r_A}\sigma_c(\mathbf{r}_1,\mathbf{r}_2,...\mathbf{r}_n)$$

where μ_i and M_A are "effective" masses for electrons and nuclei to which are assigned values which conform to the Born–Oppenheimer hypothesis ($M_A \gg \mu_i$). Δ_{ij} are Lagrangian multipliers defined by the constraints conditions for the electrons (IIA3.8), while σ_c are expressions for the constraints involving only nuclear coordinates $\mathbf{r}_I$ ($I = 1,...n$) and are needed to maintain the molecular structure. Since the electron and nuclear velocities can be assumed to be temperature-dependent quantities, different thermal processes like melting, annealing, or quenching can be simulated by varying simultaneously the degrees of freedom of the electrons and nuclei. With an algorithm similar to the simulated annealing[66] (but not based on Monte Carlo sampling) the QMD is able to give equilibrium structures at $T = 0$, which would correspond to the absolute minimum on the BO surface provided that the adopted rate of "cooling" is slow enough. Other QMD experiments carried out at $T > 0$ can give information about the existence of equilibrium molecular structures corresponding to local minima lying at higher energy.

The QMD method offers several conceptual advantages with respect to the conventional quantum mechanical methods. However, its rate of convergence, accuracy and applicability seems to be bound to two difficulties. The first concerns the Δt parameter step which is required to be sufficiently small, thus increasing the number of steps for each trajectory. The second difficulty is certainly represented by the plane-wave expansion. The plane waves are delocalized functions and all attempts to use them to describe localized (atom-like) electronic states results in a very slow convergence. This is the reason why QMD has always been applied in connection with effective potentials (ECP)[67] which avoid the representation of the electronic core states. In addition, when reliable ECPs exist, the QMD method is expected to work better for elements with diffuse valence orbitals than for elements of low atomic numbers. In addition, the QMD methods are usually applied in the context of spin-polarized (spin-unrestricted) formalism and LSD approximation for the E_{xc} functional.

4. *Symmetry, Topology, and Electron-Counting Rules*

In all branches of physics and particularly in molecular and cluster quantum chemistry, the symmetry of the nuclear frame plays a key role, being the cause (and the consequence, at the same time) of the intrinsic symmetry of the electronic wave function. The interplay between the symmetry of the nuclear frame and the symmetry of the wave function is so evident that the appearance (or absence) of specific electronic properties (dipole moments, anisotropy in polarizability, number of infrared—or Raman—active vibrational modes, and number and intensity of the photoabsorption bands) can be considered as an indication of the existence (or absence) of specific elements of space symmetry. Since a correct electronic wave function must belong to a single irreducible representation of the symmetry group to which the nuclear frame belongs, it is obvious that the non-Abelian character of a high-symmetry group corresponds to degeneracies of the electronic wavefunctions.

In this respect the behavior of the elemental clusters can serve as a very characteristic example. It is to be expected that they tend to assume a very symmetric shape, in order to maximize the interatomic bonding interactions. This usually corresponds also to a maximal average number of nearest neighbors (average coordination number) for each atom. This fact is clearly documented by the analysis of the preferred geometries generated by simple two-body classical potentials.[68] Such predictions, however, are expected to be physically relevant only for clusters composed of weakly polarizable atoms, which interact among themselves like (nearly) rigid spheres. This is the case of the van der Waals clusters of rare gas atoms.

In the case of metal atoms (and in some respect also of covalent elements) the electronic distribution around each nucleus can be markedly dependent upon the type and number of the surrounding atoms since hybridization and electron polarization occur. Therefore the global topology of the cluster can influence the specific electronic configuration of each individual atom. The fact that the electron distribution may be inhomogeneous even in clusters of high symmetry is just a specific characteristic which distinguishes clusters from bulk materials.

Such specific features of clusters clearly also influence the choice of computational methods. In particular, the basis sets employed in calculations must contain "polarization functions" well adapted to describe the distortion that valence electrons can undergo. Limitation in the size of the basis sets are often a necessary compromise in order to make possible the investigation of a wide range of cluster sizes; but also in this case the inclusion of polarization functions seems to be essential.

The topology and the related symmetry characteristics of a cluster often depend mainly on the number of valence electrons which effectively contribute to the cluster bonding. Therefore it is not surprising to observe that elements with the same atomic ground state form clusters with identical topologies. This is particularly evident, for instance, for the elements of the groups Ia and Ib, all characterized by a single s valence electron. This observation is important, since basic information about preferred geometries and general rules for cluster growth can be obtained from highly accurate calculations on clusters of elements with low atomic number, and then applied to a broader class of clusters.

In contrast to closed shell systems (with no unpaired electrons), or open-shell systems with nondegenerate one-electron levels, Jahn–Teller (JT) distortions can occur for systems with degenerate one-electron levels. Distortions lower the symmetry and remove the degeneracy.

Usually, JT distortions, acting along a non-totally symmetric normal coordinate, have small amplitude for molecules like transition-metal complexes, but in the case of clusters characterized by shallow BO surfaces large geometry modifications can take place (see section II.A.3). Of course, when the number of electrons is sufficiently high to completely fill the set of degenerate one-electron levels, no JT distortion can occur and the cluster has a closed-shell configuration, usually with a very compact structure.

For finite symmetry groups the assignment of a one-electron function to a specific irreducible representation is analogous to the assignment of the atomic angular momentum quantum number and its compo-

nents m_l for atoms.

As a simple illustrative example, let us mention that molecules with eight valence electrons are particularly stable [e.g. CH_4 (T_d), NH_3 (C_{3v}), H_2O (C_{2v}), HF ($C_{\infty v}$)]. They can be considered as derived from "united atoms" with electronic configuration $1s^22s^22p^6$ (Ne) perturbed by a "ligand field" of symmetry T_d, C_{3v}, C_{2v}, and $C_{\infty v}$, respectively. The following relations are obvious: $1s^22s^22p^6$ (atom) → $1a_1^22a_1^21t_2^6$ (T_d)] → $1a_1^22a_1^23a_1^2e^4$ (C_{3v}) → $1a_1^22a_1^23a_1^21b_1^21b_2^2$ (C_{2v}) → $1\sigma^22\sigma^23\sigma^21\pi^4$ ($C_{\infty v}$). The symmetry of the (closed-shell) molecule (taking also into account the presence of electron lone pairs) is always the highest possible one. These rules are well known in chemistry as "electron-counting rules": they have been empirically applied to both organic and inorganic compounds[69] and can be derived from simple considerations on the combined symmetry properties of the nuclear frame and of the total electronic wave function.

Recently, the electron-counting rules for spherical[70-72] and ellipsoidal[73] jellium models of clusters (cf. section II.B.6) have been proposed as an explanation of the so called "magic numbers" of the valence electrons in clusters which exhibit large stability (cf. ref 7). The basic assumption of the jellium models is that the nearly free conduction electrons move in the potential of a smeared positive charge of atomic nuclei screened by core electrons. It is frequently argued that this model is particularly appropriate for alkali-metal clusters since the alkali metals are very soft and consequently the position of atomic cores is not fixed. Various further assumptions[4,74] are made about the effective potential seen by the conduction electrons (cf. section II.B.6).

The most simple and consequently the most appealing cluster form is a sphere, but for clusters with incomplete electron shells ellipsoidal geometries are often assumed. The similarities with the models of atoms and atomic nuclei are obvious. The possibilities of meaningfully defining the ellipsoidal models for very small clusters is limited. The frequent assumption[73] that Na_3 and Na_4 are prolate and Na_5, Na_6, and Na_7 are oblate spheroids is difficult to accept since all these clusters are planar (Na_3, Na_5, Na_6) or nearly planar (Na_6, Na_7).

In the effective single-particle Hamiltonian, the potential is either a fixed function (e.g. Woods–Saxon potential[75]) or it depends in a self-consistent way upon the electron density, e.g. it satisfies the Poisson equation. The fixed potential can, for example, have the form of the three-dimensional harmonic oscillator potential, or of the infinite spherical well potential. Very appealing are the potentials taken over from nuclear physics which represent some kind of transition between these two extreme cases. Their use stresses similarities between clusters and atomic nuclei. The involved numerical parameters give to these models some flexibility, mainly for the cluster shapes which deviate from the spherical geometry.

The sequence in which the one-electron functions are occupied depends, in the one-electron approximation, strongly on the number and positions of their nodal surfaces. The presence of nodal surfaces of a given one-electron function in the region of attractive potential reduces its contribution to the attractive potential energy and increases its contribution to the positive kinetic energy. The detailed sequence of the one-electron levels depends upon the form of the effective potential which acts on the electrons; however, some general rules nearly independent of the particular potential can be formulated. This occurs mainly if the cluster exhibits at least an approximate symmetry or high compactness. Evidently, the symmetry is a necessary condition for the existence of the nonaccidental degeneracies of the one-electron levels but it is not a strictly necessary condition for the formulation of approximate rules concerning the sequence of the levels.

Let us consider briefly, for the sake of illustration, three simple one-particle systems: the hydrogen atom, the three-dimensional isotropic harmonic oscillator, and a particle confined in a square well with infinitely high walls. In the H atom the sequence of atomic orbital energies depends only on the total number of nodal surfaces ($n - 1$), where n is the main quantum number. The principal quantum number on which the energy depends is $N = n - 1$. The sequence of one-electron energy levels for the isotropic three-dimensional harmonic oscillator depends only on the total order $m = m_x + m_y + m_z$ of the polynomial which describes the nodal surfaces. In this case, $N = 2(n - 1) - l$. The sequence of the levels associated with the square well depends on the total number of nodal spheres and of nodal planes as well. The nodal spheres are much more energetically unfavorable than the nodal planes. The differences in rules determining principal quantum numbers for the three systems can be understood if one considers the effective potential $V(r)$. In the case of the H atom, for instance, the dependence upon r is convex and diverges at $r = 0$. In the case of the harmonic oscillator the function $V(r)$ is concave.

The energy sequence of the H atomic orbitals is (1s), (2s,2p), (3s,3p,3d), (4s,4p,4d,4f), (5s,5p,5d,5f,5g) which can be considered as a sequence of degenerate subshells. The number of electrons in "closed shells" is n_s = 2, 10, 28, 60, etc. In the case of the isotropic harmonic oscillator the sequence of the shells is (1s), (2p), (3d,2s), (3p,4f), (5g,4d,3s), (6h,5f,4p) with n_s = 2, 8, 20, 40, 70, 112. The sequence of shells for the square-well model is (1s), (2p), (3d), (2s), (4f), (3p), (5g), (4d), (6h), (3s) with n_s = 2, 8, 18, 20, 34, 40, 58, 68, 90, 92, etc. The jellium-like effective potential must have properties intermediate between the square-well model and the isotropic harmonic oscillator model.[76]

The validity of the Woods–Saxon[75] potential or of the square-well potential for large clusters is documented by the experimental findings on abundances for very large Na,[77] Cs–O, Cs–SO_2,[78] Ag,[79] and Au[79] clusters which exhibit supershell structure.

From the above mentioned rules the correlation between the results obtained from the assumed spherical (jellium) potential and those obtained from a molecular potential can be understood at least for cluster sizes up to 40 in a straightforward manner due to the symmetry. Therefore the shell-closing and electron-counting rules and "magic numbers" for the spherical (or spheroidal) jellium model should be interpreted as equivalent to the more general rules for molecular systems, being simply translated into the language (and notation) of a particular physical model (cf. also ref 80).

Two severe limitations should nevertheless be emphasized. The whole argumentation is based on the dominant importance of the one-electron part of the Hamiltonian. In the case where electron correlation is very important, deviations from the electron counting

rules can be expected. Moreover, if the dimensionality of the system changes completely, different rules are valid. For example, the two- and three-dimensional symmetrical clusters exhibit electronic configurations fulfilling different "shell closing" regularities.

B. Concepts of Solid-State Theory and Mathematically Related Notions in Other Fields of Science

The common feature of the methods used in solid-state theory and especially in the theory of metals is the key role played by translation symmetry and its consequences. The reason for this is not only simplifications which make easier an appropriate treatment of large systems with many electrons, but also the success of very simple approaches like the free-electron and nearly free electron methods in explaining and estimating some fundamental properties of metals. Plane wave expansions and the Fourier transform are very appropriate and powerful tools. It is possible to show that plane waves represent solutions of the Hartree–Fock theory of free electron gas.

The electron waves can be scattered by atomic nuclei, or the waves representing the nearly free valence electrons in a metal are assumed to be scattered by the potential caused by the atomic cores. It is suggestive to divide the whole space of the metal into the regions close to the atomic nuclei and the remaining space in which the electrons are free. Different successful theoretical methods for metals are based on this model. The muffin tin type potential is very appealing since the spherical symmetry of the regions around the atomic sites models automatically at least the important local symmetry properties in the neighborhood of atomic cores or nuclei. Many properties are in any case qualitatively determined by the lattice symmetry which is clearly demonstrated by the interesting results obtained with the Kronig–Penney model (cf. ref 81).

The concept of scattering of electron waves is very attractive and useful since there is an analogy with the scattering of electromagnetic and electron waves in the X-ray and electron diffraction in real crystals, respectively.

The experience gained from the successful application of the methods such as Green's function and second quantization procedures in the solid-state and nuclear physics suggests their use in the field of elemental clusters. For example, assumptions about the spherical form of the cluster and about an appropriate spherical potential facilitates the use of procedures well established in solid-state theory.

1. One-Electron Approximation in Solid-State Theory

Some characteristic features of theories typical of the solid state will be outlined in this section in order to emphasize their mutual similarities and differences (cf., e.g., refs 81–83).

A plane wave of the form

$$\psi_{\mathbf{k}}(\mathbf{r},t) = Ae^{i(\mathbf{kr}-\mathbf{k}^2t/2m)} = Ae^{i(\mathbf{kr}-\epsilon_{\mathbf{k}}t)} \quad \text{(IIB1.1)}$$

and a wave packet

$$\psi = B\int g(\mathbf{k})e^{i(\mathbf{kr}-\mathbf{k}^2t/2m)}\,\mathrm{d}\mathbf{k} \quad \text{(IIB1.2)}$$

are the simple basic notions of the one-electron theory of metals and they often serve as starting points of more sophisticated methods. The plane wave $\psi_{\mathbf{k}}(\mathbf{r},t)$ is an eigenfunction of the momentum operator with the eigenvalue $\mathbf{k}$ and is the solution of the free-electron Schrödinger equation with the energy

$$\epsilon_k = k^2/2m \quad \text{(IIB1.3)}$$

The Bloch theorem states that the wave function has the form of plane waves modulated by the lattice period

$$\psi(\mathbf{r}) = e^{i\mathbf{kr}}u_{\mathbf{k}}(\mathbf{r})$$

with

$$u_{\mathbf{k}}(\mathbf{r}+I) = u_{\mathbf{k}}(\mathbf{r}) \quad \text{(IIB1.4)}$$

where $I = (m\mathbf{a} + n\mathbf{b} + p\mathbf{c})$ and $\mathbf{k} = 2\pi(l_1/M)\mathbf{a}' + (l_2/N)\mathbf{b}' + (l_3/P)\mathbf{c}')$. $\mathbf{a}$, $\mathbf{b}$, $\mathbf{c}$ and $\mathbf{a}'$, $\mathbf{b}'$, $\mathbf{c}'$ are the fundamental vectors of the lattice and of the reciprocal lattice, respectively. m, n, p, and l_1, l_2, l_3 are integers, and M, N, P are the integers in the Born–von Karman boundary conditions ($l_1 = 0,...,M-1$; $l_2 = 0,...,N-1$; $l_3 = 0,...,P-1$).

The analogous form of the free-electron wave functions and the one-electron functions in the periodic lattice is evident and leads to the concepts of effective mass and group velocity of the electron wave packet in the crystal lattice (Wannier function).

The basic idea of many solid-state theories is to use the Fourier transform of the Bloch periodic term $u(\mathbf{r})$ over the reciprocal lattice $\mathbf{g}$ (compare also with (IIA3.5)):

$$\psi_{\mathbf{k}} = e^{i\mathbf{kr}}u_{\mathbf{k}}(\mathbf{r}) = \sum_{\mathbf{g}}\nu(\mathbf{k}+\mathbf{g})\exp[i(\mathbf{k}+\mathbf{g})\mathbf{r}] \quad \text{(IIB1.5)}$$

with

$$\nu(\mathbf{k}+\mathbf{g}) = [1/2\pi]^3\int\psi_{\mathbf{k}}\exp[-i(\mathbf{k}+\mathbf{g})\mathbf{r}]\,\mathrm{d}\mathbf{r} \quad \text{(IIB1.6)}$$

The substitution of the expression IIB1.5 in the one-electron time-independent Schrödinger equation with the effective potential $\hat{W}$ yields for the energy E an infinite system of equations in the Fourier transforms:

$$[(\mathbf{k}+\mathbf{g})^2 - E + \langle\mathbf{k}+\mathbf{g}|\hat{W}|\mathbf{k}+\mathbf{g}\rangle]\nu(\mathbf{k}+\mathbf{g}) + \sum_{\mathbf{g}'\neq\mathbf{g}}\langle\mathbf{k}+\mathbf{g}|\hat{W}|\mathbf{k}+\mathbf{g}'\rangle\nu(\mathbf{k}+\mathbf{g}') = 0 \quad \text{(IIB1.7)}$$

The free-electron theory assumes $\hat{W} = 0$ and the eigenvalues are given by the equation:

$$E = (\mathbf{k}+\mathbf{g})^2 = K_0^2 \quad \text{(IIB1.8)}$$

In the nearly free electron theory a linear combination of plane waves belonging to the same irreducible representation is considered and the potential due to the atomic cores is assumed to be so small that perturbation theory can be employed.

The augmented plane-wave methods and the KKR technique (Korringa,[84] Kohn and Rostocker[85]) use the already mentioned idea of appropriate partitioning of the crystal space. The crystal space is modeled within the spherical muffin-tin regions with spherical potential around the atoms and within the interspaces with constant potential. The augmented plane wave is a plane wave in the interspaces among the spherical "atomic regions" and linear combination of products of spherical harmonics and radial functions in the "atomic regions". It is necessary to take care about the appropriate matching on the surfaces of the spheres. In the

KKR approaches the scattering of the plane waves in the interspaces among the atomic regions by the effective potential of the atomic sites is then investigated either with scattering matrix or the Green's function method. In this connection also the concept of pseudopotential is successfully applied. The projection on the complement of the one-electron functions describing the core states leads to various forms of pseudopotentials (cf. section II.A.1).

The tight binding method of LCAO approximation assumes that the one electron function has the form

$$\psi_{\mathbf{k}}(r) = N^{-1/2} \exp(-i\mathbf{kr}) \sum_{m,n,p,\chi} \exp[i\mathbf{k}(\mathbf{r} + \mathbf{R}_{mnp})]\phi_{\chi}(\mathbf{r} - \mathbf{R}_{mnp}) \quad \text{(IIB1.9)}$$

where $\phi_{\chi}(\mathbf{r} - \mathbf{R}_{mnp})$ is the basis function located in the point $\mathbf{R}_{mnp}$. The formal analogy with (IIB1.5) is obvious as well as the rough similarity of the LCAO-like basis functions and Wannier's orbitals.

The Hartree–Fock approximation is based on assumptions which are indetical in solid-state theory and in molecular physics. By using the formalism of the second quantization the very useful concept of holes in the conduction band can be introduced. The interaction among electrons and holes in metals and semiconductors as well as of excitations can be treated in a very convenient way. All these concepts of solid-state theory can be translated into the language of molecular physics without any difficulty.

The calculation of the exchange terms necessary in the Hartree–Fock treatment is difficult in problems of solid-state physics. For this reason, the estimate of the exchange energy term based on the free-electron calculations is introduced in the Hartree–Slater equations (compare section II.A.1). The Kohn–Sham theorem[31] guarantees that the observables in the ground state can, in principle, be determined from a functional of the electron density. Therefore, the evident computational advantages of the local electron density methods, which originated in solid-state theory, lead to their frequent application for the treatment of finite systems.

2. Green's Functions

Since the Green's function technique is common to many different approaches simple definitions of the Green's operator are given in this section. This can be helpful for the understanding of links among the important concepts applied in the cluster theory.

Green's Operators. The Green's operator $\hat{G}(E)$ associated with the operator $\hat{H}$ has the property (cf., e.g., refs 81,86–89):

$$(E\hat{I} - \hat{H})\hat{G}(E) = \hat{I} \quad \text{(IIB2.1)}$$

where $\hat{I}$ is the identity operator.

For the one-electron case, this definition can be written in the coordinate representation as

$$(E - \hat{H}(\mathbf{r}))G(\mathbf{r},\mathbf{r}':E) = \delta(\mathbf{r} - \mathbf{r}') \quad \text{(IIB2.2)}$$

where

$$G(\mathbf{r},\mathbf{r}':E) = \langle \mathbf{r}|\hat{G}(E)|\mathbf{r}'\rangle \quad \text{(IIB2.3)}$$

is the Green's function in the usual notation.

Since the operator $\hat{G}$ is a function of $\hat{H}$, its spectral representation has the form

$$\hat{G}(E) = \sum_j \frac{|E_j\rangle\langle E_j|}{(E - E_j)} \quad \text{(IIB2.4)}$$

where E_j are the eigenvalues of the Hamiltonian $\hat{H}$.

In the one-electron case, the corresponding coordinate representation is

$$G(\mathbf{r},\mathbf{r}':E) = \sum_j \langle \mathbf{r}|E_j\rangle\langle E_j|\mathbf{r}'\rangle(E - E_j)^{-1} = \sum_j \frac{\psi_j(\mathbf{r})\psi_j^*(\mathbf{r}')}{(E - E_j)} \quad \text{(IIB2.5)}$$

where $\psi_j(\mathbf{r}) = \langle \mathbf{r}|E_j\rangle$ are the eigenfunctions of the one-electron Schrödinger equation in the coordinate representation.

Of course, the singularities of the Green's function are again the eigenvalues of the operator $\hat{H}$. However, various methods can be developed by taking advantage of some useful properties of Green's operators or Green's functions, such as for example the connection between the Green's operator $\hat{G}_0$ of the Hamiltonian $\hat{H}_0$ and the Green's operator $\hat{G}$ of the perturbed Hamiltonian $\hat{H} = \hat{H}_0 + \hat{V}$. It is simple to prove the Dyson equation, which has the form

$$\hat{G} = \hat{G}_0 + \hat{G}_0\hat{V}\hat{G} = \hat{G}_0\sum_{n=0}^{\infty}(\hat{V}\hat{G}_0)^n = \hat{G}_0\hat{T}\hat{G}_0 \quad \text{(IIB2.6)}$$

where

$$\hat{T} = \hat{V}\sum_{n=-1}^{\infty}(\hat{G}_0\hat{V})^n \quad \text{(IIB2.7)}$$

The representation of $\hat{T}$ is the **T** matrix which is useful in scattering theory.

The infinite sum in the Dyson relation can be formally solved under the assumption that the perturbation $\hat{V}$ is small:

$$\hat{G} = \hat{G}_0/(\hat{I} - \hat{V}\hat{G}_0) = (\hat{I} - \hat{G}_0\hat{V})^{-1}\hat{G}_0 \quad \text{(IIB2.8)}$$

The possibility of summations in the Green's function method is very efficiently used in various approximate treatments which make it possible to carry out the process which has been formally outlined here. Evidently the operator $\hat{G}$ has the poles of the operator $(\hat{I} - \hat{G}_0\hat{V})^{-1}$ which can be also quite different from the poles of $\hat{G}_0$.

In the coordinate representation the Dyson equation takes the form of an integral equation

$$G(\mathbf{r},\mathbf{r}';E) = G_0(\mathbf{r},\mathbf{r}';E) + \int G_0(\mathbf{r},\mathbf{r}'';E)\, V(\mathbf{r}'')G(\mathbf{r}'',\mathbf{r}';E)\, d\mathbf{r}'' \quad \text{(IIB2.9)}$$

Another useful property of the Green's operator is that the eigenket $|E_j\rangle$ of the Hamiltonian $\hat{H}$ can be expressed in terms of the eigenkets $|E_n^0\rangle$ of the Hamiltonian $\hat{H}_0$:

$$|E_j\rangle = |E_j^0\rangle\delta(E_j;E_j^0) + \hat{G}_0\hat{V}|E_j\rangle \quad \text{(IIB2.10)}$$

where the first term in the equation must be considered only if the eigenvalues of $\hat{H}$ and $\hat{H}_0$ coincide. The sum of the infinite series gives for $\delta(E_j;E_j^0) = 0$ the following formal result:

$$|E_j\rangle = \hat{G}_0\hat{T}|E_j^0\rangle = \hat{G}_0\hat{V}(\hat{I} - \hat{G}_0\hat{V})^{-1}|E_j^0\rangle \quad \text{(IIB2.11)}$$

According to (IIB2.9) the coordinate representation of the free particle Green's function is simply defined as

$$G_0(\mathbf{r},\mathbf{r}';E) = (1/N)\int \frac{\exp[ik(\mathbf{r}-\mathbf{r}')]}{(E-k^2+i\delta)}\,d\mathbf{k} \equiv (i/2K_0)[e^{-iK_0(\mathbf{r}-\mathbf{r}')} - e^{+iK_0(\mathbf{r}-\mathbf{r}')}] = G_0(\mathbf{r}-\mathbf{r}';E) \quad \text{(IIB2.12)}$$

where the small imaginary quantity $i\delta$ must be introduced to make the integration meaningful. $\pm K_0$ are the poles ($E = K_0^2$). The advantage of treating the perturbation of free-electron systems using the Green's method is a consequence of the simple form of the Green's function which can be utilized for the treatment of the scattering of the plane waves. For example, the scattering of a one-dimensional plane wave $(2\pi)^{-1/2}\exp(iK_0x)$ produced by the perturbation $V(x)$ in the interval $x_1 < x < x_2$ results in the one-electron wave function

$$|\psi(x)\rangle = (1/\sqrt{2\pi})e^{iK_0x} + (1/2iK_0)e^{\pm iK_0x}\int_{x_1}^{x_2} e^{\mp iK_0x'}V(x')|\psi(x')\rangle\,dx' \quad \text{(IIB2.13)}$$

where the upper signs are valid for $x > x_2$ (transmitted wave) and the lower signs for $x < x_1$ (reflected wave).

The use of the Green's functions (GF) allows a direct computation of properties due to the perturbation. In the more conventional methods, the effect of any perturbation can be investigated only if detailed information about the whole manifold of the eigenstates of the unperturbed system is available. The equations for the Green's functions in the simple cases can be directly found and consequently the Green's functions method is a useful alternative to the customary approach to the calculation of the response of a quantum mechanical system to a perturbation.

Double-Time Green's Functions. Since time-dependent processes are of special interest in the cluster theory it is appropriate to introduce a generalization of the Green's functions. By using the Heisenberg picture for the operator $\hat{A}(t)$ and for the wave function $|\psi(t)\rangle$

$$\hat{A}(t) = \exp(i\hat{H}t)\hat{A}\exp(-i\hat{H}t)$$

$$|0\rangle = e^{i\hat{H}t}|\psi(t)\rangle \quad \text{(IIB2.14)}$$

the definition of the double-time Green's function for the reference state $|0\rangle$ is (cf., e.g., refs 46 and 88)

$$\langle\langle\hat{A}(t);\hat{B}(0)\rangle\rangle = i\{\mp\theta(t)\langle 0|\hat{A}(t)\hat{B}(0)|0\rangle + \theta(-t)\langle 0|\hat{B}(0)\hat{A}(t)|0\rangle\} = i\sum_n\{\mp\theta(t)\langle 0|\hat{A}|n\rangle\langle n|\hat{B}|0\rangle e^{it(E_0-E_n)} + \theta(-t)\langle 0|\hat{B}|n\rangle\langle n|\hat{A}|0\rangle e^{it(E_n-E_0)}\} \quad \text{(IIB2.15)}$$

where $\hat{A}(t)$ and $\hat{B}(t)$ are operators in the Heisenberg picture and $\theta(t)$ is the Heaviside step-function:

$$\theta(t) = 1 \text{ if } t > 0 \qquad \theta(t) = 0 \text{ if } t < 0 \quad \text{(IIB2.16)}$$

The plus and the minus sign in (IIB2.15) is valid for the operators which preserve the particles number and for those which do not, respectively.

The Fourier transform of the Green function is defined as

$$\langle\langle\hat{A};\hat{B}\rangle\rangle_\omega = \lim_{\eta\to 0}\sum_n\left\{\pm\frac{\langle 0|\hat{A}|n\rangle\langle n|\hat{B}|0\rangle}{\omega+(E_0-E_n)+i\eta} + \frac{\langle 0|\hat{B}|n\rangle\langle n|\hat{A}|0\rangle}{\omega-(E_0-E_n)-i\eta}\right\} \quad \text{(IIB2.17)}$$

The physical interpretation of the double-time Green's function is in principle very simple and pictorial. The double-time Green's function is the probability amplitude that the measurement of the observable $\hat{A}$ yields the result $\langle\psi(t)|\hat{A}|\psi(t)\rangle$ in the state $|\psi(t)\rangle$ at the time t after the measurement of the observable $\hat{B}$ in the state $|0\rangle$ at the time 0, and vice versa. No other perturbation should occur in the time interval $(0, t)$.

If both operators $\hat{A}$ and $\hat{B}$ are set equal to the electric dipole moment operator, then the real part of $\langle\langle\hat{A};\hat{B}\rangle\rangle_\omega$ takes the usual form of the frequency-dependent polarizability

$$\langle\langle\mathbf{r};\mathbf{r}\rangle\rangle_\omega = 2\lim_{\eta\to 0}\sum_n \omega_{n0}|\mu_{n0}|^2/(\omega_{n0}^2-\omega^2+2i\omega\eta) \quad \text{(IIB2.18)}$$

where

$$\mu_{n0} = \langle n|\mathbf{r}|0\rangle \qquad \omega_{n0} = E_n - E_0 \quad \text{(IIB2.19)}$$

For the mean polarizability defined as

$$\bar{\alpha}(\omega) = (1/3)\{\alpha_{xx}(\omega)+\alpha_{yy}(\omega)+\alpha_{zz}(\omega)\} \quad \text{(IIB2.20)}$$

the following relation is valid:

$$\bar{\alpha}(\omega) = (2/3)\sum_n\frac{\omega_{n0}}{\omega_{n0}^2-\omega^2}|\mu_{n0}|^2 = \sum_n f_{n0}/(\omega_{n0}^2-\omega^2) \quad \text{(IIB2.21)}$$

where the oscillator strength f_{n0} is related with the transition dipole moment μ_{no} through the equation

$$f_{n0} = (2/3)\omega_{n0}|\mu_{n0}|^2 \quad \text{(IIB2.22)}$$

The expression for the mean static polarizability reads

$$\bar{\alpha}(0) = \sum_n f_{n0}/\omega_{n0}^2 \quad \text{(IIB2.23)}$$

If a single transition ω_{j0} is of predominant importance, the expressions for static and dynamic polarizabilities take on a very simple form due to the Kuhn–Thomas rule:

$$\bar{\alpha}(0) = N/\omega_{j0}^2 \qquad \bar{\alpha}(\omega) = N/(\omega_{j0}^2-\omega^2) \quad \text{(IIB2.24)}$$

where N is the number of electrons.

In this manner, the connection between the Green's operators and the physical observables which are useful in the theory of spectroscopical properties of clusters has been established. Further connections with the time-dependent local density approximation (TDLDA), random-phase approximation (RPA) (see sections II.B.4 and II.B.5) and plasmon theory are outlined in the Appendixes.

3. Correlation Effects in Solid-State Theory

Although the forces acting in molecules and solids are of the same Coulombic nature, the methods useful and feasible for the treatment of electron correlation are different in these two theoretical fields. Generally speaking, the basic difference in solid-state theory originates from the necessity to describe the interaction of many electrons acting partly over large distances. This kind of difficulty is already present in the quantum theoretical description of large molecular systems (particularly of those which are not very stable) and is known as size correlation defect (or size-inconsistency) (cf. section II.A.2).

The large difficulties with the correlation problem in

solid-state theory are avoided mainly with the methods similar to those which have been successfully applied also in the quantum field theory and in elementary particle physics. These approaches use the Green's functions, propagators, and "vacuum amplitudes"[86] of the investigated systems. This is the reason why some aspects of the Green's function theory have been outlined in sections II.B.2 and Appendixes.

Since the Green's functions of various kinds (like single-particle (G_1), two-particle (G_2) propagators, etc.) give, in principle, full information about the studied system, it is desirable to work out their efficient implementation for practical calculation.

One possibility is to solve a chain of the coupled nonlinear differential equations involving the "hierarchy" of G_k's.[46,86,89] Usually some approximations for G_2 are assumed and in this way the system of equations is terminated. This method is also used in quantum chemistry under the name "coupled-cluster method". The other method is to expand the propagator (or "vacuum amplitude"[86]) in an infinite perturbation series and to carry out some kind of partial summation to infinite order. The use of Feynman's diagrams makes possible a bookkeeping and a systematic selection of such contributions which allows a "selective" summation of the perturbation series due to some common repetitive building elements of the diagrams. This kind of methods commonly used for the investigation of electron correlation in molecular systems, are known in quantum chemistry as "many-body perturbtaion theory".

4. Time-Dependent Properties, Random-Phase Approximation, and Tamm–Dancoff Approximation

The response of an electronic system to a time-dependent perturbation (e.g. the interaction with electromagnetic field) can be described in two different conceptual frameworks. The perturbation can be considered as causing jumps to the excited states of the unperturbed system or as the time development of the perturbed system.

Since the spectroscopic properties of clusters and their comparison with the absorption behavior of solid-state systems are of present interest, several examples of the treatment of related subjects will be briefly sketched here, in order to illustrate useful analogies which are based on interactions among single excitations.

Let us mention two cases which are at first sight not connected with cluster physics but nevertheless show formal similarities to the theory used in the spectroscopy of clusters. There are localized and delocalized excitons.

In the theory of Wannier excitons the wave function $|\phi\rangle$ of the excited state is assumed to have a form of a linear combination of the monoexcitations from a Bloch wave of the valence band to a Bloch wave of the conduction band:[81]

$$|\phi\rangle = \sum_{k_1 k_2} c_{k_2 k_1} \hat{E}_{k_2 k_1} |0\rangle \qquad \text{(IIB4.1)}$$

where the Bloch wave k_1 belongs to the valence band and Bloch wave k_2 to the conduction band and $|0\rangle \equiv |\phi_0\rangle$ is the ket for the fully occupied valence band. Note that many-electron excitations are excluded. Therefore, the assumption that one-electron functions have the form of Bloch waves is essential for the theory of the quasiparticles known as "Wannier's delocalized excitons".

If the single electron excitation is described again as a creation of a hole in the valence band and a particle in the conduction band, but both the particle and the hole have been described by relatively well localized Wannier functions, the localized Frenkel's exciton is created. The wave function of the excited state has now the form of a linear combination of the monoexcitations from Wannier localized functions of the valence band to Wannier functions of the conduction band.

Let us emphasize that the theory of both Wannier's and Frenkel's exciton[81] models can be characterized within the Hartree–Fock approximation as monoexcitations of quasiparticles. If the one-electron states are delocalized, it is more appropriate to consider a linear combination of excitations between pairs of Bloch functions. Since the definition of the Wannier orbitals is based on the inverse Fourier transform, a good description of the valence band with Wannier orbitals is possible only if the valence band is fully occupied. Therefore, Frenkel's excitons describe better the excitation process for insulators or semiconductors in which the one-electron states can be localized.

A very simple wave function of an excited state of an agglomerate of atomic nuclei and electrons is given in the form of a linear combination of Slater determinants which represent monoexcitations ϕ_i^p with respect to the single Slater determinant ($\phi_0 \equiv |0\rangle$) describing the HF ground state of a closed-shell electronic system. An advantage of this form of wave function is that the matrix elements of the Hamiltonian $\hat{H}$ between the ϕ_0 and ϕ_i^p are equal to zero due to the Brillouin theorem. Evidently, within this approximation transition energies can be determined only qualitatively, since the ground state is calculated in the one-electron approximation only and the wave functions of excited states do not contain double and higher order excitations with respect to ϕ_0. Nevertheless, this very simple single CI (SCI) approach combined with the Pariser–Parr–Pople semiempirical π-electron theory yielded in the early days of quantum chemistry satisfactory results for some characteristic properties of the spectra of aromatic hydrocarbons.[90]

The Tamm–Dancoff approach (TDA), which is commonly used in nuclear physics, is formally completely analogous to the SCI method. In this approximation the wave function for an excited singlet state has the form

$$|\psi\rangle = \sum_{pj} Y_{pj} \hat{\mathcal{E}}_{pj} |0\rangle = \hat{R}|0\rangle \qquad \text{(IIB4.2)}$$

with Lie algebra generators (cf. (IIA2.4))

$$\hat{\mathcal{E}}_{pj} = \hat{a}^\dagger_{p\alpha}\hat{a}_{j\alpha} + \hat{a}^\dagger_{p\beta}\hat{a}_{j\beta} \qquad \text{(IIB4.3)}$$

where j and p label the occupied and unoccupied spatial orbitals in the ground state $|0\rangle$.

The operator

$$\hat{R} = \sum_{pj} Y_{pj} \hat{\mathcal{E}}_{pj} \qquad \text{(IIB4.4)}$$

includes only the excitations from the "Fermi sea" of occupied orbitals j in $|0\rangle$ into the manifold of empty orbitals p (particle-hole excitations).

The secular problem

$$\langle 0|\hat{\mathcal{E}}_{kq}\hat{H}\hat{\mathcal{E}}_{pj}|0\rangle - \delta_{jk}\delta_{pq}E = 0 \qquad \text{(IIB4.5)}$$

is the condition for solving the system of equations

$$\sum_{pj} Y_{pj}[\langle 0|\hat{\mathcal{E}}_{kq}\hat{H}\hat{\mathcal{E}}_{pj}|0\rangle - E\delta_{jk}\delta_{pq}] = 0 \quad \text{(IIB4.6)}$$

The random-phase approximation (RPA) can be considered as a generalization of the TDA. One of the ways to obtain the random-phase equations is to consider the time dependent Hartree–Fock approach. Another possibility is the derivation based on the equation of motion method.[91,92] In the former approach the time-dependent wave function $|\psi(t)\rangle$ results from the unitary transformation of a Slater determinant $|0\rangle$:

$$|\psi(t)\rangle = e^{i\hat{\beta}(t)}|0\rangle \quad \text{(IIB4.7)}$$

with the Hermitian operator $\hat{\beta}(t)$ which considers monoexcitations only:

$$\hat{\beta}(t) = \sum_{s\neq r}\beta_{s,r}(t)\hat{\mathcal{E}}_{sr} = \sum_{s\neq r}\beta^*_{s,r}(t)\hat{\mathcal{E}}_{rs} = \hat{\beta}^\dagger(t) \quad \text{(IIB4.8)}$$

For a small perturbation the relation

$$|\psi(t)\rangle = |0\rangle + i\sum_{pj}\beta_{pj}(t)\hat{\mathcal{E}}_{pj}|0\rangle \quad \text{(IIB4.9)}$$

is approximately valid. The linear dependence of the function $|\psi(t)\rangle$ upon single excitations shows its connection with a TDA wave function.

If the Ehrenfest theorem holds for an arbitrary time-independent operator $\hat{A}$

$$(\partial/\partial t)\langle\psi(t)|\hat{A}|\psi(t)\rangle = i\langle\psi(t)|[\hat{H},\hat{A}]|\psi(t)\rangle \quad \text{(IIB4.10)}$$

then for the wave function of type (IIB4.9) the equation assumes the form

$$i\sum_{pj}[\dot{\beta}_{pj}\langle 0|\hat{A}\hat{\mathcal{E}}_{pj}|0\rangle - \dot{\beta}^*_{pj}\langle 0|\hat{\mathcal{E}}_{jp}\hat{A}|0\rangle] =$$
$$i^2\sum_{pj}[\beta_{pj}\langle 0|[\hat{H},\hat{A}]\hat{\mathcal{E}}_{pj}|0\rangle - \beta^*_{pj}\langle 0|\hat{\mathcal{E}}_{jp}[\hat{H},\hat{A}]|0\rangle] \quad \text{(IIB4.11)}$$

Since $\hat{A}$ can be an arbitrary one-electron spin-independent operator:

$$\hat{A} = \sum_j \hat{a}(j) = \sum_{s,r}\hat{\mathcal{E}}_{s,r}\langle s|\hat{a}(1)|r\rangle \quad \text{(IIB4.12)}$$

equation IIB4.11 must be valid for $\hat{\mathcal{E}}_{kq}$ as well as for $\hat{\mathcal{E}}_{qk}$ and the following system of equations is achieved:

$$i\dot{\beta}_{qk} =$$
$$\sum_{pj}\{\beta_{pj}(\langle k\rightarrow q|\hat{H}|j\rightarrow p\rangle - \delta_{jk}\delta_{pq}E_0) - \beta^*_{pj}\langle\overset{j\rightarrow p}{k\rightarrow q}|\hat{H}|0\rangle\} - i\dot{\beta}^*_{qk}$$
$$= \sum_{pj}\{\beta^*_{pj}(\langle j\rightarrow p|\hat{H}|k\rightarrow q\rangle - \delta_{jk}\delta_{pq}E_0) - \beta_{pj}\langle 0|\hat{H}|\overset{j\rightarrow p}{k\rightarrow q}\rangle\} \quad \text{(IIB4.13)}$$

with

$$E_0 = \langle 0|\hat{H}|0\rangle \qquad |j\rightarrow p\rangle = 1/\sqrt{2}\hat{\mathcal{E}}_{pj}|0\rangle$$
$$|\overset{j\rightarrow p}{k\rightarrow q}\rangle = (1/2)\hat{\mathcal{E}}_{pj}\hat{\mathcal{E}}_{qk}|0\rangle \quad \text{(IIB4.14)}$$

The Fourier transforms $\beta_{pj}(\omega) = Y_{pj}$ and $\beta^*_{pj}(\omega) = Z_{pj}$ satisfy the RPA system of equations

$$\sum_{pj}\{[\langle k\rightarrow q|\hat{H}|j\rightarrow p\rangle - \delta_{jk}\delta_{pq}(E_0+\omega)]Y_{pj} - \langle\overset{j\rightarrow p}{k\rightarrow q}|\hat{H}|0\rangle Z_{pj}\} = 0$$

and

$$\sum_{pj}\{-\langle 0|\hat{H}|\overset{j\rightarrow p}{k\rightarrow q}\rangle\ Y_{pj} + [\langle j\rightarrow p|\hat{H}|k\rightarrow q\rangle - \delta_{jk}\delta_{pq}(E_0-\omega)]Z_{pj}\} = 0 \quad \text{(IIB4.15)}$$

with the secular condition for ω

$$\begin{vmatrix}(\mathbf{A}-\omega\mathbf{I}) & \mathbf{B}\\ \mathbf{B}^\dagger & (\mathbf{A}+\omega\mathbf{I})\end{vmatrix} = 0 \quad \text{(IIB4.16)}$$

where $\mathbf{I}$ is identity matrix and

$$\mathbf{A} = [\langle k\rightarrow q|\hat{H}|j\rightarrow p\rangle - \delta_{jk}\delta_{pq}E_0] =$$
$$[(\epsilon_p-\epsilon_j)\ \delta_{jk}\delta_{pq} + 2[jq|pk] - [jq|kp]]$$

and

$$\mathbf{B} = -[\langle\overset{j\rightarrow p}{k\rightarrow q}|\hat{H}|0\rangle] = [-2[jk|pq] + [jk|qp]] \quad \text{(IIB4.17)}$$

The labels of the rows and columns in the determinant (IIB4.16) are the monoexcitation $j\rightarrow p$ and $k\rightarrow q$, respectively. If Z_{pj} is set equal to zero the TDA type of equations results. The monoexcitations $j\rightarrow p$ and $p\rightarrow j$ are called in the RPA method forward and backward transitions. The calculated weights of the forward monoexcitations are usually larger than those of backward transitions. The roots of (IIB4.16) yield frequencies or transition energies.

The connection between the TDA and RPA approaches is even more evident if the system of equations IIB4.15 is derived from the Ehrenfest theorem for three quantities: the operators $\hat{\mathcal{E}}_{lk}$, the ground state $|E_0,t\rangle = \exp(-iE_0t)|0\rangle$, and the excited state $|E,t\rangle = \exp(-iEt)\hat{W}|0\rangle$ with

$$\hat{W} = \sum_{sr}X_{sr}\hat{\mathcal{E}}_{sr} \quad \text{(IIB4.18)}$$

where l, k, r, and s are labels of arbitrary orbitals. The Ehrenfest theorem yields

$$i\frac{\partial}{\partial t}\langle E_0,t|\hat{\mathcal{E}}_{lk}|E,t\rangle = (E_0-E)e^{i(E_0-E)t}\langle 0|\hat{\mathcal{E}}_{lk}\hat{W}|0\rangle =$$
$$e^{i(E_0-E)t}\langle 0|\ [\hat{\mathcal{E}}_{lk},\hat{H}]\hat{W}|0\rangle \quad \text{(IIB4.19)}$$

or

$$\sum_{sr}\{(E_0-E)\ \langle 0|\hat{\mathcal{E}}_{lk}\hat{\mathcal{E}}_{sr}|0\rangle + \langle 0|\hat{\mathcal{E}}_{sr}\hat{H}\hat{\mathcal{E}}_{lk}|0\rangle -$$
$$\langle 0|\hat{H}\hat{\mathcal{E}}_{lk}\hat{\mathcal{E}}_{sr}|0\rangle\}X_{sr} = 0$$

The simple derivation of the RPA (TDHF) equations reveals the basic assumptions from which the RPA theory starts: the time variation of $|\psi(t)\rangle$ allows only for the monoexcitations from the Slater determinant $|0\rangle$. This variation should be also quite small to justify the approximations introduced in the general expression for $|\psi(t)\rangle$ which is linearly time dependent on Lie algebra generators (cf. (IIB4.9)). The relations IIB4.16 give the frequencies $\omega = E - E_0$ of the free oscillations which in general are not too far from the excitation energies given by the Tamm–Dancoff approximate method. The interaction among the individual particle-hole excitations can in principle yield some frequencies which differ appreciably from the individual particle-hole excitations. The presence of matrix elements between the ground state $|0\rangle$ and the doubly excited configurations in (IIB4.15) and (IIB4.16) besides the exclusive consideration of monoexcitations in the definition IIB4.9 of the state $|\psi(t)\rangle$ shows that the interaction between ground state $|0\rangle$ and doubly excited configurations is partly taken into account in the RPA. The energies of doubly excited configurations do not figure in the RPA equations at all. The oscillator strengths of such combined excitations can differ from those calculated with the Tamm–Dancoff approach since the interferences due to the signs of individual contributions to the wave functions of the excited state

can influence the results very drastically. Evidently, only the monoexcitations belonging to one irreducible representation of the symmetry group of the investigated system can be involved in the TDA or RPA equations.

5. Time-Dependent Local Density Approximation

The change of the Fourier component of the electron density in the coordinate representation $\rho(\mathbf{r},\omega)$ due to external perturbation Hamiltonian

$$\hat{V} = \int \rho(\mathbf{r},t)\phi(\mathbf{r},\omega)e^{-i\omega t}\,d\mathbf{r} \qquad \text{(IIB5.1)}$$

can be written with the help of the susceptibility $\chi(\mathbf{r},\mathbf{r}';\omega)$ as

$$\delta\rho(\mathbf{r},\omega) = \int \chi(\mathbf{r},\mathbf{r}';\omega)\phi(\mathbf{r}',\omega)\,d\mathbf{r}' \qquad \text{(IIB5.2)}$$

The spectral representation of the susceptibility connected with the Green's function is

$$\chi(\mathbf{r},\mathbf{r}';\omega) = \sum_n \left\{ \frac{\langle 0|\hat{\rho}(\mathbf{r})|n\rangle\langle n|\hat{\rho}(\mathbf{r}')|0\rangle}{\omega - (E_n - E_0) + i\eta} - \frac{\langle 0|\hat{\rho}(\mathbf{r}')|n\rangle\langle n|\hat{\rho}(\mathbf{r})|0\rangle}{\omega + (E_n - E_0) + i\eta} \right\} \qquad \text{(IIB5.3)}$$

where $|n\rangle$ and E_n are the exact eigenstates and energies of the unperturbed system (cf. (IIB2.17) and (A23)).

The frequency-dependent polarizability in the z direction is (cf. (IIB2.18))

$$\alpha_{zz}(\omega) = -\int z\chi(\mathbf{r},\mathbf{r}';\omega)z'\,d\mathbf{r}\,d\mathbf{r}' = 2\sum_n \frac{|\mu_{0n}|^2(E_n - E_0)}{(E_n - E_0)^2 - (\omega + i\eta)^2} \qquad \text{(IIB5.4)}$$

The usually applied procedure approximates the change of the electron density by using simple assumptions for the susceptibility (cf. refs 93 and 94)

$$\delta\rho(\mathbf{r},\omega) = \int \chi_0(\mathbf{r},\mathbf{r}';\omega)\,V(\mathbf{r}',\omega)\,d\mathbf{r}' \qquad \text{(IIB5.5)}$$

where χ_0 is taken, for instance, from some one-electron approximation such as local density procedure (LDA) (cf. Eq. (A20))

$$\chi_0(\mathbf{r},\mathbf{r}',\omega) = \sum_{i,j} \frac{(n_i - n_j)}{\omega - (\epsilon_j - \epsilon_i) + i\eta} \varphi_i^*(\mathbf{r})\varphi_j(\mathbf{r})\varphi_j^*(\mathbf{r}')\varphi_i(\mathbf{r}') = \sum_{i(\text{occ})} \{\varphi_i^*(\mathbf{r})\varphi_i(\mathbf{r}')G_0(\mathbf{r},\mathbf{r}';\epsilon_i + \omega) + \varphi_i(\mathbf{r})\varphi_i^*(\mathbf{r}')G_0^*(\mathbf{r},\mathbf{r}';\epsilon_i - \omega)\} \qquad \text{(IIB5.6)}$$

The Green's functions are known for simple cases such as a jellium sphere[94] and can be used explicitly in the integral on the right-hand side of (IIB5.6).

The Coulombic potential due to the induced changes in the charge distribution of electrons V_c as well as the induced exchange–correlation potential V_{ex} can be added to the external perturbation potential V. The correction V_{ex} is of course specific for the LDA method. This approach, used for example by Zangwill and Soven[95] and Puska et al.,[93] has been applied by Ekardt[94,96,97] for the calculation of the photoabsorption cross section

$$\sigma(\omega) = 4\pi(\omega/c)\ \text{Im}\ \alpha(\omega) \qquad \text{(IIB5.7)}$$

for the spheric and spheroidal jellium type models of the alkali-metal clusters.

6. Jellium Model

The jellium model mentioned already in the section II.A.4 in connection with the "magic numbers" is used also in cluster physics for the investigation of the response of the cluster to both, time-independent and time-dependent perturbations. Since the assumptions introduced in the definition of the effective potential can have considerable effect on the theoretical prediction of cluster properties such as static and dynamic polarizabilities, transition energies, and intensities of absorption, it seems appropriate to recall the forms of the jellium potential frequently used in literature.

The spherical, spheroidal, and ellipsoidal geometries assumed for clusters substantially facilitate the calculations as well as qualitative considerations.[71,7]

A potential of the form

$$U(\mathbf{r}) = -[U_0/\exp[(\mathbf{r} - \mathbf{r}_0)/\epsilon] + 1] \qquad \text{(IIB6.1)}$$

where

$$\mathbf{r}_0 = r_s n^{1/3} = (3/4\pi)[\rho_0 n]^{1/3} \qquad \text{(IIB6.2)}$$

with the electron density ρ_0 and number of atoms n has been used by Knight et al. (cf. ref 70). Clemenger[73] applies the Nilsson potential[98] under assumption of the ellipsoidal form of the system. Various modifications of the effective potential have been introduced, e.g. locating centers of simple pseudopotentials in the supposed positions of atoms.

Other kinds of effective one-electron potentials are introduced in the framework of density functional procedures (cf. refs 72, 99, and 100). In the local approximation of the Kohn–Sham density functional method (LDA)[31] the following system of equations is solved self-consistently (cf. (IIA1.20)):

$$\rho(\mathbf{r}) = \sum_i |\varphi_i(\mathbf{r})|^2$$

$$-\frac{1}{2}\nabla^2\varphi_i(\mathbf{r}) + V_{\text{eff}}(\mathbf{r})\,\varphi_i(\mathbf{r}) = \epsilon_i\varphi_i(\mathbf{r})$$

$$V_{\text{eff}} = -4\pi(\rho(\mathbf{r}) - \rho_0\theta(R - r)) + \mu_{xc}(n\mathbf{r}) \qquad \text{(IIB6.3)}$$

where $\theta(R - r)$ is a step function and cluster radius R depends upon n and ρ_0 (cf. (IIB6.2))

$$R^3 = (3/4\pi)n\rho_0 \qquad \text{(IIB6.4)}$$

The effective potential V_{eff} is self-consistent in the framework of the model and simplifications introduced. Also these approaches can be combined with a simple pseudopotential V_c, e.g. of the form[101]

$$V_c = 0 \qquad r > r_c$$

$$V_c = -Z/r \qquad r < r_c \qquad \text{(IIB6.5)}$$

where Z is the valence of the atom and r is the distance from the center of the pseudopotential.

The rearrangement[102] of the terms in the expression for the energy in the density functional method (IIA1.19) is the basis of calculations of the cluster structures with the Madelung energy combined with an appropriate pseudopotential assumptions (see refs 103 and 104).

The use of the jellium model for the alkali-metal clusters is usually justified by the large softness of the alkali-metal agglomerates. It is often argued that the

positions of atoms in clusters are anyway not sure because the Born–Oppenheimer energy minima are quite flat. In our opinion the studies using the jellium model can describe some cluster properties quite well, mainly if they depend upon the completely general rules (like symmetry, counting rules, etc.) so that the assumption of the jellium potential is not the determining factor. Nevertheless, changes in the cluster topology can sometimes have pronounced consequences for their electronic structure, and therefore more sophisticated description of the complicated cluster structure is essential for some properties.

7. Plasmons

The free oscillations of the electron gas in metals which cannot be described in terms of single-electron excitations are called plasmons in analogy to the oscillations in a plasma composed of positive and negative charges. If a more or less uniform distribution of the positive charge in the simple jellium model of metals is accepted the deviation from charge neutrality acts as the restoring force and can cause free oscillations of the resulting effective charge. In the jellium model of a finite metallic body some of these oscillations are modified, of course, by the presence of an additional restoring force due to the interaction between the positive jellium charge cloud in the metal and the neutral region of the vacuum. The additional spilling of electronic charge causes a further restoring force, and different frequencies of the surface plasmon result.

Since the classical theory of electronic charge oscillations is quite widely used in the theory of cluster spectroscopy it is useful to review shortly the classical theory of oscillations in a uniform electron gas. In this derivation we do not use the atomic units in order to show clearly the dimensions of the quantities involved. The equilibrium electron charge density ρ_0 is compensated by the positive background.

The deviation from the equilibrium electron density (cf. refs 89 and 105)

$$\delta\rho(\mathbf{r},t) = \rho_0 - \rho(\mathbf{r},t) \qquad \text{(IIB7.1)}$$

gives rise to the electric field $\mathbf{E}$ satisfying Poisson's equation:

$$\operatorname{div} \mathbf{E}(r,t) = -e\delta\rho(\mathbf{r},t) \qquad \text{(IIB7.2)}$$

The time-derivative of the linearized equation of continuity

$$\frac{\partial\delta\rho}{\partial t} + \rho_0 \operatorname{grad} \mathbf{v} = 0 \qquad \text{(IIB7.3)}$$

where $\mathbf{v}$ is the velocity of the electron, can be combined with Newton's second law:

$$m\rho_0\frac{\partial \mathbf{v}}{\partial t} = -e\rho_0 E \qquad \text{(IIB7.4)}$$

and the equation for harmonic oscillations of the perturbed charge density follows

$$\frac{\partial^2 \delta\rho(\mathbf{r},t)}{\partial t^2} = -\omega_p^2\delta\rho(\mathbf{r},t) \qquad \text{(IIB7.5)}$$

The plasma frequency ω_p depends only on the average electron density ρ_0 and universal constants

$$\omega_p = \sqrt{\frac{e^2\rho_0}{m}} \qquad \text{(IIB7.6)}$$

or in atomic units

$$\omega_p = \sqrt{\rho_0} \qquad \text{(IIB7.7)}$$

A more realistic model of motion of an electron in a metal in the periodic electric field

$$E_x = E_0 e^{i\omega t} \qquad \text{(IIB7.8)}$$

takes into account the restoring force $\omega_0^2 x_j$ and the damping $\gamma\dot{x}_j$. The equation of the motion for the j-th electron reads

$$-eE_0e^{i\omega t} = m(\ddot{x}_j + \gamma\dot{x}_j + \omega_0^2 x_j) \qquad \text{(IIB7.9)}$$

If all electron coordinates x_j oscillate with the frequency ω the polarizability, defined as

$$\alpha_{xx} = \rho_0 e\sum_j x_j/E_x \qquad \text{(IIB7.10)}$$

is equal to

$$\alpha_{xx}(\omega) = \omega_p^2/(\omega_0^2 - \omega^2 + i\gamma\omega) \qquad \text{(IIB7.11)}$$

where ω_0 can be expressed with the help of the static polarizability $\alpha_{xx}(0)$ and the plasma frequency ω_p (cf. definition IIB7.6) as

$$\omega_0^2 = \frac{\omega_p^2}{\alpha_{xx}(0)} \qquad \text{(IIB7.12)}$$

The expression for the imaginary part of the dynamic polarizability, which is the interesting quantity for the light absorption, is

$$\operatorname{Im}(\alpha_{xx}(\omega)) = \frac{\gamma\omega\omega_p^2}{(\omega_p^2/\alpha_{xx}(0) - \omega^2)^2 + \gamma^2\omega^2} \qquad \text{(IIB7.13)}$$

This formula is very often applied in the spectroscopy of clusters in connection with photoabsorption cross sections and will be used in section IV.D.2. It is useful to notice that the "plasma" frequency ω_p depends only upon the electron density, and consequently it yields the right order of magnitude of the wavelengths of the absorbed light.

The photoabsorption cross section is given by the relation

$$\sigma \approx \omega\operatorname{Im}(\alpha_{xx}(\omega)) = \omega_p^2\frac{\omega^2\gamma}{(\omega^2 - \omega_0^2)^2 + \omega^2\gamma^2} \qquad \text{(IIB7.14)}$$

After these well known facts have been reviewed, several consequences resulting from the general quantum theory of the response for an arbitrary system of electrons only weakly interacting with an external field will be pointed out, in order to avoid confusion of notions which sometimes occurs in the cluster theory.

In the usual quantum theory of plasmons the electron density oscillations are described by means of the time-dependent operator $\hat{\rho}$ in the Heisenberg picture:

$$\hat{\rho}_H = \sum_{\mu,\nu}\hat{E}^H_{\nu\mu}\varphi^*_\nu\varphi_\mu = \sum_{\mu,\nu}e^{i\hat{H}t}\hat{E}_{\nu\mu}e^{-i\hat{H}t}\varphi^*_\nu\varphi_\mu \qquad \text{(IIB7.15)}$$

The summation is taken over the complete basis of the one-electron spin orbitals μ and ν. The excitation operator $\hat{E}_{\nu\mu}$ replaces the spin orbital φ_μ by the spin orbital φ_ν (cf. (IIA2.4)).

For the evaluation of the equation of motion (cf. (IIB4.10) and ref 89) for the Lie algebra generator in the Heisenberg picture

$$i\frac{\partial}{\partial t}\hat{E}^H_{\lambda\kappa} = e^{i\hat{H}t}[\hat{E}_{\lambda\kappa},\hat{H}]e^{-i\hat{H}t} \qquad \text{(IIB7.16)}$$

the explicit expression for the commutator $[\hat{E}_{\lambda\kappa},\hat{H}]$ is needed. Let us assume the Hamiltonian for the system of interacting electrons in the form

$$\hat{H} = \sum_{\mu}[\epsilon_\mu\hat{n}_\mu - \sum_{i\rho}\langle\rho i||\mu i\rangle\hat{E}_{\rho\mu}] + (1/4)\sum_{\mu,\rho,\nu,\sigma}\langle\rho\sigma||\mu\nu\rangle[\hat{E}_{\rho\mu}\hat{E}_{\sigma\nu} - \delta_{\mu\sigma}\hat{E}_{\rho\nu}] \qquad \text{(IIB7.17)}$$

where $\langle\rho\sigma||\mu\nu\rangle = [\rho\sigma|\mu\nu] - [\rho\sigma|\nu\mu]$, ϵ_μ are the Hartree–Fock eigenvalues, and $|i\rangle$ are the occupied spin orbitals in the UHF procedure (cf. ref 106).

The commutator $[\hat{E}_{\lambda\kappa},\hat{H}]$ can be partitioned in two components:

$$[\hat{E}_{\lambda\kappa},\hat{H}] = [\hat{E}_{\lambda\kappa},\hat{H}]_1 + [\hat{E}_{\lambda\kappa},\hat{H}]_2 \qquad \text{(IIB7.18)}$$

$[\hat{E}_{\lambda\kappa},\hat{H}]_1$ is an expression which is linear in Lie algebra generators $\hat{E}_{\sigma\rho}$ ($\sigma \neq \rho$) which are not number operators $\hat{n}_\rho$. $[\hat{E}_{\lambda\kappa},\hat{H}]_2$ is an expression which is bilinear in $\hat{E}_{\sigma\rho}$($\sigma \neq \rho$).

By using the commutation relations which directly follow from the definition of the Lie algebra as well as the "anticommutation" relations

$$\hat{E}_{\lambda\kappa}\hat{E}_{\sigma\rho} + \hat{E}_{\lambda\rho}\hat{E}_{\sigma\kappa} = \delta_{\kappa\sigma}\hat{E}_{\lambda\rho} + \delta_{\rho\sigma}\hat{E}_{\lambda\kappa} \qquad \text{(IIB7.19)}$$

valid for fermions (cf. ref 47), the following general relations is found:[106]

$$[\hat{H},\hat{E}_{\lambda\kappa}]_1 = (\epsilon_\lambda - \epsilon_\kappa)\hat{E}_{\lambda\kappa} + \sum_{\rho\neq\mu}\langle\kappa\rho||\mu\lambda\rangle\hat{E}_{\rho\mu}(\hat{n}_\lambda - \hat{n}_\kappa) + \sum_{\mu,\rho}[\hat{E}_{\rho\kappa}\langle\mu\rho||\mu\lambda\rangle - \hat{E}_{\lambda\rho}\langle\mu\rho||\mu\kappa\rangle][\hat{Q}\hat{n}_\mu - \hat{P}\hat{m}_\mu] \qquad \text{(IIB7.20)}$$

Here $\hat{m}_\mu = 1 - \hat{n}_\mu$ is the "number operator for a hole" in the spin orbital μ, $\hat{P}$ is the projector on the Fermi sea of occupied spin orbitals, $\hat{Q} = \hat{I} - \hat{P}$ is the projector on the space of virtual spin orbitals.

$$[\hat{H},\hat{E}_{\lambda\kappa}]_2 = (1/2)\sum''_{(\mu,\rho,\sigma)}\hat{E}_{\sigma\rho}[\langle\sigma\mu||\rho\lambda\rangle\hat{E}_{\mu\kappa} - \langle\rho\mu||\sigma\kappa\rangle\hat{E}_{\lambda\mu}] \qquad \text{(IIB7.21)}$$

$\sum''_{(\mu,\rho,\sigma)}$ means the summation over the indices of the spin orbitals which do not lead to "contractions" according to the commutation (IIA2.5) or anticommutation (IIB7.19) relations.

If the contribution $[\hat{H},\hat{E}_{\lambda\kappa}]_2$ (cf. (IIB7.18)) is neglected the equation of motion (IIB7.16) takes the form

$$-i\frac{\partial}{\partial t}\hat{E}^H_{\lambda\kappa} = (\epsilon_\lambda - \epsilon_\kappa)\hat{E}^H_{\lambda\kappa} + \sum_{\rho\neq\mu}\langle\kappa\rho||\mu\lambda\rangle\hat{E}^H_{\rho\mu}(\hat{n}^H_\lambda - n^H_\kappa) + \sum_{\mu,\rho}[\hat{E}^H_{\rho\kappa}\langle\mu\rho||\mu\lambda\rangle - \hat{E}^H_{\lambda\rho}\langle\mu\rho||\mu\kappa\rangle][\hat{Q}\hat{n}^H_\mu - \hat{P}\hat{m}^H_\mu] \qquad \text{(IIB7.22)}$$

where ϵ_κ are the Hartree–Fock eigenvalues. Consequently,

$$-i\frac{\partial}{\partial t}\langle 0|\hat{E}^H_{\lambda\kappa}|0\rangle = (\epsilon_\lambda - \epsilon_\kappa)\langle 0|\hat{E}^H_{\lambda\kappa}|0\rangle + \sum_{\rho\neq\mu}\langle\kappa\rho||\mu\lambda\rangle\langle 0|\hat{E}^H_{\rho\mu}(\hat{n}^H_\lambda - \hat{n}^H_\kappa)|0\rangle + \sum_{\mu,\rho}\langle 0|[\hat{E}^H_{\rho\kappa}\langle\mu\rho||\mu\lambda\rangle - \hat{E}^H_{\lambda\rho}\langle\mu\rho||\mu\kappa\rangle](\hat{Q}\hat{n}^H_\mu - \hat{P}\hat{m}^H_\mu)|0\rangle \qquad \text{(IIB7.23)}$$

If one assumes that the correction from the last term of (IIB7.23) is relatively small and the Fourier transform of (IIB7.23) is carried out, then the following holds:

$$\langle 0|\hat{E}^\omega_{\lambda\kappa}|0\rangle = \frac{(\bar{n}_\lambda - \bar{n}_\kappa)}{\epsilon_\lambda - \epsilon_\kappa - \omega}\sum_{\rho\neq\mu}\langle\kappa\rho||\lambda\mu\rangle\langle 0|\hat{E}^\omega_{\rho\mu}|0\rangle \qquad \text{(IIB7.24)}$$

where $\bar{n}_\kappa$ and $\bar{n}_\lambda$ are the approximate average occupation numbers of the one-electron states κ and λ. Equation IIB7.24 describes the Coulombic interaction among the one-electron density matrix elements.

Only the components of the electron density operator which belong to a given irreducible representation Γ of the symmetry group of the system are interesting. If we label these contributions in the Heisenberg picture with the symbol $\mu\nu \in \Gamma$ then the expectation value for this component can be written in the following form:

$$\bar{\rho}^{(\omega)}_\Gamma = \sum_{\kappa\lambda\in\Gamma}\langle 0|\hat{E}^\omega_{\kappa\lambda}|0\rangle\varphi^*_\kappa\varphi_\lambda = \sum_{\kappa\lambda\in\Gamma}\frac{(\bar{n}_\lambda - \bar{n}_\kappa)}{(\epsilon_\lambda - \epsilon_\kappa - \omega)}\sum_{\mu\rho\in\Gamma}\langle\kappa\rho||\lambda\mu\rangle\langle 0|\hat{E}^\omega_{\rho\mu}|0\rangle\varphi^*_\kappa\varphi_\lambda \qquad \text{(IIB7.25)}$$

Equation IIB7.15 can be substantially simplified as, for example, in the case of free-electron gas (cf. (IIB7.40)) for which $\varphi^*_\kappa\varphi_\lambda = \varphi^*_\rho\varphi_\mu$ holds. Therefore, if

$$\langle\kappa\rho||\lambda\mu\rangle \approx v_\Gamma \text{ for } \kappa\lambda \in \Gamma \text{ and } \mu\rho \in \Gamma \qquad \text{(IIB7.26)}$$

and all other integrals $\langle\kappa\rho||\lambda\mu\rangle$ have negligible values, then it is possible to write approximately for the expectation value of the electron density the following expression:

$$\bar{\rho}^\omega_\Gamma = v_\Gamma\,\bar{\rho}^\omega_\Gamma\sum_{\kappa\lambda\in\Gamma}\frac{(\bar{n}_\lambda - \bar{n}_\kappa)}{\epsilon_\lambda - \epsilon_\kappa - \omega)}$$

or

$$1 = v_\Gamma\sum_{\kappa\lambda\in\Gamma}\frac{(\bar{n}_\lambda - \bar{n}_\kappa)}{(\epsilon_\kappa - \epsilon_\kappa - \omega)} = v_\Gamma\,[G^{(0)}_\Gamma(\omega) + G^{(0)}_\Gamma(-\omega)] \qquad \text{(IIB7.27)}$$

where (cf. refs 89 and 107)

$$G^{(0)}_\Gamma(\omega) = \sum_{\kappa\lambda\in\Gamma}\frac{\bar{n}_\kappa(1 - \bar{n}_\lambda)}{\omega - (\epsilon_\lambda - \epsilon_\kappa)} = \langle 0|\hat{G}^{(0)}_\Gamma(\omega)|0\rangle \qquad \text{(IIB7.28)}$$

is the matrix element of the Green's operator for the monoexcitations in the oscillating state $|0\rangle$. This is the equation for free oscillations with frequency ω_Γ for the irreducible representation Γ. Equation IIB7.27 is also the condition for solving the system of equations (IIB7.24) if (IIB7.26) holds.

Another derivation of the equation for a free oscillating system is also quite instructive. The Fourier transform of the time-dependent Schrödinger equation is

$$(\omega - \hat{H}_0)|\psi(\omega)\rangle = \hat{V}|\psi(\omega)\rangle \qquad \text{(IIB7.29)}$$

if both $\hat{H}_0$ and $\hat{V}$ are time independent and the inverse Fourier transform of the wave function is defined as

$$|\psi(\omega)\rangle = (1/\sqrt{2\pi})\int_{-\infty}^{+\infty} e^{i\omega t}|\psi(t)\rangle\,dt \qquad \text{(IIB7.30)}$$

The Fourier transform belonging to the irreducible representation Γ of the symmetry group of the system is

$$|\psi(\omega_\Gamma)\rangle = \hat{G}^\Gamma_0(\omega)\hat{V}|\psi(\omega_\Gamma)\rangle \qquad \text{(IIB7.31)}$$

where the Green's operator is defined as

$$\hat{G}_0^{\Gamma}(\omega_{\Gamma}) = \hat{\Gamma}\hat{G}_0(\omega_{\Gamma}) = \sum_{j\in\Gamma} \frac{|j\rangle\langle j|}{(\omega_{\Gamma} - \bar{E}_j^0)} \quad \text{(IIB7.32)}$$

with

$$\hat{H}_0|j\rangle = E_j^0|j\rangle \quad \text{(IIB7.33)}$$

and $\hat{\Gamma}$ is the projector on the manifold $|j\rangle$ and $j \in \Gamma$. It follows

$$1 = \langle\psi(\omega_{\Gamma})|\hat{G}_0^{\Gamma}(\omega)\hat{V}|\psi(\omega_{\Gamma})\rangle \quad \text{(IIB7.34)}$$

If it is assumed that

$$V_{jk} = v_{\Gamma} \text{ for } j,k \in \Gamma \quad \text{(IIB7.35)}$$

then

$$1 = v_{\Gamma} \sum_{j\in\Gamma} \frac{1}{(\omega_{\Gamma} - E_j^0)} \langle\psi(\omega_{\Gamma})|j\rangle \sum_{k\in\Gamma} \langle k|\psi(\omega_{\Gamma})\rangle \quad \text{(IIB7.36)}$$

If moreover $\langle\psi(\omega_{\Gamma})|j\rangle \approx 1/\sqrt{N}$ the condition for the frequency ω_{Γ} reads

$$1 = v_{\Gamma} \sum_{j\in\Gamma} (\omega_{\Gamma} - E_j^0)^{-1} \quad \text{(IIB7.37)}$$

which has a form similar to the relation IIB.7.27.

The simple connection with the Green's operator concept as well as the approximations involved are evident. If the "free oscillation frequency" ω_{Γ} is large in comparison to the energy differences

$$\omega_{\Gamma} \gg (\epsilon_{\lambda} - \epsilon_{\kappa}) \quad \text{(IIB7.38)}$$

then it holds

$$\omega_p^2 = \omega_{\Gamma}^2 = v_{\Gamma} \sum_{\kappa\lambda\in\Gamma} (\bar{n}_{\lambda} - \bar{n}_{\kappa})(\epsilon_{\kappa} - \epsilon_{\lambda}) \quad \text{(IIB7.39)}$$

and ω_p can be considered as "generalized plasmon frequency".

Equation IIB7.27 can be also derived with the Green's function technique in the random-phase approximation in which only the summation over ring diagrams is retained.[89] The assumption of the treatment used in this section are evidently equivalent to the random-phase approach.

It is very useful and illustrative to derive the explicit expression for the plasma frequency ω_p in the classical limit of the free electron model of metals.

The assumption IIB7.26 that all integrals $\langle\chi\rho||\lambda\mu\rangle$ have a common value v_{Γ} for a given irreducible representation is fulfilled for free-electron gas (cf. (IIB1.1)).

$$v_{\mathbf{q}} = (1/V^2) \int\int \frac{d\mathbf{r}\, d\mathbf{r}'}{|\mathbf{r} - \mathbf{r}'|} e^{i((\mathbf{k}_3-\mathbf{k}_2)\mathbf{r}+(\mathbf{k}_4-\mathbf{k}_1)\mathbf{r}')} = (1/\mathbf{q}^2V)\delta(\mathbf{k}_1 + \mathbf{k}_2 - \mathbf{k}_3 - \mathbf{k}_4) \quad \text{(IIB7.40)}$$

where

$$\mathbf{q} = (1/2)(\mathbf{k}_1 + \mathbf{k}_3 - \mathbf{k}_2 - \mathbf{k}_4) \quad \text{(IIB7.41)}$$

This means that in the summation in (IIB7.37) are considered single excitations which satisfy the ring condition (IIB7.40). If these conditions are not satisfied, the definition of the plasmon is not well grounded.

In the random-phase approximation the excitations from the one-electron state $|\lambda\rangle = |\mathbf{k}\rangle$ into the state $|\kappa\rangle = |\mathbf{k} + \mathbf{q}\rangle$ as well as from the one-electron state $|\kappa\rangle = |\mathbf{k} - \mathbf{q}\rangle$ into the state $|\lambda\rangle = |\mathbf{k}\rangle$ are considered.

The contribution for $\lambda = \mathbf{k}$ and $\lambda = \mathbf{k} - \mathbf{q}$ to the summation in (IIB7.39) is

$$(\epsilon_{\mathbf{k}+\mathbf{q}} + \epsilon_{\mathbf{k}-\mathbf{q}} - 2\epsilon_{\mathbf{k}})/\omega_p^2 = \mathbf{q}^2/\omega_p^2 \quad \text{(IIB7.42)}$$

where the relation IIB1.3 for the energy of a free wave has been used (cf. ref 89).

The expression for the plasma frequency ω_p obtained as a limiting case ($\mathbf{q} \to 0$) of the quantum mechanical approach has the classical form (cf. (IIB7.7))

$$\omega_p^2 = v\mathbf{q}^2 \sum_{\mathbf{k}} \bar{n}_{\mathbf{k}} = \rho_0 \quad \text{(IIB7.43)}$$

The relation IIB7.27 for the "free-oscillation frequencies" ω_{Γ} results from the interaction among the single excitations belonging to the irreducible representation Γ. Every other ω_{Γ} lies between a pair of monoexcitation energies $\omega_{\lambda\kappa} = \epsilon_{\lambda} - \epsilon_{\kappa}$ with exception of one which can be outside of the range of the $\omega_{\lambda\kappa}$'s. The interaction described in (IIB7.27) includes in principle all single excitations but if some $\omega_{\lambda\kappa}$ are very near to the root ω_{Γ} these electron-hole excitations play a dominant role in the interaction. Only if a root ω_{Γ} is quite far from the dense band of $\omega_{\lambda\kappa}$'s the interaction among many electron-hole excitations is of comparable importance and the corresponding cross section can be large since no interference takes place. This is clearly only a limiting case if some specific conditions are fulfilled. A simple example is the free-electron gas in the random-phase approximation ($\omega_{\Gamma} = \omega_p$).

If the "band" of the monoexcitation energies is not dense enough or if the symmetry of the system is low, then further complications can be expected leading for example to large cross sections inside of the energy "band" of single excitations. The two electron excitations do not play any role in the concept of plasmons although they can in some cases be quite important.

It has been shown that the concept of collective "plasma" oscillations is a special case of the general interaction among individual monoexcitations. The necessity to consider explicit interaction among monoexcitations is in general a consequence of a convenient methodological and conceptual approach customary in solid-state physics and molecular physics as well. The excitations of the many-electron systems cannot in general be satisfactorily described in the one-electron approximation, but it is convenient to use the solution of the many-electron problems with the one-electron approach as a suitable starting point.

More specifically, in the absorption spectroscopy of molecules the excited states which can be described as a result of a single monoexcitation are an exception. For example, the very intense "B_b absorption bands" of linear polyacenes exhibit intriguing simularities with "giant resonances" of alkali-metal clusters. A very simple semiempirical Pariser–Parr–Pople (PPP) π-electron theory of conjugated hydrocarbons predicts that only electron transition from the ground state to the $1^1B_{3u}^+$ state (polarized along the longer axis of the polyacenes) leads to an intense absorption peak.[90] The plus and minus signs label representations of the "alternant symmetry" which causes certain pairs of single excited configurations to be degenerate. In the PPP approach the $1^1B_{3u}^+$ wave function is the proper linear combination of only a few one-electron excitations. The linear combination leading to $1^1B_{3u}^-$ state is optically forbidden and all other transitions (e.g. to $^1B_{2u}^+$) have small intensities.

The transition energy to the state $1^1B_{3u}^+$ decreases

from roughly 6 eV for benzene to 5 eV for pentacene and the intensity of the $1^1B_{3u}^+$ transition nearly doubles. The analysis of the whole phenomenon, which is in agreement with experiments,[108] is very transparent.[90] As in the case of alkali metal clusters the symmetry and geometry cause interference phenomena among interacting monoexcitations.

From this example a conclusion can be drawn that the interaction among monoexcitations is a very general concept which is useful for the description of the influence of the electromagnetic field on any electronic system, which is not necessarily metallic.

The validity of (IIB7.25) for the frequencies ω of the oscillating system is not limited to any special case and it represents a link between the theory of volume plasmon, surface plasmon, and a response of a highly symmetrical molecular system to the interaction with the electromagnetic field. In the case of a surface plasmon the bands of one-electron volume states and possibly of one-electron surface states should be involved in the interaction of particle-hole transitions. Consequently, there should exist a resulting collective mode with a frequency which differs substantially from those of single particle-hole excitations. The presence of a surface necessarily changes the plasmon frequency, but evidently its order of magnitude will remain unchanged with respect to the bulk plasmon frequency. This is due to the common nature of the collective mode of surface and volume plasmons. It is possible to assume that (IIB7.39) determines also the surface plasmon frequency but the occupation numbers $\bar{n}_\lambda$ differ from those for the volume plasmon and two-dimensional $\mathbf{k}$ vectors figure in (IIB7.40–IIB7.42).

The simple derivation of the plasmon theory outlined above shows that the following conditions must be simultaneously fulfilled:

(i) A plasmon should result from the interaction of a very large (in the limit infinite) number of electron-hole transitions.

(ii) All these particle-hole excitations play a comparable role.

(iii) The plasmon excitation frequency differs substantially from all the frequencies of individual monoexcitations.

(iv) Strong interference phenomenon is present.

(v) Moreover, the usual concept of the plasmon allows for transitions into the one-electron states without respecting their occupancy in the ground state (random-phase approximations). This assumption is important in taking the limit $\mathbf{q} \rightarrow 0$ in order to obtain the classical expression for plasma frequency ω_p (cf. (IIB7.43)).

In the theory of the surface plasmons analogous basic assumptions are made as in the case of volume plasmons. Consequently, the same conceptual analysis applies.

8. Comparison of the Collective Effects in the Quantum Molecular Theory and Solid-State Theory

From various theoretical approaches for the determination of the response of a quantum mechanical system to a perturbation it is possible to trace a common assumption: The excitation of the system is described as a linear combination of single electron excitations or, in other words, as interaction among electron–hole states.

The excited states in the Tamm–Dancoff procedure are linear combinations of configurations arising by a replacement of a molecular orbital occupied in the ground-state Slater determinant by a virtual orbital. In the time-dependent Hartree–Fock theory (random-phase approximation) the oscillating state is a linear combination of single excitations. In the theory of Wannier's and Frenkel's excitons the linear combinations of single excitations are used for the definitions of the notions of excitons. In the quantum mechanical theory of plasmons the spectral decomposition yielding the eigenstates of the unperturbed system shows that only single excitations from a reference state are considered in this theory. The analysis of equivalent treatments with the Green's functions and polarization propagators yields the same picture. Here the assumptions which are equivalent to the Hartree–Fock approximation and to the RPA approach are taken into account for the solution of the problems.

Statements about the nature of the binding in relatively small clusters and about the similarity of clusters with the condensed matter are often made with the help of the plasmon notion. Consequently, some clarification of the plasmon concept is a quite interesting and challenging task in the cluster theory.

As commented at the end of the previous section (section II.B.7) several specific conditions for linear combinations of monoexcitations must be simultaneously fulfilled for plasmons justifying their distinction from the excitations known in molecular systems. Therefore, the notion of the plasmon can be clearly defined only for very large systems with a quasicontinuous spectrum of particle–hole excitation energies. The state whose energy lies outside of the band belonging to specific irreducible representation of the symmetry group can be named a plasmon state and can be distinguished from the correlated particle–hole states characterized by a linear combination of a limited number of dominant contributions of particle–hole excitations.

Let us repeat that the appearance of "interferences" causing very large differences in the excitation cross sections can occur easily due to various signs of the coefficients of the contributing leading configurations.

The quantum chemistry methods which account for electron-correlation effects contain also interactions among single and higher order excitations. We have tried in the section II.B to emphasize the inherent similarities of the treatment of the many-electron effects in the quantum chemistry and in the solid-state theory making a distinction between correlation effects which are a different type of collective effects than those responsible for excitons, plasmons, etc.

III. Ground-State Properties

A. Methodological Requirements for Application of Quantum Chemistry

A few methodological problems have to be solved when studying the ground-state properties of the elemental clusters. First, the experimental data available are scarce and can be correlated with the true physical observables only in an indirect way. Therefore, the accuracy and reliability of the adopted methodological and computational approaches cannot be surely

checked by direct comparison between theoretical and experimental values. In addition, the incomplete experimental data do not allow us to formulate a simplified computational scheme based on a set of empirically determined parameters. For instance, empirical classical potentials like those used successfully in molecular mechanics and dynamics of complex systems cannot be easily derived in the case of clusters, especially those composed of metallic elements. All these considerations lead to the conclusion that the adopted methodological approach must be characterized by a very well defined internal consistency, avoiding unnecessary approximations which can affect the results in an uncontrolled manner. In addition, the computational method must incorporate the most specific features of the electron–nucleus and electron–electron potential.

Moreover, the energy accompanying the formation of the cluster from the constituent atoms and its fragmentation to clusters of smaller dimensions (phenomena which are related to experimental observations) is expected to be dominated by electron correlation effects. As a consequence, it is necessary to adopt methods yielding a correct estimate of the correlation effects, either in the framework of CI approaches (if possible, size-consistent ones), or by means of a density functional scheme, incorporating, however, at least the self-interaction corrections.

Another aspect, which is of basic importance for the choice of a computational method, is connected with the fact that usually it is not sufficient to compute physical observables for a single (very small) cluster with high sophistication, but it is of greater interest to follow a trend of computed values in a range of nuclearities, as large as possible. A compromise between accuracy and simplicity of the method must be accepted. Typically, the choice of the size of the basis sets and the inclusion of polarization functions, are obviously determined by the size of the clusters considered. Analogously, the extent of the CI treatment is limited when a large number of electrons have to be correlated. Of course, very accurate calculations on small clusters are of essential importance in the framework of broad and systematic studies, because they allow one to estimate the limitations of more approximate treatments.

B. Stability, Fragmentation, and Geometry of Clusters

Theoretical methods fulfilling the methodological requirements discussed above can be very useful in determining the trend of physical observables in a series of clusters with increasing size.

The most interesting ground-state properties of clusters are (i) the geometries of the stable conformers with the lowest energies, (ii) the corresponding binding energies per atom E_b/n ($E_b/n = (nE_1 - E_n)/n$, E_n being the total energy of the n-atom cluster), (iii) the ionization potentials and electron affinities (IP = $E_n^+ - E_n$; EA = $E_n - E_n^-$, $E_n^\pm$ being the energy of the charged n-atom cluster). In addition, quantities directly related to the electronic distribution in clusters and with its response to static external fields (dipole moments, static polarizabilities, etc.) are of basic importance for description of the specific features of the cluster electronic structure.

As is well known, clusters can undergo fragmentation when they possess a high internal temperature. For a given nuclearity, n, the theoretical study of the energetics of the process $A_n \rightarrow A_{n-m} + A_m$, i.e. the identification of the most favorable pairs $(n - m)$ and m, is useful for interpreting a variety of phenomena observed experimentally. In this respect, the energy quantity that is convenient for future discussion can be defined as $\Delta E_{n,m} = E_{n-m} + E_m - E_n$. In particular, $\Delta E_{n,1}$ and $\Delta E_{n,2}$ are measures of the tendency of an n-atom cluster to dissociate one atom or one dimer, respectively, leading to a species of nuclearity $(n - 1)$ and $(n - 2)$.

The quantity $\Delta E_{n,1} = E_{n-1} + E_1 - E_n$ is also used to define the second difference $\Delta^2 E_n = \Delta E_{n,1} - \Delta E_{n+1,1} = E_{n-1} + E_{n+1} - 2E_n$ which is another useful quantity as a measure of the stability toward fragmentation. Negative values of $\Delta^2 E_n$ indicate that the process $2A_n \rightarrow A_{n-1} + A_{n+1}$ can easily take place. A positive value of $\Delta^2 E_n$ shows that the fragmentation of a cluster with n atoms ($A_n \rightarrow A_{n-1} + A_1$) is energetically less favorable than the dissociation channel for a cluster with $n + 1$ atoms: ($A_{n+1} \rightarrow A_n + A_1$).

1. Neutral Clusters

Alkali-Metal Clusters. Among the alkali metals, a theoretical treatment of lithium requires the smallest computational effort. This is the main reason why the lithium clusters have been theoretically studied so intensively, in spite of the fact that little is known experimentally. This explains also why the number of ab initio studies on Li_n clusters[62,61,109–135] is higher than for Na_n clusters.[110,114,131,136–143] For K_n clusters only a few theoretical papers have been published,[140,141,144] mainly dealing with species of relatively low nuclearity.

Investigation of Na_n and K_n (with $n \leq 20$) are nowadays possible at a high level of accuracy due to the availability of reliable ECP's,[34,35,37,39,40] which can be conveniently combined with one of the approaches proposed for the description of the core polarization potential (CPP) or core valence correlation (CVC)[145–148] effects. As pointed out in rigorous studies on alkali dimers,[147] the CVC effects are responsible for the contraction of the equilibrium bond distances and the increase of the E_b/n, IP, and AE values. The effects are of increasing importance as the polarizability of the core of the constituent atoms increases. CVC contributions are nearly negligible for Li_2 (and Li_n) but play a determining role in K_2.[147]

Ab initio studies of optimum geometries and stabilities of alkali-metal clusters should be carried out adopting basis sets which necessarily include at least p polarization functions:[149,1,150] they are expected to be essential particularly for small species and less important for larger systems which assume preferentially three-dimensional structures. In fact in the latter case, functions of high angular momentum on one site can be easily mimicked by low angular momentum functions centered on the surrounding atoms. All the papers discussed in the following discussion seem to fulfill these basic methodological requirements although to a different extent.

The studies on Na_n species have been carried out also by using LSD methods ($n \leq 8$)[151–154] or with the QMD method of Car and Parrinello[65] also on larger systems.[155–157] In particular very recent LSD–QMD work

on Na_n (n = 2–10,13,18 and 20)[157] makes possible a comparison with the predictions obtained from other theoretical approaches.

The various theoretical studies generally agree upon the basic topologies of Li_n, Na_n, and K_n clusters. Figure 1a shows the most stable structures obtained from a HF optimization[62] of lithium clusters (n = 2–10). The optimum HF interatomic distances have been uniformly scaled by minimizing the extrapolated MRDCI energies.[48,49] The procedure is expected to take into account the effect of the electron correlation on the lithium–lithium distances but, obviously, is not equivalent to a full geometry optimization at CI level. It has been shown[62] that such partial CI geometry optimization has a nonnegligible effect on the computed E_b/n values. All other papers on Li_n clusters cited above have presented investigations limited mainly to clusters with n = 2–6 atoms. Figure 1b displays the best HF geometries for Na_n ($n \leq 9$).[142] The same topologies have been found to be the preferred ones also for K_n systems.[140,141] The study of Boustani et al.[62] is the only one which includes also a systematic theoretical vibrational analysis, which is essential in order to prove that the different conformers are real local minima on the $(3n - 6)$-dimensional surface.

Up to Li_5 the most stable forms are planar. For Li_6 three isomers with low energies have been identified, namely the planar one (D_{3h}), the pentagonal pyramid (C_{5v}), and the bicapped tetrahedron (C_{2v}): they are characterized by E_b/n values equal to 0.673, 0.675, and 0.660 eV, respectively.[62] The relative stability of the Li_n hexamers has been recently reinvestigated in detail by Koutecky et al.[134] The study shows how the prediction of the most stable conformer can easily depend upon the basis set chosen and the correlation treatment. By using a contracted 6s3p basis, the only real minima found at the SCF level are singlet states of C_{5v}, D_{3h}, and C_{2v} geometries (see above) and only one triplet state of C_{2v} symmetry. The sequence of the E_b/n values computed at SCF level 0.275 ($^1A_1$, C_{2v}), 0.296 ($^3B_1$, C_{2v}), 0.291 ($^1A_1$, D_{3h}), and 0.265 eV ($^1A_1$, C_{5v}) is changed by the correlation treatment according to 0.732 ($^1A_1$, C_{2v}), 0.718 ($^1A_1$, C_{5v}), 0.718 ($^1A_1$, D_{3h}), and 0.731 eV ($^3B_1$, C_{2v}). These results confirm the degeneracy of the forms D_{3h} and C_{5v} but, at the same time, point out that the C_{2v} form (which is formed by three condensed tetrahedra) exhibits a particularly high stability.

The existence of isomers lying so close together in energy seems to be a general characteristic for the hexamers of the Ia elemental clusters; probably because they represent the transition point between planar and three-dimensional structures. This is confirmed also by studies on Na_6 which gave E_b/n values for the D_{3h} and C_{5v} forms that differed by about 0.010, 0.004, and 0.003 eV, according to the results of refs 142, 140, and 138, respectively. The three studies adopted basis sets of type AE 3s3p, ECP 3s1p1d, and AE 6-21G, respectively, while correlation effects have been accounted for in the framework of MRDCI, CIPSI, and MP4 methods, respectively. Clearly the determination of the exact energy ordering of the isomers would require much more elaborate calculations. In particular, in the case of sodium and potassium clusters, the computational method should include an adequate treatment of the CVC effects. The recent geometry optimization[158] in the framework of the SCF ECP–CVC procedure for Na_6 yields the following E_b/n values for D_{3h}, C_{5v}, and C_{2v} structures: 0.131, 0.096, and 0.065 eV, respectively. The corresponding CI values are 0.478, 0.476, and 0.436 eV. Also LSD calculations[154] predicted the C_{5v} isomer to be

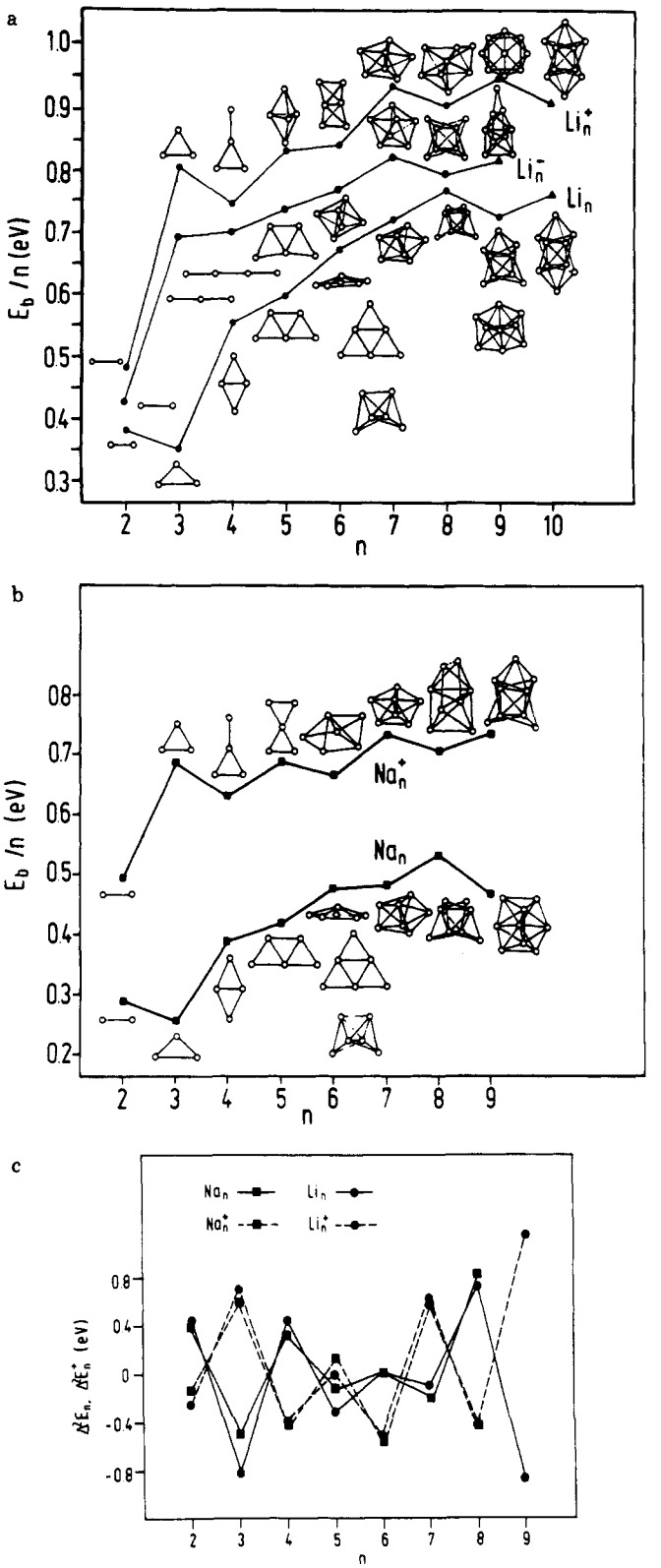

Figure 1. The CI binding energy per atom E_b/n as a function of the nuclearity n for (a) neutral, anionic, and cationic Li_n clusters and for (b) neutral, and cationic Na_n clusters. The topologies of the HF-optimized geometries are shown. (c) The measures of stabilities Δ^2E_n and $\Delta^2E_n^+$ for neutral (—) and cationic (---) Li_n and Na_n clusters are shown in part c. Small, but appropriate AO basis sets are used (for details cf. refs 62, 133, 142, and 143).

nearly degenerate (within 0.04 eV) with the D_{3h} planar form. Note, that for an internal temperature of the cluster in the range of 400–500 K, the value of kT is 0.03–0.04 eV.

An ECP–CIPSI study of K_n ($n \leq 6$) has been reported in refs 140 and 141 by using a 3s1p1d basis and carrying out an extensive correlation treatment. Core–valence correlation effects have been considered by means of a perturbation approach.[148] For the hexamer K_6, the theory again predicts a near degeneracy between the C_{5v} and D_{3h} isomers.

The above results show that in the case of hexamers the pentagonal pyramid is one of the low-energy conformers. Forms including regular or slightly distorted pentagons and pentagonal bipyramids have been found as stable geometries for clusters with $n = 7, 9, 10$[62,142] and for largers ones.[159] In the case of Li_7, the exact D_{5h} symmetry has been confirmed also from the analysis of the experimental EPR hyperfine constants for the species studied in a frozen matrix[160] (see also ref 113).

From Figure 1, parts a and b, it is apparent that the octamers are characterized by high stability. The most stable Li_8 cluster identified by HF-CI geometry optimization[62] belongs to the T_d point group, being composed of a tetrahedron with all the faces symmetrically capped, while the LSD method[154] suggests that the most stable form of Na_8 should have a D_{2d} geometry which is a deformed section of the fcc lattice. Another compact form for octamer is the square antiprism with D_{4d} symmetry. Recently,[162] the three forms T_d, D_{2d}, and D_{4d} of Na_8 have been reoptimized at the ECP–CVC level, by using a basis set of type 3s3p. Extensive MRDCI treatments including large set of reference configurations have been carried out. The best CI energies have been computed equal to −1.65840, −1.65614, and −1.65261 au, for the T_d, D_{2d}, and D_{4d} form, respectively. However, it has been shown[162] that the D_{2d} and D_{4d} transform into the T_d minimum without any energy barrier.

The T_d structure of the octamer is associated with an electronic configuration of type $1a_1^2 1t_2^6$ which is obviously related with the s^2p^6 configuration of the spherical potential. This clearly shows the connection between the predictions formulated on the basis of molecular[1,62,164,165] and spherical jellium approaches.[7,15,70] The latter method suggests that the octamer must be particularly stable due to the fact that eight valence electrons fill completely the 1s and 1p shells. In the molecular approach, the same conclusion about the cluster stability can be drawn from the observation that a set of degenerate MO's, which correspond to a very compact and symmetrical nuclear frame, is fully occupied. It must be noted, that the a_1 MO and the t_2 MO's have s and p character, respectively, in the sense that they can be projected on (and only on) the spherical harmonics with $l = 0$ and $l = 1$, respectively, located at the origin.

The occurrence of degeneracies of the "p" orbitals, is therefore a specific consequence of the symmetry of the nuclear frame. The D_{2d} and D_{4d} structures have the three highest MO's nearly (but not exactly) degenerate. This explains easily why the two forms exhibit so pronounced stability although smaller than the T_d form.

Starting from the octamer, the most favored growing sequence for the cluster seems to be that of capping progressively the six concave surfaces formed by two atoms of the outer and two atoms of the inner tetrahedron, respectively. Each capping atom forms two additional (distorted) tetrahedra and this sequence of clusters ends with a 14-atom species with a very compact (T_d) structure, characterized by high stability. Notice, that the 13-atom cluster considered in such a path of growing has no relation with the icosahedral or cubooctahedral forms, which have been considered in HF-CI for Li_{13}[161] and LSD studies for Na_{13}.[154,157]

Alkali-metal clusters with $n > 14$ have not been studied systematically by using ab initio HF-CI methods. Probable geometries for large clusters composed of atoms with one-valence electron have been obtained from the Hückel-type empirical calculations.[163] Very recent LSD–QMD work[157] contains equilibrium structures of Na_{18} and Na_{20} as well as those at higher temperature.

A few possible forms for the 20-atom clusters (the next "magic numbers" of the jellium model) have been computed and optimized (with symmetry constraints) for lithium with a basis of type 2s1p[164,165] and for Na in the framework of the ECP–CVC approach.[166]

Two low-energy forms of Li_{20} both have T_d symmetry. The first (the most favored at the CI level) is composed of three "spherical" shells composed of 4, 4, and 12 atoms (4, 4, 12), while the second cluster is just a part of the fcc lattice (see Figure 5 of ref 164). The two clusters have the same electronic configuration $1a_1^2 1t_2^6 2a_1^2 2t_2^6 1e^4$. However, the T_d(fcc) isomer has the highest occupied MO's $2a_2$, $2t_2$, and 1e distributed in a range of about 0.7 eV, while these levels are virtually degenerate for the (4, 4, 12) T_d structure. In the latter case the 12 electrons $2a_1^2 2t_2^6 1e^4$ fill completely a system of six "degenerate" orbitals, which corresponds to the filling of the 2s and 1d shells of the spherical jellium potential.[7,70]

This is again an evident example of the combined role played by the symmetry of the nuclear frame and electronic wave function: the exact or nearly exact degeneracy of (completely filled) one-electron levels is an important factor for the cluster stability.

The results commented above concerning the clusters of larger nuclearity ($n > 8$) cannot be presently considered as complete and systematic. A more detailed investigation is needed in order to obtain reliable information about the trend of the E_b/n and $\Delta^2 E_n$ quantities in this range of the cluster size. In addition, the calculations reported (mainly for Li_n) are not sufficient to show clearly which path of cluster growth is the preferred one, namely that producing structures with symmetry characteristic for the bulk (e.g. fcc) or structures which still include pentagonal-like subunits.

In general, for neutral and charged Li_n and Na_n clusters, E_b/n increases with n as shown in Figure 1, parts a and b. Exceptions have been found, however, for the trimers and for Li_9 and Na_9: in the first case E_b/n decreases because the trimers are species of particularly low stability. For $n = 9$ the decrease in E_b/n is a consequence of the pronounced stability of the octamers. It is well recognized that the E_b/n quantity of the alkali clusters is strongly dominated by correlation effects. The correlation energy accounts for about 50% of the stability of Li_n clusters and even more than 90% in the case of small Na_n and K_n clusters. It has been shown[140,145] that the HF method—when all the core polarization contributions are neglected—is unable

to yield Na and K dimers, trimers, and tetramers stable with respect to atomization.

Even–odd alternations become more evident when the Δ^2E_n function is considered (see Figure 1c). The Δ^2E_n curves for Li_n, Na_n, and K_n show basically the same trend: sharp minima occur for n = 3, 9 and less pronounced minima for n = 5, 7. Correspondingly, maxima are present for even n and they are more pronounced for n = 2, 4, and 8, than for n = 6, indicating that the clusters with an even number of atoms survive fragmentation easier than those with an odd number of atoms.

The conclusion that clusters with an even number of atoms n are always more stable than those with the (n + 1) and (n − 1)—atoms cluster has been drawn from the UHF-MP4 study of ref 138, but such an evidence is not present in results of other works.[142,62,154] This also reflects the fact that the Δ^2E_n curves reported by Ray[138] have even–odd oscillation more pronounced (in particulary for n = 6) than the curves of Figure 1c.

The trend of the Δ^2E_n values computed by the majority of the theoretical works confirms that the process $A_n \rightarrow A_{n-2} + A_2$ is favored for n even, while for odd number of atoms the preferred fragmentation leads to a (n − 1)—atom cluster.[141,167-174]

For very large Ia and Ib clusters special stability has been predicted and experimentally found[76-79] for the magic numbers 40, 58, 92, 138, 198, etc. These magic numbers which are predicted, among others, by the Wood–Saxon potential and jellium model, can be understood considering the Bohr's correspondence principle between quantum and classical motion.[15]

Alkaline Earth Metal Clusters. Ground-state geometries and stabilities of IIa-atom clusters have been investigated theoretically by using a variety of basis sets and electron correlation methods. It has been shown that a correct description of species such as Be_2, Be_3, and Be_4 even at the semiquantitative level (see ref 175 and references therein) is very difficult in spite of their small size and small number of electrons. Quantitative predictions of properties of Be clusters involve substantially larger computational and methodological difficulties than those met in studying Ia-elemental clusters. For instance, the size-consistency effects which are absent in Li_2 and which can be overcome with a full (or nearly full) CI valence electrons treatment for Li_n ($n \leq 4$–6) is expected to play a big role in IIa-atom clusters. Atoms of the group IIa have a closed-shell ground state and all the available theoretical results on clusters seem to suggest that small Be_n and Mg_n species also have a closed-shell configuration. This fact, which would simplify the theoretical treatment, is, on the contrary, complicated by the occurrence of large effects due to the s–p near degeneracy.

A recent study of Lee et al.[175] on small Be_n and Mg_n (n = 3, 4, 5) summarizes all these difficulties, showing at which level of sophistication the calculations on IIa-atom clusters must be carried out in order to obtain quantitatively correct results. The Be_3 (D_{3h}) cluster studied with a 7s3p2d1f basis and the coupled cluster (CC) method including single and double excitations (CCSD) is characterized by E_b/n = 0.260 eV and a Be–Be bond distance of 2.24 Å. When a similar basis (5s3p2d1f) is used and the correlation treatment is extended at the MRCI level, the estimated value of E_b/n is nearly double (0.486 eV) with respect to the previous one, while the Be–Be distance (2.22 Å) seems to be almost unaffected. For Be_4 (T_d), the value E_b/n = 0.838 eV at an equilibrium bond length of 2.06 Å has been calculated at the same level of approximation. The trigonal-bipyramidal form of Be_5 is characterized by E_b/n = 0.71 eV with the two independent Be–Be distances equal to 2.03 and 2.08 Å. The E_b/n value for Be_5 has been obtained with a CCSD treatment (7s3p2d basis) and, therefore, must be compared with the corresponding values consistently obtained for Be_3 and Be_4, 0.106 and 0.64 eV, respectively. These results show that an enormous increase in E_b/n is produced by a multireference CI treatment and, at the same time, that E_b/n is probably a rapidly convergent quantity as the cluster size increases. The same rapid convergence occurs for the equilibrium Be–Be distances. The electronic structure and the basic quantities for the ground state of Mg_3, Mg_4, and Mg_5 follow the same trend.

The SCF method is unable to describe stable Mg_n clusters ($n \leq 5$) and the single reference CI methods (CPF and CCSD) are unable to correct the HF inadequacies completely. Only the MRCI level of theory seems to be adequate in this case. For instance, for the trimer Mg_3 E_b/n = 0.056 eV, obtained with a basis 5s3p1d, increases to 0.091 eV with a basis 7s6p3d1f. The latter, however, is not a practicable basis for calculations on larger systems.

Results obtained at comparable level (CCSD with basis set 6s5p2d) for the series Mg_3, Mg_4, and Mg_5 (E_b/n = 0.014, 0.114, and 0.114 eV and equilibrium bond distance r_e = 4.00, 3.23, and [3.16, 3.53] Å, respectively) show that the trend is indeed parallel to that discussed for Be_n.

For the study of clusters with higher nuclearity application of the theory at a lower level of sophistication has to be accepted. Marino et al.[176] investigated in a systematic manner the series Be_n with n = 3, ...7, considering a large number of different geometry configurations and different spin multiplicities by means of UHF-MP4 methods. For Be_n, using a 6-31G basis, E_b/n values were computed equal to −0.001, 0.421, 0.467, 0.435, and 0.498 eV for n = 3, 4, 5, 6, and 7, respectively. The clusters have the following best structures: equilateral triangle, tetrahedron, trigonal bipyramid, octahedron, and pentagonal bipyramid with Be–Be equilibrium distances equal to 2.48, 2.11, [2.04, 2.12], 2.09, [2.03, 2.17] Å. The high spin states seem to be increasingly favored as the nuclearity increases. In agreement with other studies, Marino et al.[176] found that up to Be_5 the cluster ground states are singlet states, while the lowest triplet (quintet) state (often with different symmetry of the nuclear frame) lies higher by about 1.37 (2.81) and 0.54 (1.83) eV in Be_4 and Be_5, respectively. On the contrary, Be_6 (O_h) has a quintet ground state, although the first singlet (D_{3d}) is only at 0.13 eV higher in energy. Similarly, the quintet ground state of Be_7 (D_{5h}) is more stable than the first triplet (centered hexagon, D_{6h}) and the first singlet of the heptagon (D_{7h}) by about 0.19 and 0.57 eV, respectively.

In recent calculations[177] the problem of the spin multiplicity of the ground state of Be_{13} (which has been assumed to be a singlet in previous calculations[180]) has been investigated for the cluster geometries optimized under D_{3h} (hcp) or D_{3d} (fcc) symmetry constraint. The following stabilities have been computed: E_b/n = 1.124, 1.201, and 1.257 eV for $^1A_1$ (D_{3h}), $^5A_2''$ (D_{3h}), and ^3A_g (D_{3d})

states, respectively, at the MP4 (SDTQ) level of theory by using a 4s2p basis. Inclusion of d polarization functions (4s2p1d) does not alter the computed trend for E_b/n, thus confirming that $^3A_{1g}$ is the ground state of Be_{13}.

The largest Be clusters investigated so far are Be_{51} and Be_{57},[178] Be_{63},[179a] Be_{69},[179b] Be_{81} and Be_{87},[179c] and Be_{55}.[180] In all cases ECP approaches have been adopted, using basis sets of type 2s1p[178,179] and 3s2p.[180] For an assumed singlet ground state, the conclusion has been reached[180] that Be_{55} prefers an fcc type structure instead of the hcp of the bulk metal. The two other clusters, Be_{51} and Be_{57} are assumed to possess D_{3h} symmetry,[178] and in the singlet ground state have E_b/n equal to 1.117 and 1.103 eV, respectively. While the first quintet state of Be_{51} lies 2.01 eV above the ground state, the first triplet for Be_{57} is much closer in energy (0.58 eV). However, the ground state of the Be_{63},[179] turns out again to be an open shell $^5E''$ (D_{3h}), with E_b/n = 1.072 eV. There is no substantial difference in values of the binding energy per atom for Be_{51}, Be_{57}, and Be_{63} at this level of calculation. For the ground states of Be_{69}, Be_{81} ($^3E''$), and Be_{87} ($^1A_1'$), the E_b/n increases slightly to 1.22, 1.23, and 1.24 eV, respectively. It seems that Be_{69} and Be_{81} exhibit bulk-like behavior, while several anomalies concerning different properties have been obtained for Be_{87} (cf. ref 179c).

Notice that calculations on large clusters at the HF level only[178-180] are probably of limited validity for quantitative purposes, since accurate studies on small Be_n and Mg_n clusters have shown that correlation effects are essential in determining correct values and ground-state multiplicities. However, approximate calculations on high nuclearity systems may help in suggesting trends and regularities in a series of clusters.

Other UHF-MP2 calculations adopting a basis set of the STO-6G* type have been recently reported for Mg_n ($2 \le n \le 4$) clusters for which an E_b/n value has been computed (approximate data obtained from Figure 8 of ref 181) as 0.45, 0.60, and 0.90 eV, respectively. Taking into account the extent of the basis and the quality of the CI expansion adopted, these E_b/n values seem to be overestimated (when compared with the accurate results of ref 175), probably partly due to a basis-set superposition error.

Finally, the only example of LSD calculations reported on the series Mg_n (n = 2, ...6)[182] is worth mentioning. The optimized structures up to Mg_5 are in general agreement with the results of HF-type methods.[175,176] On the contrary, Mg_6 has a shape of a bipyramid with rectangular basis (an octahedron with two axial distortions) in the singlet ground state. This is in disagreement with the findings of Marino et al.[176] and is one of the examples known in which the LSD favors more the low-spin states while the HF method (combined with a limited CI) favors high spin multiplicity probably because of the presence of large exchange contributions.[183]

Ia–IIa Mixed-Metal Clusters. In a series of papers[184-186] the electronic structure of the clusters composed of Ia-group metal atoms and of only one IIa-group atom has been investigated at the ab initio level (SCF-MRDCI). Cluster geometries optimized at the HF level are reported in Figure 2a, for the $MgNa_k$ species (k = 1, ...8). The mixed dimer MgNa does not show an appreciable stability. Also the $MgNa_2$ and $MgNa_3$ systems are characterized by a relatively small value of E_b/n (0.22 and 0.27 eV, respectively). Note, that for a mixed cluster the following definition holds: $E_b/n = E_b/(k+1) = [E(AB_k) - E(A) - kE(B)]/n$, where A and B are IIa- and Ia-group elements, respectively.

Starting only at $MgNa_4$, the cluster appears to be characterized by an enhanced stability, showing that the IIa-group atom has little tendency to form only one or two Mg–Na bonds. In larger clusters the Mg atom takes the central position of a regular polygon or polyhedron (in the absence of Jahn–Teller distortions), therefore assuming the highest possible coordination number. In the range of the investigated cluster sizes, a pronounced increase of E_b/n occurs for k = 4 and, in particular, for k = 6. The 8 valence electron cluster $MgNa_6$ (O_h) (see Figure 2a) has an electronic configuration of type $1a_{1g}^2 1t_{1u}^6$ which is formally identical to the configurations $1a_1 1t_2^6$ of T_d or s^2p^6 of spherical symmetry. This is a further example of a high symmetrical nuclear frame which, when combined with a closed-shell electronic configuration, gives rise to a particularly stable species.

A comparison of E_b/n for three series of mixed cluster $MgNa_k$, $MgLi_k$, and $BeLi_k$ is shown in Figure 2b. E_b/n are relatively smoothly increasing functions with the number of valence electrons N. The values of E_b/n for N = 8–10 do not differ substantially. E_b/n for $BeLi_k$ has substantially larger values for $k \ge 4$ than the corresponding curves for $MgNa_k$ and $LiNa_k$, illustrating a stronger role of the Be atom in hybridization.

Other studies on mixed Ia–IIa clusters have been carried out at ab initio levels[111,122,124,125,187,188] or by using LDA approach.[189] The number of isomers considered in these latter investigations is, however, much smaller than in refs 184–186, and no substantial improvement in the description of this class of clusters can be deduced.

Ib-Group Metal Clusters. It is often assumed that Cu, Ag, and Au atoms behave in a similar manner as the Ia atoms in metal–metal bond formation, due to the fact that the Ia and Ib elements have an ns^1 valence configuration. This is equivalent to assume that the $(n-1)d^{10}$ shell does not play a significant role in bond formation. However, some important electronic effects have to be taken into account in order to understand the limits inherent in the chemical analogy between Ia and Ib elements. The $(n-1)$d electrons do not contribute to a large extent, in a direct way, to the metal–metal bond, which is expected to be dominated by the s–s interaction, accompanied by a small contribution from the np orbitals, due to polarization effects. However, a more precise estimate of the relative importance of the role of the d orbitals may be derived from accurate wave functions of small Ib-atom clusters. For instance, from the data reported by Walch et al.[190] for relativistic ECP (RECP)-CPF calculations on Ib trimers, the following average electron configurations can be obtained for Cu_3 and Ag_3, in their ground state (C_{2v},$^2B_2$): s(0.937)p(0.240)d(9.823) and s(0.883)p(0.197)d(9.920), respectively. It must be noted that even a small d–s–p hybridization can give significant contribution to some molecular properties. In addition, the d–s correlation energy can be a determining factor for stabilizing the metal–metal bond. This is clearly proved by the rich literature on the Cu_2 dimer (see ref 6 and references therein). Clearly, the necessity of considering

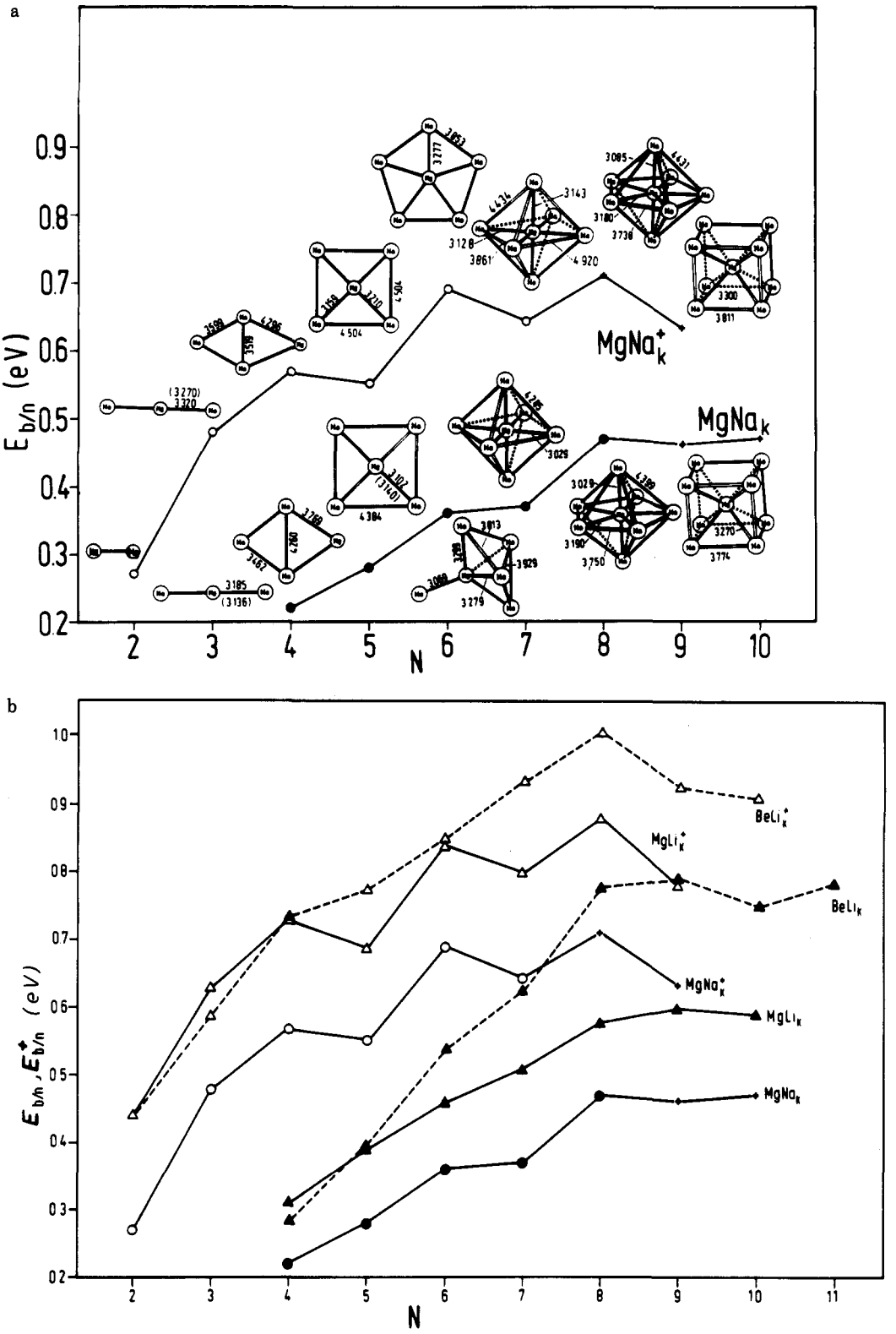

Figure 2. (a) The CI binding energy per atom E_b/n for neutral and charged $MgNa_k$ as functions of the number of valence electrons N. The HF-optimized geometries are drawn (cf. ref 186). (b) Comparison of the CI E_b/n for neutral and charged $MgNa_k$, $MgLi_k$, and $BeLi_k$ as functions of N (cf. refs 184 and 186).

the Ib atoms as 11 valence electron atoms limits the applicability of the theoretical methods including CI correlation to a series of clusters of small nuclearity.

A very appealing approach overcoming such a basic difficulty should be based on the description of the d–s and d–p correlation in terms of an "ad hoc" core–valence correlation potential (CVC), allowing the inclusion of the $(n - 1)d^{10}$ shell into the core. Obviously the procedure, combined with ECP or RECP, is also aimed at reducing the SCF calculation to the s valence electrons only. Recently, the problem has been investigated for Cu_n and Cu_n^-[191] by comparing the results of ECP–CVC calculations with those of other ECP studies[190] (for n = 1–3) in which the $3d^{10}$ electrons are explicitly correlated. Differences between the electron detachment energies for Cu_n^- computed by the two approaches

fall into the range of 0.08–0.36 eV. An attempt to describe Ib atoms as one-electron systems by means of a suitable CVC operator has been proposed earlier by Flad et al. (ref 192 and references therein) in the framework of the so-called "energy adjusted" ECP method. Detailed comparison between Ia (Li, Na, and K) and Ib (Cu and Ag) atom clusters has been presented.[192] It is important to note that the RECP methods can include relativistic effects only partially and that these effects are of increasing importance going from Cu to Au (see for instance refs 36, 193–198).

Relativistic scattered wave (RSW) calculations have been carried out by Arratia-Perez and Malli on Ag_4 and Ag_5 clusters.[193,198] For the Ag_5 species the total valence populations have been computed as equal to s(1.030)-p(0.213)d(9.874) for axial and s(0.717)p(0.383)d(9.822) for equatorial Ag atoms. It is important to note that such values are very close to those reported above for RECP–CPF calculations on Ag_3. However, it has been pointed out[193] that at a nonrelativistic level the MO's of symmetry e′ composed mainly of d atomic functions have a nonbonding character, while they contribute to the cluster stability because of their relativistic radial expansion.

Accurate AE (Cu) and RECP–MCPF (Ag and Au) calculations using a 6s5p3d (Cu) and 5s5p4d (Ag and Au) basis set describing the $(n-1)s^2(n-1)p^6(n-1)d^{10}ns^1$ configuration have been reported[190,199] for Cu_n, Ag_n, and Au_n ($2 \le n \le 5$). The correlation treatment for the X_n (X = Cu, Ag, Au) clusters is applied to 11 electrons per atom.

The following best geometries have been found: obtuse ($^2B_2$) or acute ($^2A_1$) triangles (X = Cu, Ag), rhombus and planar-trapezoidal forms for X_4 and X_5, respectively. The X–X bond distances for increasing cluster nuclearity are in the range 2.37–2.47 Å for Cu_{3-5}; 2.67–2.84 Å for Ag_{3-5}, and are close to 2.76 Å in Au_4 and Au_5. In this respect, all the Ib-atom clusters considered have basic topologies identical to those of the alkali metals (see Figure 1).

The spin density distribution in Ag_5 has been interpreted on the basis of EPR hyperfine constants as strongly localized on two atoms and less pronounced on other centers (refs 200 and 201 and references therein). This suggested that the structure of Ag_5 could be a (Jahn–Teller) distorted trigonal bipyramid. Such a structure is similar to that assumed in the nonrelativistic scattered wave (SW)[202] and RSW calculations on Ag_5.[198] However, the MCPF results of ref 199 show that the distorted trigonal bipyramid and the square pyramid of Ag_5 are 0.31 and 0.76 eV higher in energy than the trapezoidal structure. The spin distribution of the latter is also consistent with the experimental EPR observations.

The ground-state geometrical structure and stability of Cu_4 and Ag_4 clusters has been studied with RECP–MRSDCI and RECP–CASSCF methods by Balasubramanian and Feng.[203] By means of relativistic CI[204] including explicitly the spin–orbit coupling operator, it has been shown that spin–orbit effects are small for Ag_4 which prefers the rhombic structure. The $^3B_2$ states for the rhombus and square arrangements of Cu_4 lie at 0.75 and 0.82 eV above the ground state $^1A_1$ (D_{2h}) at CASSCF level, while an MRSDCI treatment yields 1.10 and 1.29 eV, respectively.

For a linear arrangement of Ag_4 $^1\Sigma_g^+$ state is found to be low lying. It is located 0.14 eV at the CASSCF and 0.38 eV at the MRSDCI level above the ground state $^1A_1$ (D_{2h}). The CASSCF method gives 10 singlet and triplet states of different symmetry within an energy range of about 1.0 eV.

The Au_4 tetramer has been studied with the same methodological approach adopted for Cu_4 and Ag_4.[205,206] The best estimate of the stability of Au_4 ($^1A_1$, D_{2h} rhombus) is E_b/n = 1.713 eV which must be compared with the corresponding values for Cu_4 and Ag_4:[203] E_b/n = 2.277 and 1.311 eV, respectively. The IP_v values have been computed as equal to 7.8, 5.8, and 6.7 eV for Cu_4, Ag_4, and Au_4. The gold tetramer is therefore markedly more stable than Ag_4, a fact which can be completely ascribed to relativistic effects, such as the mass–velocity contraction of the outermost s orbitals.

Rigorous and systematic quantum chemical investigations of Ib-atom clusters with nuclearity $n > 5$ have not yet been reported, and, most likely, cannot be carried out at present due to obvious computational limitations. At the same time, however, also a more approximate but systematic study covering a broader range of nuclearities is also lacking. In as much as the metal–metal bond in Ib-elemental clusters is determined mainly by the s valence electrons, the above discussed results concerning basic cluster topologies clearly show a close similarity with the results obtained for the alkali metal clusters.

IIIa- and IVa-Elemental Clusters. Clusters of the boron and carbon groups will be considered here just to point out the similarities and differences with the clusters discussed previously, which are composed of elements with essentially metallic character. Recent reviews on carbon[9,14] and silicon[5] clusters have been published.

Overview and comments on the theoretical works done on Al_n systems can be found in ref 2 (and references therein). On the contrary, very few calculations have been reported on neutral[207] and cationic[208] B_n clusters.

B_n (n = 4–10) clusters considered in a linear arrangements should exhibit a feromagnetic behavior, a conclusion based on a VB analysis of the UHF wave function.[209,210]

A recent systematic study has been carried out at the HF (AE)-CI level, using a double-ζ basis set with polarization function (DZ+P).[211] The resulting best geometries of B_n ($n \le 8$) are reported in Figure 3a. The strong tendency of the boron clusters to assume planar configurations is apparent with the exception of B_7. Note, however, that the heptamer is a hexagonal pyramid (C_{6v}) with the apical atom just slightly above the plane. This structure, therefore, is very similar to a B_7 unit of the hcp lattice. B_8 has a D_{7h} symmetry with a boron atom in the center of a heptagon, therefore, in an unusual coordination mode. E_b/n values ranging from about 1.2 eV (B_2) to 3.0 eV (B_8) have been computed by using MRDCI or direct CI methods[211] (see Figure 3b).

The planar structures of B_n are consistent with the chemical characteristics of the boron atom which, having only three valence electrons, strongly prefers to assume an sp^2 type hybridization. This is obviously true for B–B bonds, while in presence of electron-donor elements the boron can also assume a three-dimensional coordination.

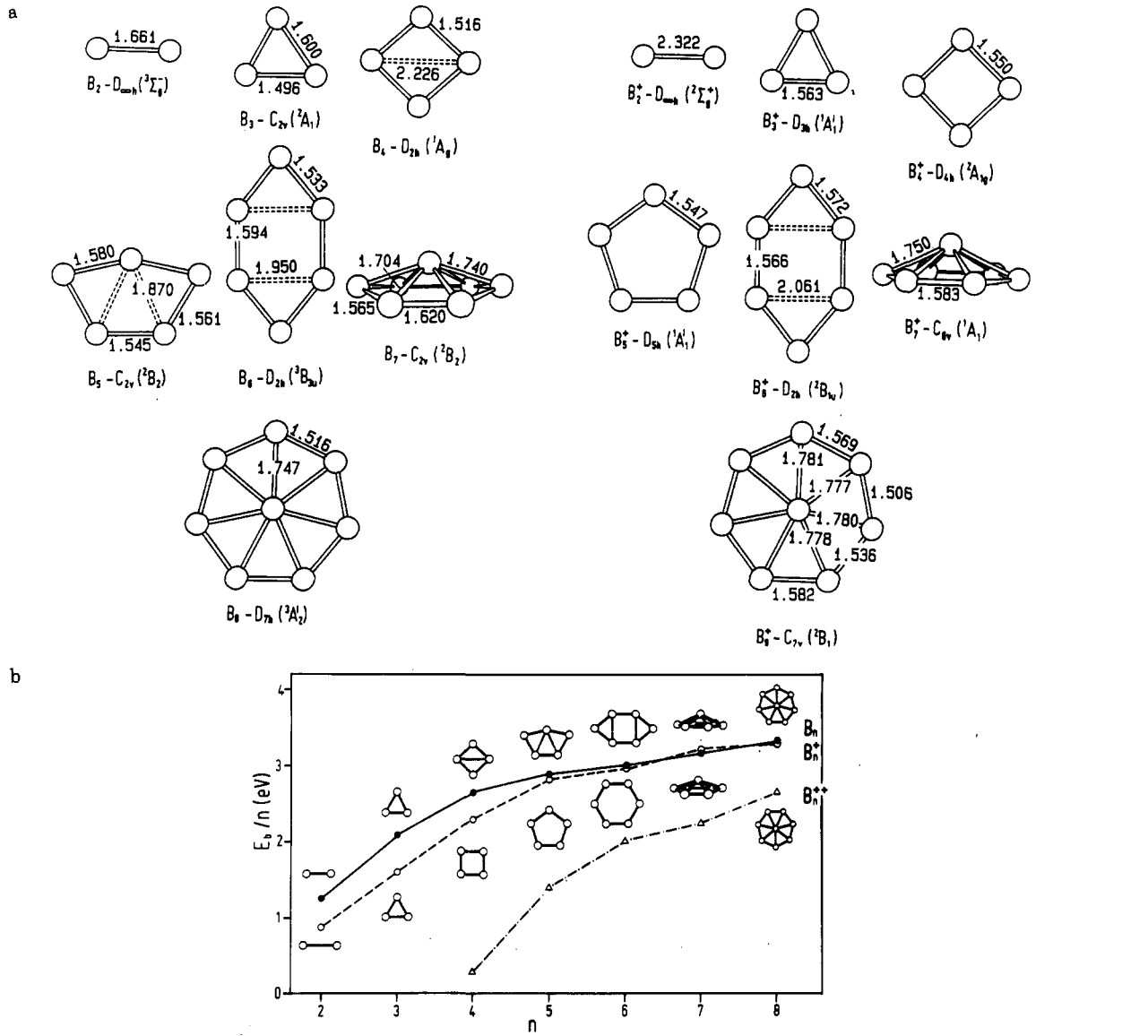

Figure 3. (a) The best geometries of B_n^+ and B_n ($n \leq 8$) clusters obtained by the HF procedure with use of a DZ+P basis set.[211] (b) The CI binding energy per atom E_b/n as a function of the nuclearity n for neutral, singly, and doubly charged B_n clusters. The topologies of the optimized geometries are drawn.

Ab initio calculations on Al_n[212] (n = 2, ...6, 13) have shown that up to Al_5 the best geometrical structures are overall similar to those of B_n clusters. However, Al_6 seems to prefer the O_h geometry (E_b/n = 1.47) while the form analogous to B_6 (see Figure 3b) is slightly less stable E_b/n = 1.25 eV). Al_{13} is found to be icosahedral (E_b/n = 1.11 eV) although the D_{2h} symmetry which is a planar section of an hcp lattice has comparable stability (E_b/n = 1.08 eV).

In the very systematic investigations carried out by Raghavachari et al. (ref 213, and see also ref 14 and references therein) the best geometries of C_n (n = 3, ...10) clusters have been determined. The clusters with an odd number of atoms are linear chains, those with an even number of atoms have cyclic structures with $n/2$-fold symmetry. Thus C_6, C_8, and C_{10} assume geometries with D_{3h}, D_{4h}, and D_{5h} symmetry, respectively (see Figure 4). However, the ground-state energy for the linear structure of C_4 is only negligibly higher than for the rhombic geometry (cf. ref 214).

Reference 5 collects and comments on the most recent quantum chemical studies on Si_n clusters, mainly carried out by Raghavachari. Figure 5 shows that planar forms exist only up to Si_4. For nuclearities $n \geq$

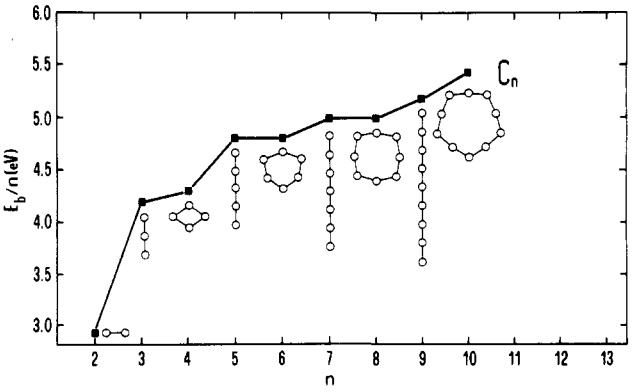

Figure 4. E_b/n as a function of nuclearity n for neutral C_n ($n \leq 10$) clusters. Topologies of the best optimized structures are drawn (HF (6-31G*) and MP2-4 calculations[213]).

basically built from distorted tetrahedral units. None of the low energy forms, however, are related with the bulk-type structures.

IIIa- and IVa-elemental clusters differ substantially in shape from the Ia-, Ib-, and IIa-metal clusters. The obvious observation is that the elements of the boron

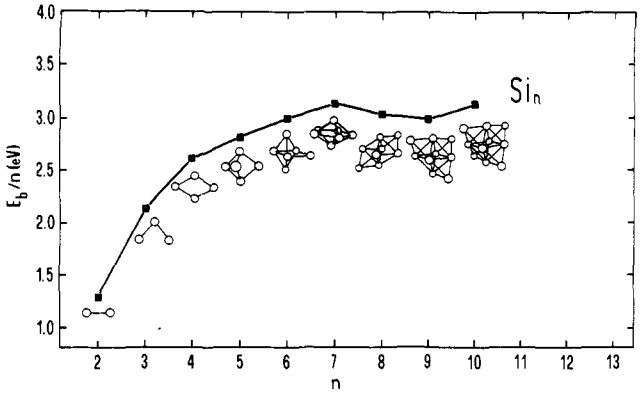

Figure 5. E_b/n as a function of nuclearity n for neutral Si_n ($n \leq 10$) clusters. Topologies of the best optimized structures are drawn (HF (6-31G*) and MP2-4 calculations[5]).

ground electronic state. Therefore, the p electrons (and p orbitals) are expected to play a determining role in the formation of the bonds in clusters. In addition, the tendency of individual elements to assume sp, sp^2, or sp^3 hybridization is the factor determining the preference for linear, planar, or three-dimensional geometry. This can be clearly understood by comparing B_n and Al_n clusters: the three-dimensional structures for the latter appear already for a smaller nuclearity than for the former. In C_n, both for linear and cyclic structures, a tendency of each carbon atom to interact with one or two nearest-neighbor atoms is apparent, which means the formation of multiple C–C bonds. Silicon, on the contrary, essentially favors structures with single Si–Si bonds, in which sp^3 hybridization is well developed.

In the case of Ia and Ib metals, the p orbitals act mainly as polarization functions, and therefore the three-dimensional structures become energetically favored only when a high number of metal–metal bonds can be formed, that is for a relatively high coordination numbers. The role played by the p orbitals is even more evident for Be_n and Mg_n where, starting from the T_d tetramers, a true hybridization (and not only weak polarization) occurs.

2. Cationic Clusters

Alkali-Metal Clusters. Several theoretical studies have addressed the problem of ionization for Li_n, Na_n, and K_n clusters and the consequent changes in shape and stability. These studies aim to determine both the vertical (IP_v) and adiabatic (IP_a) values of the ionization potentials. Of course, the calculation of IP_a requires, in principle, the knowledge of the optimum geometry of the ground state of the cationic clusters. In this respect, the computational difficulties met in the case of neutral clusters have to be mentioned once again, in order to emphasize that the existence of several isomers for the cationic clusters can make the determination of IP_a difficult. Studies based on HF-CI methods have been carried out on the Li_n^+ ($n \leq 6$)[62,111,128,131,164] species, while refs 62 and 164 also contain results for higher nuclearities ($6 \leq n \leq 10$). Electronic structures of the cationic Na_n^+ clusters (or simply IP_v values for Na_n) have been computed in the framework of the HF[131,138–140,143] or LSD[154] theoretical methods. In Figure 1, parts a and b, the best geometries for the Li_n^+ and Na_n^+ species are shown.[62,143] Several important changes in the best nuclear arrangements caused by the ionization process have to be noted. For Li_3 the isosceles triangle becomes equilateral, and the rhombic form of Li_4 transform into a T shape (C_{2v}). The pentamer and hexamer prefer to assume a three-dimensional structure (D_{3h} and D_{2d}, respectively) while Li_7^+ and Na_7^+ preserve their exact D_{5h} symmetry. The cationic octamer is no longer a tetrahedron but a capped pentagonal bipyramid. Li_9^+ has the form of a centered square antiprism, while the C_{2v} structure of Na_9^+ has slightly lower energy than the centered square antiprism. Finally, Li_{10}^+ is a three-capped pentagonal bipyramid.

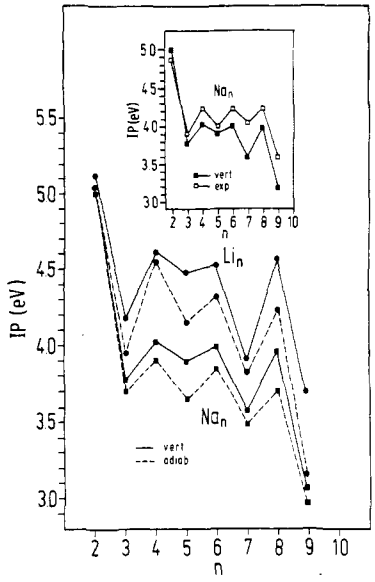

Figure 6. Vertical and adiabatic ionization potentials (IP_v and IP_a) for Li_n and Na_n clusters defined as $E_{CI}(M_n^+) - E_{CI}(M_n)$ as functions of the nuclearity n. A comparison between the calculated IP_v of Na_n and the measured IP[216] is in the window. For details see refs 62 and 143. The vertical process is assumed to take place at the fixed geometry of the neutral species and in the adiabatic process the cationic geometry is allowed to relax.

As expected, due to the geometrical reconstruction of cations with respect to neutral clusters, the IP_a values differ appreciably from the corresponding IP_v. For Li_n, the differences $\Delta IP = IP_v - IP_a$ (which are always positive) have values equal to 0.2, 0.4, 0.2, 0.3, and 0.5 eV for $n = 3$, 5, 6, 8, and 9, respectively. In the other cases, ΔIP values are usually smaller than 0.1 eV.[62] The absolute values of IP_v and IP_a, as well as the differences ΔIP, seem to be markedly dependent upon the theoretical approach adopted for their evaluation and in particular upon the basis set. For instance, in refs 120 and 124 IP_v values equal to 4.33 (3.67), 3.09 (3.16), 3.79 (3.60), and 3.05 (1.99) eV have been computed at SCF (CI) level by using the STO 6G basis, for the clusters Li_n ($n = 2$–5), respectively. These IP values are consistently smaller by about 0.6–1.0 eV with respect to the values of the ref 62 for $n = 2$, ...5 and ref 215 for $n = 2$, 3. The inadequacy of the STO 6G basis is evident if one considers that the values of IP_v computed by Rao et al.[120,124] for Li_n are even smaller than the values experimentally measured for the corresponding Na_n clusters.[12]

As Figure 6 shows the behavior of IP_v and IP_a for Li_n and Na_n as a function of the cluster size is quite parallel, as is also the case for the K_n species studied in ref 140. The ionization potentials are characterized by a pronounced even–odd alternation which is present both in the theoretical and experimental sets of data (for a recent review of the experimental values see refs 12, 18, and 216 and references therein). IP values decrease with the increasing cluster size toward a limit which should correspond to the work function for the bulk metal (2.4, 2.3, and 2.2 eV for Li, Na, and K, respectively). All the reported theoretical data lie, however,

considerably (about 1.5 eV) above the asymptotic value. This is certainly due to the relatively small nuclearities so far investigated. On the other hand, theoretical estimates are lacking for cluster sizes so large that extrapolation to the bulk value would be meaningful. Therefore, the question "is the IP value of the cluster a reliable quantity to prove the appearance of a metallic behavior?" and "how large must a cluster be in order that its IP approximately matches the bulk value?" still remain open and difficult questions.

As shown in Figure 1c, the Δ^2E_n values computed for Li_n^+ and Na_n^+ clusters show an even–odd alternation which is complementary to that of neutral clusters. The behavior, however, can be easily rationalized in terms of the number of valence electrons. Both for neutral and cationic clusters, the Δ^2E_n values are always large and positive for an even number of valence electrons and negative for odd. This means that while for neutral clusters processes like $A_{2m} \rightarrow A_{2m-2} + A_2$ are favored, the cationic clusters follow a fragmentation path of type $A_{2m+1}^+ \rightarrow A_{2m-1}^+ + A_2$. Such behavior of the alkali-metal clusters is predicted by all the ab initio calculations, which perfectly agree with the available experimental data based on photofragmentation experiments carried out on Na_n and K_n species.[167,172-174,217,218]

Alkaline Earth Metal Clusters. Little has been reported for ionization energies of IIa-elemental clusters and the stability of geometry-relaxed cationic Be_n^+ and Mg_n^+, Mg_n^{2+} clusters. The works of Durand[219] and Durand et al.[220] are aimed at analyzing and interpreting the collective effects following the (single and double) ionization processes in terms of static and dynamic polarization. The dynamic polarization, which can be taken into account by means of CI or effective VB treatments, overcomes the inadequacy of the estimate of the ionization energy based only on the SCF energy differences. Neutral and cationic Mg_n ($n \leq 7$) have been studied by using an ECP (basis 4s3p1d)-CVC-CIPSI method. Vertical and adiabatic ionization energies range from about 6.8 (Mg_2) to 6.1 eV (Mg_7). The corresponding IP_a have values lower by about 0.4–0.8 eV (approximate data obtained from Figure 12 of ref 219). It is important to notice that even–odd oscillations of IP's as a function of the nuclearity, characteristic for alkali-metal clusters, are almost completely absent for the IIa clusters. In particular, the IP_a quantities show a smooth convergence toward a value of 5.53 eV evaluated for a Mg_{17} cluster (hcp unit cell). However, this value is considerably higher than the 3.79 eV for the photoelectric work function of Mg bulk.

Reuse et al.[182] reported LSD values of E_b/n for Mg_n and Mg_n^+ ($n \leq 6$), together with a computed atomic ionization energy IP_1 of 7.63 eV (the experimental value is 7.64). It is easy to show that the adiabatic ionization potential for the n-atom cluster obeys $IP_a = n[(E_b/n) - (E_b^+/n)] + IP_1$, where E_b^+/n is the binding energy per atom for a cationic species: $E_b^+/n = [(n-1)E_1 + E_1^+ - E_n^+]/n$. Therefore the data of Table I in ref 182, allow us to compute the values IP_a = 6.33, 5.86, 6.31, 5.48, and 5.77 eV for n = 2–6 which, when compared with the HF-CI values of Durand et al.,[219,220] seem to be consistently smaller by about 0.4–0.5 eV, and, which exhibit a well-pronounced even-odd alternation.

Ia–IIa Mixed-Metal Clusters. Only one systematic ab initio study has been reported on cationic $MgLi_k^+$, $MgNa_k^+$, and $BeLi_k^+$ mixed clusters.[184-186] The structures and stabilities E_b/n for the $MgNa_k^+$ cations are reported in Figure 2a. It is apparent that the ionization

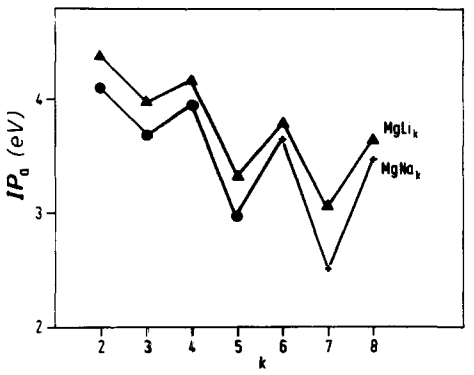

Figure 7. The adiabatic ionization potentials (IP_a) for MgY_k (Y = Li and Na) as a function of k. They are obtained as the CI ground-state energy difference between cationic and neutral species at their best geometries (cf. ref 186).

of the neutral $MgNa_k$ clusters has two important effects. First, there is a strong increase in E_b/n values, even in the case of very small clusters (k = 1–3), which become quite stable species. Second, the topologies for the cations are nearly always coincident with those of the neutral clusters, a fact which was not observed in the case of homogeneous Ia-elemental clusters. An exception occurs for $MgNa_5^+$, which assumes a D_{5h} pentagonal structure, thus requiring an important nuclear rearrangement of the neutral precursor. Again, close similarity between the topologies and a parallel trend in E_b^+/n values have been computed for the $MgNa_k^+$, $MgLi_k^+$, and $BeLi_k^+$ series of clusters (see Figure 2b).

The computed IP_a values for the $MgLi_k$ and $MgNa_k$[186] clusters are reported in Figure 7. Alternation occurs for even and odd k. Higher IP_a values for even k are reminiscent of the situation found for the homogeneous Li and Na clusters and confirm that systems with an even number of valence electrons are characterized by large stability. Notice that the IP_a behavior of $MgNa_k$ and $MgLi_k$ as functions of cluster size is parallel. However, the IP_a's of the $MgNa_k$ series have lower values than those of the $MgLi_k$ species.

3. Anionic Clusters

The recent development of experimental techniques allows the preparation of mass-selected anionic clusters and their spectroscopical investigation (see section IV), thus opening a new route to study directly the electronic structure of such complex systems. Since the measured quantities are often closely dependent on the cluster shape, the spectroscopical results can offer indirect but precise information about the preferred geometries.

From a theoretical point of view the Li_n^- species are the simplest examples of metallic anionic clusters, and their study should require a relatively small computational effort. However, two important methodological aspects have to be pointed out. First, in order to describe correctly the electronic structure of negatively charged clusters a special choice of the atomic basis set might be necessary, especially for the smallest clusters in which the amount of net negative charge on each center is relevant. Second, the correct prediction of the electron affinity EA, both vertical (EA_v) or adiabatic (EA_a), requires a more extended treatment of the correlation effects than for neutral clusters. In fact, the one-electron methods may be qualitatively correct for predicting ground-state properties of neutral species or for the evaluation of IP's but usually yield quite unacceptable values for EA. This is particularly valid for small metallic anionic clusters which are characterized

by low values of EA, since they possess an extra electron only loosely bound.

The importance of the correlation effects for determining correct EA values (i.e. E_n^- energies) has an obvious impact also on the procedure adopted for geometry optimization, which, to some extent, should be carried out with correlation effects taken into account.

Therefore, despite the chemical simplicity of the Li_n^- clusters, their study with rigorous quantum mechanical methods may turn out to be a nontrivial task. This is the main reason why very few systematic investigations concerning Ia-metal anionic clusters are known.

The study of Boustani and Koutecký[133] on Li_n^- ($n \leq 9$) uses a small basis set 3s1p augmented by a diffuse s function necessary to improve the estimate of the atomic EA. Several different conformers have been studied in order to identify the most stable geometries. Theoretical vibrational analysis has been performed at the RHF level to check if the stationary point on the BO surface is a local minimum.

Figure 1a reports the trend in the E_b/n values computed at the MRDCI level with the corresponding best cluster topologies. The E_b^-/n values are intermediate between those of neutral and cationic clusters and increase regularly (without pronounced even–odd alternation) in the investigated range of nuclearity. Notice a rapid increase of E_b^-/n value for the trimer and a sharp increase for the heptamer, followed by a decrease for octamer. The trend is analogous to that computed for E_b^+/n values and is complementary to the curve of E_b/n values for the neutral clusters. High IP or low AE values for Li_8 indicate a particular stability which characterizes the clusters with eight valence electrons. Note, however, that Li_7^- is no longer a pentagonal bipyramid, but assumes a structure of C_{3v} symmetry (see Figure 3 of ref 62), which is the second most stable form for the neutral cluster. The D_{5h} structure presents imaginary frequencies. The Li_8^- cluster has a tetrahedral form, with the electronic configuration of type $1a_1^2 1t_2^6 2a_1^1$. Other structures derived from the fcc lattice are less stable than the T_d form.

Åkeby et al.[191] have reported a theoretical SCF-CI study on Cu_n^- ($n \leq 10$) in which the copper atom is treated as a single valence electron atom, but all the core–valence interaction terms have been included in the ECP or CVC operator.

The best cluster geometries found in ref 191 do not coincide, in general, with those reported in ref 133 for Li_n^-. In particular, Cu_4^- is found to be a rhombus, 0.25 eV more stable than the linear form, which seems to be the best one for Li_n^-. Cu_6^- assumes the form of a bicapped tetrahedron (C_s) instead of the bipyramidal structure found for Li_6^-. The largest clusters investigated ($n = 7$–10) also differ in the preferred structures from the Li_n^- clusters. It has been pointed out[191] that the core–valence 3d–4s correlation considered by means of the effective CVC operator is responsible for an important stabilization of the planar or three-dimensional structures with respect to linear ones. In fact, the linear structures (for instance, for Cu_4^-) are found to be preferred in absence of core–valence correlation. On the basis of these results, the claim has been made that some discrepancies between the best geometries for Cu_n^- and Li_n^- could be due just to the fact that standard HF-CI calculations on Li_n^- [133] do not consider the core–valence correlation effects. This problem, however, should be more carefully investigated, since the very accurate results concerning the dimer[147] do not show large CVC effects for lithium. Ab initio ECP calculations with and without CVC corrections for Na_4^- yield in both cases slight preference for the linear geometry with respect to the rhombic ones. Other aspects considered in the study of ref 191 will be reviewed in section IV.C.3, in the context of electron-detachment spectroscopy.

4. Consequences of Shell-Closing and Jahn–Teller Effects for Cluster Properties

Several specific features of the geometrical and electronic structure of the elemental clusters presented in the previous sections can be interpreted and rationalized in terms of general and simple rules.

Elemental clusters, especially the larger ones, have a pronounced tendency to assume very compact and symmetrical structures. As a consequence of compactness and symmetry of the nuclear frame, degeneracies of the one-electron energy levels occur. Since the cluster geometries necessarily belong to subgroups of the spherical group, it is obvious that the actual ordering and degeneracy character of the one-electron levels can be correlated with the corresponding quantities of an idealized superatom. In fact, in previous sections examples have been presented of electronic configurations of clusters (expressed in terms of irreducible representations of the finite groups) which can be easily translated into an atomic-like notation. This allows for a direct correlation between results based on quantum molecular methods (HF-CI or DF methods) and those obtained from the spherical jellium approach. The existence of highly symmetrical clusters (and molecules) is possible only in the absence of Jahn–Teller distortions, a condition which is certainly fulfilled for systems with a number of electrons sufficient to fill completely the sets of degenerate one-electron levels.

The existence of "closed-shell" systems which exhibit particularly high stability is a fact well recognized in the chemistry of molecules and in particular for transition-metal complexes.[17]

Such elementary principles governing the stability of a high symmetric molecular system are expected to be approximately valid also in the case of clusters which do not exhibit exact symmetry. In the presence of high compactness and approximate symmetry, the one-electron energy levels are expected to be almost degenerate. The particular stability of clusters characterized by fully occupied degenerate levels is, of course, also one leading feature of the spherical jellium theory. In this context, such a phenomenon is named "shell-closing"[76,101,221,222] and can occur only for specific numbers of electrons (magic numbers). Notice, that the magic numbers larger than 2 and 8 depend upon the particular assumptions made in defining the effective potential (cf. section II.A.4). Molecular quantum mechanical approaches are able to predict in a very natural and general way why a cluster of given nuclearity and symmetry of the nuclear frame should possess high stability. Moreover, the same theoretical approaches predict the nature of the geometrical distortions, in agreement with the Jahn–Teller (JT) theorem. A very well known example of JT instability is provided by the trimers of Ia and Ib metals for which the D_{3h} equilateral structure is a cusp on the BO surface. The JT $D_{3h} \rightarrow C_{2v}$ distortion leads to two possible stable structures: an acute and obtuse triangle. The determination of the exact energy ordering of the two conformers may require the use of elaborate computational treatments (see section IV). In an analogous fashion, it is easy to

predict that a tetrahedron, trigonal bipyramid, or octahedron cannot occur as best forms for alkali-metal clusters of nuclearity 4, 5, and 6, respectively. Oppositely, the ionization of one electron, leading to the cationic clusters, can remove the JT instability, leading to species, which are more symmetrical than the original neutral one.[62] This is the case, for instance, of the nuclearities 3, 5, and 9. On the contrary, it is clear that the ionization of highly symmetrical (closed-shell) clusters, like Li_8 (T_d), produces a cationic species with seven valence electrons with much lower symmetry (C_s, capped pentagonal bipyramid).

A more complicated situation occurs for anionic clusters of the Ia- and Ib-group elements. The structure of the cluster deviates from an idealized highly symmetrical one not only due to JT distortions but also since relatively low compactness of clusters minimizes the Coulomb repulsion due to the excess of negative charges. Large net negative charges are usually located on the exposed atoms with low coordination number. This can easily explain the existence of linear forms for trimers, tetramers and pentamers of the Ia-metal clusters.

The shell-closing phenomenon is certainly a relevant factor for the stability of a cluster. However, due to the results from jellium-type calculations its importance has been overemphasized. For larger clusters, the additional $(n + 1)$-th atom added to a compact cluster with n atoms can lower the average coordination number reducing the cluster stability due to a purely geometrical effect as experimentally found by Martin et al.[77] and pointed out by Koutecký and Fantucci in the work published in ref 20.

In fact, the E_b/n curves determined by molecular quantum methods (HF or DF) (see Figure 1, parts a and b and Figure 2, parts a and b) do not exhibit very pronounced maxima for clusters with "magic numbers" of valence electrons. On the contrary, E_b/n seems to be a fairly smooth function of n. This is a quite general tendency, which is characteristic for clusters of all the elements so far studied with rigorous theoretical models. For example, E_b/n for neutral alkali-metal dimers and octamers exhibit maxima which are also found for cations and anions with two and eight valence electrons. The clusters with three and nine valence electrons always have slightly smaller E_b/n than those with two and eight electrons, respectively. Relatively high values of E_b/n have also been calculated for Li_{20} and Na_{20}. These results are in full agreement with the qualitative analysis of section II.A.4 and with the predictions of the jellium model. Notice, however, that although the maxima of the E_b/n functions are not very pronounced, the quantities Δ^2E_n exhibit large maxima not only for clusters with two and eight but also for those with four valence electrons. The examples of mixed clusters $MgLi_k$, $MgNa_k$, and $BeLi_k$ also show more pronounced even–odd alternation for Δ^2E_k than for E_b/n. Generally, size-dependent functions of E_b/n and Δ^2E_n obtained from quantum chemical investigations contain additional information with respect to the results obtained from simple models. The deformation of the jellium sphere into spheroidal or elipsoidal shapes introduces even–odd alternations of the E_b/n and Δ^2E_n. The argument is more or less analogous to the rationalization of the cluster shape deformation due to the pseudo-Jahn–Teller effect. The jellium theory assumes that the appropriate model of the tetramer and the pentamer is a prolate and an oblate spheroid, respectively. The quantum molecular calculations predict for both clusters planar structures. The overall predictions of the jellium model for the structural deformation of clusters with nuclearity smaller than 10 are rather arbitrary (cf. section II.A.4).

It is natural to raise the question about the intrinsic nature and origin of the high abundancies experimentally observed in mass spectra of alkali-metal clusters.[70,221,223–225,170] The occurrence of maxima in the recorded intensities for specific nuclearities did contribute essentially in designing interpretative models, including magic numbers. The following question, however, must be answered in a precise way: "are the high abundances of clusters with magic numbers of valence electrons due to the intrinsic stability of the parent species A_n^+ or are they due to accumulation of stable A_n^+ species generated from dissociation processes of clusters of higher nuclearity?" Clearly, no easy answer can be obtained from the analysis of experimental data concerning clusters characterized by a relatively high internal temperature (vibrationally "hot" clusters). Recent measurements carried out on very cold clusters[226] have pointed out, in agreement with ab initio results, that the emphasis placed on the shell-closing phenomenon as being the factor principally responsible for the high abundancies should be reconsidered at least for small clusters.

C. Physical Properties Dependent on Cluster Size and Cluster Shape

As discussed previously, E_b/n is a typical quantity which depends both on the shape and the size of clusters. The computed curves for E_b/n, although yielding rich physical information, cannot be related in a direct way with any of the quantities experimentally accessible. On the other hand, experimental data for IP and EA values can be obtained with a good accuracy and for a broad class of nuclearities. Although the dependence of these quantities upon cluster size is enlightening, the information about cluster shape does not emerge from experiments. Of course, only rigorous quantum mechanical calculations based on Hamiltonians in which the positions of the individual nuclei are considered can represent a reliable tool for investigating the dependence of cluster properties on cluster shape. In this sense, not only the difficulties inherent in the assumptions of a spherical positive background can be overcome, but it is possible to point out to which extent the cluster shape is important for specific properties. In fact, it is widely recognized that a spherical jellium approach fails to yield a complete and qualitatively correct description of all the cluster properties and for this reason, the spheroidal jellium theory[73] has been introduced.

For simplicity, the following discussion will refer only to the Ia-elemental clusters. IP and EA values for alkali-metal clusters show a clear tendency toward lower and higher values, respectively, when the nuclearity increases. The trend is evident, in spite of the even–odd alternation, as already discussed. In the case of Li_n and Li_n^+,[62] the number of different isomers identified as local minima is sufficiently high to allow a discussion of the shape-dependence of the IP_a values. For the trimer the D_{3h} and $D_{\infty h}$ forms of Li_3^+ are associated with IP_a values which differ by about 0.69 eV. For tetramer only one stable (C_{2v}) isomer has been found, while for the pentamers the two forms of Li_5^+ are nearly degenerate, with IP_a values differing only by 0.03 eV. For n = 7–9 the

corresponding differences are 0.23, 0.13, and 0.30 eV. Thus, in several cases, different isomers have IP_a values characterized by differences definitely larger than the estimated experimental error, which is, for instance, in the case of Na_n clusters often smaller than 0.1 eV (see refs 8 and 256 and references therein). Therefore, the ionization potential can be considered in principle as a quantity useful for selecting among different possible cluster shapes. This, of course, is true in particular for small clusters, while in the case of large species one can expect that several isomers exist with similar compactness, symmetry, and stability both for neutral and cationic forms with corresponding very similar values of IP_a.

Analogous considerations can be applied also to the measured EA values. In this case, the combined use of experimental and theoretical results seems to be a very powerful tool for establishing (or at least suggesting) possible structures for the ground state of the anions. The EA values are often obtained from photodetachment experiments, in which transition energies to excited states of the neutral clusters are also measured (cf. section IV.C.1). The importance of rigorous quantum mechanical treatment in this context will be discussed in details in section IV.

A physical quantity directly connected with the electronic charge distribution in clusters in the ground state is the static dipole polarizability, which has been measured by means of molecular beam deflection experiments for Na_n and K_n clusters ($n \leq 40$).[227] From a theoretical point of view, static dipole polarizabilities can be computed employing the coupled Hartree–Fock theory or the finite field approach. The latter allows for the determination of the diagonal components of the polarizability tensor (α_{xx}, α_{yy}, α_{zz}) via SCF or CI calculations repeated for different values of perturbing homogenous electric field. An analogous procedure can be employed in connection with LSD calculations. In any case, the determination of reliable values for α requires the choice of sufficiently flexible basis set, since obviously in this case the description of polarization effects is essential.

Calculations of $\bar{\alpha} = (\alpha_{xx} + \alpha_{yy} + \alpha_{zz})/3$ for alkali-metal clusters have been carried out also in the framework of the jellium theory (see, for instance refs 93, 228 and 229) but the results from quantum molecular models are more relevant for a discussion of the shape dependency.

LSD methods have been employed to compute $\bar{\alpha}$ or the associated value $\beta = \bar{\alpha}_n/n\alpha_1$ (α_n and α_1 are the polarizability values for the n-atom clusters and the single atom, respectively) for a series of different isomers of Na_n clusters.[151-153]

In the latter studies, the authors have explicitly stated that $\bar{\alpha}$ is a quantity particularly sensitive to variations in the cluster shape, especially for small nuclearities. Only for specific cluster shapes which are the best ground-state geometries or energetically close lying isomers, the theory yields values whose trend is parallel to the observed trend. The results of Mullet et al.[151-153] have been recently substantially confirmed by the results of SCF and CI calculations carried out on Li_n (AE) and Na_n (ECP–CVC) clusters.[230] In Figure 8 the results for Li_n species are reported and compared with the experimental data of ref 227. Even–odd alternations are pronounced for the smallest clusters, while the averaged polarizability per atom β becomes a smooth function for higher nuclearities, in agreement with the experimental finding.

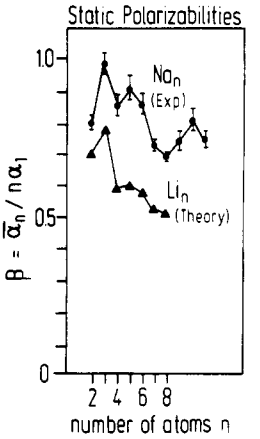

Figure 8. A comparison between calculated static polarizabilities for Li_n as a function of the cluster size[230] and the measured polarizabilities for Na_n.[227] The CI values for the static polarizabilities α are obtained by using the Hamiltonian in which a homogeneous external field E is considered, from the expression $E(E) = E_0 - \mu_0 E - (1/2)E\alpha E$, where E_0 is the energy of the unperturbed system and the dipole moment is $\mu(E) = \mu_0 + \alpha E$.

The cluster shape has even more pronounced effects on the components α_{ii} ($i = x, y, z$) than on $\bar{\alpha}$ values. For instance, the components of α for acute and obtuse forms of Na_3, reported in ref 151, are α_{xx} = 50.6, 78.8; α_{yy} = 46.6, 74.3; α_{zz} = 34.3, 36.0 Å^3, respectively (xy is the plane of the nuclear frame).

For Na_n, pairs of isomers have $\bar{\alpha}$ values equal to 76.3, 92.3 (n = 4), 100.3, 112.7 (n = 6), 111.7, 120.0 (n = 8), and 136.7, 135.3 Å^3 (n = 9). The differences, seem to decrease with the increasing nuclearity showing that large clusters, although having different shapes, are characterized by electronic distributions which respond in a similar manner to an external perturbing electric field.

D. Nature of Interatomic Interactions in Small Elemental Clusters

The study of the nature of the atom–atom interaction as characteristic of the elemental clusters can, in principle, be carried out on the basis of the analysis of the electron density of the associated wave function, determined at the HF-CI or LSD level of theory. Notice, however, that such an analysis has been carried out for alkali-metal clusters, while for other elements the analysis is limited only to the gross atomic and orbital populations.

Mulliken analysis has been reported, for instance, for Li_n and Li_n^+ clusters[62] pointing out that the p functions of Li are definitely important: in the series Li_3–Li_9 their (average) occupancy on each center ranges from 0.14 to 0.25. Therefore, the p functions cannot be considered simply as polarization functions, since they are involved in a quite important hybridization process.

The role of the polarization–hybridization functions in the electronic wave function of alkali-metal clusters as well as of other elemental clusters has been extensively discussed in several papers.[130,220,231-233] It has been concluded that the stabilizing effect of the p orbitals is essential in ab initio treatments, but it can be also described by a basis set including only s functions, provided that use is made of an appropriate model Hamiltonian. In addition, the analysis of the CI wave function in terms of VB structures, revealed the existence of important contributions from ionic structures.[115,116,234-237]

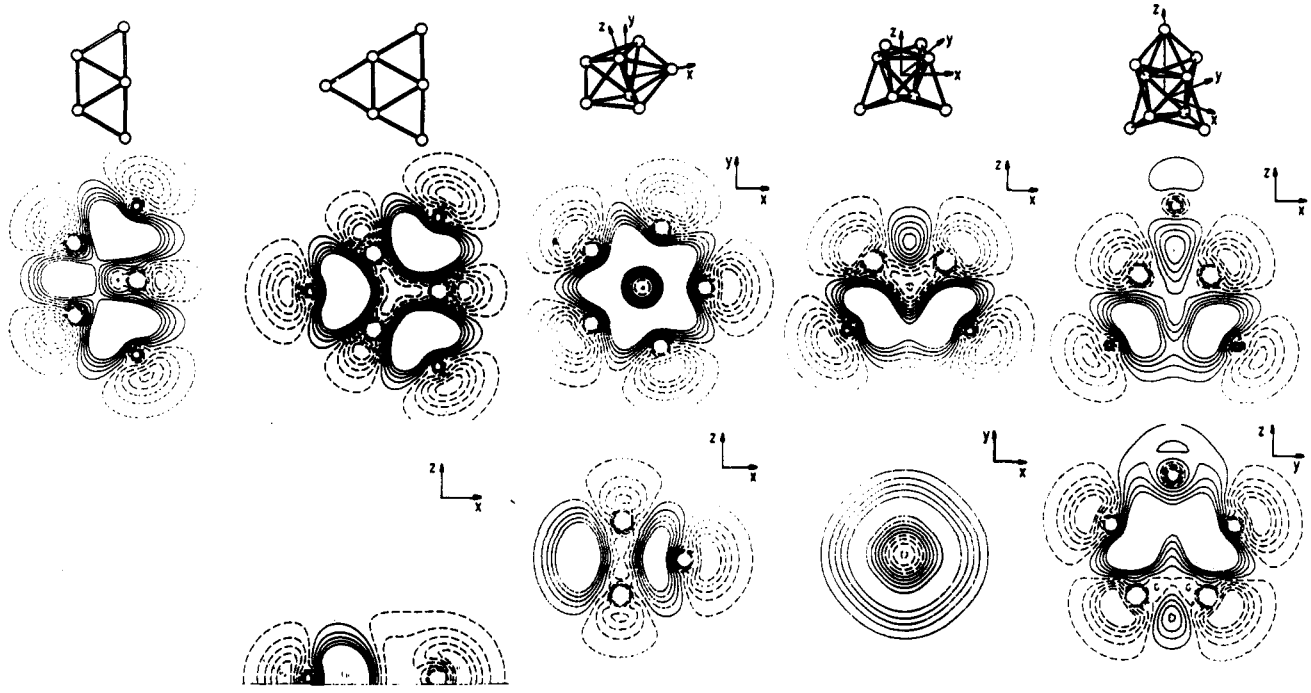

Figure 9. Difference one-electron density (DOD) maps for Li_n (n = 5–9). The coordinate axes define the planes of cuts displayed. The full and broken lines represent constant positive and negative values of DOD, respectively (cf. ref 62).

Worth mentioning are the studies[62] based on the analysis of both the total electron-density maps and distortion-density maps (obtained by subtracting out the contributions of the constituent atoms, assumed to be spherical) for a series of Li_n clusters. An accumulation of electron density in the centers of triangles in the planar forms of Li_4, Li_5, and Li_6 is apparent. Also in the case of larger three-dimensional clusters, no evidence has been obtained of accumulation of charge between pairs of atoms, which would correspond to the formation of a conventional two-center bond (cf. Figure 9). Therefore, it is possible to conclude that Li_n clusters are characterized by delocalized distribution of all the valence electrons. The SCF-MRDCI wave functions of Li_4, Li_5, and Li_6 have been analyzed by Gatti et al.[150] on the basis of the topological approach proposed by Bader.[238-240] The study did confirm the existence of maxima of electron density at the centers of triangles, a situation markedly different from that of normal molecules, for which the density maxima occur generally only at the nuclear positions. According to Bader's theory, the maxima at the nonnuclear positions have to be characterized as "nonnuclear" attractors, i.e., as central points of basins (quantum mechanical subsystems fulfilling, for instance, the local virial theorem) which essentially contribute to the cluster stability. In fact, no direct Li–Li bonds have been identified, and the bonding interactions must be classified essentially as three-center bonds. This conclusion is basically identical with that reached by Hall,[137] in a study of Na_4, Na_5, and Na_6 based on the path-integral approach. Finally, the existence of unusual metal–metal interactions caused by electrons not localized according to the usual chemical schemes has also been pointed out on the basis of GVB studies of alkali-metal clusters[117,118] and aluminum clusters.[241,242]

Concerning the electron charge distribution in clusters, it is important to emphasize a fact which is entirely evident in a molecular or chemical context, but which is often interpreted in a completely different way in the framework of the spherical jellium theory.

In the case of highly symmetrical clusters the charge distribution assumes a symmetrical shape, which is sometimes close to spherical. For instance, in the case of the octamers of the alkali-metal clusters which are composed of two tetrahedra, the charge density is composed of two quite distinct shells (see Figure 9) associated with the atoms belonging to the inner and outer tetrahedron, respectively. A situation entirely equivalent from a topological point of view is expected, for instance, in the case of the octahedral clusters $MgLi_6$ or $MgNa_6$. It is obvious that the shape of the charge density is a direct consequence of the symmetry of the assumed electron–nuclear potential. Spherical or very symmetric potentials give rise to spherical or very symmetric densities. This clearly does not mean that nearly spherical densities necessarily have to be associated with potentials in which the actual positions of the nuclei are irrelevant. Thus, the claims that spherical electron densities for alkali-metal clusters support the validity of the jellium model have to be carefully reconsidered.

E. Comparison of Concepts and Results Obtained from Quantum Molecular Methods and Other Approaches

As commented in previous sections, the different theoretical methods applied to the study of the electronic structure of clusters in their ground state are either quantum molecular methods, based on HF (or HF-CI) or DF (LSD) theories, or methods based on jellium (spherical or spheroidal) models. The methods belonging to the first group are equivalent regarding the adopted potential created by the nuclei (point charges at given spatial positions) and differ essentially by the assumed form of the exchange-correlation potential. The HF-CI methods are able to give an accurate

many-electron wave function while DF approaches are basically one-electron models. Despite these differences, the HF-CI and LSD methods, in general, are in agreement at least in the predicted trend of the computed quantities, such as the most favorable cluster geometries, cluster stability, and ionization potentials. Of course, the two groups of methods may be in disagreement as for the absolute values of some cluster properties, especially when the LSD methods are applied without self-interaction correction (SIC). It is very well known, for instance, that SIC can strongly reduce the values of the computed binding energy, which is usually overestimated by the LSD methods.

More difficult are the comparisons between the quantum molecular methods and the jellium approach, due to the large differences in the basic assumptions. The only point in which all the methods are qualitatively in agreement concerns the "spherical" clusters and their properties.[70,93,123,132,243-250] As discussed above, the agreement is due to the high symmetry of the nuclear potential. Notice, however, that also in this case the jellium model always overemphasizes the stability of the closed-shell structures. For clusters with a number of valence electrons different from one of the magic numbers, the comparison between methods using molecular and jellium potentials is difficult, since the specific features of the results depend in this case just on the departure of the actual potential from spherical symmetry. The spherical jellium models have been originally justified by the observation that alkali-metal clusters are "soft", easily melting species, for which the effective nuclear positions are irrelevant, especially at high temperature. However, the molecular dynamic studies (LSD-QMD)[157] indicate that shapes of clusters with closed electronic shells (8 and 20) deviate from the sphericity with increasing temperature. This finding does not support a spherical liquid droplet picture. Also other examples of jellium-type calculations reported in the literature do not always seem to conform to the basic hypothesis of complete atomic mobility. For instance, large clusters composed of IIa-group elements are characterized by higher stability than the corresponding clusters of the Ia group. The three-dimensional structures for Be or Mg clusters seem to be largely preferred over planar structures also in the case of very small systems. As a consequence, some of the features of the IIa-group clusters are expected to be more shape dependent than in the case of alkali clusters. Jellium calculations on Mg clusters have been reported[245,74] with the aim of discussing shell-closing properties, stability, and fragmentation channels. The problem of the electronic structure of the mixed Ia–IIa clusters has also been addressed by the jellium theories.[251,252] These clusters assume in general a very compact structure with the IIa atom at the center of the regular polyhedron. Therefore, the high symmetry of the cluster would suggest that a jellium approach is applicable. However, the strong Ia–IIa interaction, which is maximized only in the case that the IIa atom occupies a central position, makes the cluster structure much more rigid than that of the alkali metals, in contrast with the jellium potential assumption.

Finally, the reliability of the jellium approach for the study of clusters composed of heavy metals such as Al and Pb,[74,101,253] Cu,[254] and Ag[254,255] has never been demonstrated.

IV. Excited-State Properties

A. Experimental Spectroscopic Methods

In the last 5–10 years there has been a rapid development of the optical response spectroscopic techniques which aim to probe the size-dependent structural properties of clusters via their electronically excited states. They represent a more direct tool for determining the characteristic electronic and geometrical features of clusters than the previous measurements of the properties such as molecular beam abundances,[7,12,70,71,223,224] ionization potentials (see for example refs 216 and 256), polarizabilities (Na_n[227] and Al_n[257]), and chemical reactivity[18] (section III.B,C). The information about structures has been available from the ESR studies[258] in matrices, with obvious limitations such as no direct information about the particle size and the influence of the matrices (for example alkali-metal trimers[259] and heptamers[160]). The first gas-phase absorption experiments were most extensively performed on metal trimers by laser-induced fluorescence (LIF) (Na_3,[260] and Cu_3[261,262]) and multiphoton ionization (MPI) (Na_3,[263,264] Cu_3,[265] Ag_3,[266] Al_3,[267] Li_3,[268] $LiNa_2$, and Li_2Na). The interpretation of absorption spectra of trimers in terms of the dynamical Jahn–Teller model will be discussed in section IV.C.2. However, both techniques, LIF and MPI, have not been successfully applied to larger clusters in part due to the dissociative nature of their excited states. This has been recently overcome by the two complementary techniques of photodetachment[10,11,13,269-276] and photodissociation[277-283] spectroscopies, applied to negative ions and to neutral or positively charged cluster beams, respectively. Both techniques are capable of accessing a large part of the spectrum of excited states, in principle, for any cluster of any element or combination of elements, and they take into account the specific particle size.

In the framework of photodetachment spectroscopy two complementary lines have been followed by using pulsed[11,275,284] and continuous[10,271] ion sources. The photodetachment spectra using the latter technique, which has higher resolution (10 meV) but is not applicable to the far and extreme ultraviolet, have been recorded for Ib clusters: Cu_n^- (n = 2–10),[269-271] Ag_n^- (n = 2–10),[271] and Au_n (n = 1–5)[271] and for alkali-metal clusters: Na_n^- (n = 2–5,7), K_n^- (n = 2–7), Rb_n^- (n = 2–4), Cs_n^- (n = 2,3), $(NaK)^-$, $(Na_2K)^-$, $(KRb)^-$, $(KCs)^-$, $(K_2Cs)^-$, and $(RbCs)^-$.[10,276] The pulsed technique has been widely used, and numerous spectra have been measured for Ia, Ib, IIIa, and IVa clusters which are reviewed in refs 9, 11, 13, 285, and 286. From the photodetachment spectra the optically allowed and forbidden states of the neutral clusters are accessible but are obtained at the ground-state geometries of the anions. If the geometries of small neutral clusters differ from those of their anions, the structural information about the neutral species from the spectra is not direct. Also, relatively small portions of the spectra of neutral clusters are accessible through photodetachment measurements, since they are recorded summed with the vertical detachment energies (VDE), defined as the energy difference between the ground states of the anion and the neutral cluster at the geometry of the former. Nevertheless, ultraviolet photoemission spectroscopy (UPS) with photon energy of 7.9 eV has been successfully

applied (for example to C_{60}^-[9] and very recently, to the resolution of the d band for Cu_n[287]). Both powerful techniques, pulsed and continuous, produced large amounts of data, such as electron affinities EA and VDE corresponding to the onset of intensities and to the first maximum in the spectrum, as well as additional bands corresponding to excited states of the neutral clusters. Characteristic fingerprints have been found as a function of the cluster size (e.g. oscillatory behavior of EA) and the demand for theoretical interpretations became enormous. There are two major difficulties with this type of experiments: (i) the clusters produced are not supercold, and (ii) there is, in general, no selectivity among the cluster geometries studied. Difficulties on the part of the theory are also large, since there are many isomers to consider, and in the case of larger clusters the density of excited states becomes very large and prohibitive for the molecular treatment. Nevertheless, through the interplay between theory and experiment, reliable structural information about differences and similarities between anionic and neutral clusters can be obtained at least for Ia and Ib clusters.

The theoretical interpretation of the photodetachment spectra will be discussed in sections IV.C.1 and IV.D.1. Several lines have been followed: (i) electron affinities have been determined by using simple qualitative highest occupied and lowest unoccupied molecular orbitals (HOMO–LUMO) considerations based on the jellium model (e.g. for Cu_n^-),[272] (ii) more sophisticated quantum chemical approaches have recently been successfully employed, ranging from semiempirical to ab initio versions for EA of Si_n^-,[288] C_n^-,[289-292] Cu_n^-,[191,199,293-294] and (iii) complete quantum chemical interpretation of all bands of photodetachment spectra obtained by using a continuous beam has been limited until now to small alkali-metal clusters.[144,162,295]

Photodissociation spectroscopy offers a good opportunity to address the structural properties of clusters directly and large portions of optically allowed transitions have been recently covered. The first spectra of tetramers Na_4,[279] Cu_4^+,[281] and Li_4[283] have been very recently recorded by photodepletion, exhibiting a rich pattern. In the case of Cu_4^+[281] and Li_4[283] the vibronic structure of several electronic transitions has also been resolved. The complete quantum molecular interpretation of absorption spectra of alkali-metal tetramers will be discussed in section IV.C.2. The first photodissociation experiments on clusters larger than tetramers have been carried out for Na_n (n = 8, 9, 10, 12, 16, and 20),[277,296,297,298] but with low resolution and only for selected visible wavelengths, so that some spectral regions have not been covered. These measurements have been interpreted in terms of classical collective electronic oscillations in spherical, spheroidal (or elipsoidal) metal droplets, since they exhibited from one to three broad maxima (cf. section IV.D). In the case of cationic clusters K_n^+ (n = 9, 21)[278] a pronounced single intense transition was observed, resembling a "giant resonance" found for the interaction of atomic nuclei with electromagnetic radiation. Similarly the photoabsorption spectra of two closed-shell clusters Cs_8 and $Cs_{10}O$[282] have been interpreted as due to plasmon or plasmon-enhanced excitations. The high-resolution spectra for Na_n (n = 3, 4, 8, 20),[279,280,308] Li_n (n = 2–8),[283,299,300,301] and Li_yNa_x[302] also became available, covering a good part of the spectral region. These experimental findings called for theoretical interpretation using more sophisticated quantum molecular models,[158,162,300,301,303-307] since the presence of quantum effects[279,280,308,309] became evident.

B. Methodological Requirements for Application of Quantum Chemistry

One of the early successes of the quantum mechanical ab initio CI methods has been the determination of the spectroscopic properties of small molecules such as diatomics and triatomics.[310] The study of vertical excitations (i.e., in the neighborhood of the ground-state equilibrium geometries; so called spectroscopic minima) as well as geometrical relaxations in the excited states (energy potential surfaces) important for photochemical processes[311] put large demands on the computational tools. After gaining some experience, these methods have also been successfully applied to larger systems. Two factors determining the accuracy of the calculations are the choice of the atomic–orbital basis set and an appropriate treatment of the correlation effects. These requirements are much more severe for adequate description of excited states than in the case of the determination of the ground-state properties. This is true not only from the numerical point of view but also for extracting the qualitative information from the nature of the wave functions of the excited states, which is crucial for understanding the underlying principles governing the physical and chemical processes involved.

This is particularly important for the study of excited states of clusters. The difference in the nature of chemical bonding between small clusters and "normal" molecules and solids, which is present in the electronic ground state, is even more pronounced in the excited state. Since the study of the latter should serve for characterization of mostly yet unknown specific structural and electronic properties for the given size of the cluster, in connection with optical response experiments which are in progress, the approximations involved in the description of excited states should be kept at a minimum. After knowledge about the leading factors determining these characteristics is gained, the nature of the methodological simplifications acceptable in models applicable to larger clusters can be set.

The use of ab initio CI methods for the description of excited states is limited to small clusters with a small number of valence electrons. These limitations are connected with the fact that the calculation of one vertical spectrum for the ground-state equilibrium geometry of a cluster involves determination of individual electronic (quantum mechanical) excited states with given multiplicity and symmetry. This implies that the number of states in the energy regime of interest, which is several eV, can be large, and the balanced description of the close-lying excited states of the same symmetry and multiplicity is not an easy task. Therefore the ab initio CI methods have only recently been applied to the study of a number of excited states of s^1-electron metal clusters larger than trimers.[158,162,295,300,301,303-305]

Apart from their predictive power, these calculations should serve as a guidance for the other approaches, such as the ab initio response theory or the ab initio random phase approximation (RPA).

The Appropriate Atomic Orbital Basis Set. The AO basis sets are usually determined to yield an optimal

energy for an atom, but the polarization functions are added to account for the molecular environment, and the basis can be extended by adding the functions which are important in correlation treatments (there is not always a strict distinction between polarization and correlation orbitals).[310] Numerous AO basis sets are tested, mainly for the ground states, and there are many studies about the influence of polarization and correlation orbitals on the total energies, dissociation energies, bond lengths, and other ground-state properties. (The influence of polarization p functions on the stability of Li clusters has been discussed previously.[1,149]) The results of these investigations are also valid in general for excited states, and moreover, the correlation orbitals might be even more important, since reliable determination of transition energies requires adequate calculation of the difference in correlation energies for different states. However, fortunately, in a molecule or a cluster at the equilibrium geometry, or close to it, there are many molecular orbitals with adequate nodal properties which can mimic at least the angular part of correlation orbitals. Therefore, it is not always necessary to introduce many additional correlation functions in order to construct a reliable basis set for the treatment of the excited states, especially if vertical spectra at equilibrium geometries are calculated. Some diffuse functions accounting for the radial contribution of correlation orbitals might be necessary. In the case that the dissociation limits or the whole potential surfaces are needed, the additional correlation functions might be essential for the description of separated parts of the system. Moreover, in many cases, for the reliable description of excited states, orbitals with higher quantum numbers occupied in excited states but not in the ground states, i.e., "spectroscopic orbitals" have to be added.[310] The exponents of Rydberg orbitals are listed in the literature, but in many cases it is reasonable to optimize spectroscopic orbitals for the excited states of interest.

The choice of the AO basis set is closely related to the compromise between accuracy and feasibility. It is also fortunate that sometimes the description of spectroscopic properties of dimers is more difficult than that of larger systems and therefore calculations on dimers can also serve as tests of the quality of the AO basis sets. For example, in the case of Li and Na, calculations of the excited states of dimers have been carried out by using relatively large basis sets in the CI treatments prior to the calculations of excited states of alkali-metal clusters (cf. refs 303 and 304 and references therein). It has been possible to obtain CI results of comparable accuracy and in good agreement with the experimentally available spectroscopic constants for dimers by using considerably smaller basis sets: (13s3p1d/6s3p1d) for Li[303] and (12s8p1d/7s4p1d) for Na,[304] modifying the standard basis sets by adequate contractions, splitting the exponents of p functions to reach the optimal $\Delta E(^2S \rightarrow ^2P)$ atomic excitation energies, and adding one d function. These basis sets have then been employed for calculations of excited states of Li_n[303,300,301] and Na_n[304,162] and of mixed Li_xNa_y[306] clusters.

Even these basis sets which are not considered to be sufficiently large for exact treatment of very small systems become impracticable for the treatment of excited states of larger clusters, which are expected to have interesting characteristic optical response properties (for example alkali-metal clusters with 8–20 electrons). This is mainly due to the very large CI space produced by more than 200 one-electron functions if several states of the same symmetry have to be determined, and, therefore, an inevitable severe truncation of the CI expansion might introduce a substantial lack of accuracy. Therefore the use of the nonempirical effective core potentials (ECP), corrected for core valence correlation (CVC)[145] even for alkali-metal clusters such as Na_n and K_n (which has been successfully used for ground-state properties) can be useful for the description of excited states if sufficiently small AO basis sets yielding acceptable accuracy are designed. For example, (4s4p/3s3p) basis set for Na and (6s3p/4s3p) for K yield atomic properties (ionization potential, static polarizability, and excitation energies) in good agreement with the experimental and with the ab initio all-electron values. The calculated and experimental values (in parentheses) of ionization potentials of Na, IP (^2S) = 5.136 (5.139), IP (^2P) = 3.042 (3.035), and of K, IP (^2S) = 4.339 (4.340), IP (^2P) = 2.719 (2.726) eV are in good agreement.[145]

The appropriate description of anionic clusters requires the addition of some diffuse functions, since negative anions have a more expanded charge distribution than the neutral species. For example, the addition of one s diffuse function with $\alpha_S = 0.01$ to the above all-electron basis for Na atom corrects the atomic electron affinity from 0.44 to 0.539 eV, leading to a better agreement with the experimental value (0.548 eV[162]). Similarly, in the CI ECP–CVC calculations, the addition of two diffuse s functions with exponents α = 0.007, 0.0035 to the (3s3p) basis of Na, and with exponents α = 0.002, 0.001 to the (4s3p) basis of K, yields electron affinities $EA_{Na} = 0.540$ and $EA_K = 0.518$,[145] in good agreement with the experimental values of 0.548 and 0.501 eV, respectively.

The influence of correlation and spectroscopic orbitals for description of excited states of other than alkali-metal clusters will be discussed in sections IV.C.2 and IV.C.3. For example, several low-lying excited states have been determined for Ib clusters (trimers and tetramers)[203,205,312,313] as well as for C_4,[314,315] Si_3,[316] and Si_4.[317]

Methods for Calculating Excited States of Clusters. In order to study the excited states of clusters, it is necessary to use theoretical methods able to give a balanced description of excited states of different nature in an energy interval which sometimes requires determination of a large overall number of states and among them many (more than 10) of the same symmetry and multiplicity. For this purpose, only methods which take correlation effects into account are acceptable, since the SCF procedure will give a wrong ordering of states and erroneous excitation energies even for the lowest state of a given symmetry. Until now mainly vertical spectra of Ia clusters (including higher lying excited states) have been studied theoretically. The wave functions of optically allowed excited states often have pronounced multideterminantal leading features.[158,162,300,301,303-306] In the case of geometrical relaxation in excited states, these features are even more pronounced.[136,205,203] Therefore, all the theoretical methods based on a truncated single reference configuration expansion are most probably not adequate for a description of higher lying excited

states of clusters, at least not in the case of Ia and Ib clusters.

The deficiency of the truncated CI expansion is removed to a large extent in a multireference approach in which the reference space (from which single, double, or higher excitations are generated) includes all the configurations which are necessary for the zero-order description of all excited states of the same symmetry and the same multiplicity.[310,318] The aim of such approaches is the balanced description of excited states, so that the transition energies can be calculated in a reliable manner, although the full CI limit is not reached. There are several schemes used to achieve this goal and they can be compared with the full CI results feasible for smaller systems in order to estimate the errors of the approximations (cf. section II.A.2). The reference space can be formed (i) by configurations generated from the complete active space (CAS),[53b] which includes all configurations which can be obtained by distributing n electrons among m orbitals in all possible ways consistent with the symmetry and multiplicity of the state, or (ii) by selection according to energy-lowering criteria leading to a reference set of configurations which appear in the final CI expansion with weight larger than the chosen value. Then, the single and double excitations SD (usually and sometimes higher order) with respect to the reference set can be (i) all included by direct CI[53a] or (ii) the expansion can be truncated again according to the energy lowering criteria chosen (MRDCI).[48,49] Of course, the procedures confined to (i) are more exact, but they are computationally very demanding, and the limit of their applicability is easily reached in the study of excited states of clusters. A comparison and understanding of the spectral pattern for clusters of different sizes requires determination of many excited states of the same symmetry covering the whole spectral region characteristic of the physical phenomena involved.

In connection with the latter requirement, additional methodological difficulties are present, since the choice of one-electron functions for the description of many excited states of the same symmetry in truncated CI is a very important accuracy-determining step. Optimized MO's from MCSCF[318] procedure are usually designed for a given state. For the description of several excited states of the same symmetry, one can use the natural orbitals as one electron functions, or MO's from the lowest excited state of the given symmetry, making sure that the MRCI treatment includes the most important contributions to the CI expansion, so that the description of the higher excited states of the same symmetry does not substantially suffer from this deficiency. Moreover, in the case of metal clusters (e.g., alkali) the ground-state SCF wave function at equilibrium geometries with relatively high symmetry contains many energetically close lying virtual orbitals, so that the number of active orbitals to span CASSCF or MCSCF spaces often becomes prohibitively large. Therefore, a reasonable strategy seems to be to compare the methods by using the complete active space as the reference set and all SD excitations with respect to it and those which select the reference set as well as SD excitations according to the energy lowering criteria for the examples where this is feasible. After estimating the error of the less accurate scheme one can proceed with the application of the latter to determine semi-quantitatively transition energies and other spectroscopic properties for cluster of different sizes.

Table I should serve as an illustration of this strategy. It contains a comparison of transition energies for optically allowed states for the equilibrium geometry of Na_4 obtained from (i) the MRDCI[48,49,320] procedure by using the SCF MO's of the lowest state of the given symmetry; (ii) the MRDCI procedure by using iterative NO's as one electron functions in the CI; (iii) the direct CI[53a,320] procedure with full CI for four valence electrons in the active space of 25 MO's and with SD excitation in the external space of 47 MO's. The deviation in the excitation energies obtained from the MRDCI and the direct CI procedure are not larger than 0.02 eV for the lowest state of the same symmetry (cf. ref 162). Moreover, both procedures yield the equivalent leading features of the wave functions which demonstrates their multideterminantal nature even at the qualitative level of the analysis. (Notice, that the exact values of the coefficients of the leading configurations in the CI expansion given, for example, in Table I are not independent of the choice of one-electron functions.) The errors in excitation energies are surely larger if the calculations of many more than three states of the same symmetry are requested, and they might reach the value of 0.2 eV.

C. Results Obtained with CI and Related Quantum Chemical Methods

1. *Photodetachment Spectra of Anionic Ia Clusters*

Photodetachment spectra of small alkali metal-cluster anions are highly structured and have regular patterns as a function of the cluster size.[10,276] The measured photoelectron intensities are functions of the electron-binding energy which is equal to the difference between the photon energy and the measured electron kinetic energy (e.g., for recorded spectra of Ia anions the photon energy of 2.54 eV has been used). The individual peaks arise due to photodetachment transitions between the ground state of the anion and the ground and the excited states of the neutral clusters. Figure 10 illustrates that the CI energies of vertical transitions at the internuclear distance of the K_2^- anion coincide with the individual peaks of the recorded spectrum. Notice that the first peak corresponds to VDE and the next two bands arise from transitions to two triplet states of K_2. The adiabatic electron affinity EA_a corresponds to the onset of the intensity of the first peak. The vertical transitions to the excited states at the equilibrium geometry of neutral K_2 do not correspond to the positions of the band maxima. Consequently, in order to interpret the photodetachment spectra the equilibrium geometries of the anionic clusters have to be determined first and the spin multiplicity of the states has to be considered.

For small clusters, Li_n^-,[133] Na_n^-,[295,162] and K_n^-,[144] $2 \leq n \leq 5$, linear geometries minimize the Coulomb repulsion due to an extra charge located at the end of the chains and therefore it is to be expected that they are good candidates for the equilibrium geometries. All three anionic trimers are linear according to the ab initio all electron or ECP–CPP calculations. The ground-state energies of linear and rhombic tetramers are almost degenerate. The CI energy difference between the two

TABLE I. Comparison of AE-MRDCI, ECP–CVC-MRDCI, and Direct CI (close to the full CI), Ground and Optically Allowed Excited-State Properties of Na_4 up to 3.3 eV of Excitation Energies for the Optimized Ground-State Geometry of the Neutral Cluster (in D_{2h} Symmetry)

	states	E(CI)[a,b]	T_e,[c] eV	$\varphi \approx$[e]	f,[f]	E(CI)[g]	T_e,[g] eV
	$1^1A_g^a$	−647.445 83	0	0.930 $(1a_g^2 1b_{3u}^2)$		−647.448 20	0
	$1^1A_g^b$	−0.814 00	0	0.925 $(1a_g^2 1b_{3u}^2)$			0
A	$1^1B_{2u}^a$	−647.390 61	1.51	−0.453 $(1b_{3u} \rightarrow 1b_{1g})$	0.008	−647.391 38	1.55
			(1.57)[d]	−0.658 $(1b_{3u} \rightarrow 1b_{2u}, 1b_{3u} \rightarrow 2a_g)$			
				−0.375 $(1a_g \rightarrow 1b_{2u})$			
	$1^1B_{2u}^b$	−0.756 66	1.57	0.404 $(1b_{3u} \rightarrow 1b_{1g})$	0.002		
				+0.669 $(1b_{3u} \rightarrow 1b_{2u}, 1b_{3u} \rightarrow 2a_g)$			
				−0.393 $(1a_g \rightarrow 1b_{2u})$			
B	$1^1B_{3u}^a$	−647.383 31	1.71	−0.899 $(1b_{3u} \rightarrow 2a_g)$	1.180	−647.384 50	1.73
			(1.74)[d]	−0.079 $(1b_{3u} \rightarrow 3a_g)$			
	$1^1B_{3u}^b$	−0.748 81	1.77	0.912 $(1b_{3u} \rightarrow 2a_g)$	1.20		
C	$2^1B_{3u}^a$	−647.377 07	1.87	−0.109 $(1b_{3u} \rightarrow 2a_g)$	0.011		
			(1.92)[d]	+0.725 $(1b_{3u} \rightarrow 3a_g)$			
	$2^1B_{3u}^b$	−0.741 79	1.96	0.717 $(1b_{3u} \rightarrow 3a_g)$	0.016		
D	$1^1B_{1u}^a$	−647.369 93	2.07	0.569 $(1b_{3u} \rightarrow 1b_{2g})$	0.075	−647.371 23	2.09
			(2.10)[d]	+0.561 $(1b_{3u} \rightarrow 1b_{1u}, 1b_{3u} \rightarrow 2a_g)$			
				−0.235 $(1a_g \rightarrow 1b_{1u})$			
	$1^1B_{1u}^b$	−0.733 05	2.20	−0.584 $(1b_{3u} \rightarrow 1b_{2g})$	0.095		
				−0.526 $(1b_{3u} \rightarrow 1b_{1u}, 1b_{3u} \rightarrow 2a_g)$			
				+0.231 $(1a_g \rightarrow 1b_{1u})$			
E′	$2^1B_{2u}^a$	−647.355 69	2.45	0.572 $(1b_{3u} \rightarrow 1b_{1g})$	0.150		
			(2.52)[d]	0.553 $(1b_{3u} \rightarrow 1b_{2u}, 1b_{3u} \rightarrow 2a_g)$			
				−0.235 $(1b_{3u} \rightarrow 2b_{3u}, 1b_{3u} \rightarrow 1b_{1g})$			
	$2^1B_{2u}^b$	−0.719 97	2.57	+0.500 $(1b_{3u} \rightarrow 1b_{1g})$	0.027		
				−0.572 $(1b_{3u} \rightarrow 1b_{2u}, 1b_{3u} \rightarrow 2a_g)$			
				−0.291 $(1b_{3u} \rightarrow 2b_{3u}, 1b_{3u} \rightarrow 1b_{1g})$			
E	$3^1B_{2u}^a$	−647.355 28	2.46	−0.357 $(1b_{3u} \rightarrow 1b_{1g})$	0.81		
			(2.52)[d]	+0.184 $(1b_{3u} \rightarrow 2a_g, 1b_{3u} \rightarrow 1b_{2u})$			
				−0.617 $(1a_g \rightarrow 1b_{2u})$			
	$3^1B_{2u}^b$	−0.717 60	2.63	−0.522 $(1b_{3u} \rightarrow 1b_{1g})$	0.954		
				−0.095 $(1b_{3u} \rightarrow 2a_g, 1b_{3u} \rightarrow 1b_{2u})$			
				−0.553 $(1a_g \rightarrow 1b_{2u})$			
F	$2^1B_{1u}^a$	−647.344 28	2.76	−0.648 $(1b_{3u} \rightarrow 1b_{2g})$	0.796		
			(2.80)[d]	−0.297 $(1b_{3u} \rightarrow 2a_g, 1b_{3u} \rightarrow 1b_{1u})$			
				−0.501 $(1a_g \rightarrow 1b_{1u})$			
	$2^1B_{1u}^b$	−0.706 47	2.90	0.672 $(1b_{3u} \rightarrow 1b_{2g})$	0.672		
				−0.304 $(1b_{3u} \rightarrow 2a_g, 1b_{3u} \rightarrow 1b_{1u})$			
				+0.476 $(1a_g \rightarrow 1b_{1u})$			
G	$3^1B_{1u}^a$	−647.335 46	3.00	−0.472 $(1b_{3u} \rightarrow 2a_g, 1b_{3u} \rightarrow 1b_{1u})$	0.083		
				−0.493 $(1a_g \rightarrow 1b_{1u})$			
				+0.350 $(1b_{3u} \rightarrow 3a_g)$			
G′	$3^1B_{3u}^a$	−647.334 5	3.03	0.315 $(1b_{3u} \rightarrow 3a_g)$	0.002		
				−0.533 $(1b_{3u} \rightarrow 1b_{2u}, 1b_{3u} \rightarrow 1b_{1g})$			
H	$4^1B_{2u}^a$	−647.324 49	3.30	0.411 $(1b_{3u} \rightarrow 2b_{3u}, 1b_{3u} \rightarrow 1b_{1g})$	0.056		
				−0.353 $(1b_{3u} \rightarrow 2b_{1g})$			
				+0.201 $(1a_g \rightarrow 3b_{2u})$			
				+0.209 $(1b_{3u} \rightarrow 3a_g, 1b_{3u} \rightarrow 1b_{2u})$			

[a] CI energies (in au) obtained from 37M/4R (T = 1 μh), 27M/3R (T = 1 μh), and 24M/3R (T = 1 μh) for $^1B_{2u}$, $^1B_{3u}$, and $^1B_{1u}$ states, respectively. AO basis is (12s8p1d/7s4p1d). [b] CI energies (in au) obtained from the ECP–CPP 5M/1R, 20M/2R, 14M/2R, and 30M/3R MRDCI treatment (T = 0) for ^1A_g, two $^1B_{3u}$, two $^1B_{1u}$, and three $^1B_{2u}$ states, respectively. AO basis is (4s4p/3s3p). [c] Transition energies with respect to the ground state in eV. [d] In brackets the excitation energies obtained from the iterative NO procedure. [e] Leading features of the correlated wave functions. Excitations with respect to the ground state configurations are indicated. [f] Calculated oscillator strength. [g] Energies and transition energies obtained from the direct CI procedure with the 25 MO's in the internal space for which the four valence electron full CI has been carried out and with 47 MO's in the external space into which all single and double excitations with respect to internal space configurations have been included in the CI. A to H correspond to labels of experimental bonds.

isomers, ΔE_I (Li_4^-) = −0.10 eV, ΔE_I (Na_4^-) = −0.01 eV, and ΔE_I (K_4^-) = −0.067 eV, lies within the accuracy of the method employed, although in all three cases the linear geometries are slightly favored over the rhombic ones (E ($^2\Sigma_g^+$) < E ($^2B_{2u}$)), independent of the details of the treatment (addition of one diffuse s function to the AO basis set and inclusion of all triple and quadruple excitations).[295,162,144] The stabilities of the planar trapezoidal and linear anionic pentamer geometries are also comparable: ΔE_I (Li_5^-) = 0.01 eV, ΔE_I (Na_5^-) = 0.081 eV, ΔE_I (K_5^-) = −0.029 eV. In the case of Li_5^- and Na_5^- trapezoidal structures are favored, and for K_5^- the linear one has slightly lower energy. For hexamers the comparison is available between Li_6^- [133] and K_6^-.[144] In both cases the D_{4h} topologies of tetragonal bipyramids are more stable than the planar D_{3h} geometries, ΔE_I (Li_6^-) = 0.177 eV, ΔE_I (K_6^-) = 0.120 eV, and more stable than the C_{2v} face-capped trigonal bipyramids (C_{2v}) and the pentagonal pyramids (C_{5v}). Note that the trapezoidal topologies are the most stable structures of the neutral pentamers, while planar (D_{3h}), three-dimensional pentagonal pyramids (C_{5v}), and C_{2v} geometries with tetrahedral subunits of the neutral hexamers have close-lying energies (as already pointed out in section III.B.1). The C_{2v}, D_{3h}, and C_{5v} structure has the lowest energy for Li_6, Na_6, and K_6, respectively. Notice, however that the C_{5v} and D_{3h} structures are almost degenerate in all three cases.

If several anionic isomers are energetically close it is important to calculate their VDE values in order to find

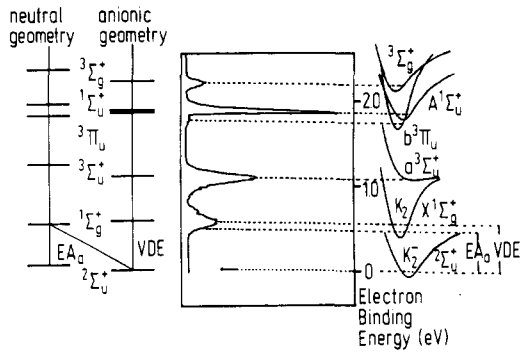

Figure 10. A comparison of calculated[144] and measured[10,276] photodetachment transitions of K_2^- (ECP-CVC-MRD-CI treatment[145]).

TABLE II. Comparison of ab Initio CI and Experimental Values for VDE and EA$_a$ of Na_n^- and K_n^- Anions

	theory		experiment[276]	
species	VDE[a]	EA$_a$[a]	VDE	EA$_a$
Na^-	0.44[b] (0.548)[c]		0.548	
Na_2^-	0.507[b] (0.542)[c]	0.427[b]	0.543 ± 0.010	0.430 ± 0.015
Na_3^-	1.174[b]	1.065[b]	1.158 ± 0.010	1.019 ± 0.060
Na_4^-(RH)[f]	0.768[b] (0.744)[c]			
Na_4^-(L)[f]	1.127[b] (1.097)[c]	0.715[b]	1.145 ± 0.030	0.91 ± 0.15
Na_5^-(PL)[f]	1.035[b] (1.024)[c]		1.200 ± 0.05	1.10 ± 0.10
Na_5^-(L)[f]	1.472[b] (1.450)[e]	0.807[b]		
K^-	0.518[d] (0.518)[e]		0.501	
K_2^-	0.575[d] (0.578)[e]	0.534[d]	0.550 ± 0.010	0.493 ± 0.012
K_3^-	1.110[d] (1.098)[e]	1.601[d]	1.043 ± 0.01	0.956 ± 0.05
K_4^-(RH)[f]	0.760[d] (0.777)[e]			
K_4^-(L)	1.073[d] (1.073)[e]	0.791[d]	1.048 ± 0.025	0.83 ± 0.10
K_5^-(PL)	0.955[d] (1.013)[e]	0.833[d]	1.045 ± 0.022	0.95 ± 0.10
K_5^-(L)	1.345[d] (1.373)[e]			
$K_6^-(D_{4h})$	0.948[d]	0.731[d]	1.091 ± 0.020	0.95 ± 0.10
$K_6^-(D_{2h})$	0.967[d]			
$K_6^-(D_{3h})$	0.770[d]			
$K_6^-(C_{5v})$	0.792[d]			

[a] The CI values in eV. [b] The AO basis set (12s8p1d/7s4p1d) and large scale CI (cf. ref 162). [c] The AO basis from b augmented with one diffuse s function with exponent α = 0.01 (cf. ref 162). [d] The ECP-CPP-CI calculations with the AO basis (4s3p) (cf. ref 145). [e] The AO basis from d augmented by two diffuse functions α = 0.002 and α = 0.001 (cf. ref 145). [f] RH, L, and PL label rhombic, linear, and planar trapezoidal structures, respectively.

out to which extent the corresponding structures contribute to the recorded spectrum, since the internal temperature of the clusters (nonequilibrium distribution) is not exactly known. If the topologies of the anionic clusters differ from the corresponding neutral ones, the VDE values will be considerably larger than in the opposite case (see Table II). If the values of the VDE's for different anionic isomers coincide with the maxima of the measured intensities, the determination of excited states for the neutral species at these anionic geometries is desirable in order to carry out the complete assignment of the spectrum.

A comparison of measured[276] and calculated photodetachment spectra of Na_{2-5}^- [295,162] and K_{2-5}^- [144] is given in Figures 11–14 (cf. also Table II). The spectroscopic patterns of Na_{2-5}^- and K_{2-5}^- in the energy interval up to 2.54 eV differ by the appearance of one additional band in the latter case. Notice that the calculated and measured atomic ^2S–^2P transition for the K atom is lower (1.62 eV) than for the Na atom (2.10 eV). For dimers and trimers the assignment of linear anionic geometries to the spectra is straightforward.

For Na_2^- and K_2^- the VDE values as well as the positions of the first triplet state $^3\Sigma_u^+$ of the neutral dimers coincide with the maxima of the first two recorded bands. The third weak band in the Na_2^- spectrum is due to the pair of $^1\Sigma_u^+$ and $^3\Pi_u$ states lying slightly above 2.0 eV. The equivalent pair of excited states of K_2 coincide with the maximum of the largest peak in spectrum of K_2^- which is located below 2.0 eV. The fourth band in the K_2^- spectrum corresponds to the location of the $^3\Sigma_g^+$ excited state (cf. Figure 11). Similarly, the two lowest states $^2\Sigma_u$ and $^2\Sigma_g$ of the neutral trimers at the anionic linear geometries are assigned to two intense peaks in spectra of Na_3^- and K_3^-. In the latter case two close-lying excited states, $2^2\Sigma_g$ and $^2\Pi_u$, located above 2.0 eV coincide with the third measured band (Figure 12).

The patterns of the K_3^- and Na_3^- spectra differ mainly by the presence of the third weak band in the former case. In order to illustrate that different geometries of neutral and anionic clusters give rise to different spectroscopic patterns, the vertical spectra for the best neutral obtuse isosceles triangles of Na_3 and K_3 have also been shown in Figure 12. The energies of the ground states of Na_3^- and K_3^- at the best geometries of the neutral species are considerably higher, by 0.378 and 0.328, respectively, than at their own best linear geometries.

Notice that if anions with an odd number of atoms have singlet ground states, the vertical transitions for the neutral species take place among doublet states but if the triplets are the ground states, transitions to quartet states can also take place.

Calculated vertical spectra of Na_4^- and K_4^- for the two best linear and rhombic geometries of the anions as well as for the best rhombic geometries of the neutral species, containing the ground states of anions and of the neutral species as well as excited states of the latter, are shown in Figure 13 together with the recorded spectra. This illustrates that (i) the vertical spectra for linear topologies differ substantially from those of the rhombic geometries and that (ii) the differences in the rhombic geometries of the neutral species and of the anions have a considerable influence on the location of excited states of different nature. In the latter case an extra electron causes a deformation of the rhombus toward a square geometry. Therefore, the lowest triplet state $^3B_{1g}$ is close to the ground state ^1A_g, as in the biradicaloid species, since this geometrical deformation is favorable for the triplet state, with the leading configurations having singly occupied HOMO and LUMO. The CI values of VDE_{RH} for rhombic anions are considerably lower than the values of VDE_L for linear anions (cf. Table II). In fact, VDE_{RH} of Na_4^- is lower than the onset of the measured intensity, while VDE_{RH}, of K_4^- just coincides with the onset of the signal. In both cases of Na_4^- and K_4^-, the vertical spectra of linear anions give rise to VDE_L, corresponding to the maxima of the first bands in the measured spectra, the $^3\Sigma_u^+$ states coincide with the second maxima, and the pairs of states $^3\Sigma_g^+$ and $^1\Sigma_u^+$ fall in the energy interval of the most intense bands. A pair of $^3\Pi_g$ and $^3\Pi_u$ states coincide with the fourth measured band in the K_4^- spectrum, which does not appear in the 2.54 eV interval of the Na_4^- spectrum. The vertical spectra for the rhombic geometries of the Na_4^- and K_4^- anions match the recorded spectra less well. For example, a pair of triplet states $^3B_{2u}$ and $^3B_{3u}$ does not coincide with high spectral in-

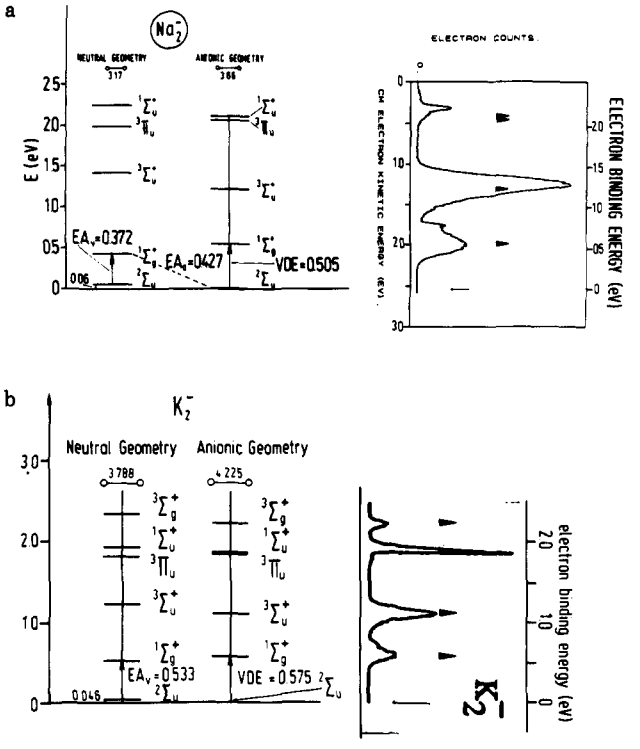

Figure 11. The CI values for vertical transitions and for EA_a of (a) Na_2^-[162] and (b) K_2^-[144] calculated (i) at the best anionic and (ii) the best neutral geometries are compared with photoelectron detachment spectra.[276] AE-CI and ECP–CVC-CI results for Na_2^-, Na_2 and K_2^-, K_2, respectively. Assignment of anionic geometry to the spectrum is labeled as ▲.

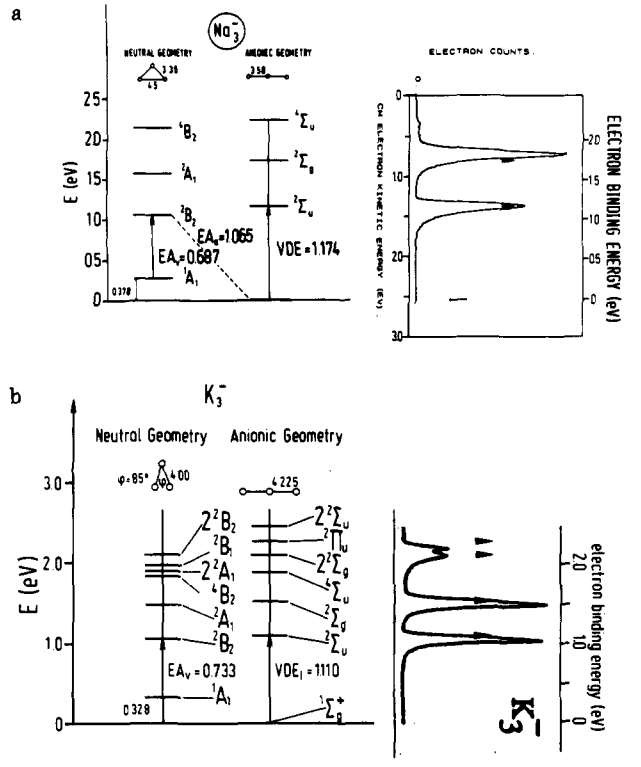

Figure 12. The CI values for vertical transitions and for EA_a of (a) Na_3^-[162] and (b) K_3^-[144] calculated (i) at the best anionic and (ii) the best neutral geometries are compared with photoelectron detachment spectra.[276] AE-CI and ECP–CVC-CI results for Na_3^-, Na_3 and K_3^-, K_3, respectively. Assignment of anionic linear geometry to the spectrum is labeled as ▲.

tensities. Since the optically allowed states lie above the whole group of triplet states and above the "optically dark" $^1B_{1g}$ state, the calculation of the transition moments would not clarify the assignment. In conclusion, the linear geometries of Na_4^- and K_4^- are dominantly responsible for the measured photoelectron detachment spectra, although the contribution of the anionic rhombic geometries is not excluded, particularly in the case of K_4^-.

The recorded K_5^- spectrum is more structured than the Na_5^- one. Nevertheless, the calculated vertical spectra for linear (L) and trapezoidal (Pl) anionic structures of both pentamers exhibit very similar patterns (cf. Figure 14). The VDE_L has a larger value than VDE_{Pl} in both cases, but they coincide with the second and first band maxima in the K_5^- spectrum, and fall in the interval of the broad feature of the Na_5^- spectrum. The excited states of the neutral species at the both trapezoidal and linear geometries of the anions match the energy intervals with high intensities. Although the calculated vertical transitions for trapezoidal geometries of the anions account for the measured spectroscopic patterns by themselves, contributions from the linear geometries cannot be completely ruled out.

The examples of calculated and measured Na_{2-5}^- and K_{2-5}^- spectra show clearly that there is a substantial difference between the geometries of anions and neutral species (which seems not to be the case for Ib anions, cf. sections III.B.3 and IV.C.3). Moreover, the structural assignment of spectra can be accomplished if in addition to the VDE values, the energies of excited states are calculated. This is also decisive for the determination of contributions from different isomers with comparable energies, which is not always possible on the basis of their VDE values. The photodetachment spectra of small alkali-metal anions exhibit very characteristic features which are due to their linear (Na_{2-4}^-, K_{2-4}^-) and planar (Na_5^-, K_5^-) geometries, although in the case of tetramers and pentamers the mixture of both is not excluded. As pointed out already, presently available experimental data might still contain a mixture of different structures, although the development of cold cluster sources is in rapid progress and the first vibrational structure of small anions has been recorded.[271]

In order to carry out the complete assignment of the photodetachment spectra in a semiquantitative way, the optimization of anionic geometries is needed, correlation effects have to be taken into account, and spin multiplicities of all excited and ground states have to be considered. For the large clusters the increasing density of optically allowed and dark excited states, especially if more than one isomer is considered, presents a problem, and simplified approaches might be useful (cf. section IV.D.1).

2. Photoabsorption Spectra of Neutral and Cationic Ia Clusters

The interpretation of absorption spectra of small clusters represents an inviting subject, where concepts taken from different fields, such as nuclear physics, solid-state physics, and quantum chemistry, require careful consideration. This is closely connected with a desire to define at which size and due to which characteristic property small clusters might or might not exhibit metal bulk properties. Since the available

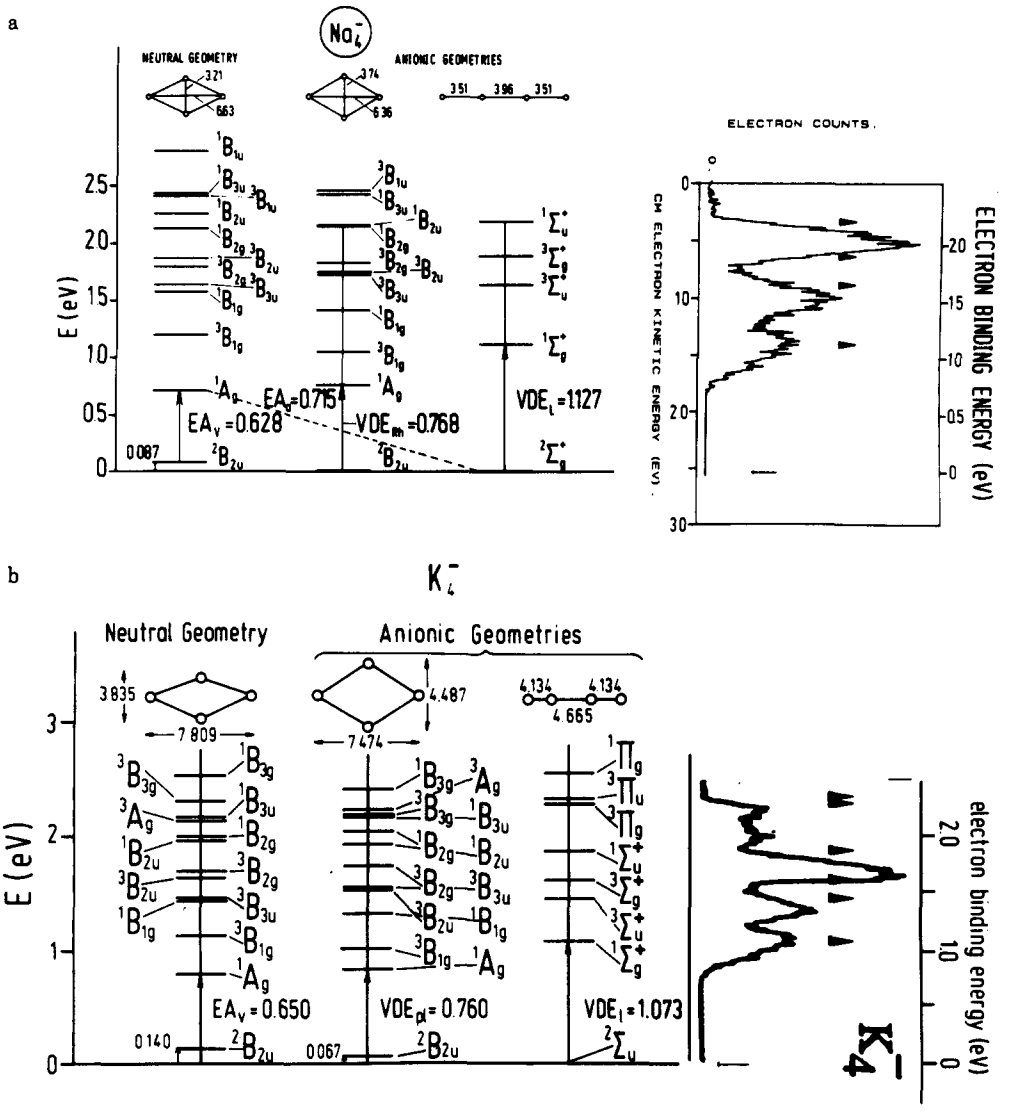

Figure 13. The CI values for vertical transitions and for EA_a of (a) Na_4^-[162] and K_4^-[144] calculated (i) at the two best anionic (linear and rhombic) and (ii) the best neutral geometries are compared with photoelectron detachment spectra.[276] AE-CI and ECP–CVC-CI results for Na_4^-, Na_4 and K_4^-, K_4, respectively. Assignment of anionic rhombus geometry to the spectrum is labeled as ▲.

experimental data are far from being complete and new measurements are in progress, there is a challenge for theoretical predictions concerning the characteristic features of the absorption spectra for clusters with planar versus three-dimensional geometries belonging to different symmetry point groups, and for those containing odd versus even numbers of valence electrons.

There are presently five different model approaches available for discussions of absorption spectra: (i) quantum chemical ab initio CI models, which have been successfully used for prediction of molecular spectroscopic properties for a long time; (ii) random-phase approximation using ab initio SCF Hartree–Fock one-electron functions which will be addressed in this section, (iii) Mie–Drude classical theory used for an estimate of the surface plasmon frequencies in spherical metal droplets; (iv) time-dependent local density approximation for modeling the optical response of clusters based on the jellium model and related methods; and (v) random-phase approximation using the jellium model. A comparison of results and concepts obtained from all these model approaches will be discussed in section IV.D.2.

Trimers. The theoretical interpretation of the pioneering experimental work on absorption spectra of Na_3[263,321,264] using the two-photon ionization (TPI) technique started more than a decade ago and later on Cu_3[265] became the classical examples of the dynamic Jahn–Teller effect due to vibronic coupling in the ground as well as in excited states. The first ab initio CEPA calculations have been carried out for the ground and excited states of Li_3,[322,323] which has been selected as a model for other trimers. These results have been scaled in order to interpret the A and B bands of the Na_3 spectrum, located at 1.85 and 2.02 eV respectively (see ref 12 and references therein). The equilateral triangle D_{3h} is the crossing point of two surfaces for the ground and excited states $[[^2E']_1, [^2E']_2; [^2E'']_1, [^2E'']_2]$. There are three equivalent wells corresponding to isosceles triangles which arise by a cyclic permutation of the apex atom. The molecule oscillates from obtuse to acute triangle without passing through the D_{3h} center. If the energy barrier between the wells is small compared to kT, so called pseudorotation occurs (dynamic Jahn–Teller molecule). In this case the ground state of the trimer is a fluxional molecule without a single well-defined geometrical structure. If kT is small or the

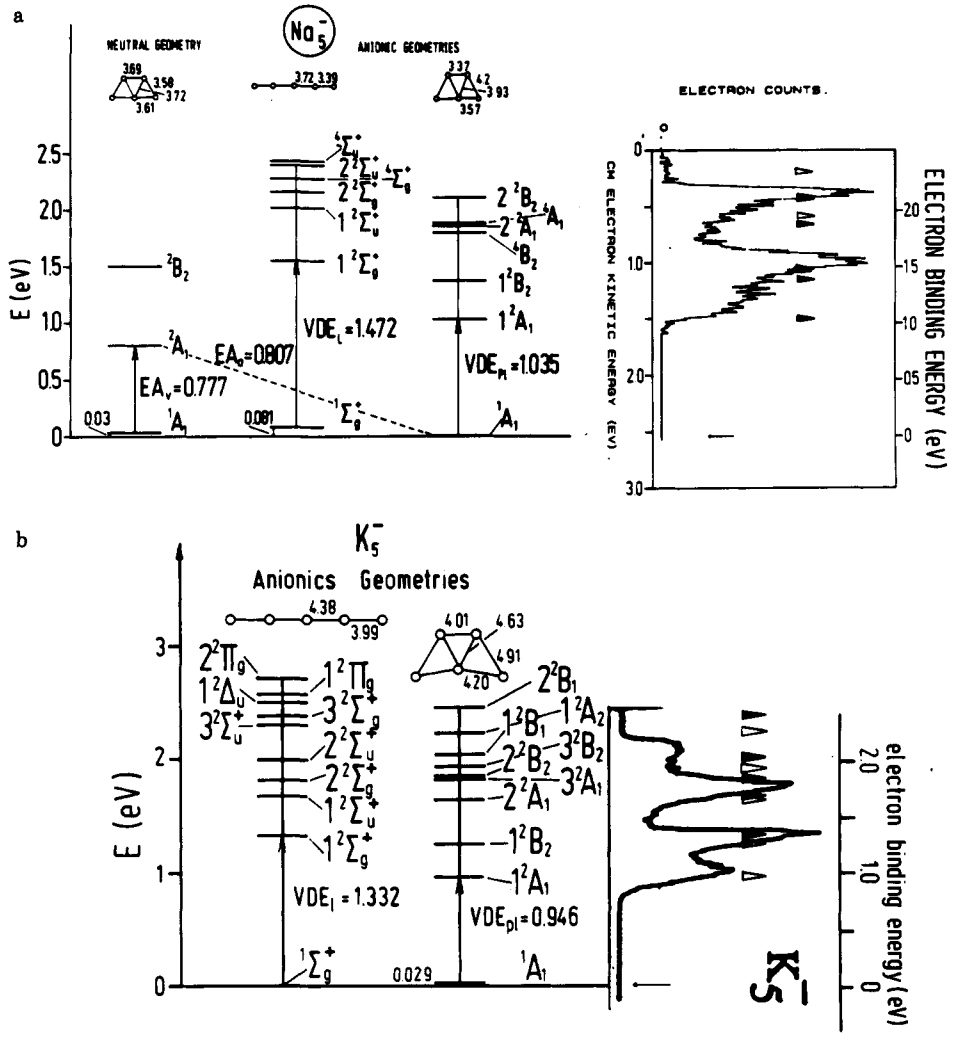

Figure 14. The CI values for vertical transitions of (a) Na_5^-[162] and (b) K_5^-[144] calculated (i) at the two best anionic trapezoidal and linear geometries are compared with photoelectrondetachment spectra.[276] AE-CI and ECP-CVC-CI results for Na_5^-, Na_5 and K_5^-, K_5, respectively. Contributions from the first and second lowest lying anionic isomer to the spectrum are labeled as ▲ and △, respectively.

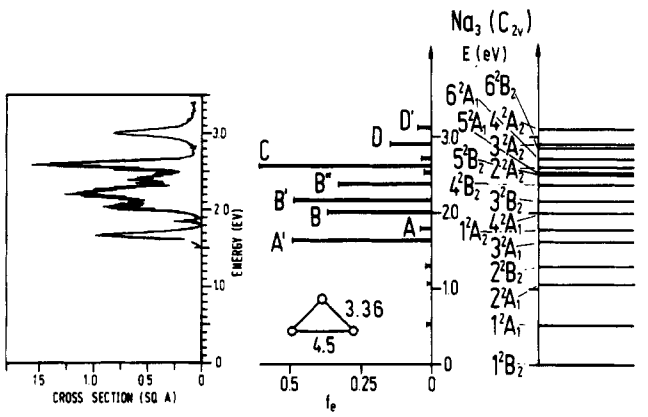

Figure 15. A comparison of the photodepletion spectrum[280] and CI optically allowed transitions (eV) and oscillator strengths f_e for Na_3 (AE-MRDCI treatment).[162]

well is deep, the trimer (Na_3) will be frozen in one of the C_{2v} wells (cf. "low"-temperature ESR spectra[259,324]). The quantitative analysis of resolved vibrational–rotational fine structure of the A and B bands of Na_3 in terms of half-integers for rotational quantum numbers J has been taken as a proof of a pseudorotation. The analysis of the experimental data suggested that the A and B bands at 1.85 and 2.05 eV originate from the $^2E' \rightarrow {}^2E''$ and $^2E' \rightarrow {}^2E'$ transitions and later found B′ and C bands (at 2.16 and 2.58 eV) from $^2E' \rightarrow {}^2E'$ and $^2E' \rightarrow {}^2E''$ transitions, respectively. ECP-GVB-CI calculations of the ground and excited states energy surfaces of Na_3[136] confirmed the $1^2E' \rightarrow 1^2E''$ assignment of the A band and suggested that the B and B′ bands are due to the three-state system $4^2A_1'$ and $3^2E'$ and the C band corresponds to the $2^2E''$ doublet. Recently seven band systems for Na_3 have also been observed by the depletion technique.[280] The location of the A, B, B′, C, and D bands is in agreement with previously measured positions[264] and additional A′ and B″ bands have been found at 1.65 and 2.40 eV, respectively. The ab initio CI calculations[162] for the optically allowed excited states of Na_3 (in the energy interval up to 3.1 eV) at the optimal ground-state geometry (obtuse isosceles triangle), as well as oscillator strengths f_e, are compared with the depletion data[280] in Figure 15. The calculation of oscillator strengths helps to clarify the assignment, since there is a large manifold of close-lying optically allowed excited states in the energy interval of 2–3 eV. The vertical transitions from the $^1B_2$ states of the obtuse isosceles triangle (arising from the Jahn–Teller distortion of the expected E′ ground state in D_{2h} symmetry) to the 1^2A_2, 4^2A_1, 3^2B_2, 2^2A_2, and 3^2A_2 states correspond to the previously found A, B, B′, C, and D bands and the A′ and B″ bands are assigned to 3^2A_1 and 4^2B_2 states. The A and A′ bands are most probably mutually

perturbed and the transitions to both 3^2A_2 and 4^2A_2 might be responsible for the D band. The calculated oscillator strengths of these optically allowed transitions are in qualitative agreement with the measured cross sections. Locations of allowed transitions together with their oscillator strengths yield an assignment of both two-photon ionization (TPI) and depletion spectra. This indicates that the surfaces of excited states may be very parallel to the ground-state energy surface and that the bands which have not been observed by the TPI technique correspond to fully dissociative excited states. Note, however, that the depletion and TPI spectra are not identical, where both are observed. There is a slight deviation in positions of optically allowed transitions.

In addition to Na_3, which is the most exhaustively studied trimer,[263,264] and for which the interpretation of the data is most complete, similar features (e.g. dynamic Jahn–Teller effect for the ground and excited states) have also been observed for Cu_3[265,262,325,326] (cf. section IV.C.3) and Li_3.[268]

For Li_3 two-band systems with resolved rovibrational structures and band heads located at 1.80 and 2.67 eV have been observed by using the TPI technique.[268] They have been labeled as the A and C bands in analogy to the Na_3 absorption spectra. The ground state as well as both excited states have been interpreted in terms of a dynamical Jahn–Teller effect. Due to the measured rovibronic pattern the conclusion has been drawn that the A and C bands originate from $^2E' \rightarrow {}^2E'$ and $^2E' \rightarrow {}^2E''$ transitions, respectively, although the perturbation of other close-lying transitions of different symmetry is not excluded. It is well established that a Jahn–Teller distortion takes place in the ground state of Li_3 leading to the $^1B_2$ state of the obtuse isosceles triangle. Although an extensive study of the ground and excited states energy surfaces of Li_3 was carried out a long time ago,[322,323] for the quantitative assignment of the recent measurements[268] additional state-of-the-art CI calculations are necessary for the surfaces of excited states.

The interpretation of absorption spectra of trimers manifesting high-resolution rovibronic structure for each electronic transition can be considered as a very special case of molecular spectroscopic studies. Only recent progress in the experimental field has opened the new possibility to investigate the size-dependent features of absorption pattern which calls for theoretical structural assignments and characterization of larger clusters.

Tetramers. The depletion spectra of alkali-metal tetramers recently recorded[279,280,283,302] offer a good opportunity for structural assignment since they represent the smallest clusters with relatively large stability. It is instructive to compare measured and calculated optically allowed transitions for Na_4,[304,162] Li_4,[303,300] and the mixed $LiNa_3$[307,306] and Li_2Na_2[307,306] tetramers with four valence electrons in order to study the dependence of the spectroscopic pattern upon their geometry and the degree of substitution.

The rhombic geometries (D_{2h}) of Na_4 and Li_4 are the most stable structures with ^1A_g ground states lying 0.256 and 0.43 eV below the energies of the lowest triplet states $^3A_2$ of deformed tetrahedron structures ($C_{2v} \approx D_{2d}$), respectively.[149,303,304] The latter have been derived by axial distortions of the tetrahedrons leading to the

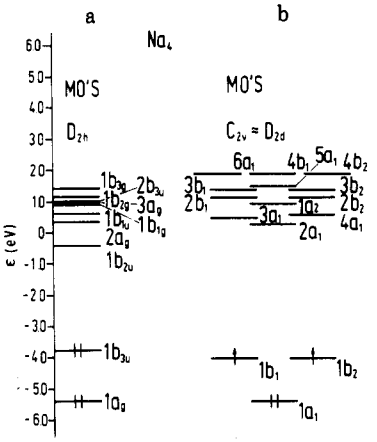

Figure 16. The MO's for Na_4 obtained (a) from the SCF procedure for the ground state of the rhombus (D_{2h} symmetry) and (b) from the SCF procedure for the $^3A_2$ state of the deformed tetrahedron (C_{2v} symmetry). Only the one-electron levels, which are relevant for the electronic excitations corresponding to the leading configurations in the CI wave functions of optically allowed states are drawn (cf. Table I).

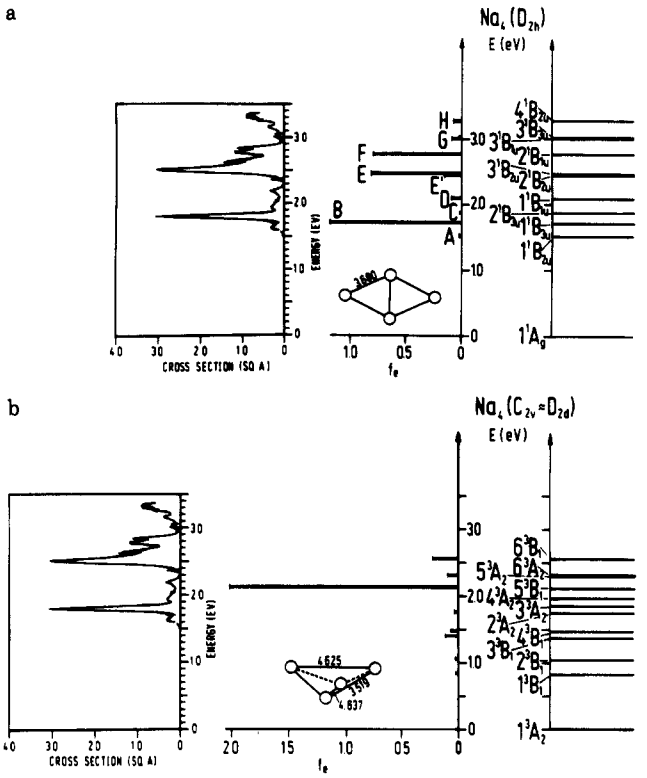

Figure 17. Comparison of depletion spectrum of Na_4[279,280] and the CI energies of optically allowed states (eV) and the oscillator strengths f_e for (a) the best neutral rhombus (singlet state) and (b) the deformed tetrahedron (best triplet state) structures.[162,304]

D_{2d} forms and by further small distortions in which the degeneracy has been completely removed (cf. section III.B.1).

The MO schemes for both the best singlet and triplet structures of Na_4 obtained at the SCF level are drawn in Figure 16 for illustrative purposes. The near-degenerate pattern and energy ordering of the virtual orbitals (although they don't have direct physical meaning) will serve as guidance for discussion of electronic excitations which have a leading role in the multideterminantal wave functions of optically allowed excited states obtained by the MRDCI method. The

excited states with CI excitation energies T_e up to 3 eV for the rhombic (D_{2h}) and deformed tetrahedron (C_{2v}) structures of Na_4 together with their oscillator strengths are compared with the recorded depletion spectrum in Figure 17a. The calculated vertical spectrum of the rhombus[304,162] exhibits three intense transitions to 1^1B_{3u}, 3^1B_{2u}, and 2^1B_{1u} states located at 1.71, 2.46, and 2.76 eV, in complete agreement with measured B, E, and F bands.[279,280] The transitions to 1^1B_{2u}, 2^2B_{3u}, 1^1B_{1u}, 3^1B_{1u}, 3^1B_{3u}, and 4^1B_{2u} with low oscillator strengths coincide with recorded A, C, D, G, and H weak bands.[279,280] Notice that in each of the three irreducible representations of the D_{2h} group there is only one transition with considerable intensity. Moreover, the leading features of the CI wave functions listed in Table I together with the MO scheme of Figure 16 illustrate that the first two $^1B_{3u}$ states have largest contributions from the singly excited configurations: ($1b_{3u} \rightarrow 2a_g$) or ($1b_{3u} \rightarrow 3a_g$) while all $^1B_{2u}$ and $^1B_{1u}$ states have three or four leading configurations among which one is doubly excited: ($1b_{3u} \rightarrow 2a_g$, $1b_{3u} \rightarrow 1b_{2u}$) and ($1b_{3u} \rightarrow 2a_g$, $1b_{3u} \rightarrow 1b_{1u}$), respectively, and the others are singly excited with respect to the ground state configuration ($1a_g^2 1b_{3u}^2$).

Notice also that the several excited states belonging to the same irreducible representation have common leading configurations, whereby just coefficients and signs with which they enter linear combinations are different, substantially influencing the values of the oscillator strengths for transitions to these states. Consequently, there are interference phenomena within each irreducible representation in the case of homogeneous tetramers, giving rise to one transition with large and to others with low oscillator strengths (1^1B_{3u} versus 2^1B_{3u}; 2^1B_{2u} versus 1^1B_{2u} and 4^1B_{2u}; 2^1B_{1u} versus 1^1B_{1u} and 3^1B_{1u}).

The described leading features of the correlated wave functions remain unchanged also when the natural orbitals (NO) are used instead of MO's as one electron functions in the CI, and the transition energies do not differ substantially as shown in Table I. A comparison between transition energies and oscillator strengths for allowed transitions obtained from AE-CI and ECP-CVC-CI is also given in Table I, illustrating that the latter procedure yields acceptable results. Therefore it can be applied for a study of absorption spectra of larger clusters. It has already been discussed in section IV.B that the fine details of the CI treatment do not substantially influence the excitation energies and oscillator strengths, although a large-scale multireference SD-CI is inevitable for the assignment of the rhombic Na_4 to the measured spectrum, as will be shown later in connection with the applicability of the RPA method.

The question can be raised whether the other isomers contribute to the spectrum and how different geometry influences the spectroscopic pattern. The calculated vertical spectrum with respect to the triplet ground state $^3A_2$ of the distorted tetrahedron (cf. Figure 17b) yields the transition to 5^3B_1 at 2.12 eV with dominant oscillator strength resembling a giant resonance.[162] The wave functions of the 5^3B_1 state is dominated by three singly excited configurations ($1a_1^2 2a_1^1 1b_1^1$), ($1a_1^1 1b_2^2 1b_1^1$), and ($1a_1^2 1b_2^1 1a_2^1$) with respect to the triplet ground state configuration ($1a_1^2 1b_1^1 1b_2^1$). For all other transitions low intensity has been calculated. The calculated spectroscopic pattern for Na_4 with C_{2v} symmetry does not correspond to the measured one. Since the energy of the $^3A_2$ state is 0.24 eV higher than that of the ^1A_g state of the rhombus, the conclusion can be drawn that there is no contribution from this isomer and that only the rhombic structure is responsible for the recorded spectrum. However, the finding that even the four valence electrons of a deformed tetrahedron structure can give rise to a spectroscopic pattern with one dominant intense transition illustrates that the appearance of the single or few intense transitions in the depletion spectrum is not necessarily proof of the existence of surface plasmons due to a collective excitation. Of course, the individual particle–hole excitations are not sufficient for the description of excited states, which means that the many-electron picture has to be used instead of the one-electron description. Moreover, it seems that the symmetry of the cluster is one of the determining factors for the appearance of the giant resonances, as will also be pointed out for larger clusters. If the geometry of the cluster belongs to a point group for which the degenerate one-electron levels are present, among which few mutually interacting particle–hole excitations take place, the intense transition can occur to the state in which those configurations play a leading role. The location of the intense transition is closely connected with an energy gap of one-electron levels among which excitations take place, and this is again dependent on the structure of the cluster.

A comparison of the absorption of Na_4 obtained from the CI calculations and from the RPA technique using the same ab initio ground-state SCF one-electron functions (Figure 18) illustrates explicitly the influence of the type of electron excitations on the location and the oscillator strengths of the transitions. As pointed out in section II.B.4, the RPA approach accounts for interactions among single excitations as well as between the ground-state and doubly excited configurations, but not among the double excitations. Consequently, the oscillator strengths of transitions to $^1B_{3u}$ states and their energies obtained from the RPA method agree well with those calculated by CI, since one or two configurations with single excitations have a leading role in their wave functions (cf. Tables I and III). The discrepancy between results obtained from both methods is large for excitation energies and oscillator strengths of other optically allowed transitions to $^1B_{2u}$ and $^1B_{1u}$ states, as illustrated in Figure 18, since one of the leading configurations in the corresponding wave functions contains double excitations which are not accounted for in the RPA approach on the same footing as the single ones (cf. Tables I and III). Note, that the excitation energies obtained from the TDA approximation, which takes into account just interaction among single excitations, are just slightly higher (not more than 0.2 eV) with respect to the RPA ones, and the values of oscillator strengths are also larger in the former case (cf. Table III). This comparison is instructive since it clearly demonstrates that the successful applicability of the RPA for the complete interpretation of absorption spectra is limited to cases in which the single excitations represent the leading features of the wave functions (cf. section II.B.4) as it will be also demonstrated on a number of examples throughout this section. However for tetramers the RPA does not yield satisfactory description of spectra.

The calculated[303,300] and measured[283,300] depletion spectra of Li_4 shown in Figure 19 exhibit striking sim-

TABLE III. Comparison of Transition Energies and Oscillator Strengths Obtained from the AE-RPA and AE-TDA for Na_4 D_{2h} Structure[a]

state	T_e(RPA),[b] eV	T_e(TDA),[b] eV	f_e(RPA)[c]	f_e(TDA)[c]	leading excitation (RPA):[d] $c^2 \geq 0.10$
1^1B_{1u}	2.45	2.51	0.539	0.574	0.95 ($1b_{3u} \rightarrow 1b_{2g}$)
2^1B_{1u}	3.09	3.20	0.476	0.835	0.95 ($1a_g \rightarrow 1b_{1u}$)
3^1B_{1u}	4.76	4.77	0.003	0.004	0.88 ($1a_g \rightarrow 2b_{1u}$)
4^1B_{1u}	5.01	5.13	0.158	0.396	0.87 ($1b_{3u} \rightarrow 2b_{2g}$)
5^1B_{1u}	5.66	5.70	0.016	0.099	0.88 ($1a_g \rightarrow 3b_{1u}$)
1^1B_{2u}	2.22	2.26	0.306	0.228	0.84 ($1b_{3u} \rightarrow 1b_{1g}$), 0.10 ($1a_g \rightarrow 1b_{2u}$)
2^1B_{2u}	2.60	2.81	0.701	1.299	0.92 ($1a_g \rightarrow 1b_{2u}$)
3^1B_{2u}	3.67	3.71	0.036	0.134	0.90 ($1b_{3u} \rightarrow 2b_{1g}$)
4^1B_{2u}	4.50	4.61	0.070	0.287	0.71 ($1a_g \rightarrow 2b_{2u}$), 0.16 ($1b_{3u} \rightarrow 3b_{1g}$)
5^1B_{2u}	4.68	4.68	0.000	0.007	0.56 ($1a_g \rightarrow 3b_{2u}$), 0.18 ($1a_g \rightarrow 2b_{2u}$), 0.11 ($1b_{3u} \rightarrow 3b_{1g}$)
1^1B_{3u}	1.73	1.81	1.111	1.433	0.81 ($1b_{3u} \rightarrow 2a_g$), 0.11 ($1b_{3u} \rightarrow 3a_g$)
2^1B_{3u}	2.06	2.07	0.078	0.192	0.87 ($1b_{3u} \rightarrow 3a_g$)
3^1B_{3u}	3.25	3.26	0.207	0.311	0.63 ($1b_{3u} \rightarrow 4a_g$), 0.28 ($1b_{3u} \rightarrow 5a_g$)
4^1B_{3u}	3.58	3.60	0.050	0.016	0.69 ($1b_{3u} \rightarrow 5a_g$), 0.28 ($1b_{3u} \rightarrow 4a_g$)
5^1B_{3u}	4.13	4.19	0.014	0.047	0.86 ($1a_g \rightarrow 2b_{3u}$)

[a] The ground-state SCF one-electron functions have been used employing AO basis (12s8p1d/7s4p1d). [b] Excitation energies. [c] Oscillator strengths. [d] Leading excitations with respect to the ground-state configuration ($1a_g^2 1b_{3u}^2$).

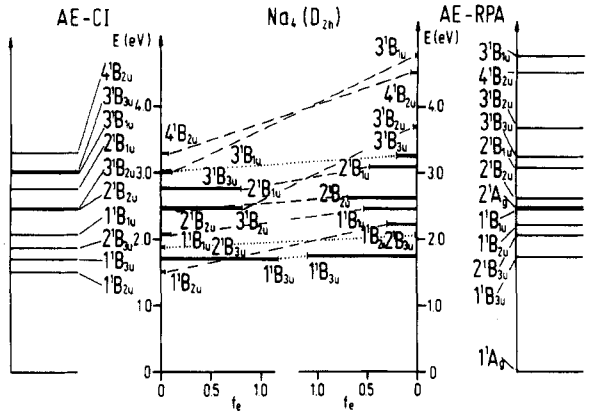

Figure 18. Comparison of ab initio AE-CI and RPA transition energies (eV) and oscillator strengths f_e for optically allowed states of Na_4 (D_{2h}) rhombic structure.

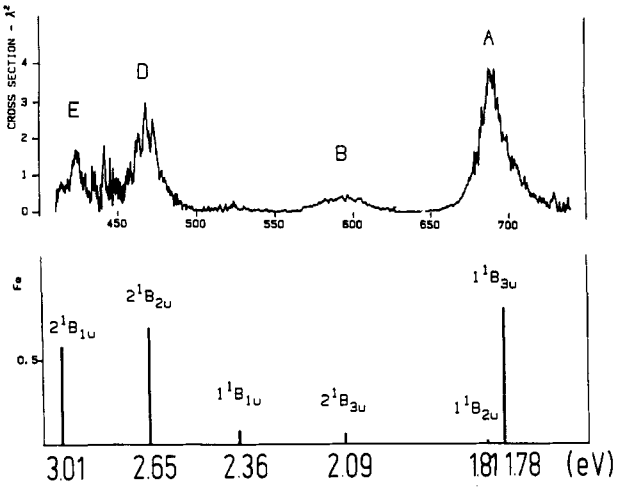

Figure 19. Comparison of the photodepletion spectrum[283] and CI optically allowed transitions (nm) and oscillator strengths f_e of Li_4.[303]

ilarities with those obtained for Na_4.[304,279] Again the transitions from the ^1A_g ground state of the best rhombic geometry to 1^1B_{3u}, 2^1B_{2u}, and 2^1B_{1u} located at 1.78, 2.65, and 3.01 eV, respectively, have considerable values of oscillator strengths in decreasing order and correspond to the recorded spectrum with bands maxima located at 1.80, 2.65, and 3.01 eV labeled as A, D, and E, respectively, which are only slightly red shifted with respect to those found for Na_4. The energy of the 1^1B_{1u} state lies in the region of the A band, and the transition to 2^1B_{3u} at 2.09 eV coincides with the weak B band recorded at 2.08 eV. The measured spectrum can again be assigned as due to the rhombic ground state geometry of Li_4.[303,300] The leading features of the excited states are analogous to those of Na_4. The only difference between Li_4 and Na_4 spectra is the smaller number of recorded weak bands in the former case, but the overall spectral pattern remains unchanged.

A study of excited states of heterogeneous tetramers serves as a good example for finding out to which extent the number of valence electrons and the position of the nuclei determine the spectral pattern. For $LiNa_3$ there are two energetically close-lying planar rhombic isomers with the Li atom located on the short $(LiNa_3)_s$ and on the long $(LiNa_3)_l$ diagonal, respectively. The energy difference is $\Delta E_I = -0.082$ eV in the favor of the former one. Three planar isomers have been found for Li_2Na_2 with Li_2 lying on short diagonal, long diagonal, and the side of a rhombus having small energy differences $\Delta E_I = -0.193$ and -0.110 eV with respect to the first one.[307,306]

In order to carry out the structural assignment to the recorded spectrum[302,327] the optically allowed excited states of both $LiNa_3$ isomers (C_{2v}) are compared in Figure 20. Again, there are three intense transitions from the $^1A_1$ ground state of $(LiNa_3)_s$ to 2^1B_2, 5^1A_1 (6^1A_1), and 3^1B_1 states located at 1.73, 2.53 (2.54), and 2.80 eV, respectively, coinciding with recorded bands having large cross sections. There is close analogy to the B, E, and F bands of Na_4. Transitions to 3^1B_2 and to 2^1B_1 states correspond to the weaker fine structure with slightly larger oscillator strengths than those calculated for the C and D bands of Na_4.[302,307,306,327] The rhombic $(LiNa_3)_s$ structure accounts fully for the recorded spectrum. However, the other $(LiNa_3)_l$ isomer gives rise to an almost identical spectrum. In the ground state the role of the HOMO and LUMO orbitals has been exchanged with respect to $(LiNa_3)_s$ due to Li substitution at the long diagonal. The contribution of the second isomer to the spectrum may depend on the height of the barrier separating both species, since the temperature is not known. The calculated barrier between the two isomers is not negligible (~0.5 eV), although this investigation has not been completed. The

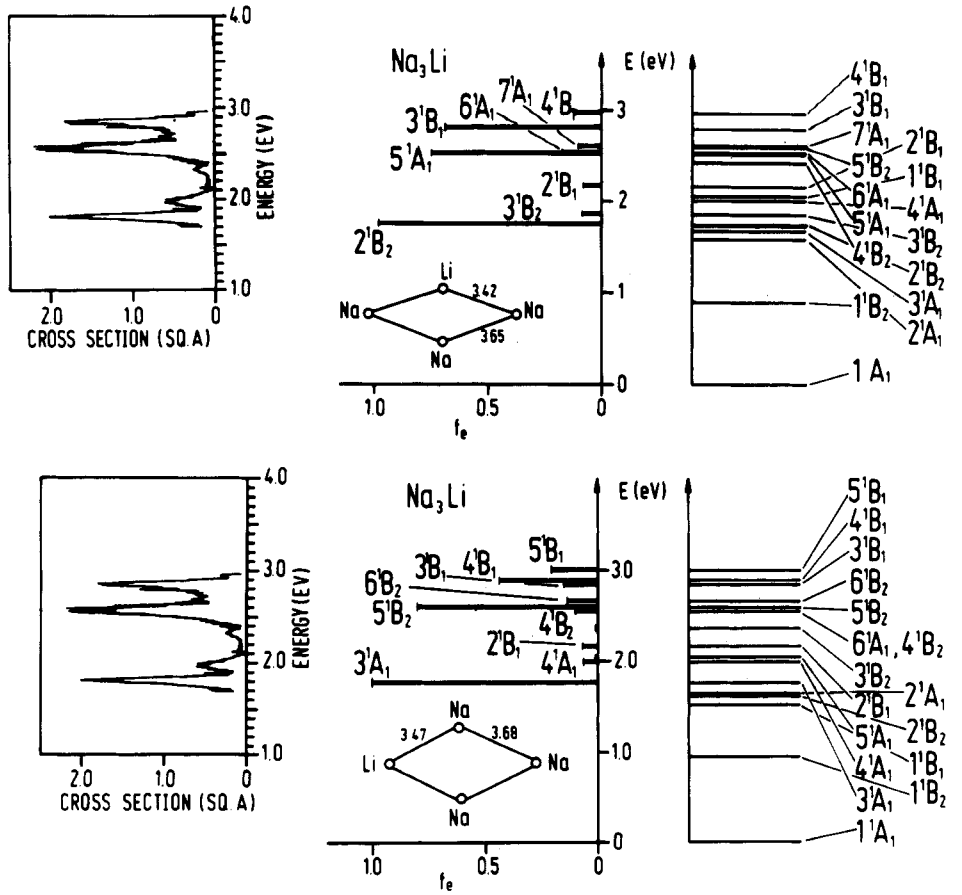

Figure 20. Comparison of photodepletion spectrum[302,327] and CI optically allowed transitions (eV) and oscillator strengths f_e of two $LiNa_3$ isomers.[306]

Li–Na as well as Na–Na bond lengths in both isomers do not substantially differ from each other and the MO energy schemes are almost identical. Since among many energetically close lying states there is always one intense transition in each irreducible representation it is not surprising that both structures yield almost equivalent spectroscopical patterns.

In comparison with homogeneous clusters, increasing the amount of Li introduces some new features into the absorption spectrum[302,327] as shown in Figure 21, since four intense transitions are present for Li_2Na_2. Calculated energies of excited states and oscillator strengths for the $(Li_2Na_2)_s$ isomer with Li_2 on the short diagonal (which is the most stable ground-state structure) illustrate that there are now two intense transitions in each irreducible representation. The leading features of the wave functions of the 1^1B_{3u} and 2^1B_{3u} states are determined by two configurations with comparable weights arising from excitations $1b_{3u} \rightarrow 2a_g$ and from $1b_{3u} \rightarrow 3a_g$ of the ground state configuration $(1a_g^2b_{3u}^2)$. For the other $(Li_2Na_2)_l$ isomer with Li_2 on the longer diagonal the oscillator strength of the transition to the 2^1B_{3u} state is negligibly small and the calculated spectroscopic pattern with three dominant transitions resembles the one obtained for the homogeneous Na_4 cluster. Since the location of other intense transitions to 1^1B_{3u}, 2^1B_{2u}, and 2^1B_{1u} states are in good agreement with three of four recorded intense bands, the contribution from this isomer is not excluded. Similarly, the calculated spectrum of the third Li_2Na_2 isomer with Li–Li as next nearest neighbors accounts for a part of the recorded spectrum. However, only the $(Li_2Na_2)_s$ isomer with the lowest ground-state energy gives rise to four intense transitions and to the fine structure[307,306] of the recorded spectrum.[302,327]

These examples illustrate clearly that besides the number of valence electrons and the common planar structure, the location of Li atoms is important for the complete assignment of the recorded spectrum.

Na_5. The optically allowed transitions have been calculated with the ECP–CPP–CI method[158] for two Na_5 structures: the planar (C_{2v}) and the deformed trigonal bipyramid (C_{2v}). The reliability of ab initio ECP–CPP–CI versus ab initio all-electron results for the determination of absorption spectra has been illustrated earlier on the example of Na_4. The ground state $^2A_1$ of the planar geometry is more stable (for 0.23 eV) than the $^2B_1$ state, which is the ground state of the bipyramid.[142] A comparison of one-electron levels for both structures, given in Figure 22, illustrates that there are more closely lying almost degenerate MO's present for the planar structure than for the bipyramid. Moreover, the HOMO–LUMO energy gap is smaller for the latter, which is the less-stable structure, indicating that the transition energies for the lowest lying optically allowed states might have smaller values than in the former case. A comparison of calculated locations of the optically allowed excited transitions up to 3.0 eV and the oscillator strengths for both structures are given in Figure 23. The calculated vertical spectrum for planar Na_5 exhibits large oscillator strengths for transitions to 4^2B_2 and 5^2B_2 located at ~2.0 eV and for the transitions to the 8^2A_1 and 9^2A_1 states at ~2.5 eV, respectively. In the energy interval 2.5–3.0 eV no intense

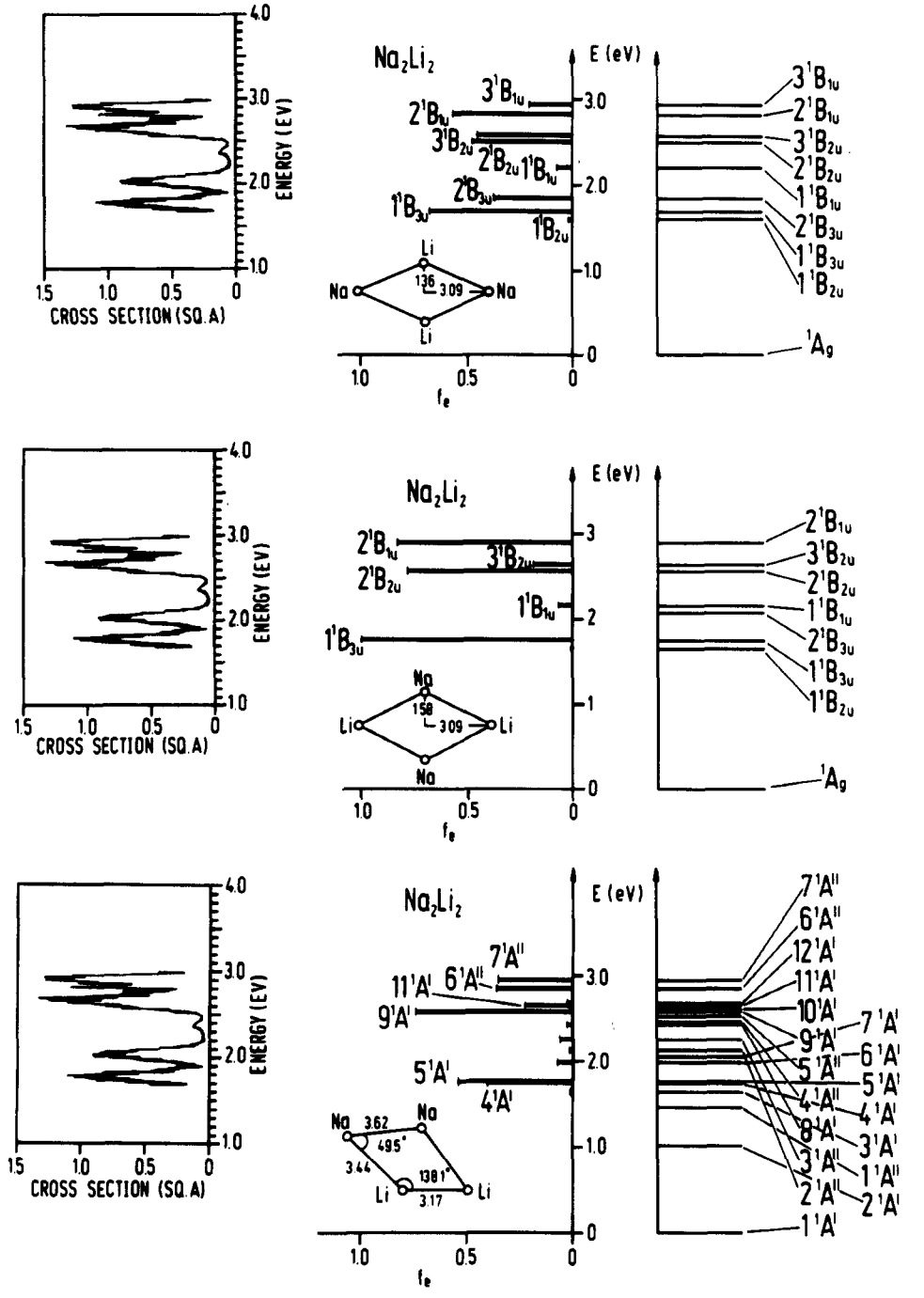

Figure 21. Comparison of photodepletion spectrum[302,327] and CI optically allowed transitions (eV) and oscillator strengths f_e of three Li_2Na_2 isomers.[306]

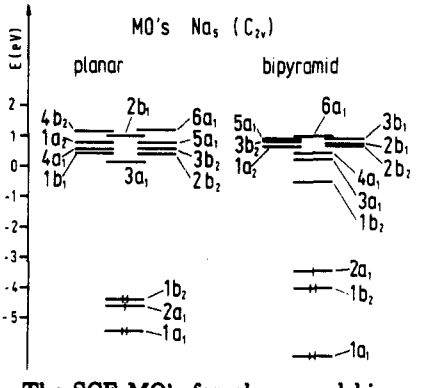

Figure 22. The SCF MO's for planar and bipyramidal Na_5 structures (C_{2v}).[158]

transitions have been calculated. In the case of the bipyramid there are more transitions with considerable oscillator strengths than in the former case, and they are distributed over the whole energy interval 2.0–2.8 eV.

Although absorption spectra recorded at high resolution are not yet completed, it is likely that only the planar structure is responsible for the spectrum.[329]

Na_n (n = 6, 8, 20). The theoretical investigation of absorption spectra for Na_6,[158] Na_8,[305,162] and Na_{20}[328] and their comparison is of particular interest for several reasons: (i) A transition between planar and three-dimensional structures occurs for alkali-metal hexamers for which three energetically close lying geometrical structures have been found: almost degenerate planar

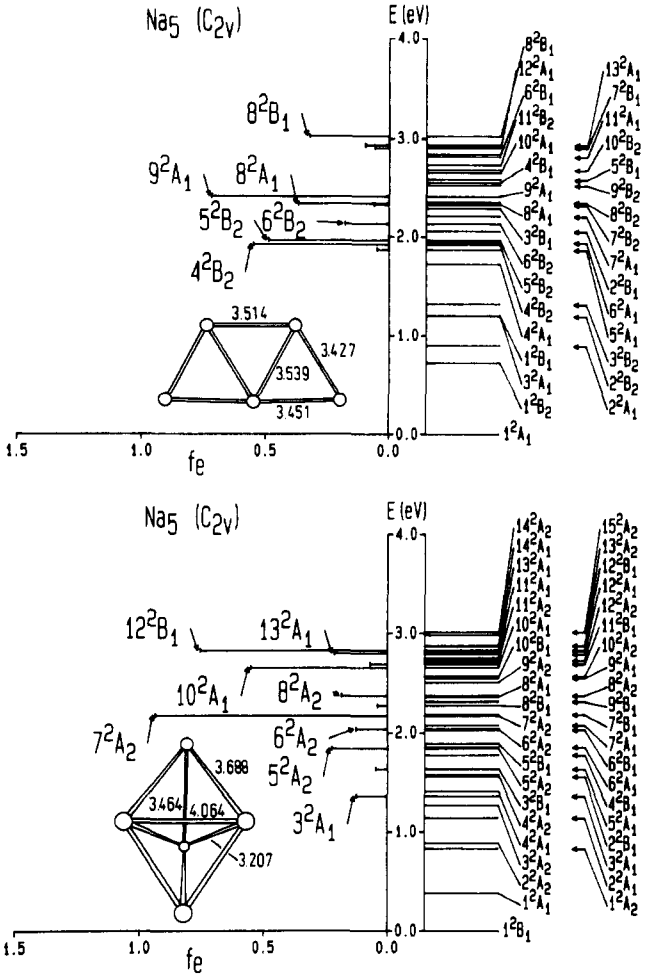

Figure 23. The CI optically allowed transitions (eV) and oscillator strengths f_e for planar and bipyramidal structure of Na_6.[158]

($D_{3h} \rightarrow C_{2v}$) and a "flat" pentagonal pyramid ($C_{5v} \rightarrow C_s$) (with energy difference $\Delta E_I = -0.014$ eV, separated by a negligible barrier) and the three-dimensional C_{2v} structure built from the tetrahedral units with $\Delta E_I = -0.250$ eV with respect to the planar one[142,158] which has the lowest energy. Notice that geometry optimizations for planar and pentagonal pyramid yield slight deviations from the highly symmetrical point groups. Therefore, the ($D_{3h} \rightarrow C_{2v}$) and ($C_{5v} \rightarrow C_s$) labels are introduced. Recent experiments[298,329] indicate that the absorption spectrum of Na_8 exhibits a dominant transition at ~2.07 eV (600 nm) (see Figure 25) and an additional weaker band at ~2.88 eV (430 nm). (ii) Na_8 and Na_{20} with 8 and 20 valence electrons represent particularly stable clusters with closed shells. Moreover, "giant resonances" have been measured at ~500 nm (2.5 eV) for Na_8[277,279,280] and Na_{20}.[296,297,308] In addition, a fine structure at ~700 nm and at ~600 nm for Na_8[279,280] and a broad band at 400–450 nm for Na_{20}[308] have recently been found via the high-resolution depletion technique. (iii) An understanding of reasons for similarities and differences in the absorption spectra of Na_6, Na_8, and Na_{20} represents one of the essential issues concerning specific structural properties as a function of the cluster size. Very recent ab initio ECP–CI and ab initio ECP–RPA work which is still in progress will be addressed in this section. A comparison with results for Na_6, Na_8, and Na_{20} obtained by using the RPA based on the jellium model with the harmonic oscillator potential will be made in section IV.D.2.

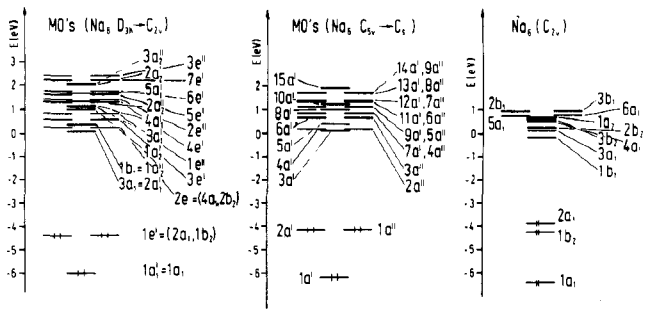

Figure 24. The SCF MO's for planar, "flat" pyramidal and three-dimensional C_{2v} structures of Na_6. $D_{3h} \rightarrow C_{2v}$ and $C_{5v} \rightarrow C_s$ label a small deviation from the higher symmetry groups for the optimized geometries.

The ground-state SCF MO levels for three Na_6 structures are given in Figure 24 for illustrative purposes. Two closely related ($D_{3h} \rightarrow C_{2v}$) and ($C_{5v} \rightarrow C_s$) topologies with almost degenerate pairs of one-electron levels and HOMO–LUMO energy gaps ~4.5 eV differ from the one-electron scheme of C_{2v} Na_6 structure for which the degeneracy is not present. A comparison of calculated spectra for three structures with excitation energies up to 3.0 eV and the oscillator strengths using CI and RPA techniques[158] is given in Figures 25 and 26, respectively. The dominant pair of transitions located at ~2.1–2.2 eV is present for both the planar Na_6 and for the flat pentagonal pyramid. The CI and RPA wave functions of the 4^1A_1 and 3^1B_2 states of the planar structure contain as the two largest contributions singly excited configurations arising by promoting an electron from almost degenerate $1e' \approx (2a_1,1b_2)$ to $2e' \approx (4a_1,2b_2)$ one-electron levels, although the CI wave functions also contain a few additional leading configurations with coefficients > 0.1 (cf. Table IV). Consequently, the transition energies obtained by the RPA technique are only negligibly higher with respect to the CI ones for these two states (cf. Table V). In addition to these dominant transitions there are several excited states located between 2.8 and 3.2 eV which have some oscillator strength, so that a broad band with lower intensity is expected in this region (cf. Figure 25). However, there is a substantial difference between the CI and RPA results for these higher lying excited states concerning their location and oscillator strengths, since the leading configurations of the CI wave functions contain double excitations which cause lowering of the transition energies and the oscillator strengths relative to RPA. In particular, RPA yields a considerably larger f_e value for transition to the 3^1B_1 and its location is ~0.3 eV higher with respect to the corresponding CI state (cf. Figures 25 and 26 and Tables IV and V).

The analysis of the results obtained from the RPA and the CI procedures for the ($D_{3h} \rightarrow C_{2v}$) structure of Na_6 offers a good opportunity to point out that one has to be aware of approximations involved in different treatments in order to judge the reliability of their predictions (cf. sections II.A.2 and II.B.4). For example, the location of the 3^1B_1 state for planar Na_6 obtained from the RPA treatment, which is not adequately described due to a lack of interactions among double excitations, coincides accidentally with the region of a low intensity band observed, although its oscillator strength is too large and similar to those calculated for the 4^1A_1 and 3^1B_1 states. All three RPA states together exhaust 63% of the sum of oscillator strengths which is 5.4 in

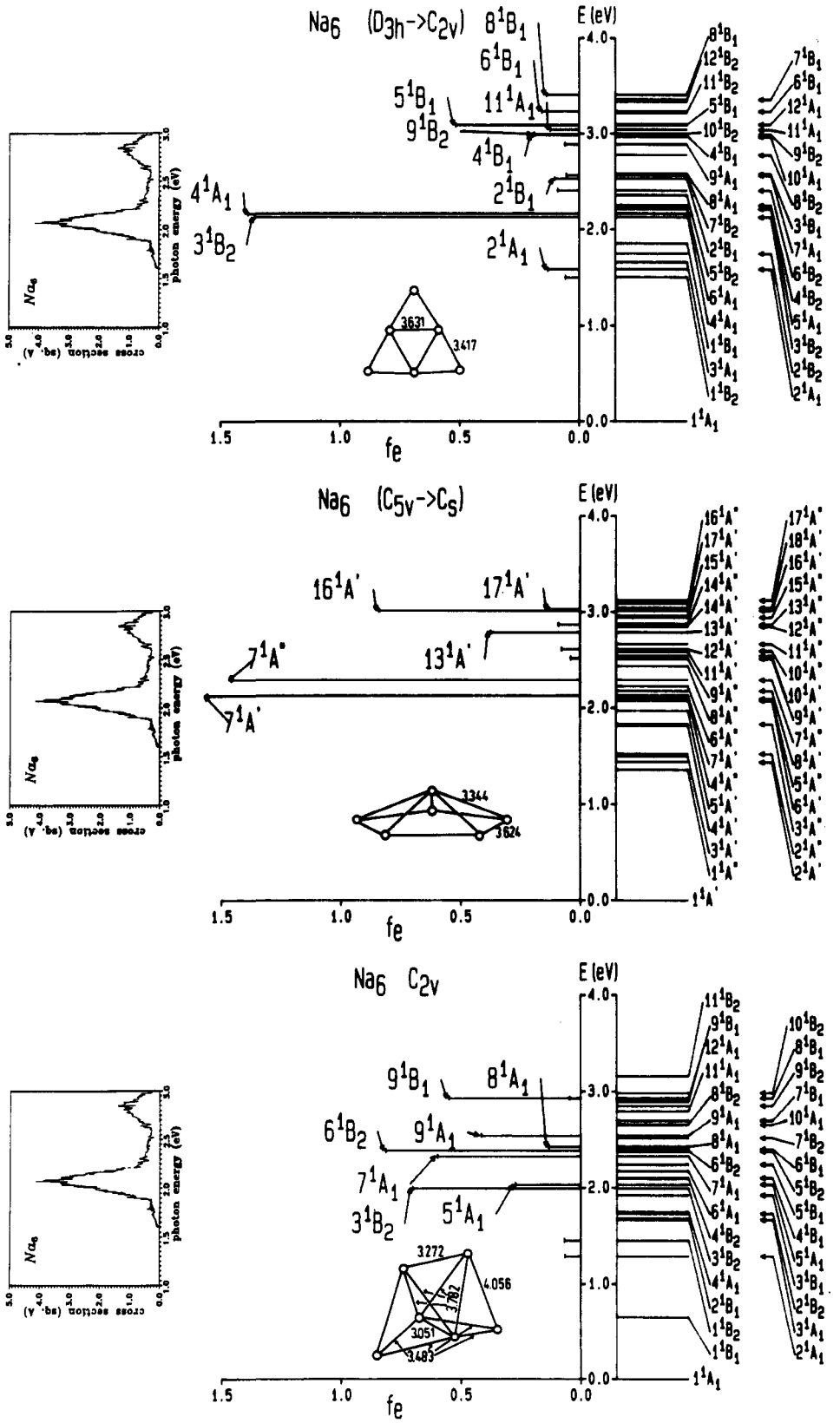

Figure 25. Comparison of photodepletion spectrum[329] and CI optically allowed transitions (eV) and oscillator strengths f_e for three Na_6 structures:[158] $D_{3h} \rightarrow C_{2v}$, C_{5v}, and C_{2v}.

the energy interval up to 4.0 eV. The RPA prediction of ~2:1 intensity for the bands located at 2.24 and 2.85 eV, respectively, is not in agreement with the CI results[158] and experiment.[329]

Since the MO scheme of the pyramidal ($C_{5v} \rightarrow C_s$) structure is very similar to the ($D_{3h} \rightarrow C_{2v}$) one, an analogous situation to that described for the 4^1A_1 and 3^1B_2 states has been found for the location, oscillator strengths, and the leading features of the wave functions for the $7^1A''$ and $7^1A'$ states (cf. Figure 25). Dominant intense transitions to these states give rise to the overall similar spectra of the ($D_{3h} \rightarrow C_{2v}$) and ($C_{5v} \rightarrow C_s$)

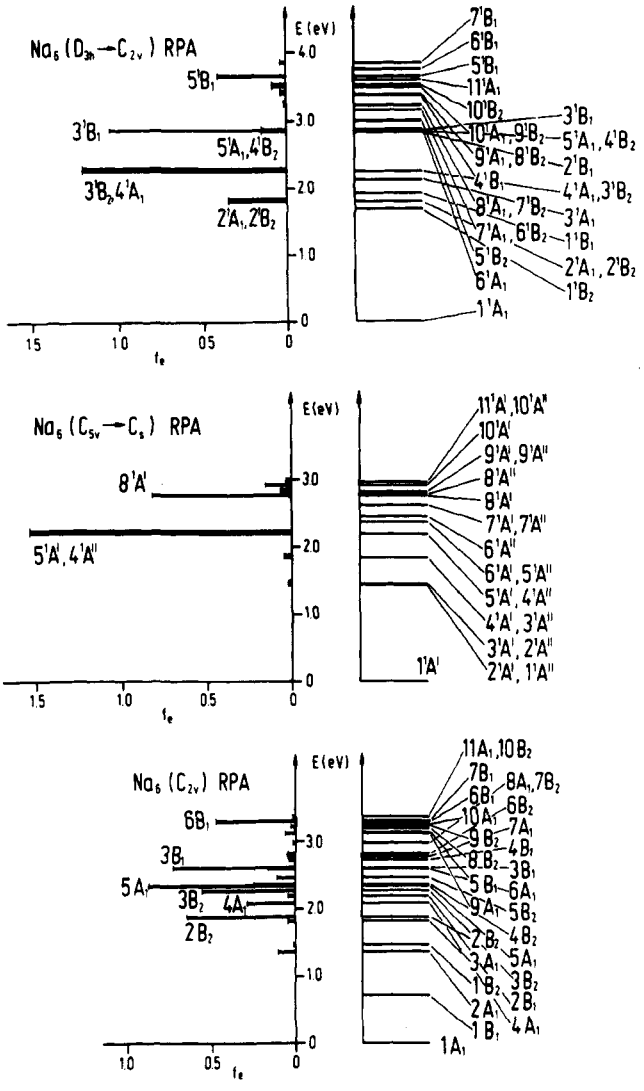

Figure 26. The RPA (based on the SCF procedure) transition energies (eV) and oscillator strengths f_e for three Na_8 structures:[158] $D_{3h} \rightarrow C_{2v}$, $C_{5v} \rightarrow C_s$, and C_{2v}.

structures which differ from each other only in details. Notice, that the ($C_{5v} \rightarrow C_s$) topology differs from the ($D_{3h} \rightarrow C_{2v}$) one only in the position of the out-of-plane atom.

In contrast, the C_{2v} structure seems to produce a different spectroscopical pattern with several intense transitions between 2.0 and 2.8 eV. Also, the location and oscillator strengths of the transitions obtained from the CI and RPA technique differ substantially from each other. It is likely that the C_{2v} structure, which is less stable than the other two, is not responsible for the observed Na_6 spectrum.[329]

The example of Na_6 illustrates clearly that the assumption about averaging of geometries, which will smear out the structural properties in the sense of an oscillation among many energetically close lying structures contributing to a broad absorption band, is not valid.[330-332] If this were the case, the contribution from the C_{2v} structure would also be seen in the absorption spectrum. Namely, a broad band at ~2.5 eV would have to be observed in addition to an intense band located at ~2.0 eV and the weak one at ~2.8 eV due to the planar ($D_{3h} \rightarrow C_{2v}$) and ($C_{5v} \rightarrow C_s$) structures. Only the two latter bands have been recorded.[329] Recent QMD work[157] in which also the structures at high temperature have been considered indicate strongly that the mobility of atoms is not so large as expected.

From a comparison between the CI and RPA results a rough estimate can be made that a dominant intense transition can already arise due to an interaction of very few (two or three) particle-hole excitations among degenerate or almost degenerate pairs of one-electron levels. For example, two single particle-hole transitions contribute ~78% to the RPA wave function of the 3^1B_2 and 4^1A_1 state of ($D_{3h} \rightarrow C_{2v}$) structure. In this case the RPA will reproduce this part of the spectrum well. The approximate location of the intense transition depends roughly upon the energy difference between the one-electron levels among which excitations occur. The one-electron level scheme is determined by symmetry, geometry, and the potential. Therefore, differences between these RPA results and those based on the jellium model oscillators can be expected (cf. section IV.D.2).

The number of valence electrons available to occupy the degenerate or almost degenerate one-electron levels is closely connected with the symmetry of the stable cluster geometry. In a fact, the most stable Na_8 cluster is the highly symmetric T_d tetracapped tetrahedron (cf. section III.B.1). In this context the number of valence electrons is connected with the appearance of characteristic features in the absorption spectra, but the existence of one dominant intense peak is not necessarily dependent only on the number of valence electrons corresponding to a closed shell (8,20) (compare Na_6).

As already pointed out in section III.B.1, geometry optimization of Na_8 in the framework of the HF analytical gradient method carried out for an antiprism with the D_{4d} symmetry and a deformed section of the fcc lattice leading to the geometry with the D_{2d} symmetry, respectively, yields ground-state energies which are only slightly higher than the T_d one (cf. section III.B.1). The D_{2d} and D_{4d} structures have been considered since they have been found as stable isomers in the LSD[154] and LSD–QMD work[157] and they certainly belong to a class of compact and symmetrical geometries. Therefore, it is of interest to find out to which extent their spectral pattern is different from the one calculated for the T_d structure. The CI energy ordering for the three structures remains the same as in the SCF case.[162] The optimization of geometry at the large-scale CI level in the framework of CASSCF is not practicable, and pointwise CI optimization is not particularly instructive due to the very shallow energy surfaces. A comparison between the measured absorption spectrum[279,280] and the calculated energies for allowed transitions with corresponding oscillator strengths for all three T_d, D_{2d}, and D_{4d} structures[305,162] is given in Figure 27. The one-electron level schemes of Figure 28 will again be helpful for discussing the nature of the excited states of different Na_8 structures. For the T_d structure, the 4^1T_2 state located at 2.49 eV (498 nm) has dominant oscillator strength and coincides with the maximum of the observed intense band. There are only three leading configurations in the wave function of the 4^1T_2 state, arising from single excitations from $1t_2$ to $3t_2$ and the 1e MO's (cf. Figure 28). There are two close-lying states, 5^1T_2 and 6^1T_2, blue shifted with respect to 4^1T_2 also lying in the energy interval of the observed intense band. The 6^1T_2 and 4^1T_2 have similar leading terms in the corresponding wave func-

TABLE IV. Transition Energies and Oscillator Strengths Obtained from the ECP–CVC-CI Procedure for the Na_4 ($D_{2h} \rightarrow C_{2v}$) Structure

state	E, au[a]	T_e, eV[b]	f_e[c]	Ψ[d]
1^1A_1	−1.2379	0.00		0.91 ($1a_1^2 2a_1^2 1b_2^2$)
2^1A_1	−1.1797	1.59	0.1330	−0.72 ($2a_1 \rightarrow 3a_1$) − 0.26 ($2a_1 \rightarrow 4a_1$) −0.19 ($1b_2 \rightarrow 2b_2$) + 0.19 ($2a_1 \rightarrow 7a_1$) +0.18 ($2a_1 \rightarrow 6a_1$)
3^1A_1	−1.1770	1.66	0.0025	−0.55 ($2a_1 \rightarrow 4a_1$) + 0.54 ($1b_2 \rightarrow 2b_2$) +0.21 ($2a_1, 1b_2 \rightarrow 4a_1, 2b_2$)
4^1A_1	−1.1583	2.17	1.3862	0.52 ($1b_2 \rightarrow 2b_2$) + 0.50 ($2a_1 \rightarrow 4a_1$) −0.39 ($2a_1 \rightarrow 3a_1$) + 0.15 ($1a_1 \rightarrow 4a_1$)
5^1A_1	−1.1565	2.22	0.0016	0.42 ($1a_1 \rightarrow 3a_1$) + 0.30 ($2a_1, 1b_2 \rightarrow 3a_1, 2b_2$) +0.25 ($2a_1 \rightarrow 5a_1$) −0.24 ($2a_1^2 \rightarrow 3a_1, 4a_1$) + 0.16 ($2a_1^2 \rightarrow 3a_1^2$)
6^1A_1	−1.1553	2.25	0.0186	0.41 ($1a_1 \rightarrow 4a_1$) + 0.27 ($1b_2^2 \rightarrow 4a_1^2$) +0.25 ($1b_2^2 \rightarrow 3a_1, 4a_1$) +0.25 ($2a_1, 1b_2 \rightarrow 4a_1, 2b_2$) −0.21 ($1b_2 \rightarrow 3b_2$) − 0.19 ($1b_2 \rightarrow 4b_2$) −0.18 ($2a_1^2 \rightarrow 4a_1^2$) − 0.15 ($1b_2 \rightarrow 8b_2$)
7^1A_1	−1.1437	2.56	0.0555	0.37 ($2a_1 \rightarrow 5a_1$) + 0.36 ($1b_2 \rightarrow 3b_2$) +0.25 ($2a_1^2 \rightarrow 3a_1^2$) − 0.25 ($1b_2^2 \rightarrow 3a_1^2$) +0.22 ($2a_1 \rightarrow 6a_1$) +0.16 ($2a_1 \rightarrow 13a_1$) + 0.16 ($1a_1, 2a_1 \rightarrow 3a_1^2$) −0.15 ($1b_2^2 \rightarrow 3a_1, 4a_1$)
8^1A_1	−1.1431	2.58	0.0026	−0.40 ($2a_1 \rightarrow 6a_1$) − 0.30 ($1b_2 \rightarrow 4b_2$) −0.24 ($2a_1, 1b_2 \rightarrow 3a_1, 4a_1$) −0.23 ($2a_1 \rightarrow 13a_1$) − 0.20 ($1b_2 \rightarrow 8b_2$) −0.20 ($2a_1^2 \rightarrow 3a_1, 4a_1$) −0.17 ($2a_1^2 \rightarrow 2b_2^2$) + 0.17 ($2a_1 \rightarrow 7a_1$)
9^1A_1	−1.1318	2.89	0.0612	0.34 ($2a_1, 1b_2 \rightarrow 3a_1, 2b_2$) − 0.30 ($1b_2 \rightarrow 3b_2$) −0.28 ($2a_1 \rightarrow 5a_1$) + 0.26 ($2a_1 \rightarrow 6a_1$) +0.22 ($2a_1^2 \rightarrow 3a_1^2$) − 0.21 ($1a_1 \rightarrow 4a_1$) −0.20 ($1b_2^2 \rightarrow 3a_1^2$) + 0.16 ($1a_1, 2a_1 \rightarrow 3a_1^2$)
10^1A_1	−1.1289	2.97	0.0001	0.47 ($1b_2 \rightarrow 3b_2$) − 0.43 ($2a_1 \rightarrow 5a_1$) +0.22 ($2a_1, 1b_2 \rightarrow 4a_1, 2b_2$) +0.20 ($1a_1 \rightarrow 3a_1$) + 0.16 ($1b_2 \rightarrow 2b_2$) −0.15 ($2a_1 \rightarrow 4a_1$)
11^1A_1	−1.1261	3.04	0.1224	−0.44 ($1b_2 \rightarrow 4b_2$) − 0.30 ($1a_1 \rightarrow 4a_1$) +0.27 ($2a_1, 1b_2 \rightarrow 4a_1, 2b_2$) + 0.26 ($2a_1 \rightarrow 6a_1$) −0.18 ($1b_2 \rightarrow 8b_2$) +0.19 ($2a_1 \rightarrow 5a_1$)
12^1A_1	−1.1241	3.10	0.0331	0.29 ($2a_1, 1b_2 \rightarrow 4a_1, 2b_2$) −0.29 ($1b_2 \rightarrow 3b_2$) −0.24 ($2a_1^2 \rightarrow 2b_2^2$) + 0.24 ($1b_2^2 \rightarrow 2b_2^2$) −0.24 ($1a_1 \rightarrow 3a_1$) − 0.23 ($1b_2 \rightarrow 4b_2$) −0.21 ($2a_1 \rightarrow 5a_1$) + 0.19 ($1b_2^2 \rightarrow 4a_1^2$) −0.17 ($1a_1 \rightarrow 4a_1$)
1^1B_1	−1.1698	1.85	0.0000	−0.89 ($2a_1 \rightarrow 1b_1$)
2^1B_1	−1.1450	2.53	0.1039	0.63 ($2a_1 \rightarrow 2b_1$) + 0.32 ($2a_1, 1b_2 \rightarrow 1b_1, 2b_2$) −0.24 ($1a_1 \rightarrow 1b_1$) +0.17 ($1a_1, 2a_1 \rightarrow 3a_1, 1b_1$) − 0.16 ($2a_1 \rightarrow 3b_1$) +0.16 ($2a_1^2 \rightarrow 3a_1, 1b_1$)
3^1B_1	−1.1432	2.58	0.0290	0.58 ($1b_2 \rightarrow 1a_2$) − 0.27 ($2a_1 \rightarrow 2b_1$) +0.26 ($1b_2^2 \rightarrow 4a_1, 1b_1$) −0.20 ($1a_1 \rightarrow 1b_1$) + 0.19 ($2a_1, 1b_2 \rightarrow 1b_1, 2b_2$) −0.16 ($1b_2 \rightarrow 3a_2$)
4^1B_1	−1.1283	2.98	0.1947	0.50 ($2a_1, 1b_2 \rightarrow 1b_1, 2b_2$) − 0.26 ($1b_2 \rightarrow 1a_2$) −0.25 ($2a_1 \rightarrow 2b_1$) −0.22 ($2a_1^2 \rightarrow 3a_1, 1b_1$) +0.18 ($1a_1, 2a_1 \rightarrow 3a_1, 1b_1$) −0.16 ($2a_1, 1b_2 \rightarrow 3a_1, 1a_2$)
5^1B_1	−1.1244	3.09	0.5177	−0.43 ($2a_1 \rightarrow 2b_1$) − 0.30 ($1b_2 \rightarrow 1a_2$) +0.28 ($1a_1, 2a_1 \rightarrow 3a_1, 1b_1$) −0.26 ($1a_1 \rightarrow 1b_1$) + 0.21 ($2a_1^2 \rightarrow 3a_1, 1b_1$) +0.19 ($2a_1, 1b_2 \rightarrow 1b_1, 2b_2$) +0.18 ($2a_1, 1b_2 \rightarrow 3a_1, 1a_2$) −0.15 ($1a_1, 2a_1 \rightarrow 4a_1, 1b_1$)
6^1B_1	−1.1192	3.23	0.1577	−0.58 ($2a_1 \rightarrow 3b_1$) + 0.23 ($1a_1, 2a_1 \rightarrow 4a_1, 1b_1$) +0.22 ($1b_2 \rightarrow 1a_2$) −0.22 ($1b_2^2 \rightarrow 4a_1, 1b_1$) + 0.18 ($2a_1^2 \rightarrow 4a_1, 1b_1$) −0.17 ($2a_1 \rightarrow 7b_1$)
7^1B_1	−1.1146	3.35	0.0336	0.47 ($2a_1 \rightarrow 3b_1$) + 0.28 ($2a_1, 1b_2 \rightarrow 1b_1, 2b_2$) −0.25 ($2a_1 \rightarrow 4b_1$) − 0.24 ($1b_2^2 \rightarrow 4a_1, 1b_1$) +0.21 ($2a_1^2 \rightarrow 3a_1, 1b_1$)

TABLE IV (Continued)

state	E, au[a]	T_e, eV[b]	f_e[c]	Ψ[d]
8^1B_1	−1.1128	3.41	0.1374	0.40 ($2a_1 \rightarrow 4b_1$) + 0.28 ($1a_1 \rightarrow 1b_1$) −0.21 ($2a_1$, $1b_2 \rightarrow 3a_1$, $1a_2$) +0.21 ($2a_1$, $1b_2 \rightarrow 1b_1$, $2b_2$) −0.19 ($1a_1$, $2a_1 \rightarrow 4a_1$, $1b_1$) −0.17 ($1b_2^2 \rightarrow 4a_1$, $1b_1$) + 0.16($2a_1 \rightarrow 8b_1$) −0.16 ($1b_2^2 \rightarrow 3a_1$, $1b_1$)
1^1B_2	−1.1828	1.50	0.0583	−0.85 ($1b_2 \rightarrow 3a_1$)
2^1B_2	−1.1736	1.75	0.0062	−0.52 ($2a_1 \rightarrow 2b_2$) − 0.46 ($1b_2 \rightarrow 4a_1$) −0.30 ($2a_1^2 \rightarrow 3a_1$, $2b_2$) −0.25 ($2a_1$, $1b_2 \rightarrow 3a_1$, $4a_1$)
3^1B_2	−1.1597	2.13	1.3567	0.48 ($1b_2 \rightarrow 4a_1$) − 0.42 ($2a_1 \rightarrow 2b_2$) +0.32 ($2a_1$, $1b_2 \rightarrow 3a_1$, $4a_1$) −0.25 ($2a_1^2 \rightarrow 3a_1$, $2b_2$) + 0.22 ($1a_1 \rightarrow 2b_2$) −0.17 ($1b_2 \rightarrow 5a_1$)
4^1B_2	−1.1551	2.25	0.0063	0.34 ($1a_1 \rightarrow 2b_2$) + 0.30 ($2a_1^2 \rightarrow 3a_1$, $2b_2$) +0.23 ($1b_2 \rightarrow 5a_1$) −0.23 ($2a_1$, $1b_2 \rightarrow 2b_2^2$) −0.22 ($2a_1$, $1b_2 \rightarrow 3a_1$, $4a_1$) +0.19 ($2a_1 \rightarrow 4b_2$) +0.15 ($2a_1$, $1b_2 \rightarrow 3a_1$, $5a_1$)
5^1B_2	−1.1513	2.36	0.0010	−0.59 ($2a_1$, $1b_2 \rightarrow 3a_1$, $4a_1$) +0.21 ($2a_1^2 \rightarrow 3a_1$, $2b_2$) −0.18 ($2a_1 \rightarrow 3b_2$) −0.17 ($2a_1$, $1b_2 \rightarrow 3a_1$, $7a_1$)
6^1B_2	−1.1495	2.41	0.0907	0.32 ($1b_2 \rightarrow 5a_1$) − 0.29 ($2a_1$, $1b_2 \rightarrow 3a_1^2$) −0.26 ($1b_2 \rightarrow 7a_1$) −0.21 ($1b_2 \rightarrow 3a_1$) −0.19 ($2a_1$, $1b_2 \rightarrow 3a_1$, $5a_1$) −0.19 ($2a_1$, $1b_2 \rightarrow 2b_2^2$) +0.17 ($1b_2 \rightarrow 8a_1$) − 0.17 ($2a_1^2 \rightarrow 3a_1$, $2b_2$) −0.16 ($2a_1$, $1b_2 \rightarrow 3a_1$, $7a_1$) −0.16 ($1a_1 \rightarrow 2b_2$)
7^1B_2	−1.1435	2.57	0.0303	−0.28 ($1b_2^2 \rightarrow 4a_1$, $2b_2$) − 0.27 ($2a_1 \rightarrow 3b_2$) −0.25 ($1b_2 \rightarrow 6a_1$) +0.23 ($1b_2 \rightarrow 7a_1$) − 0.22 ($2a_1^2 \rightarrow 3a_1$, $2b_2$) −0.22 ($2a_1 \rightarrow 4b_2$) + 0.21 ($1b_2 \rightarrow 5a_1$) +0.17 ($2a_1$, $1b_2 \rightarrow 3a_1^2$) − 0.17 ($1b_2 \rightarrow 13a_1$)
8^1B_2	−1.1359	2.78	0.0276	−0.50 ($2a_1 \rightarrow 3b_2$) − 0.30 ($2a_1^2 \rightarrow 3a_1$, $3b_2$) −0.24 ($1b_2 \rightarrow 5a_1$) −0.20 ($2a_1$, $1b_2 \rightarrow 3a_1$, $4a_1$) +0.17 ($1b_2 \rightarrow 6a_1$) + 0.17 ($2a_1$, $1b_2 \rightarrow 4a_1^2$) +0.16 ($2a_1^2$, $1b_2 \rightarrow 3a_1$, $4a_1^2$)
9^1B_2	−1.1280	2.99	0.1897	0.30 ($1b_2^2 \rightarrow 4a_1$, $2b_2$) − 0.29 ($2a_1 1b_2 \rightarrow 2b_2^2$) +0.27 ($1b_2^2 \rightarrow 3a_1$, $2b_2$) + 0.20 ($2a_1$, $1b_2 \rightarrow 3a_1^2$) −0.20 ($2a_1^2 \rightarrow 3a_1$, $2b_2$) − 0.20 ($2a_1$, $1b_2 \rightarrow 3a_1$, $5a_1$) −0.20 ($1b_2 \rightarrow 7a_1$)
10^1B_2	−1.1277	3.00	0.0039	0.36 ($2a_1 \rightarrow 4b_2$) − 0.30 ($1b_2 \rightarrow 6a_1$) −0.30 ($1a_1 \rightarrow 2b_2$) +0.19 ($1a_1$, $2a_1 \rightarrow 3a_1$, $2b_2$) − 0.18 ($2a_1 \rightarrow 2b_2$) +0.17 ($1b_2 \rightarrow 5a_1$) −0.17 ($2a_1 \rightarrow 7b_2$) − 0.16 ($1b_2 \rightarrow 8a_1$) +0.16 ($1b_2 \rightarrow 7a_1$)
11^1B_2	−1.1197	3.22	0.0131	−0.30 ($2a_1$, $1b_2 \rightarrow 3a_1^2$) + 0.26 ($1b_2 \rightarrow 9a_1$) +0.26 ($1b_2^2 \rightarrow 3a_1 2b_2$) −0.25 ($1b_2 \rightarrow 8a_1$) − 0.24 ($1b_2 \rightarrow 5a_1$) +0.20 ($1b_2 \rightarrow 7a_1$) −0.18 ($2a_1$, $1b_2 \rightarrow 3a_1$, $9a_1$) +0.17 ($2a_1$, $1b_2 \rightarrow 3a_1$, $5a_1$)
12^1B_2	−1.1154	3.33	0.0360	0.52 ($1b_2 \rightarrow 9a_1$) +0.38 ($1b_2 \rightarrow 8a_1$) +0.22 ($2a_1$, $1b_2 \rightarrow 3a_1$, $9a_1$) −0.19 ($1b_2^2 \rightarrow 3a_1$, $2b_2$) −0.18 ($1b_2 \rightarrow 6a_1$)

[a] The CI energies obtained from MRDCI treatments employing AO basis (4s4p/3s3p): 57M/12R (T = 2.7 μh), 49M/8R (T = 1.2 μh), and 62M/12R (T = 2.3 μh) for $^1A_1$, $^1B_1$, and $^1B_2$ states, respectively. [b] Transition energies. [c] Oscillator strengths. [d] Leading excitations of the wavefunction. Excitations with respect to the ground-state configuration are indicated. The configurations with the coefficients $|c| \geq 0.15$ are listed.

tions, but the coefficients of the single excitations and their signs give rise to a different interference and therefore a smaller transition dipole results in the former case. Notice that the lower lying optically allowed transitions to the 1^1T_2, 2^1T_2, and 3^1T_2 states located at 1.58, 1.68, and 2.08 eV, respectively, have considerably lower oscillator strengths. The leading configuration of the 1^1T_2 state arises from a HOMO–LUMO excita-

TABLE V. Comparison of Transition Energies and Oscillator Strengths Obtained from the ECP–CVC-RPA and ECP–CVC-TDA Approaches for the Na_8 ($D_{3h} \rightarrow C_{2v}$) Structure[a]

state	T_e (RPA)[b]	T_e (TDA)[b]	f_e (RPA)[c]	f_e (TDA)[c]	leading excitations (RPA):[d] $\|c\| \geq 0.2$
2^1A_1	1.80	1.84	0.34	0.41	0.88 ($2a_1 \rightarrow 3a_1$)
3^1A_1	2.12	2.15	0.00	0.00	−0.67 ($2a_1 \rightarrow 4a_1$) − 0.67 ($1b_2 \rightarrow 2b_2$)
4^1A_1	2.24	2.35	1.20	1.20	0.63 ($2a_1 \rightarrow 4a_1$) − 0.63 ($1b_2 \rightarrow 2b_2$)
5^1A_1	2.84	2.91	0.14	0.14	−0.55 ($2a_1 \rightarrow 5a_1$) + 0.55 ($1b_2 \rightarrow 3b_2$)
6^1A_1	2.87	2.94	0.00	0.00	−0.66 ($2a_1 \rightarrow 5a_1$) − 0.66 ($1b_2 \rightarrow 3b_2$)
7^1A_1	3.15	3.16	0.00	0.00	−0.60 ($2a_1 \rightarrow 6a_1$) + 0.39 ($2a_1 \rightarrow 7a_1$), −0.39 ($1b_2 \rightarrow 4b_2$) − 0.34 ($2a_1 \rightarrow 10a_1$)
8^1A_1	3.22	3.26	0.01	0.01	0.66 ($1b_2 \rightarrow 4b_2$) + 0.33 ($2a_1 \rightarrow 7a_1$), +0.32 ($2a_1 \rightarrow 5a_1$) − 0.32 ($1b_2 \rightarrow 3b_2$)
9^1A_1	3.38	3.39	0.03	0.03	−0.83 ($2a_1 \rightarrow 10a_1$)
10^1A_1	3.48	3.49	0.08	0.15	−0.63 ($2a_1 \rightarrow 7a_1$) − 0.43 ($2a_1 \rightarrow 6a_1$), −0.36 ($2a_1 \rightarrow 3a_1$)
11^1A_1	3.59	3.69	0.00	0.00	−0.87 ($1a_1 \rightarrow 3a_1$)
1^1B_1	1.92	1.95	0.0	0.00	−0.90 ($2a_1 \rightarrow 1b_1$)
2^1B_1	2.83	2.83	0.0	0.00	−0.62 ($2a_1 \rightarrow 2b_1$) − 0.62 ($1b_2 \rightarrow 1a_2$)
3^1B_1	2.85	2.94	1.04	1.17	0.67 ($2a_1 \rightarrow 2b_1$) − 0.67 ($1b_2 \rightarrow 1a_2$)
4^1B_1	3.36	3.37	0.0	0.00	0.63 ($2a_1 \rightarrow 3b_1$) − 0.40 ($2a_1 \rightarrow 4b_1$), −0.40 ($1b_2 \rightarrow 2a_2$)
5^1B_1	3.63	3.68	0.40	0.57	0.76 ($1a_1 \rightarrow 1b_1$) − 0.39 ($2a_1 \rightarrow 4b_1$), +0.39 ($1b_2 \rightarrow 2a_2$)
6^1B_1	3.75	3.76	0.0	0.00	−0.47 ($2a_1 \rightarrow 4b_1$) − 0.47 ($1b_2 \rightarrow 2a_2$)
					+0.44 ($2a_1 \rightarrow 5b_1$) − 0.40 ($2a_1 \rightarrow 3b_1$)
7^1B_1	3.84	3.85	0.03	0.06	−0.57 ($2a_1 \rightarrow 4b_1$) + 0.57 ($1b_2 \rightarrow 2a_2$), +0.52 ($1a_1 \rightarrow 1b_1$)
8^1B_1	4.07	4.08	0	0.0	0.73 ($2a_1 \rightarrow 5b_1$) + 0.46 ($2a_1 \rightarrow 3b_1$)
9^1B_1	4.28	4.40	0.38	0.98	−0.65 ($2a_1 \rightarrow 6b_1$) + 0.65 ($1b_2 \rightarrow 3a_2$)
10^1B_1	4.36	4.36	0.00	0.0	−0.54 ($2a_1 \rightarrow 6b_1$) − 0.54 ($1b_2 \rightarrow 3a_2$), +0.43 ($2a_1 \rightarrow 5b_1$)
1^1B_2	1.69	1.71	0.00	0.00	−0.66 ($2a_1 \rightarrow 2b_2$) + 0.66 ($1b_2 \rightarrow 4a_1$), 0.88 ($1b_2 \rightarrow 3a_1$)
3^1B_2	2.24	2.35	1.20	1.55	0.63 ($2a_1 \rightarrow 2b_2$) + 0.63 ($1b_2 \rightarrow 4a_1$)
4^1B_2	2.84	2.91	0.14	0.33	−0.55 ($2a_1 \rightarrow 3b_2$) − 0.55 ($1b_2 \rightarrow 5a_1$)
5^1B_2	2.99	2.99	0.00	0.00	0.60 ($2a_1 \rightarrow 3b_2$) − 0.60 ($1b_2 \rightarrow 5a_1$)
6^1B_2	3.15	3.16	0.0	0.00	−0.60 ($1b_2 \rightarrow 6a_1$) + 0.39 ($2a_1 \rightarrow 4b_2$), +0.39 ($1b_2 \rightarrow 7a_1$) − 0.34 ($1b_2 \rightarrow 5a_1$)
7^1B_2	3.22	3.26	0.00	0.00	0.66 ($2a_1 \rightarrow 4b_2$) − 0.33 ($1b_2 \rightarrow 7a_1$), +0.32 ($2a_1 \rightarrow 3b_2$) + 0.33 ($1b_2 \rightarrow 5a_1$)
8^1B_2	3.38	3.39	0.03	0.04	0.83 ($1b_2 \rightarrow 10a_1$)
9^1B_2	3.48	3.49	0.08	0.15	−0.63 ($1b_2 \rightarrow 7a_1$) − 0.43 ($1b_2 \rightarrow 6a_1$), −0.36 ($1b_2 \rightarrow 3a_1$)
10^1B_2	3.51	3.51	0.00	0.00	−0.53 ($1b_2 \rightarrow 8a_1$) − 0.53 ($2a_1 \rightarrow 5b_2$)

[a] The ground-state SCF one-electron functions have been used employing AO basis (4s4p/3s3p). [b] Transition energies. [c] Oscillator strength. [d] Leading excitations with respect to the ground-state configuration ($1a_1^2 2a_1^2 1b_2^2$).

tion ($1t_2 \rightarrow 2a_1$) and the composition of the 2^1T_2 and 3^1T_2 wave functions is dominated by three configurations arising from single excitation from $1t_2 \rightarrow 2t_2$ and to the 1e MO's. These two weak transitions coincide with the measured fine structure, red shifted with respect to the dominant transition (for details cf. ref 162).

The closely related D_{2d} Na_8 structure again exhibits dominant features at ~2.5 eV, which correspond to the calculated transitions to the 3^1B_2 and 6^1E states. This is easy to understand by comparing the one-electron schemes for the T_d and D_{2d} structures. The symmetry lowering in the latter splits the degeneracy of t_2 representation into e and b_2, giving rise to two transitions which have large oscillator strengths and almost coincide in energy. The transition to the 2^1B_2 state at 2.09 eV with small but not negligible oscillator strength corresponds again to the measured fine structure.

In the case of the antiprism (D_{4d}) the dominantly intense transition to the 4^1E_1 state at 2.7 eV is slightly blue shifted relative to the maximum of the measured cross section and the weak transtions do not correspond to the measured fine structure. The one-electron levels of this compact and highly symmetrical structure (Figure 28) do not substantially differ from those of the T_d and D_{2d} structures. Correspondingly, the leading features of the wave functions of the 4^1E state are determined by single excitations similar to the case of the states of the T_d and D_{2d} structures to which intense transitions have been found. Although the absorption spectrum calculated for the antiprism contains a single intense transition, the agreement with the locations of observed bands is not as good as for the T_d and D_{2d} structures. Since all intense transitions for the three Na_8 structures considered are characterized by the interaction of singly excited configurations, RPA using the SCF one-electron functions yields very similar results to those obtained by the CI treatments (cf. Figure 29). In fact, for the T_d[333] and D_{2d}[158] structures for the RPA gives rise to two close-lying transitions which exhaust the large part of the sum of oscillator strengths. For D_{4d} one single transition is more dominant similar to that found by using the CI procedure. The transitions with low values of the oscillator strength are distributed over a large part of the energy interval, particular for the D_{2d} structure.

Notice that although the three structures, T_d, D_{2d}, and D_{4d} calculated for Na_8 give rise to similar spectroscopic patterns, only the first one represents an equilibrium geometry. Furthermore, it is apparent that the consideration of dynamical averaging of geometries to yield "spherical" Na_8 in which the position of the nuclei can be neglected is an inadequate assumption for this level of response measurement.[332] It is more appropriate to consider the broadening of the intense absorption band due to vibrations.

It is instructive to compare the calculated spectra for Na_6 and Na_8 and to point out similarities and differences. This is particularly interesting in the context of the previous plasmon collective mode interpretation of a "giant resonance" found for Na_8.[277,296,297] Let us compare the one-electron level schemes and the calculated spectra of the T_d Na_8 cluster with those obtained for the D_{3h} and C_{5v} structures of Na_6. The HOMO–LUMO gap is almost the same for all three structures (4.3–4.4 eV) (cf. Figures 24 and 28). In the case of Na_6 the interaction among single excitations from the highest occupied to a pair of almost degenerate one-electron levels $1e' \approx (2a_1, 1b_2) \rightarrow 2e' \approx (4a_1, 2b_2)$ corresponding

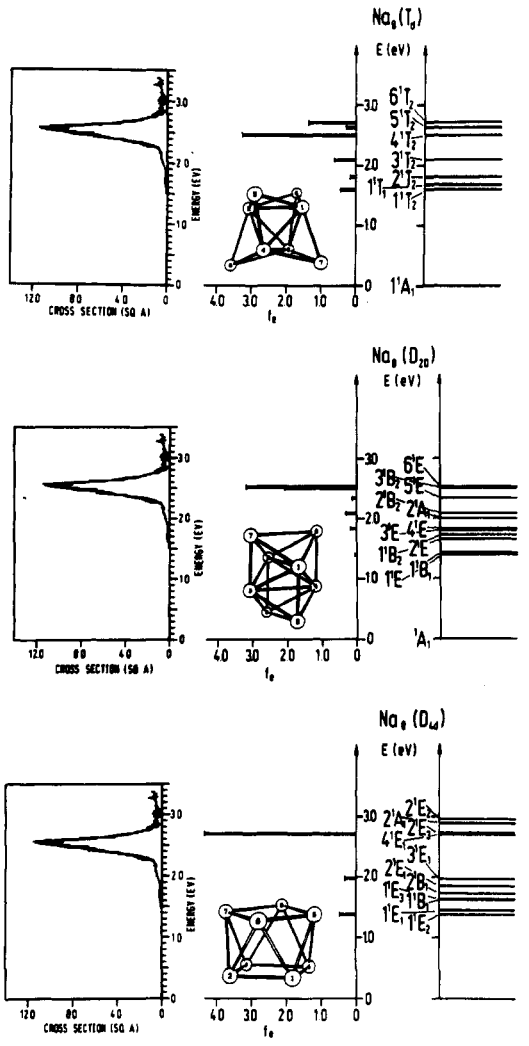

Figure 27. Comparison of photodepletion spectrum[279,280] and CI optically allowed transitions (eV) and oscillator strengths f_e of three Na_8 structures:[305,162] T_d, D_{2d}, and D_{4d}.

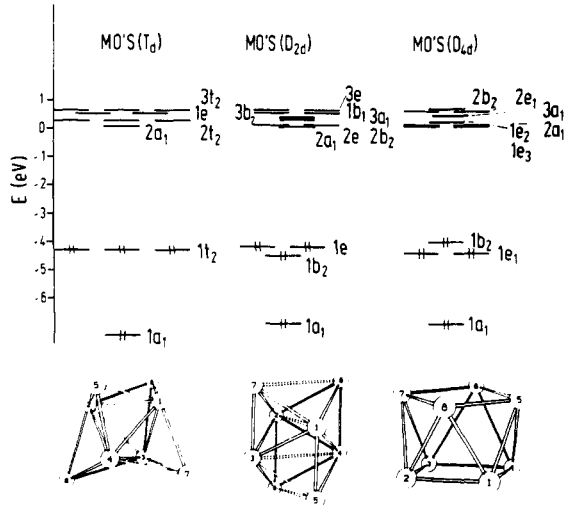

Figure 28. The SCF MO's for three energetically close lying structure of Na_8: T_d, D_{2d}, and D_{4d}.

to LUMO + 1 gives rise to a pair of states with low and high oscillator strengths (due to interference) with a dominant transition at ~2.1 eV (cf. Table IV). For Na_8 the interaction among single excitations from degenerate HOMO levels to the second and third pairs of degenerate orbitals ($1t_2 \rightarrow 3t_2$, $1t_2 \rightarrow 1e$) shifts the in-

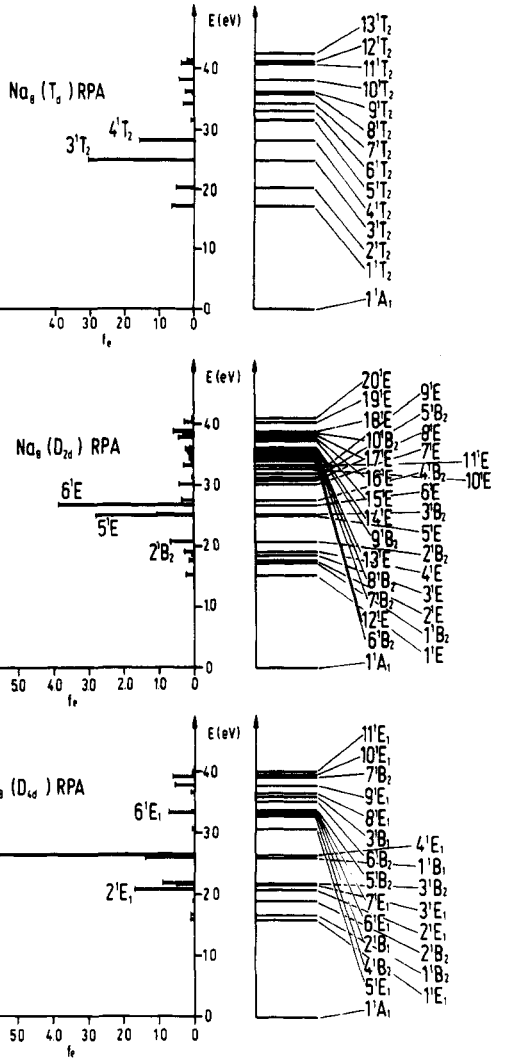

Figure 29. The RPA (based on SCF procedure) optically allowed transitions (eV) and oscillator strengths f_e for three energetically close lying structures of Na_8: T_d, D_{2d}, and D_{4d}.

tense transition to the blue by about 0.4 eV. Moreover, the weak transition in Na_8 is also located at ~2.08 eV and in the wave function of 3^1T_2 the interaction between single excitations from the $1t_2 \rightarrow 2t_2$ levels plays a leading role. In other words, the appearance of the intense transitions in the same or similar energy region for clusters of different sizes is closely connected with their geometrical structures. Both intense transitions in Na_6 and Na_8 with locations differing by ~0.4 eV, can be interpreted as due to the interference phenomena in which only a very limited number of particle–hole excitations (three) play a leading role. The interaction among these single excitations giving rise to the final quantum-mechanical states is a many-electron effect which cannot be classified as a collective mode in the sense of plasmon theory (cf. section II.B.7).

At this point it is instructive to mention that the description of the excited states of clusters in terms of interaction of individual excitations is just a way of improving the wrong starting point which is the one electron picture. However, this discussion is useful since we can distinguish between (i) individual particle–hole excitations and (ii) many-electron effects which can be qualitatively determined by (a) interaction among very few leading excitations as is the case in many molecular excited states and those (b) for which a very large

number of excitations with comparable weights is involved so that the notion of collective excitations can be introduced.

In this context, the question can be raised at which cluster size such a molecular picture will disappear. Therefore, the interpretation of the absorption spectrum of Na_{20} is of particular interest. The geometry optimization of the Na_{20} structure without symmetry constraints is not a very easy task. In analogy to Li_{20},[164] several structures have been optimized under symmetry restrictions such as the most compact highly symmetrical T_d Na_{20}, and sections of fcc and hcp lattices with T_d and D_{3h} symmetry, respectively. Other structures resulting from pentagonal growth as well as deformed sections of hcp lattices will have still to be considered (cf. ref 157). The SCF E_b/n for the T_d–fcc structure is lower than for the other two geometries. This energy ordering remains the same when the correlation energy has been estimated by a nonlocal density functional by using the HF density.[334] However, in analogy to Li_{20}, the extensive CI treatment for Na_{20} might yield the lowest energy for the most compact "spherical" T_d structure. The results at this level of calculation are not yet available. The MO schemes of both T_d structures are compared in Figure 30. The valence electrons occupying one-electron levels $1a_1$, $1t_2$, $2a_1$, 1e, and $2t_2$ in both cases can be approximately compared with 1s, 1p, 2s, and 1d orbitals of the superatom. However, there are differences in energy ordering of degenerate one-electron levels among the two structures, particularly in the case of the "spherical" T_d structure. Notice that the HOMO–LUMO ($2t_2$–$3t_2$) energy gap of the "spherical" T_d structure of Na_{20} is only ~0.5 eV smaller than for the three Na_8 geometries considered. Moreover, the HOMO–LUMO gap of Na_8 (T_d) is comparable in size with the energy difference between the 1e ≡ HOMO-1 (or $2a_1$ ≡ HOMO-2) and the LUMO of Na_{20}. If we assume, according to the analysis of the Na_6 and Na_8 results, that the dominant transition will arise by interaction among single excitations from the 2s1d type of one-electron levels (corresponding to HOMO, HOMO-1, and HOMO-2) to degenerate close-lying unoccupied orbitals, it is likely that the location of this band will not substantially differ from the one found for the Na_8 cluster.

A comparison of ECP–RPA results for Na_8 (T_d)[333] and Na_{20} (T_d)[328] with the experimental spectra is shown in Figure 31. In fact, the most intense calculated transitions are located in both cases at ~500 nm, where the giant resonances have been found. However, the second intense transition to 4^1T_2 in the case of Na_8 is slightly blue shifted relative to the measured maximum and the value of the oscillator strength is about half of that calculated for the 3^1T_2 state. For the highly symmetrical spherical Na_{20} with T_d symmetry the ECP–RPA yields a single dominant intense transition to the 9^1T_2 state, although there are two additional states with some oscillator strengths in the 450–500 nm regions where the broad band has been measured. Notice however, that for the most intense transition the oscillator strength f_e has a value of about 10. In addition to the values of f_e drawn in Figure 31a there are many small contributions in the energy interval considered. The sum of f_e is 19.1 in the energy interval up to 7.78 eV.

The number of particle–hole excitations playing a leading role in the 9^1T_2 state of $Na_{20}(T_d)$ is larger than in the case of the 3^1T_2 and 4^1T_2 states of Na_8. The weights of the three leading excitations in the 3^1T_2 state of Na_8 represent 78% of the wave function. For Na_{20} the main contributions to 9^1T_2 arise by promoting one electron from six close-lying $2a_1 \equiv 2s$ and 1e, $2t_2 \equiv 1d_\epsilon, 1d_\gamma$ occupied levels to the three lowest lying unoccupied t_2, two a_1, and $1t_1$ levels. The configurations ($2t_2 \rightarrow 1t_1$) ≡ ($1d_\gamma \rightarrow 1f_\epsilon$), ($1e \rightarrow 3t_2$) ≡ ($1d_\epsilon \rightarrow 1f_\gamma$), ($2t_2 \rightarrow 4t_2$) ≡ ($1d_\gamma \rightarrow 2p$), ($2t_2 \rightarrow 3a_1$) ≡ ($1d_\gamma \rightarrow 3s$), and ($2a_1 \rightarrow 4t_2$) ≡ ($2s \rightarrow 2p$) contribute with weights larger than 0.1 to the 9^1T_2 state of Na_{20}, making up 62% of the wave function. The labels point out a connection between the T_d and the full rotation R_3 symmetry groups. In other words, the number of leading particle–hole excitations is still not very large in Na_{20}. There are also differences between the spectra obtained from ECP–RPA for Na_8 and Na_{20} with respect to those resulting from the RPA based on the jellium model, as will be discussed in section IV.D.2, illustrating a strong dependence of the results on the details of the potential.

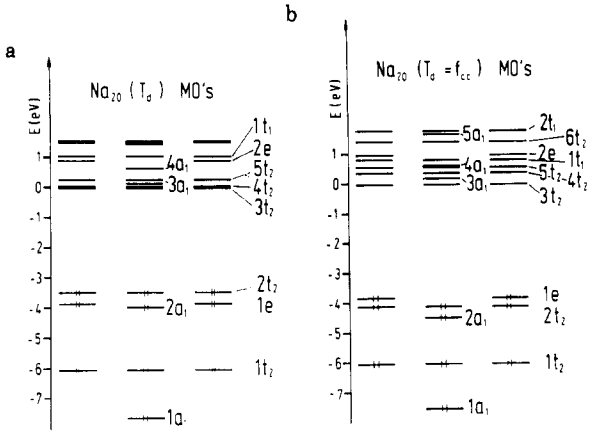

Figure 30. The SCF MO's for (a) the "spherical" T_d Na_{20} structure and (b) for the T_d geometry which is a section of the fcc lattice.

However, the T_d–fcc structure of Na_{20} gives rise to a completely different spectral pattern (cf. Figure 31b) which does not correspond to the measured one. The transition to the 6^1T_2 located at 560 nm has the largest oscillator strength, but it does not dominate the spectrum since there are two other transitions to the 7^2T_2 and 10^1T_2 states at 510 and 433 nm with relatively large intensities. The 6^1T_2 state contains four leading particle–hole transitions with weights > 0.1:($1e \rightarrow 4t_2$) = ($1d_\epsilon \rightarrow 1f_\gamma$), ($1e \rightarrow 1t_1$) ≡ ($1d_\epsilon \rightarrow 1f_\epsilon$), ($2a_1 \rightarrow 3t_2$) ≡ ($2s \rightarrow 2p$) and ($2t_2 \rightarrow 4t_2$) ≡ ($1d_\gamma \rightarrow 1f_\gamma$). Transition to this state exhausts 20% of the oscillator strength sum which equals to 19.04 over the energy interval up to 7.5 eV. The other two states, 7^1T_2 and 10^1T_2 with oscillator strength each representing ~12% of the sum contain two and three leading configurations: ($2t_2 \rightarrow 4t_2$) ≡ ($1d_\gamma \rightarrow 1f_\gamma$), ($2t_2 \rightarrow 1t_1$) ≡ ($1d_\gamma \rightarrow 1f_\epsilon$); and ($2t_2 \rightarrow 4a_1$) ≡ ($1d_\gamma \rightarrow 4s$), ($2a \rightarrow 3t_2$) ≡ ($2s \rightarrow 2p$), ($2t_2 \rightarrow 5t_2$) ≡ ($1d_\gamma \rightarrow 2d_\gamma$), respectively. There are many small contributions of the oscillator strengths for transitions distributed over the whole energy interval. Structural assignment of the recorded Na_{20} spectrum has not been completed yet. This investigation is in progress.[328] Note that experimental internal energies may in fact be a problem here.

Na_9^+. The depletion spectrum of Na_9^+ exhibits a giant resonance with a maximum located at 2.62 eV[309] just

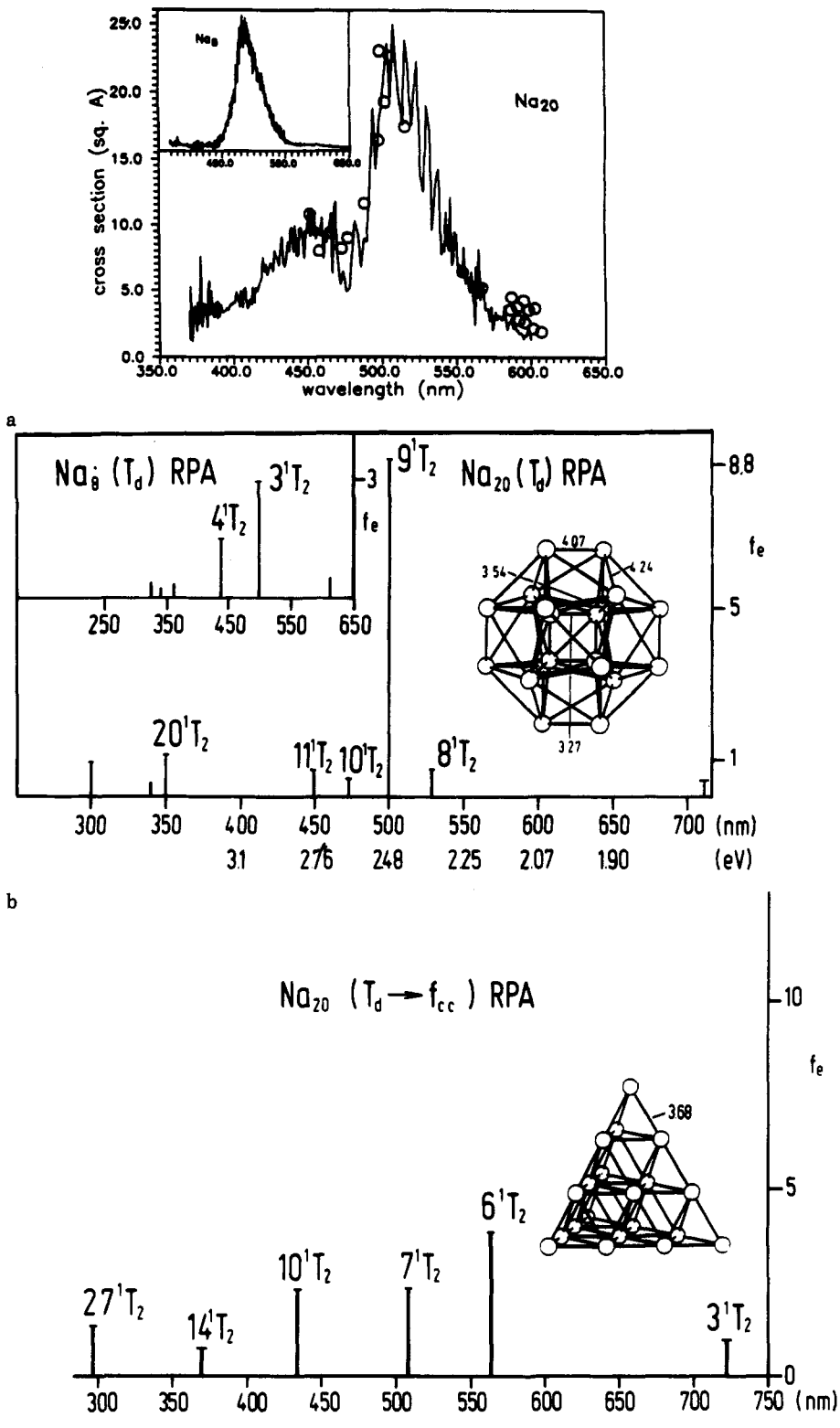

Figure 31. Comparison of the photodepletion spectrum of Na_{20}[308] and Na_8[308] and RPA optically allowed transitions (nm) and oscillator strengths f_e for (a) the highly symmetrical T_d structures of Na_{20}[328] and Na_8[333] and (b) for T_d structure of Na_{20}[328] which is a section of the fcc lattice.

slightly blue shifted with respect to the one found for Na_8. The Na_9^+ structure with C_{2v} symmetry obtained by adding one atom to the T_d structure of Na_8 has the lowest SCF energy in comparison with two other geometries optimized by the analytical gradient method under C_{4v} and D_{4d} symmetry constraints. The latter two structures are antiprismatic with the ninth atom capping one face of the Na_8 antiprism, and located in its center, respectively. The CI ground-state energies of both antiprismatic forms are 0.127 and 0.31 eV higher than the C_{2v} structure.[158,307] A comparison of one-electron levels in Figure 32 shows again that there are many close-lying levels to which particle–hole excitations will occur whose degeneracy is of course higher for the antiprisms than for the C_{2v} structure. Although the MO energies of Na_9^+ are shifted to lower values with

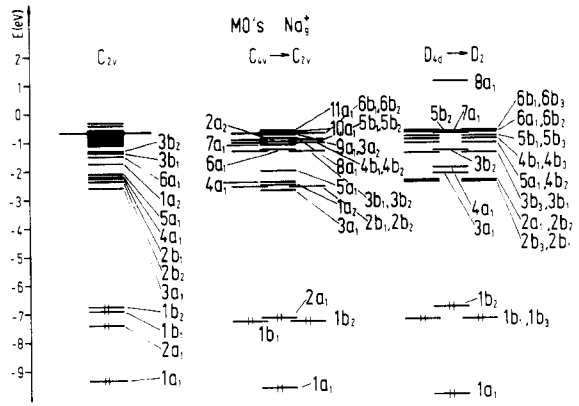

Figure 32. The SCF MO's for three energetically close lying structures of Na_9^+: C_{2v}, C_{4v}, and D_{4d}.

respect to those of Na_8 due to the lack of one electron in the field of nine nuclei, the energy gap between the levels among which excitations take place is almost the same as for Na_8 (~4.5 eV). In analogy to the previous discussion, it is to be expected that large oscillator strengths will be found for transitions to states which are located in a similar energy interval as the intense band for Na_8. Also, higher symmetrical and compact antiprisms should give rise to a smaller number of intense transition than the C_{2v} geometry.

A comparison between transition energies and oscillator strengths obtained from the ECP–CVC–CI and ECP–CVC–RPA approximations for all three Na_9^+ structures is given in Figures 33 and 34. For the C_{2v} structure the CI method yields dominant intense transitions to 7^1A_1 and 7^1B_2 states located at ~2.8 eV and two transitions at ~2.4–2.6 eV with considerable oscillator strengths. In addition weak fine structure has been located at ~2.0 eV.[307,158] An overall agreement with experimental data[309] is present, although the most intense calculated transitions lie ~0.2 eV higher than the maximum of the recorded absorption band. The dominant features of the theoretical spectrum are due to interaction among single particle–hole excitations. Therefore they are also appropriately reproduced by the RPA. However, as noticed earlier the role of double excitations seems to be larger for structures which are not highly symmetrical (e.g. C_{2v}). Therefore, in comparison with CI, the RPA yields several additional transitions with considerable intensity distributed over the broader energy interval 2.5–3.5 eV for the C_{2v} structure. Both antiprismatic forms, particularly the body centered one, give rise to dominant intensities located at 2.6–2.8 eV. The RPA yields only negligibly higher transition energies than the CI results for those states for which the high oscillator strengths have been calculated. Although an additional detailed investigation of the relative stability of the three structures of Na_9^+ might be necessary, the CI results (transition energies and oscillator strengths) for the C_{2v} and D_{4d} structures agree well with the observed spectrum.

Li_n (n = 6–8). Although the most stable ground-state structures of Li_n clusters have almost equivalent topologies to those found for Na_n, it is interesting to find out if the specific structural differences will be reflected in the absorption spectra. As mentioned earlier, the recorded and calculated absorption spectra of Li_4 and Na_4 exhibit striking similarities, and an assignment to the rhombic structure was straightforward.

For Li_6 there again are three structures of comparable stability: planar D_{3h}, flat pentagonal pyramid C_{5v}, and a C_{2v} structure containing tetrahedral subunits.[62,134,301] However, the latter has the lowest ground-state energy with respect to the former ones (0.17 eV), which is opposite to the case of Na_6. The D_{3h} and C_{5v} structures are closely connected, since the pentagonal pyramid is very flat and it transforms into the planar structure without a barrier, but the C_{2v} form is separated by a small barrier from the planar geometry.

Although the work on well-resolved absorption spectra for Li_6[301] and for Na_6,[329] as well as on the theoretical predictions for all three close-lying isomers (three-dimensional C_{2v}, planar D_{3h}, and pentagonal pyramid) is still in progress,[301,158] it is very likely that a structural difference between Na_6 and Li_6 is present. The C_{2v} structure of Li_6 which has the lowest ground-state energy gives rise to a group of transitions with considerable oscillator strengths located in the 2.4–2.6 eV energy interval. The most intense transition at 2.51 eV occurs to the 8^1A_1 state, and considerably weaker ones are located at ~1.7 eV, as shown in Figure 35. The energy difference between one-electron levels among which important excitations occur leading to the most intense transition to the 8^1A_1 state at 2.51 eV are comparable with those responsible for intense transitions in Li_7 and Li_8 clusters. For all three clusters the recorded intense transitions occur in the same energy interval (cf. Figure 36). The calculated spectral pattern obtained for the Li_6 C_{2v} structure is in complete agreement with the presently available recorded spectrum.[301] It seems that the intense band at ~2.1 eV (600 nm) present in the spectrum of Na_6[329] is absent in the case of Li_6. The planar and flat pyramidal structures of Li_6 give rise to similar spectral patterns[301] as the equivalent topologies of Na_6, with dominant feature at ~2.1 eV (600 nm). Therefore the three-dimensional Li_6 (C_{2v}) for which the dominant transitions are located at ~2.5 eV (500 nm) is the only candidate for assignment to the presently available spectrum. Although further experimental and theoretical confirmation is desirable, this is an interesting example of the pronounced structural characteristics of the absorption spectra of small clusters.

The most stable ground-state structure of Li_7 is the pentagonal bipyramid (D_{5h}).[62] For the Li_7 pentagonal bipyramid, all calculated oscillator strengths for transitions up to ~2.40 eV have negligible values. One intense transition coinciding with the maximum of the recorded band at 2.46 eV has been calculated. However, since this is an open-shell system, there are many close-lying states of the same symmetry to be determined, and it is not yet conclusive that some intense transitions blue shifted with respect to the one located at 2.46 eV might not be present.[300]

As in the case of Na_8, the tetracapped tetrahedral Li_8 structure is the most stable one and the other two D_{2d} and D_{4d} with close-lying energies do not represent local minima on the SCF surface, since they transform into the T_d form without passing over barriers[335] (cf. section III.B.1). The calculated spectra for both the T_d and D_{2d} structures of Li_8 and Na_8 have globally similar features (Figure 37) due to the symmetry and similar energy gaps between the levels among which particle–hole excitations take place. However, the energy interval in which the transitions with large intensities are located

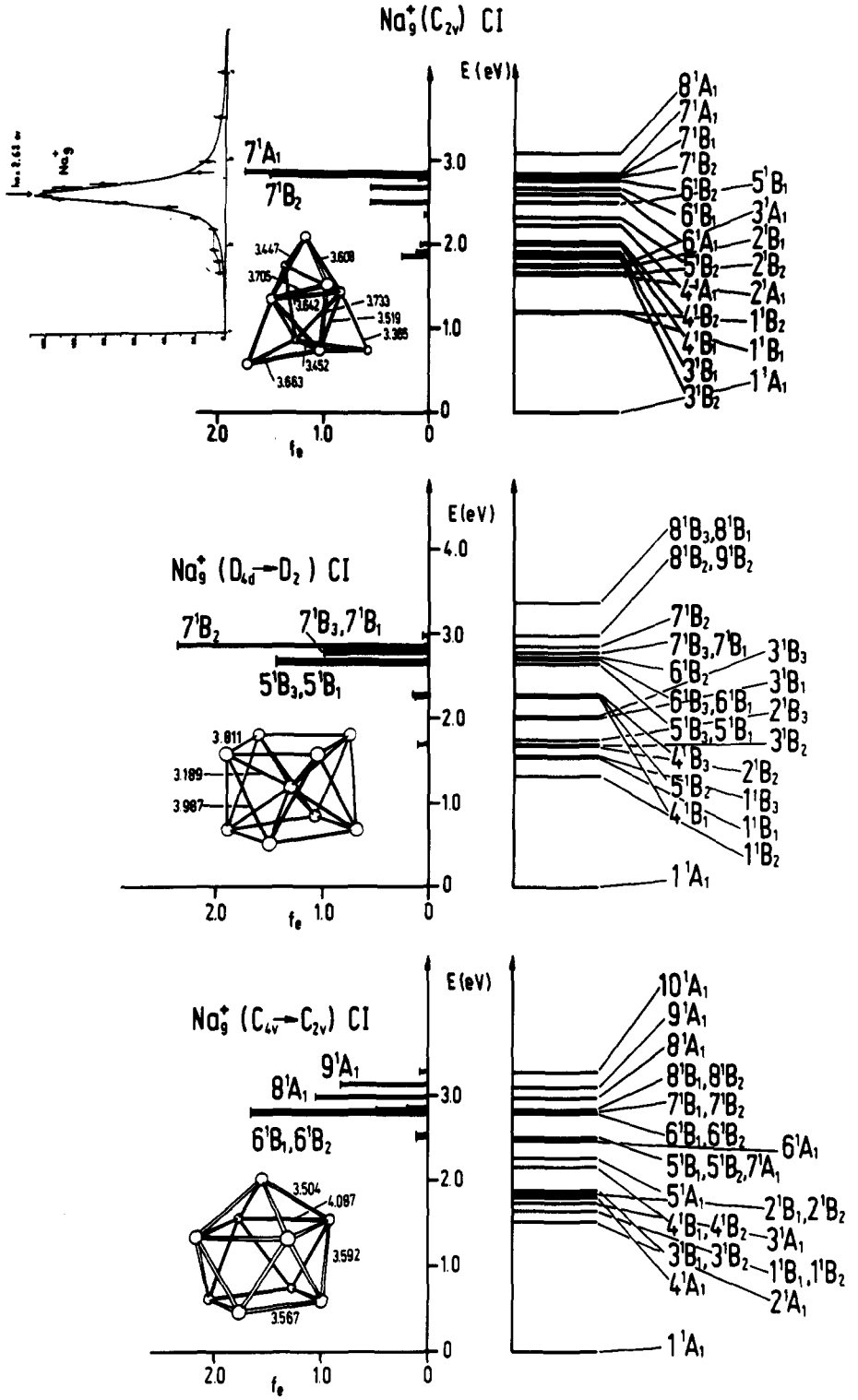

Figure 33. Comparison of the photodepletion spectrum of Na_9^+ [309] and CI optically allowed transitions (eV) and oscillator strengths f_e for three energetically close lying structures:[158,307] C_{2v}, D_{4d}, and C_{4v}.

is considerably broader in the case of Li_8 than for Na_8. Also, there is more discrepancy between the locations as well as the values of the oscillator strengths obtained from the AE-CI and AE-RPA for T_d Li_8 (cf. Figures 37 and 38) than for T_d Na_8. However, the dominant features obtained from both methods are similar although transition energies obtained from the RPA are too high in comparison with the recorded spectra. The AE-RPA method gives rise to two transitions located at ~2.4 and 3.0 eV with large and comparable oscillator strengths for the T_d structure of Li_8. For the D_{2d} structure, in addition to the most intense transition to the 6^1E state, there are transitions to three $^1B_2$ states with some oscillator strengths. The recorded depletion spectrum of Li_8 has recently become available and exhibits a dominant broad band at 450–520 nm. The assignment of the Li_8 T_d structure to the recorded spectrum is most likely, although a contribution from the other related D_{2d} structure cannot be ruled out. The energy gaps between the occupied and virtual orbitals among which important excitations take place in the wave functions for the intense transitions have very similar values for

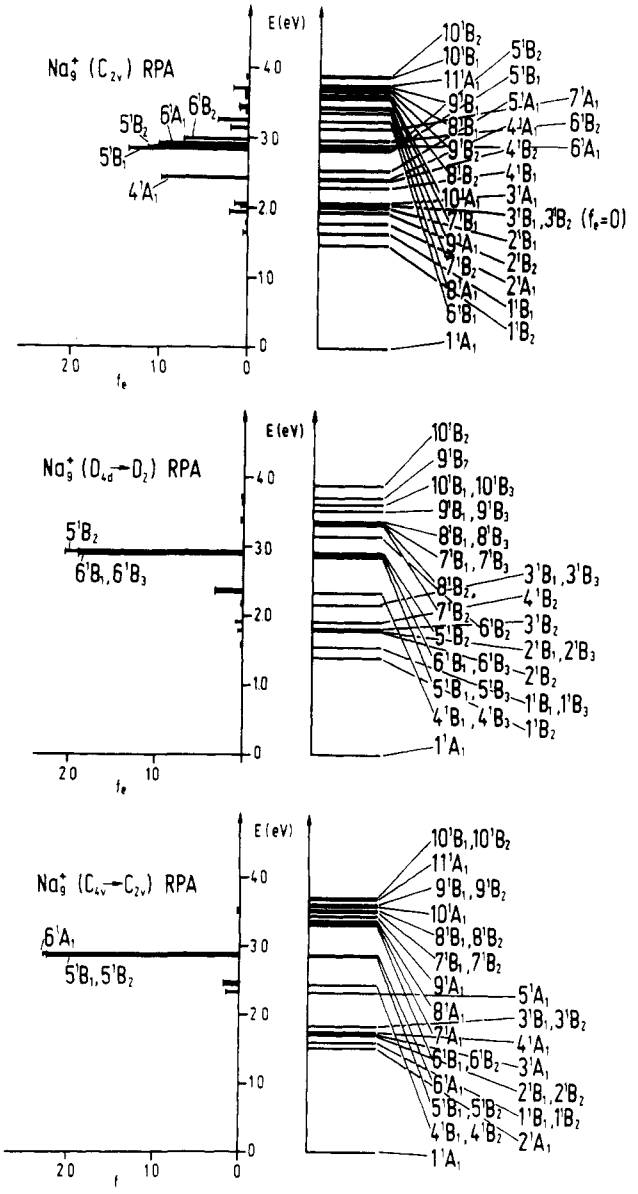

Figure 34. The RPA (based on the SCF procedure) optically allowed transitions (eV) and oscillator strengths f_e for three energetically close lying Na_9^+ structures:[159] C_{2v}, D_{4d}, and C_{4v}.

the C_{2v} Li_6, D_{5h} Li_7, and T_d Li_8 structures. This might be the reason for the almost same location of an intense transition at ~2.5 eV in all three cases.

A comparison between absorption spectra of Li_n and Na_n clusters is not yet complete and can be of significant importance for obtaining direct detailed evidence about structural properties of alkali metal clusters.

From quantum molecular description of absorption spectra of small alkali-metal clusters the following conclusions can be drawn:

(1) The appearance of dominant intense transitions is closely connected with a symmetry of the structure, the degeneracy of the one-electron levels as well as their detailed energy ordering, which is given by the potential determined by the position of the nuclei. It seems that a high degeneracy of occupied one-electron levels and close-lying triply degenerate (or almost degenerate) unoccupied levels must be available for the interacting single particle–hole excitations in order to give rise to a dominant transition.

(2) There is a substantial difference between the quantum theory of surface plasmons (section II.B.7) and CI or RPA methods (section II.A.2 and II.B.4), although all of them consider the interaction between particle–hole excitations. The frequency of the surface plasmon resulting from the quantum theory corresponds to a pole lying outside the one-electron level spectrum at an energy higher than the individual excitations (cf. section II.B.7). The interaction among excitations in the CI or RPA accounting for many-electron effects changes the energy of the resulting state with respect to the energy of the individual particle–hole excitations, giving rise to the appropriate value of the transition energy.

(3) The aim of a comparison between ab initio CI and RPA results for a number of absorption spectra for different structures has been to establish qualitative rules according to which judgement can be made under which conditions the RPA should yield reliable predictions of transition energies and oscillator strengths. The wave functions of states to which transitions with large intensities take place usually contain single excitations as leading configurations. In this case, the RPA results might be acceptable. However, there have been found many cases in which the role for interactions among double excitations is crucial for determining the spectral pattern. Additional investigations are needed before a conclusion might be drawn that, for clusters with high symmetry and high compactness, interaction among single excitations only may be sufficient for a reliable qualitative description of the absorption spectra. It seems that the ab initio RPA procedure is suitable for qualitative purposes, but it is less reliable for an assignment of a particular cluster geometry to the recorded spectrum.

(4) Large transition moments are also connected with larger polarizability of the electronic density along the symmetry axis which allows for the optical transitions. The involvement of p orbitals of Na and Li is obvious, causing in principle large polarizability already at the size of the tetramer. The appearance of one or a few dominant transitions in small alkali-metal clusters ($n \leq 20$) illustrates their very characteristic structural properties which only for considerably larger sizes where the structures turn into droplets can be adequately interpreted in the semiclassical picture of the surface plasmon, as will be discussed later in section IV.D.2. Additional experimental and theoretical data are needed in order to determine at which size approximately this transition will occur.

3. Spectroscopic Properties of Ib Clusters

Photodetachment. There are several essential difficulties in the quantitative determination of the ground and excited state properties of the neutral and anionic Cu_n, Ag_n, and Au_n clusters, as mentioned in section IV.B: (i) the correlation of d and s electrons, and therefore also large basis sets which are necessary for the approximate description of d–d correlation, as well as (ii) the treatment of the $(n + 1)$-electron system with the same accuracy as the n-electron system. In particular, if more than one valence electron per atom is correlated, the correlation of many electrons puts severe limitations on the cluster size and a size-consistent treatment of the correlation effects is important. Therefore, most of the theoretical work correlating many valence electrons per atom has been done on the

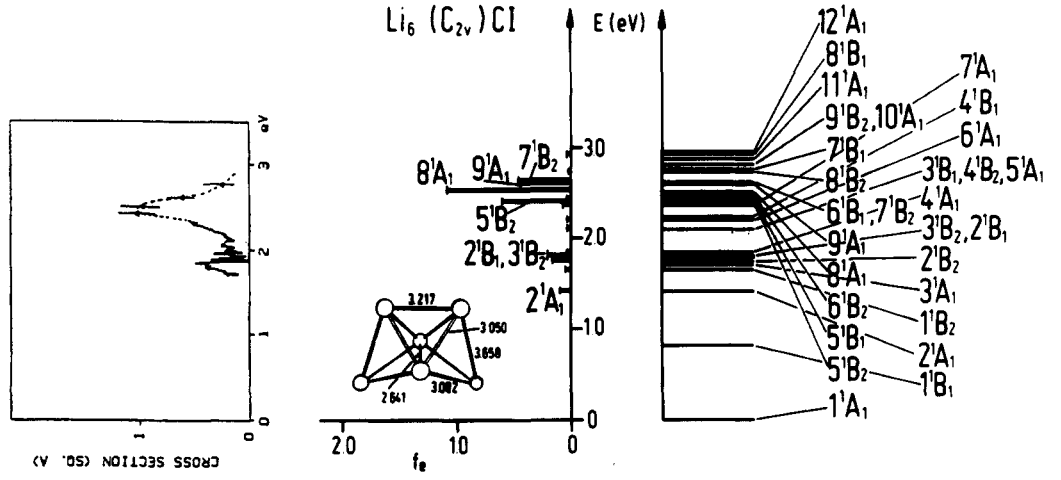

Figure 35. Comparison of the photodepletion spectrum and CI optically allowed transitions (eV) and oscillator strengths f_e for the lowest C_{2v} structures of Li_6.[301]

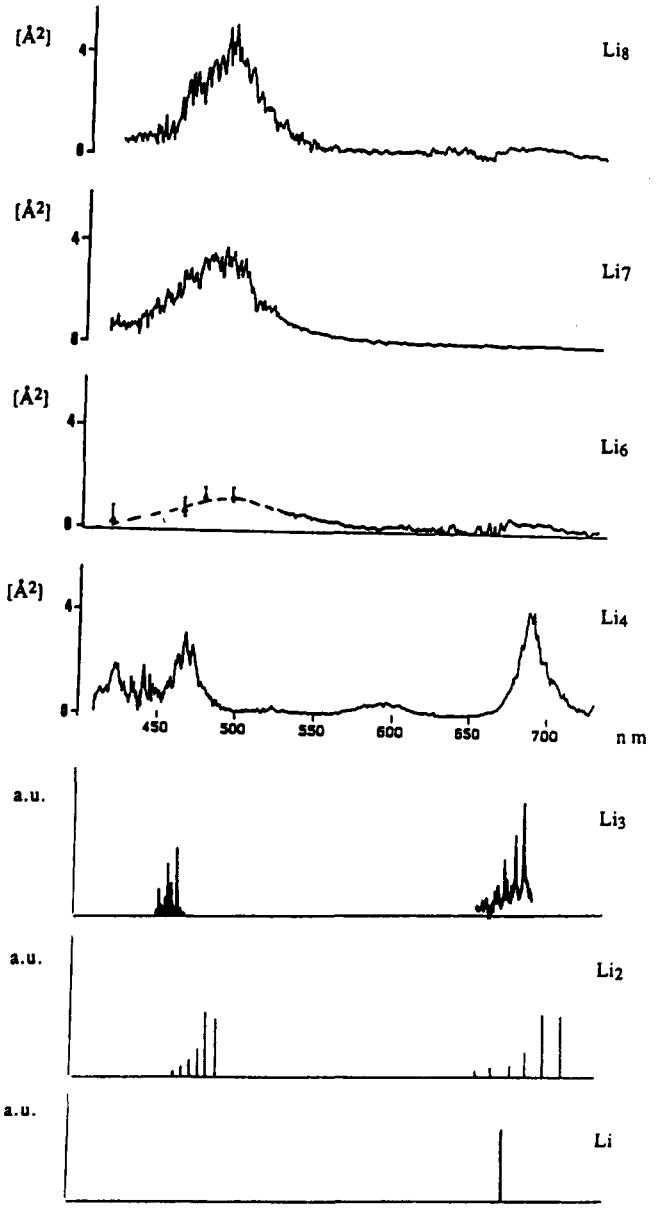

Figure 36. Photodepletion spectra of Li_n (n = 1–4, 6–8).[299,300]

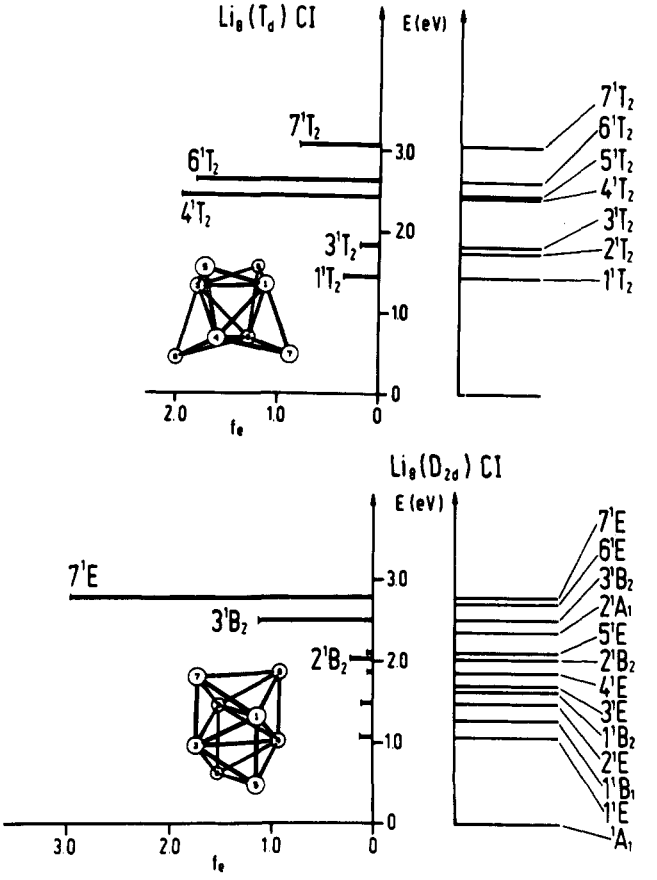

Figure 37. The CI optically allowed transitions (eV) and oscillator strengths f_e for the two most stable related structures of Li_8:[300] T_d and D_{2d}.

neutral trimers and tetramers (cf. section III.B.1). This will be addressed here only in connection with the determination of VDE and EA of anionic clusters. The theoretical description of the neutral trimers is particularly difficult, since all three of them are fluxional molecules and in some cases such as Cu_3 and Au_3, correlation effects are important even for the geometry optimization.[336] The results obtained from all-electron SCF followed by a modified coupled-pair functional (MCPF) size-consistent correlation treatment for 33 and 34 electrons are available for Cu_3 and Cu_3^-.[293,336] In the case of neutral and anionic Ag_3[336] and Au_3[294,336] the relativistic effective core potential (RECP) has been used for the inner-core electrons while the outermost core orbitals 4s and 4p for Ag and 5s and 5p for Au were included in the valence shell. Since the 5s and 6s or-

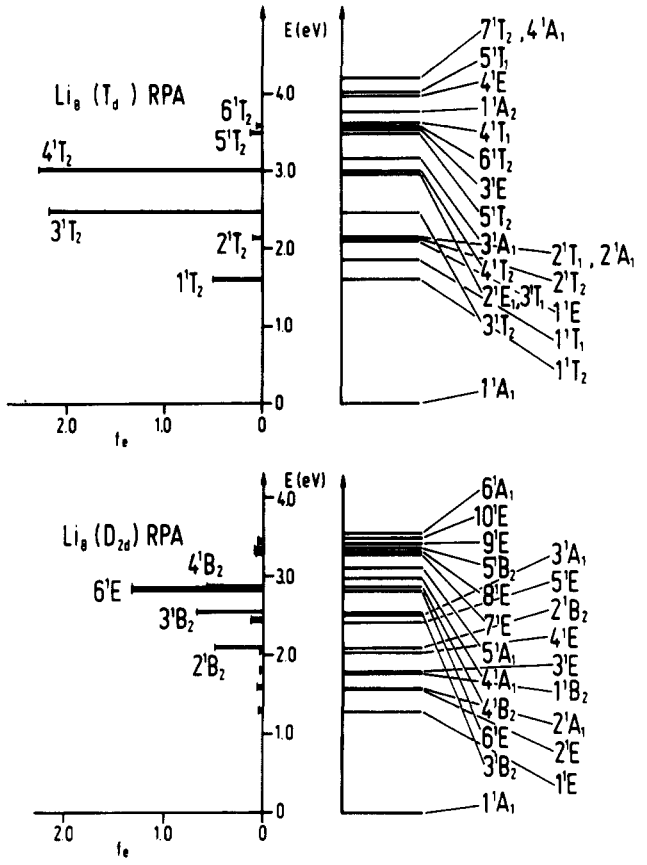

Figure 38. The RPA (based on the SCF procedure) optically allowed transitions (eV) and oscillator strengths f_e for two T_d and D_{2d} structures of Li_8.[300]

bitals have nodal spheres, the 4d and 5d electrons can correlate with 5s and 6s ones, respectively.[336] The correlation effects were accounted for by the MCPF approach. Large basis sets of the type (16s12p7d4f)/[6s3p3s1f] for Cu and (6s6p4d3f)/[5s4p4d1f] for Ag and Au have been used.[336,294] All three trimers are Jahn–Teller distorted molecules with $^2B_2$ ground states of the obtuse isosceles triangles with the bond angle only slightly larger than 60 °. The $^2B_2$ ground states are only slightly lower than the $^2E'$ states of the equilateral triangles (cf. section III.B.1). All anionic trimers are linear, since this geometry minimizes the Coulomb repulsion for the extra electron. In this respect there is close analogy to the alkali metal neutral and anionic trimers. However, it is known that even at this level of accuracy an ab initio treatment of Ib-metal clusters does not yield accurate EA's in the absolute sense. Nevertheless, if the computed EA's for the atom, diatomics, and trimers are directly multiplied by 1.3, the scaled EA values are in satisfactory agreement with the experimental values. The calculated adiabatic electron affinities for Cu_3^-, Ag_3^-, and Au_3^- without (and with) scaling including Jahn–Teller correction are 1.75 (2.24), 1.89 (2.39), and 3.26 (4.16) eV, respectively.[336] The experimental values[271] for the threshold detachment energy E_T, defined as the electron binding energy at which the intensity reaches 10% that of the lowest maximum, are 2.27 ± 0.01, 2.36 ± 0.01, and 3.4–3.95 for Cu_3^-, Ag_3^-, and Au_3^-, while the electron binding energy at the maximum of the lowest electronic transition (VDE) are 2.37 ± 0.01, 2.43 ± 0.01, and >3.5 eV, respectively. The calculated and scaled VDE values for Cu_3^- at the linear geometry are 1.97 and 2.63 eV,[337] respectively. According to Franck–Condon simulations, the observed narrow peak widths for Cu_3^- and Ag_3^- are consistent with calculations only for linear-to-linear transition ($v' = 0 \leftarrow v'' = 0$). The adiabatic electron affinity was estimated from the VDE value by subtracting the energy difference between the ground states of the neutral trimers calculated at the linear geometries of the anions and at the best geometries of the neutral ones $E\ (^2\Sigma_g^+) - E\ (^2B_2)$.[271] The Au_3^- spectrum exhibits features different from the two lighter Ib trimers. These have been assigned to a two-photon processes in which photodissociation is followed by photodetachment of the monomer and dimer fragments, since the calculated EA of 4.16 eV lies higher than the photon energy of 3.35 eV in the high resolution experiment. The experimental EA obtained by using pulsed ion sources is estimated to be ~3.9 eV.[11] The results of calculations at the same level of accuracy are available for geometries of mixed Ib trimers Au_2Cu, Au_2Ag, Ag_2Cu, Cu_2Ag, Ag_2Au, Cu_2Au, and CuAgAu as well as corresponding EA's,[336] but experimental data are not yet available.

The recorded photodetachment spectra of Ib clusters (n = 2–10) exhibit discrete isolated electronic bands (cf. Figure 39). In contrast to the nickel group clusters,[286] the relatively simple spectra of Ib-metal clusters (n = 2–10) indicate that only s valence electrons might be responsible for the relatively small number of the low-lying excited states. Therefore, simplified theoretical approaches can also be useful. Results are available presently for Cu_n ($n \leq 10$). They were obtained from the ECP approach in which copper atoms are treated as one-electron atoms.[191] This ECP (including 3d orbitals) is corrected for core–valence correlation (CPP) and correlation effects for valence s electrons are taken into account. However, a geometry optimization of the anionic structures has not been carried out. The optimized geometries of Li_n^- clusters served as starting points to select the topologies for Cu_n^- clusters (cf. section III.B.3), and then comparison of ground-state and first excited state transition energies (VDE and T_e) with measured peaks for Cu_n rather than the calculated ground state energies of anions has been used to select cluster geometries as good candidates for structural assignment.

Notice that the energy difference between the ground and first excited state of the neutral cluster (first transition energy ≡ T_{e_1}) corresponding to the energy gap between two maxima with the lowest binding energy in recorded spectrum, is often called the HOMO–LUMO gap in the literature. This stems from the qualitative considerations which have been used for the interpretation of the oscillatory behavior of T_{e_1} values as a function of cluster size, especially for even clusters. The energy gap should also decrease for large n, as the lowest excited states develop into the conduction band. The T_{e_1} energies are associated with the HOMO–LUMO gap in the case of nondegeneracy and with the even number of electrons, in the sense that, for example, the lowest lying triplet state for Cu_2 has a leading configuration in which one electron from the doubly occupied HOMO has been promoted to the LUMO: $X^1\Sigma_g^+(4s\sigma_g)^2$–$a^3\Sigma_u^+(4s\sigma_g)^1(4s\sigma_g^*)^1$. However, the calculation of the transition energy T_{e_1} involves more than just an independent-particle model as well as appropriate spin of the states under consideration. The energy of the first excited state is associated with the

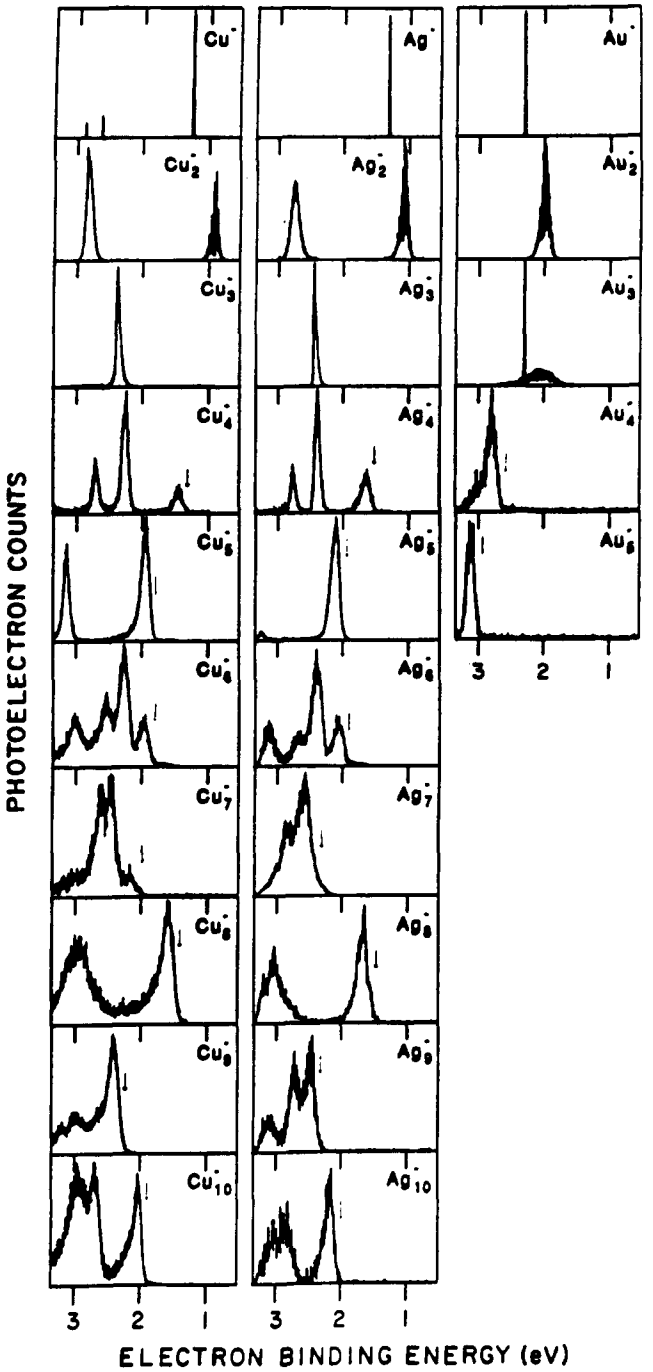

Figure 39. Comparison of photodetachment spectra of Ib anionic clusters Cu^-_{1-10}, Ag^-_{1-10}, and Au^-_{1-5} obtained by continuous beam technique.[271]

stability of the clusters. For example, T_{e_1} (Cu_2) > T_{e_1} (Cu_4) > T_{e_1} (Cu_6) < T_{e_1} (Cu_8) > T_{e_1} (Cu_{10}). Dimers and octamers are more stable than tetramers and hexamers and the HOMO–LUMO gap, as well as T_{e_1}, are larger for the former than for the latter. Notice also that, for example, HOMO–LUMO gap for K_2, K_4, and K_6 at the best geometries of the anions have values of 3.53, 3.05, and 2.8 eV, while the calculated T_{e_1} values are 0.52, 0.36, and 0.2 eV which are in agreement with the recorded spectra are presented in section IV.C.1.

Recent calculations of EA for Ib clusters up to pentamers,[199] carried out by using the MCPF method and correlating both the d and s electrons in the framework of an all-electron treatment for Cu_n and of relativistic ECP for Ag_n and Au_n, have confirmed results on Cu_n

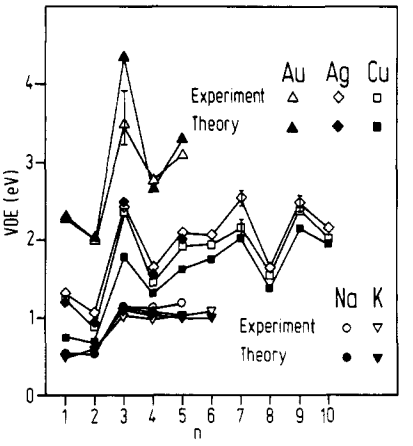

Figure 40. Comparison of measured VDE values for Ia[276] and Ib[271] clusters and calculated values for Na^-_n,[295,162] K^-_n,[144] Cu^-_n,[191] Ag^-_n,[199] and Au^-_n.[199]

obtained by using a simplified procedure.[191] Also in the case of Ag^-_4 and Au^-_5 the planar rhombic and trapezoidal geometries have been found to be the most stable, similarly to the case of the neutral ones. When scaled by the factor 1.3, the calculated values for EA are in satisfactory agreement with experimental VDE values.[271] The scaling factor has been envisaged as a correction for missing atomic electron correlation effects.[312]

A comparison of experimental and available theoretical VDE values for small Ib and Ia anionic clusters is given in Figure 40. There is a pronounced alternation between even and odd numbered clusters (odd > even), particularly for Ib metal clusters, with a general increasing tendency as a function of a cluster size, although it seems that several hundreds of atoms are needed to reach the work function values (4.65, 4.26, and 5.10 eV for Cu, Ag, and Au, respectively). Since the neutral clusters with an even number of valence electrons are more stable than those with an odd number, the accommodation of an extra electron leading to the anionic species is less favorable in the former than in the latter cases. Therefore, the VDE and EA are smaller for even than for odd numbered clusters. The general behavior of VDE for Ib clusters as a function of cluster size is parallel; the values for Au_n are just shifted by 1 eV with respect to those measured for Ag_n and Cu_n. The ECP calculations of VDE, correlating only s electrons for Cu_n[191] (scaled to account for missing atomic electron correlation effects), and without geometry optimization, reproduce the experimental trend qualitatively. The scaled VDE values obtained correlating s an d electrons of Cu_{2-5}, Ag_{2-5}, and Au_{2-5} for optimized anionic structures compare well with the experimental values.

The VDE's obtained from the AE-CI and ECP–CPPCI procedures for Na^-_n and K^-_n at their best geometries (cf. section IV.C.1) are in satisfactory agreement with the experimental values. The alternation in the VDE values for n = 4–6 is much less pronounced for alkalis than for Ib clusters. This is most probably due to structural differences of their anionic geometries. It is to be expected that a larger odd–even alternation will be present if the geometries of the anions do not substantially differ from those of the neutral ones. This for example is not the case for Na^-_4, K^-_4, and K^-_6 (cf. section IV.C.1). The linear forms (L) for Na^-_4 and K^-_4

have slightly lower energies than the rhombic ones (RH), but this is energetically unfavorable for the neutral tetramers and therefore VDE_L is considerably larger than VDE_{RH}. In contrast, the most stable geometries of anionic and neutral Ib tetramers seem to be the rhombic forms, and therefore the VDE's are relatively small and not considerably larger than the electron affinities EA. Hexamers represent special cases, since for neutral alkali-metal clusters the planar and the three-dimensional structures are in a competition. Anionic hexamers seem to prefer a square-bipyramidal geometry or a deformed C_{2v} structure, and therefore it is to be expected that the VDE values will be high. Drawing the analogy, a similar situation might be present for Ib anionic hexamers, indicating that their geometries may substantially differ from the neutral ones, which is not the case for tetramers and pentamers.[199]

In conslusion, although there are some similarities between Ia and Ib anionic clusters, it is not possible to use information available from alkali-metal cluster to make straightforward structural assignment for coinage metal clusters.

The interpretation of photodetachment spectra of larger Ib clusters for which the jellium model has been used will be briefly discussed in section IV.D.1.

Absorption Spectroscopy. The most extensively studied systems are again the trimers (cf. ref 6), and among them Cu_3. According to the SCF-SD-CI calculations[325] the ground-state energy surface of Cu_3 is also extremely flat, with the $^2B_2$ state of the obtuse isosceles triangle being slightly lower than the $^2A_1$ state of the acute one due to a Jahn–Teller distortion. The calculated barrier for pseudorotation is only 171 cm^{-1}. Two groups of low-lying excited states have been calculated,[325] a 3s Rydberg state of $^2A'_1$ symmetry located at 2.14 eV and a 3d → 4s excited state at 2.40 eV, which correlates with a $^2E''$ state of D_{3h} symmetry, were candidates for the interpretation of the absorption spectra. The $^2E' \rightarrow {}^2A'_1$ transition does not involve the dynamical Jahn–Teller effect and the $^2E' \rightarrow {}^2E''$ transition does. There has been controversy about the assignment of the measured transition at 2.3 eV, which seems to be settled as $^2E' \rightarrow {}^2A'_1$ assignment.[265]

Several excited states of Ag_3 have been calculated by using relativistic ECP and correlating the 5s electrons only.[338a] Later, Rydberg orbitals were added and the ground-state properties of the neutral and cationic Ag_3 as well as several excited states have been determined, correlating 5s and 4d electrons.[338b] Recent gas-phase spectroscopy experiments[339] on Ag_3 reported a vibronic spectrum with an origin at 3.35 eV as the result of a one-photon resonant two-step ionization process. Although there is an excited $^2E''$ state calculated in this energy interval (3.26) with some oscillator strength, additional work is necessary in order to secure a full assignment. Presently, a dynamical Jahn–Teller effect for the ground state of Ag_3, with a barrier height calculated[190] at about 100 cm^{-1}, agrees with the experiment. The conjecture has been made on the basis of vibronic structure that there might be a higher barrier to pseudorotation in the excited states,[339] but this remains to be examined.

The excited states of Ib tetramers still represent an inviting but not simple field for theoreticians. The first absorption spectrum of a Ib tetramer has recently been published.[281] The photodissociation spectrum for Cu_4^+ in the visible region (710–370 nm)[281] exhibits 10 electronic transitions and seven of them show vibrational fine structure. There are two groups of transitions located at ~650 nm and in the energy interval 450–370 nm. Since the question has been raised whether the group of transitions at ~600 nm corresponds to a d → s type of transition which does not change drastically from atom to bulk, theoretical work on the ab initio level would be helpful for addressing this problem.

Although the ground-state properties of Ib tetramers have become available recently at a high computational level as discussed in section III.B.1, there are almost no calculations for the excited states. An exception is a study of the ground state and the two lowest excited states (triplet and singlet) of Au_4.[205] A relativistic core potential and correlation employing the MCSCF/MRSDCI method including d electrons have been used. The effect of the spin–orbit term has also been investigated by using the relativistic CI method. The rhombic structure has been found to be the most stable in the singlet ground state. The surfaces of the first excited singlet and triplet states corresponding to the HOMO–LUMO transition seem to be very flat, since the energies at their own square and rhombic geometries almost coincide. The energy of the lowest triplet state at the optimized tetrahedron geometry is higher than for the rhombic or square geometries, which is opposite to the cases of Li_4 and Na_4. Also, the splitting between the $^3B_{1g}$ and $^1B_{1g}$ states seems to be smaller than in the case of alkali tetramers. However, optically allowed excited states have not yet been calculated. It would be interesting to know how much excitations from the d shell will complicate the absorption pattern of the neutral Ib tetramers with respect to the relatively simple but rich spectra of the alkali-metal tetramers.

D. Comparison and Analysis of Concepts and Results Obtained from Quantum Chemical Methods and Other Approaches

1. Photodetachment Spectra

The HOMO–LUMO energy difference and the LUMO energy of the anions obtained from the jellium model have been used for the interpretation of the UPS spectra of Cu_n (n = 6–41).[272] The qualitative agreement between theory and experiment is very good, exhibiting a particular drop in the EA values for clusters 8, 20, and 40 as well as 14 and 34. It has been assumed that there is no geometrical change between the anions and the neutral clusters. It is to be expected that for the stable clusters with n = 4, 8, and 20 the HOMO–LUMO gap is larger than in the case of less stable ones. In analogy to molecules, the lowest excited states of the stable species are usually, but not necessarily, lying higher in energy than the states of less stable ones. Consequently, the finding that the energy difference between the first two peaks in the photodetachment spectra is particularly large for n = 4, 8, and 20 can easily be explained as due to larger HOMO–LUMO gaps of these very stable species with respect to other less stable ones. This qualitative consideration is model independent. Also the low values for VDE or EA for stable molecules are then connected with the high energy of the HOMO

for anions which causes their relatively low stability. The even–odd alternations of the EA as a function of n are also easy to understand without using any particular model. Let us assume a decrease in the MO energy with cluster size. Neglecting electron–electron repulsion, as is the case in the simple theories, the HOMO of the neutral system with an odd number of electrons is analogous to the doubly occupied HOMO of the anion. Therefore the energy of the singly occupied HOMO of the anion with an even number of atoms is higher than the energy of the doubly occupied HOMO for the anionic system with an odd number of atoms. The latter may easily be lower than the energy of the singly occupied MO of the next larger anion with an even number of atoms. These simple qualitative considerations are very useful for understanding a general trend in the measured observables.

However, at least for the smaller clusters, the methods which can be used for a satisfactory interpretation of the photodetachment spectra have to provide reliable predictions of geometry, spin multiplicity, and stability of the anionic and neutral clusters. Furthermore, the correlation effects and the spin multiplicity for the ground and excited states of the neutral species have to be accounted for in order to predict the adequate energy ordering of excited states of different nature (cf. section IV.C.1).

2. Absorption Spectra

Classical Theory. As mentioned in section IIB, the Mie–Drude classical free-electron theory for surface plasmons has been frequently used for the interpretation of absorption spectra of small alkali-metal clusters.[277,296-298,278] The classical model of a damped oscillator applied to the electron polarization under the influence of an electric field has been defined in section II.B.7. The imaginary part of the polarizability $\alpha_{xx}(\omega)$ given by (IIB7.11) is connected with the photoabsorption cross section (cf. (IIB7.14)):

$$\sigma \approx \omega \, \mathrm{Im}(\alpha_{xx}(\omega)) = \omega_p^2 \omega^2 \gamma / [(\omega^2 - \omega_0^2)^2 + \omega^2 \gamma^2] \qquad \text{(IVD2.1)}$$

where ω_p is volume plasma frequency and γ is a damping factor which is inversely proportional to the electron mean free path.

The frequency-dependent polarizability has the maximum value for $\omega_0 = \omega_s = \omega_p/\sqrt{\alpha(0)}$. The same relation can be obtained from the quantum mechanical expression for the static polarizability, assuming that a single transition takes place ($\omega_{no} = \omega_0$):

$$\bar{\alpha}(0) = \frac{\omega_p^2}{N} \sum_n \frac{f_{n0}}{\omega_{n0}^2} \approx \frac{\omega_p^2}{\omega_s^2} \qquad \text{(IVD2.2)}$$

where f_{n0} is the oscillator strength for the $0 \rightarrow n$ transition and N is the number of electrons (cf (IIB2.21–IIB2.24)). However, there are two conditions under which the damped oscillator model formally yields the classical limit of the quantum mechanical expression: (i) Each electron reacts in the same manner to the effective electric field which allows for an interpretation of $\omega_p^2 = e^2N/m_e$ as the frequency of the volume plasmon and of $\alpha(0)$ as the static polarizability. (ii) The sum rule for all electronic transitions considered, must be fulfilled, and only then the relation $\omega_s = \omega_0$ holds for the surface plasmon frequency ω_s.

The restoring force with the proportionality constant $\omega_p^2/\alpha(0)$ (cf. (IIB7.12)) depends upon the shift of the electronic cloud with respect to the charge of the fixed atomic nuclei.

The concept of the "collective motion or plasmon" in the classical model can be correlated with an analogue of the self-consistent one-electron picture, in the sense that each electron reacts to the effective electric field but modified by the actual electron density. In other words, the volume plasmon, which is a well-defined collective mode in the quantum mechanics of very large systems, yields in the classical limit a good estimate of the plasma frequency which depends on the electron density only. However, the surface plasmon involves additional assumptions about the nature of the restoring force and therefore "quantum effects" will inevitably be present in small clusters of finite dimension. Consequently, the concept of surface plasmon, using a simple damped oscillator model, can only yield an estimate of the interval in which the frequency of the adsorbed light is to be expected if static polarizability $\alpha(0)$ is taken from experiment or calculations and the damping factor γ is fitted to the experiment. The static polarizability $\alpha(0)$ will then determine a position of the absorption band, and γ is closely connected with the band width.

For spherical particles only one resonance frequency can be obtained and in order to explain the appearance of other transitions the three-dimensional oscillator has been optimized, giving rise to "axial ratios" D_j/D_i used in the relation connecting surface plasmon frequencies ω_{si} and averaged static polarizability:[277,296-298]

$$\omega_{si}^2 = \frac{N^2}{3m_e\bar{\alpha}}\left[1 + \frac{D_j}{D_i} + \frac{D_k}{D_i}\right] \qquad (i \neq j \neq k = 1, 2, 3) \qquad \text{(IVD2.3)}$$

The axial ratios of sodium clusters have been determined by using a self-consistent spheroidal jellium model.[72]

The ellipsoidal and spheroidal deformation of a cluster leads to three or two frequencies, respectively, since in this manner distinct polarizabilities along corresponding axes are introduced. For spherical clusters all the oscillator strength should be exhausted in a single transition, while for spheroidal clusters one peak should have twice the oscillator strength of the other (ellipsoidal shell model (ESM)). According to ESM theory the "closed-shell" clusters such as Na_8, Na_{20}, and Na_{40} should exhibit a single giant resonance, and other open-shell clusters one or two additional peaks.

For the classical monovalent metal sphere $\alpha = N\mathbf{r}_s^3$ where $\mathbf{r}_s$ is the Wigner–Seitz radius (cf. ref 82) of the metal, the classical surface plasma resonance wave length for Na is 365 nm (3.4 eV) ($\mathbf{r}_s$ = 4 au). In the jellium model the electronic charge density can "spill out" from the rigid positive background charge. Therefore, a size-dependent red shift of the surface plasma mode with decreasing sphere size has been predicted.[94]

The first experimental data on the absorption of Na_n (n = 8–10, 12, 20) clusters exhibited one, two, or three intense and broad bands.[277,296,297] Since the classical

ESM model using measured polarizabilities gave rise to resonance frequencies in the measured interval, roughly agreeing with the recorded bands, as for example in the case of Na_{8-10}, the conclusion has been made about the presence of surface plasma resonances already in small alkali-metal clusters.[277,296,297] However, several new features appeared later. In the framework of the classical model the experimental data are described better for some very small clusters than for the larger ones. For clusters with n = 6–12 the ESM yields better rough estimate of the bands than for n = 13–40.[298] The measured dipole strength per atom decreases with cluster size, indicating that the additional absorption occurs outside the measured energy interval.

For Na_8 and Na_{20} the "plasma resonances" have been calculated at 2.59 and 2.67 eV, respectively, assuming a spherical shape for both clusters. For Na_6, which has oblate spheroidal shape according to ESM, two bands with 2:1 intensities have been predicted. As already discussed in section IV.C.2, recent experiments exhibit in addition to giant resonances, the red-shifted fine structure for Na_8,[279,280] and the blue-shifted band with smaller but considerable intensity for Na_{20}.[308] Also, the well-resolved spectrum of Na_6 is dominated by one intense transition at ~2.05 eV and there is a considerably weaker broad transition at ~2.8 eV.[329] The simple classical theory is capable of predicting only the range of the energy interval in which intense absorption bands appear in the case of Na_n and K_n. For Li_n the Mie–Drude jellium frequencies lie ~1 eV higher in the UV region than the recorded absorption bands. In order to take into account the higher electron binding it has been proposed to introduce the effective optical mass m^* similarly as for the bulk near the Fermi level.[300] For clusters with the average distance of 3.1 Å the correction of m^*/m = 2.04 has been calculated, which shifts the "plasmon frequency" to the measured wavelength interval.

It is not surprising that additional absorption bands appear in the absorption spectra of small clusters which cannot be accounted for in classical model, or that predicted positions and intensities of bands do not agree consistently with the spectroscopic pattern. The quantum effects must be appreciable in systems such as small alkali-metal clusters. Because of the classical limits of quantum effects, the right order of magnitude of predicted "plasma frequency" is to be expected. The problem with the physical interpretation of the classical theory is that the agreement between the experimental findings and theoretical predictions do not improve systematically with the increasing cluster size for $n \leq$ 40. This behavior contradicts the idea that the free-electron nature of a cluster becomes more apparent with increasing cluster size. The appearance of a small number of intense transitions in absorption spectra and their partial agreement with the predictions in the framework of classical Mie–Drude theory does not justify the conclusion that the collective plasma oscillations are present for alkali-metal clusters of any size.[298]

Time-Dependent Local Density Approximation Based on the Jellium Model. In order to account for the quantum effects of the absorption spectra of small alkali-metal clusters two other approaches in the framework of the jellium model have been used: the time-dependent local density approximation (TDLDA)[340,94,341] and the RPA.[332,342-344]

In the TDLDA,[94] which makes use of Kohn–Sham orbitals, the imaginary part of the dynamic polarizability $\mathrm{Im}(\alpha(\omega))$, corresponding to the interaction of single particle–hole transitions, exhibits peaks connected with the poles of the Green's functions. Consequently, the characteristics of the imaginary part of the dynamic polarizability are also due to the electronic correlation effects which are partly taken into account in TDLDA. The calculated maxima of $\mathrm{Im}(\alpha(\omega))$ have been assigned to surface plasmons at about 2.6–2.9 eV and to the considerably blue-shifted volume plasmons, while other fine "cusps" have been identified as single particle–hole pair excitations.

The size dependence of quantum size effects has been illustrated, comparing results for sodium spheres of n = 20, 92, and 198 valence electrons.[94] The shifts of peaks with respect to poles of the Green's functions (which are related to the unperturbed Hamiltonian) can be understood as due to the perturbation introduced through the effective potential. The maxima superposed on the continuous "background" are due to inclusion of electron correlation, which can lead to considerable enhancement of some transition intensities, similar to the case of the CI or RPA procedures.

As pointed out in refs 341 and 331, many approximations are involved in TDLDA on the basis of the jellium model and the positions of maxima and fine cusps cannot be used for quantitative purposes, since they are strongly dependent on the potential used. Nevertheless, the inclusion of quantum effects in the framework of TDLDA illustrated the crudeness of the classical Mie–Drude approach.[94] The use of the approximate one-electron Green's functions based on jellium local electron density in the framework of TDLDA (cf. section II.B.5 and Appendixes) shows a connection of this approach with the other methods applied in the theory of cluster spectroscopy, since the poles of Green's functions correspond to the energies of the individual particle–hole transitions. Various rough approximations to the effective potential make it possible to obtain the absorption cross sections by a direct integration in space. Since the TDLDA approach includes different approximations and assumptions than other quantum mechanical methods, it yields only additional supporting information on small clusters, but it can be valuable for large metallic clusters. The evaluation and interpretation of the TDLDA results is quite difficult, since the influence of the assumptions about the effective potential, as well as other approximations, are not very transparent.

Random-Phase Approximation Based on the Jellium Model. The calculations of transition energies and oscillator strengths for the interpretation of absorption spectra within the mean-field framework (jellium) using the RPA are parallel to those performed for studies of giant resonances in nuclei. Notice, however, that although methodological tools are applicable in different fields, there is substantial difference in the nature of the forces giving rise to the giant dipole resonances in nuclei (GDR) and those responsible for electronic transitions with large intensities in clusters resembling a GDR (short range versus Coulomb forces).

The spherical clusters such as Na_8, Na_{20}, Na_9^+, Na_{21}^+,[342a] K_9^+, K_{21}^+,[342b] and Na_{40}[344] as well as Cs_8 and $Cs_{10}O$[332] have been studied. In the case of Na_8 a single state at ~2.8 eV exhausting ~75% of the total oscil-

lator strength according to the energy-weighted sum rule has been found and is dominated by the interaction among three single particle–hole transitions. For Na_{20} two lines at 2.6 and 2.9 eV have been located with almost equal values of the oscillator strengths similar to the case of TDLDA. The associated wave functions contain about 10 forward going amplitudes and about six backward going amplitudes. These intense transitions have been called collective states (Na_8) or fragmented collective states (Na_{20}). It has been found that one single particle–hole transition is responsible for the so called "fragmentation of the plasmon" in Na_{20},[342a] since a spectrum with a dominant single peak has been obtained when this particle–hole transition was excluded from the interaction.

For cationic clusters K_9^+, K_{21}^+, and K_{22}^+ a single peak carrying most of the oscillator strength has been obtained by using the jellium-RPA[342b] method. This has been explained as due to particularly deep potentials of the cationic clusters relative to the neutral one. The particle–hole transition which was responsible for the "fragmentation" of the "collective state" in the case of neutral clusters has a much higher energy for cations and therefore does not contribute essentially in the interaction with other particle–hole transitions that give rise to the state with the large oscillator strength. The experimentally recorded spectra of K_9^+, Na_9^+, and K_{21}^+ exhibit dominant single peak features. However, the widths of the bands are not small. In the case of Na_{21}^+ two close-lying bands with large intensity have been measured.[309] Recently an ellipsoidal shell-model average potential has been introduced in the RPA study of Na_6, Na_{10}, and Na_{12},[345] giving rise to more than one intense transition. In addition, a broadening of the band (cf. refs 346 and 347) has been simulated by Lorentzian functions in order to obtain a qualitative agreement with experiment.

Notice that the role of a single particle–hole transition interacting with a "plasmon" in the physical interpretation of the spectra should be considered with caution. As mentioned earlier, the individual particle–hole transition does not have any direct physical meaning. Its individual contributions to the states can of course change the energy and oscillator strength of the transition particularly when an interaction with other particle–hole transitions is energetically favorable, is symmetry allowed, and when the nodal properties of the one-electron functions among which transitions occur have significant influence on the magnitude of the allowed dipole transitions. These basic features are accounted for in the RPA theory. Contributions of individual particle–hole transitions to the RPA wave functions of the states having significant influence on the oscillator strength produce interference phenomenon common in molecular spectroscopy.

A Comparison of Jellium RPA with ab Initio RPA and CI Results. It is very instructive to compare the RPA-jellium results with those obtained from the RPA on the basis of the nonempirical SCF-ECP approach and results from the CI treatments in order to clarify the notions necessary for the interpretation.

Let us first compare the results obtained from the jellium RPA and the ab initio RPA on the basis of the SCF Roothaan procedure for Na_8 and Na_{20}, which differ mainly in the detailed form of the assumed potential. The most compact spherical geometries, such as T_d structures, are very suitable for this comparison. As shown in section IV.C.2, ab initio RPA for Na_8 yields two close-lying states at 2.48 and 2.8 eV with oscillator strengths 2.83 and 1.65, respectively (cf. Figure 29), which exhaust 37% and 22% of the sum of oscillator strengths, which is equal to 7.58 in the energy interval up to 6 eV, in contrast to a single dominant transition obtained from the jellium RPA (cf. Figure 31a). In the case of Na_{20} (T_d) the dominant single feature with 54% of the sum of oscillator strengths ($\sim$19.1 in the energy interval up to 7.8 eV) has been calculated by using ab initio RPA in contrast to the above mentioned jellium results with a large portion of the oscillator strengths distributed between two transitions. These discrepancies clearly illustrate that the classification of the physical phenomena responsible for the pattern of absorption spectra of small alkali-metal clusters, as "collective" state or "fragmented collective" state on the basis of calculations of oscillator strength using jellium RPA, is rather arbitrary. In fact, introduction of changes in the potential through "nonjellium effects" strongly influences the results, as illustrated in ref 332. For Na_6 the ab initio RPA as well as the CI calculations yield different spectroscopic patterns for the planar and for the three-dimensional C_{2v} structure, illustrating that the averaging of geometries is not a suitable assumption.[347]

In the case of cations a comparison between jellium- and ab initio-RPA results is available only for Na_9^+. As illustrated in Figure 33 the structures of high symmetry, such as antiprisms D_{4d} and C_{4v} exhibit a dominant transition located at $\sim$2.8 eV and a fine structure shifted to the red. It is remarkable that the antiprismatic structures with eight valence electrons (Na_8 and Na_9^+) have a tendency to yield a single intense transition. In contrast, the C_{2v} structure of Na_9^+ with the lowest ground-state energy gives rise to several transitions with considerable oscillator strengths due to the lower symmetry and they are distributed over the energy interval in which a dominant band has been recorded. The transition energies obtained from ab initio RPA are all blue shifted with respect to the experimental results. A dependence of the spectral pattern on the geometry of the cationic cluster is clearly demonstrated. As already mentioned, the jellium RPA gives rise to a single intense transition for Na_9^+.[342a]

In summary, the results obtained from ab initio RPA calculations for optimized structures with the lowest energies for Na_8 and Na_9^+ differ qualitatively from those resulting from the jellium RPA. The discrepancy is present also for Na_{20}, but in this case it is still an open question whether the T_d structures ("spherical" or a section of fcc lattice) considered in the ab initio RPA calculations are the most stable geometries.

A comparison between the ab initio RPA and the CI results made in section IV.C.2 served to illustrate the role of the explicitly considered interaction among doubly excited configurations. It has been shown that qualitative agreement is present only for some parts of the spectra, i.e. for the states with dominant contributions of single excitations, while for other parts of the spectra the discrepancy is large even from a qualitative point of view. It is not yet possible to state completely generally that RPA reproduces the dominant features well and the fine structure less well.

From a comparison of results obtained using different

approaches which account for quantum effects the following conclusions can be drawn:

(i) The interaction among single excitations or particle–hole transitions giving rise to the final states is a manifestation of a many-electron effect, which means that electrons cannot be treated independently of each other as in the one-electron description (by a single particle–hole transition). This is a completely general characteristic of several phenomena of a very different physical nature such as excitations in molecular systems, excitons, plasmons etc. The necessity of considering the interactions among single excitations is simply a basic manifestation of the many-electron nature of a realistic quantum mechanical model. Only if the number of strongly interacting monoexcitations that contribute with nearly equal weights to the wave functions is very large and if other conditions listed in section II.B.7 are simultaneously fulfilled is it justified to use the notion of plasmon. An appropriate treatment of correlation effects as such does not justify the use of this notion. In the case of small alkali-metal clusters very often the leading features of two (or three) optically allowed states are determined by the same particle–hole transitions, e.g., three such transitions, but they enter with different coefficients and different phase in the linear combinations, giving rise to interference phenomena leading to a large oscillator strength for a transition to one state and a very weak one to the other.

(ii) The locations of intense transitions and the oscillator strengths are both strongly dependent on the energy ordering of the one-electron levels among which excitations take place, and this is determined through a potential which depends on the positions of nuclei and on the approximations introduced in the Hamiltonian.

Interpretation of Spectra. Comparing all the theoretical and experimental results concerning absorption spectra of small alkali-metal clusters presently available, the following conclusions can be drawn:

(i) Characteristic features, such as a very small number of intense transitions, are due to a delicate interplay between the electronic and geometrical structure of the clusters (including symmetry). Valence electrons in Ia clusters are delocalized, since they form many-center delocalized bonds (cf. section III.D). Therefore, their excitation is not localized in the sense of partly or entirely breaking two-center bonds. Consequently, many-electron effects accounted for by electronic correlation play a specially important role. This is, of course, the sort of collective effect that is present in many molecules as for example in the case of delocalized π-electrons in conjugated hydrocarbons.

(ii) A very large oscillator strength can result for one or a few transitions also from the interaction of a very small number of leading excitations due to interference phenomena (analogous to the selection rules).

(iii) The number of strongly interacting monoexcitations can be applied as a rough criterion for classification of collective effects present for plasmons. If the number of dominant configurations is small, the usual correlation effects are present. The limiting case of the plasmon is reached if the number of configurations with equal weights in the wave function is so large that the individual excitations cannot be identified, so that integration over their manifold is necessary, as shown in section II.B.7. However, notice that for any truncated correlated wave function this analysis is strongly dependent upon the choice of the one-electron functions.

(iv) The concept of the splitting of a surface plasmon due to the interaction of the plasma frequency with a single particle–hole transition represents an arbitrary definition, unless a nearly infinite number of equally contributing particle–hole transitions is involved in the interaction.

(v) Similarly as in the case of some ground-state properties, certain features of excited-state properties are independent of the model used, since they are dictated by the global symmetry of the system.

V. Summary

We have shown that a number of valuable general rules governing the electronic and geometrical structure of small elemental clusters have resulted from quantum chemical investigations. They concern, for example, symmetry, shape, stability, and a number of physical observables. The predictive power of these relatively accurate methods, although still limited to small clusters with a small number of valence electrons, has been clearly demonstrated by successful structural and spectroscopic assignments and interpretation of the optical response properties. For example, at the present time the direct experimental information on cluster geometry is available only for very small clusters by analysis of the vibronic structure, which has not yet been resolved for the larger ones. In the latter case only a comparison between accurate theory and experiment makes it possible to gain knowledge about the geometries and specific electronic properties such as the type of excitations responsible for the spectroscopic pattern.

As illustrated on a number of examples, in spite of a relatively large mobility of alkali-metal atoms in small clusters, the positions of their nuclei cannot be ignored. After all, the positions of the nuclei are respected in solid-state theories for metal bulk and surfaces taking into account three- or two-dimensional periodicity.

Many recent advances in cluster science have been achieved due to the joint effort by nuclear and solid-state physicists aiming to gain understanding of the reasons for the appearance of similarities between properties of atomic nuclei and clusters. In this connection quantum chemistry can play an important role as a guide for extracting the essentials from the allowable simplifications which can be introduced in approximate theories.

Recent experimental trends toward the production of clusters under well-defined conditions (e.g. low temperature), as well as the preparation of small and very large clusters under the same conditions, offer a new challenge for future theoretical developments. They should permit the quantitative predictions of structure and properties of medium-size clusters and contribute toward a qualitative understanding of the behavior of large clusters.

VI. Appendixes

A. Green's Functions and Interaction Picture

The direct use of the Green's functions is in general very difficult and therefore various approximate

methods are very often used. For this purpose, the separation of the Hamiltonian $\hat{H}$ in the perturbation $\hat{V}$ and the unperturbed Hamiltonian $\hat{H}_0$ is advantageous. Usually, $\hat{H}_0$ is chosen to be a one-electron operator.

It is very convenient to apply the interaction picture[89]

$$|\psi_I(t)\rangle = \exp(i\hat{H}_0 t)|\psi(t)\rangle$$

$$\hat{A}_I(t) = e^{i\hat{H}_0 t}\hat{A}(t)e^{-i\hat{H}_0 t} \tag{A1}$$

where

$$\hat{H}_0 = \hat{H} - \hat{V}(t) \tag{A2}$$

for the calculations in the framework of the linear response theory.

The time-dependent Schrödinger equation in the interaction picture has the form

$$i\frac{\partial|\psi_I(t)\rangle}{\partial t} = \hat{V}_I(t)|\psi_I(t)\rangle \tag{A3}$$

where $\hat{V}(t)$ is the time-dependent perturbation which has been switched on at the time $t = 0$.

The formal solution is

$$|\psi_I(t)\rangle = -i\int_0^t \hat{V}_I(\tau)|\psi_I(\tau)\rangle\, d\tau + |0\rangle = \hat{U}(t)|0\rangle \tag{A4}$$

It can be shown that the double-time Green's function can be written in the interaction picture as

$$\langle\langle A(t);\hat{B}(0)\rangle\rangle = i\{\mp\theta(t)\langle 0|\hat{A}_I(t)\hat{U}(t)\hat{B}_I(0)|0\rangle + \theta(-t)\langle 0|\hat{B}_I(0)\hat{U}(-t)\hat{A}_I(t)|0\rangle\} \tag{A5}$$

(cf. (A4) for the definition of the operator $\hat{U}$).

The formal solution (A4) of the Schrödinger equation (A3) in the first-order perturbation approximation is

$$|\psi_I(t)\rangle = \left(1 - i\int_0^t \hat{V}_I(t-\tau)\, d\tau\right)|0\rangle = \left(1 + i\int_0^t \hat{V}_I(t-\tau)\, d(t-\tau)\right)|0\rangle \tag{A6}$$

The expectation value of an operator $\hat{A}$ in the linear response theory takes the form

$$\langle\psi(t)|\hat{A}|\psi(t)\rangle - \langle 0|\hat{A}|0\rangle = \delta\langle\hat{A}\rangle =$$
$$-i\int_0^t d\tau\, \langle 0|\hat{A}e^{i(E_0-\hat{H}_0)(t-\tau)}\hat{V}(\tau) - \hat{V}(\tau)e^{i(E_0-\hat{H}_0)(\tau-t)}\hat{A}|0\rangle =$$
$$i\int_{-\infty}^{+\infty} d\tau\, \theta(t-\tau)\langle 0|[\hat{V}_I(\tau),\hat{A}_I(t)]|0 =$$
$$-\int_{-\infty}^{+\infty} d\tau\, \theta(t-\tau)\, \langle\langle\hat{A}(t);\hat{V}(\tau)\rangle\rangle + \text{compl conj} \tag{A7}$$

with $\hat{A}(t) = 0$ for $t < 0$. From the last expression in the equation (A7) the connection of the linear response theory with Green's functions is clear.

B. Green's Functions in the One-Electron Approximation

Because of the important role of the free-electron wave in the solid-state theory let us mention that the Heisenberg picture of the Lie algebra generator $\hat{E}_{\mathbf{k},\mathbf{k}'}$ describing the excitation from the free-electron wave $|\psi_{\mathbf{k}}\rangle$ with the impulse $\mathbf{k}$ to $|\psi_{\mathbf{k}'}\rangle$ is simply

$$\hat{E}^{(H)}_{\mathbf{k}'\mathbf{k}} = e^{i(\epsilon_{\mathbf{k}'}-\epsilon_{\mathbf{k}})t}\hat{E}_{\mathbf{k}'\mathbf{k}} \tag{A8}$$

For the discussion of the approximate procedures used in the cluster theory the consideration of the one-electron Hamiltonian as the unperturbed Hamiltonian is of interest. The free-electron case is an example of a more general relation valid for an unperturbed system described by an one-electron Hamiltonian $\hat{H}_0$. $\hat{H}_0$ always can be written in terms of occupation number operators as

$$\hat{H}_0 = \sum_j \omega_j \hat{n}_j \tag{A9}$$

For the Heisenberg picture of the operator $\hat{A}$ the following general relation is valid:

$$\hat{A}^{(H)} = e^{+i\hat{H}t}\hat{A}e^{-i\hat{H}t} = \hat{A} + (it)[\hat{H},\hat{A}] + \frac{1}{2!}(it)^2[\hat{H},[\hat{H},\hat{A}]] + \frac{1}{3!}(it)^3[\hat{H}[\hat{H},\hat{A}][\hat{H},\hat{A}]] + \ldots = e^{it\hat{\hat{H}}}\hat{A} \tag{A10}$$

where the "super-operator" $\hat{\hat{H}}$ is defined as[46] $\hat{\hat{H}}\hat{A} = [\hat{H},\hat{A}]$.

By using (A9) for $\hat{H}_0$ and (IIA2.5) the commutator $[\hat{H}_0,\hat{E}_{kl}]$ takes the form

$$\sum_j \omega_j[\hat{n}_j,\hat{E}_{kl}] = (\omega_k - \omega_l)\hat{E}_{kl} \tag{A11}$$

and consequently according to (A10) it holds

$$\hat{E}^{(H_0)}_{kl} = e^{i(\omega_k-\omega_l)}\hat{E}_{kl} \tag{A12}$$

For any operator $\hat{A}$ in the one-electron approximation the following relation is valid:

$$\hat{A}^{(H_0)} = \sum_{l,k} a_{lk}e^{i(\omega_l-\omega_k)t}\hat{E}_{lk} \tag{A13}$$

Consequently, the intermediate picture of a density operator

$$\hat{\rho}(\mathbf{r},\mathbf{r}') = \sum_{l,k}\hat{\mathcal{E}}_{lk}\, \varphi_l^*(\mathbf{r})\, \varphi_k(\mathbf{r}') \tag{A14}$$

is

$$\hat{\rho}^{(H_0)}(\mathbf{r},\mathbf{r}',t) = \sum_{lk}\hat{\mathcal{E}}_{lk}\, e^{i(\omega_l-\omega_k)t}\varphi_l^*(\mathbf{r})\varphi_k(\mathbf{r}')$$

where $\varphi_l(\mathbf{r})$ is the eigenfunction of the Hamiltonian $\hat{H}_0$ with the eigenvalue ω_l. Let us consider the "excitation" propagator defined as

$$\langle\langle\hat{E}_{lk}(t);\hat{E}_{nm}(t')\rangle\rangle_0 = -i\{\theta(t-t')\langle 0|\hat{E}_{lk}^{(H_0)}(t)\hat{E}_{nm}^{(H_0)}(t')|0\rangle + \theta(t'-t)\langle 0|\hat{E}_{nm}^{(H_0)}(t')\hat{E}_{lk}^{(H_0)}(t)|0\rangle\} =$$
$$-ie^{i(\omega_l-\omega_k)(t-t')}\{\theta(t-t')n_l m_k + \theta(t'-t)n_k m_l\}\delta_{lm}\delta_{kn} =$$
$$i\langle\langle\hat{a}_k(t);\hat{a}_n^\dagger(t')\rangle\rangle_0\langle\langle\hat{a}_l^\dagger(t);\hat{a}_m(t')\rangle\rangle_0 \tag{A15}$$

since for the one-electron double-time Green's functions in one-electron approximation holds:

$$\langle\langle\hat{a}_k(t);\hat{a}_n^\dagger(t')\rangle\rangle_0 = i\delta_{kn}e^{i\omega_k(t-t')}\{n_k\,\theta(t'-t) - m_n\theta(t-t')\}$$

$$\langle\langle\hat{a}_l^\dagger(t);\hat{a}_m(t')\rangle\rangle_0 = i\delta_{lm}e^{i\omega_l(t-t')}\{m_l\,\theta(t'-t) - n_m\,\theta(t-t')\} \tag{A16}$$

where n_k is the occupation number, and $m_k = 1 - n_k$. The circumstance that the two-electron Green's functions assigned to H_0 is possible to express as products of one-electron Green's functions is the consequence of one-electron character of the Hamiltonian $\hat{H}_0$.

C. Polarization and Dipole Propagators

The polarization propagator has generally the form

$$\langle\langle\hat{\rho}(\mathbf{r},t);\hat{\rho}(\mathbf{r}',t')\rangle\rangle = i\langle 0|T\{\hat{\rho}(\mathbf{r},\mathbf{r},t)\hat{\rho}(\mathbf{r}',\mathbf{r}',t')\}|0\rangle \tag{A17}$$

where T is the time ordering operator.

If $|\psi_0\rangle = |0\rangle$ is a ground-state ket in one-electron approximation with the effective Hamiltonian $\hat{H}_0$ (cf (A9)) then the polarization propagator is

$$\langle\langle\hat{\rho}(\mathbf{r},t);\hat{\rho}(\mathbf{r}',t')\rangle\rangle_0 = i\sum_{nklm}\varphi_l^*(\mathbf{r})\varphi_k(\mathbf{r})\varphi_n^*(\mathbf{r}')\varphi_m(\mathbf{r}')\langle\langle\hat{E}_{lk}(t);\hat{E}_{nm}(t')\rangle\rangle_0 = i\sum_{lk}e^{i(\omega_l-\omega_k)(t-t')}\varphi_l^*(\mathbf{r})\varphi_l(\mathbf{r}')\varphi_k(\mathbf{r})\varphi_k^*(\mathbf{r}')\{\theta(t-t')\hat{n}_l\hat{m}_k + \theta(t-t')\hat{n}_k\hat{m}_l\} \quad (A18)$$

The Fourier transform reads

$$\langle\langle\hat{\rho}(\mathbf{r},\omega);\hat{\rho}(\mathbf{r}',\omega)\rangle\rangle_0 = \sum_{lk}\left[\frac{n_l m_k}{\omega-(\omega_l-\omega_k)+i\eta} - \frac{n_k m_l}{\omega-(\omega_l-\omega_k)-i\eta}\right]\varphi_l^*(\mathbf{r})\varphi_l(\mathbf{r}')\varphi_k(\mathbf{r})\varphi_k^*(\mathbf{r}') = \chi^0(\mathbf{r},\mathbf{r}',\omega) \quad (A19)$$

The polarization propagator can be expressed in terms of one-electron Green's functions due to the one-electron character of the Hamiltonian $\hat{H}_0$:

$$\chi_0(\mathbf{r},\mathbf{r}';\omega) = \sum_l m_l\{\varphi_l^*(\mathbf{r})\varphi_l(\mathbf{r}')G(\mathbf{r},\mathbf{r}';\omega_k+\omega) + \varphi_l^*(\mathbf{r}')\varphi_l(\mathbf{r})G^*(\mathbf{r},\mathbf{r}';\omega_k-\omega)\} \quad (A20)$$

where

$$G(\mathbf{r},\mathbf{r}';E) = \sum_k n_k\varphi_k^*(\mathbf{r})\varphi_k(\mathbf{r}')/(E-\omega_k) \quad (A21)$$

The expression (A20) is used in the calculations of linear response with the jellium model.[93,94,340]

The mutual Coulombic interaction between the charge distributions $\rho(\mathbf{r})$ and $\rho(\mathbf{r}')$ can be to the first order expressed simply with Green's functions

$$\text{real}\left\{\int\chi_0(\mathbf{r},\mathbf{r}',\omega)\hat{V}(\mathbf{r},\mathbf{r}')\,d\mathbf{r}d\mathbf{r}'\right\} = \sum_{l,k}n_k m_l\left\{\frac{1}{(\omega_l-\omega_k)-\omega} - \frac{1}{(\omega_k-\omega_l)-\omega}\right\}K_{kl} = 2\sum_{l,k}n_k m_l\frac{(\omega_k-\omega_l)K_{kl}}{(\omega_l-\omega_k)^2-\omega^2} \quad (A22)$$

$\chi_0(\mathbf{r},\mathbf{r}';\omega)$ is clearly the independent-particle density–density correlation function and K_{kl} is the exchange integral.[94,340]

Similarly the dipole propagator in the one-electron approach has the form

$$\int\langle\langle\hat{\mu}(\mathbf{r},\omega);\hat{\mu}(\mathbf{r}',\omega)\rangle\rangle_0\,d\mathbf{r}d\mathbf{r}' = \sum_{lk}\left\{\frac{n_l m_k}{\omega-(\omega_l-\omega_k)+i\eta} - \frac{n_k m_l}{\omega-(\omega_l-\omega_k)-i\eta}\right\}|\mu_{lk}|^2 \quad (A23)$$

where

$$\mu_{lk} = \int\varphi_l^*(\mathbf{r})x\varphi_k(\mathbf{r})\,d\mathbf{r} \quad (A24)$$

In this section the two electron propagators have been discussed since the processes during which the number of particles remains constant are for us of special interest. If the ionization potential or electron affinity were discussed in more detail the one-electron propagators or Green's functions (cf. e.g. Refs 86, 89) would be important. In this case, the operators which figure in the definition (IIB2.15) would be the creation and annihilation operators of the second quantization. The one-electron Green's functions are very useful for the investigation of the fundamental properties of the quasiparticles.

In summary, many common features of the approaches used in the theory of clusters (e.g. theory of plasmon and the TDLDA approximation) can be well understood if the connection with Green's functions is properly worked out.

Acknowledgments. We thank our co-workers Mr. A. Blase, Dr. I. Boustani, Mrs. G. Bravo-Perez, Mr. J. Gaus, Mr. J. Pittner, and Mr. C. Scheuch and colleagues Dr. C. Gatti, Dr. M. F. Guest, and Dr. S. Polezzo who have substantially contributed to the work included in the review. We thank Mrs. A. Polinske for typing the manuscript and Mrs. C. Cornelissen and L. Češpiva for technical help. We extend our thanks to Prof. M. M. Kappes, Dr. M. Broyer, Dr. J. P. Wolf, Prof. L. Wöste, and Dr. C. Brechignac for providing us with their data prior to publication. This work has been supported by the Deutsche Forschungsgemeinschaft (Sfb 337, Energy transfer in molecular aggregates) and the Consiglio Nationale delle Ricerche (CNR). We dedicate this contribution to R. Stephen Berry in occasion of his 60th birthday.

VII. References

(1) Koutecký, J.; Fantucci, P. *Chem. Rev.* **1986**, *86*, 539–587.
(2) Halicioglu, T.; Bauschlicher, C. W., Jr. *Rep. Prog. Phys.* **1988**, *51*, 883–921.
(3) Mingos, D. M. P.; Johnson, R. L. *Struct. Bonding* **1987**, *68*, 29–87.
(4) Manninen, M. In *Condensed Matter Theories*, 3rd ed.; Arponen, J. S., Bishop, R. F., Manninen, M., Eds.; Plenum Publishing; New York, 1988; pp 221–234.
(5) Raghavachari, K. *Phase Trans.* **1990**, 24–26; 61–90.
(6) Morse, M. D. *Chem. Rev.* **1986**, *86*, 1049–1109.
(7) De Heer, W. A.; Knight, W. D.; Chou, M. Y.; Cohen, M. L. *Solid State Phys.* **1987**, *40*, 93–181.
(8) Kappes, M. M. *Chem. Rev.* **1988**, *88*, 369–389.
(9) Curl, R. F.; Smalley, R. E. *Science* **1988**, *242*, 1017–1022.
(10) Arnold, S. T.; Eaton, J. G.; Patel-Misra, D.; Sarkas, H. W.; Bowen, K. H. In *Ion and Cluster Ion Spectroscopy and Structure*; Maier, J. P., Ed.; Elsevier: Amsterdam, 1989; pp 417–472.
(11) Cheshnovsky, O.; Pettiette, C. L.; Smalley, R. E. In *Ion Spectroscopy and Structure*; Maier, J. P., Ed.; Elsevier: Amsterdam, 1989; pp 373–415.
(12) Schumacher, E. *Chimia* **1988**, *42*, 357–376.
(13) Smalley, R. E. In *Cluster Spectroscopy*; Bernstein, E. R., Ed.; Elsevier: Amsterdam, 1988.
(14) Weltner, W., Jr.; Van Zee, R. *Chem. Rev.* **1989**, *89*, 1713–1747.
(15) Björnholm, S. *Contemp. Phys.* **1990**, *31*, 309–324.
(16) Cohen, M. L.; Knight, W. D. *Phys. Today* **1990**, 42–50.
(17) Mingos, D. M. P.; Slee, T.; Lin, Z. *Chem. Rev.* **1990**, *90*, 383–402.
(18) Kaldor, A.; Cox, D. M.; Zakin, M. R. *Adv. Chem. Phys.* (Prigogine, I., Rice, S., Lawley, K., Eds.) **1990**, *70*, 211–261.
(19) Jena, P., Rao, B. K., Khanna, S. N., Eds. *Physics and Chemistry of Small Clusters*; Plenum Press: New York, 1986.
(20) Träger, F.; zu Putlitz, G. *Metal Clusters*; Springer-Verlag: Berlin 1986.
(21) Hilf, E. R.; Kramer, F.; Wien, K. *PDMS and Clusters*; Lectures Notes in Physics, Springer-Verlag: Berlin, 1987.
(22) Jortner, J., Pullman, A., Pullman, B., Eds. *Large Finite Systems*; Reidel: Dordrecht, 1987.
(23) Benedek, G., Martin, T. P., Pacchioni, G., Eds. *Elemental and Molecular Clusters*; Springer-Verlag: Berlin, 1988.
(24) Chapon, C., Gillet, M. F., Henry, C. R., Eds. *Small Particles and Inorganic Clusters*; Springer-Verlag: Berlin, 1989.
(25) Haberland, H., Ed. *Clusters of Atoms and Molecules*; Springer-Verlag: Berlin, in press.
(26) McWeeny, R.; Sutcliffe, B. T. In *Methods of Molecular Quantum Mechanics*; Academic Press: London, 1969.
(27) McWeeny, R. *Methods of Molecular Quantum Mechanics*; Academic Press: London, 1989.

(28) Szabo, A.; Ostlund, N. S. In *Modern Quantum Chemistry*; MacMillan Publ. Co.: New York, 1982.
(29) Hohenberg, P.; Kohn, W. *Phys. Rev. B* **1964**, *136*, 864–871.
(30) Levy, M. *Proc. Natl. Acad. Sci. U.S.A.* **1979**, *76*, 6062–6065.
(31) Kohn, W.; Sham, L. J. *Phys. Rev.* **1965**, *140A*, 1133–1138.
(32) The Kohn–Sham orbitals are usually expanded in a set of nuclei-centered functions (Gaussians or Slater orbitals) or plane waves. See, for instance: Snijders, J. G.; Baerends, E. J.; Vernsoijs, P. Internal Report, Free University, Amsterdam, 1981. Dunlap, B. I.; Connolly, J. W. D.; Sabin, J. R. *J. Chem. Phys.* **1979**, *71*, 3396–3402; *J. Chem. Phys.* **1979**, *71*, 4493–4499. See also refs 64 and 65.
(33) Parr, R. G.; Yang, W. *Density Functional Theory of Atoms and Molecules*; Oxford University Press: New York, 1988.
(34) Szasz, L. *Pseudopotential Theory of Atoms and Molecules*; John Wiley: New York, 1985.
(35) Balasubramanian, K.; Pitzer, K. S. In *Ab Initio Methods in Quantum Chemistry-I*, Prigonine, I., Rice, S., Lawley, K., Eds., *Adv. Chem. Phys.* **1987**, *67*, 287–319.
(36) Pyykkö, P. *Chem. Rev.* **1988**, *88*, 563–594.
(37) Hay, P. J.; Wadt, W. R. *J. Chem. Phys.* **1985**, *82*, 270–283.
(38) Hay, P. J.; Wadt, W. R. *J. Chem. Phys.* **1985**, *82*, 299–310.
(39) Wadt, W. R.; Hay, P. J. *J. Chem. Phys.* **1985**, *82*, 284–298.
(40) Stevens, W. J.; Basch, H.; Krauss, M. *J. Chem. Phys.* **1984**, *81*, 6026–6033.
(41) Hamann, D. R.; Schlüter, M.; Chiang, C. *Phys. Rev. Lett.* **1979**, *43*, 1494–1497.
(42) Bachelet, G. B.; Hamann, D. R.; Schlüter, M. *Phys. Rev. B* **1982**, *26*, 4199–4228.
(43) Pettersson, L. G. M.; Wahlgren, U.; Gropen, O. *J. Chem. Phys.* **1987**, *86*, 2176–2184.
(44) Dolg, M.; Wedig, H.; Stoll, H.; Preuss, H. *J. Chem. Phys.* **1987**, *86*, 866–872.
(45) Shavitt, I. In *Methods of Electronic Structure Theory*; Schaefer, H. F., III, Ed.; Plenum Press: New York, 1977.
(46) Jörgensen, P.; Simons, J. *Second Quantization Methods in Quantum Chemistry*; Academic Press: New York, 1981.
(47) Koutecký, J.; Laforgue, A. *Int. J. Quantum Chem.* **1977**, *11*, 505–523.
(48) Buenker, R. J.; Peyerimhoff, S. D. *Theor. Chem. Acta* **1974**, *35*, 33–58.
(49) Buenker, R. J.; Peyerimhoff, S. D.; Butcher, W. *Mol. Phys.* **1978**, *35*, 771–791.
(50) Ahlrichs, R.; Scharf, P.; Erhardt, C. *J. Chem. Phys.* **1985**, *82*, 890–898.
(51) Ahrichs, R.; Scharf, P. In *Ab Initio Methods in Quantum Chemistry-I*, Prigogine, I., Rice, S., Lawley, K. P., Eds.; *Adv. Chem. Phys.* **1987**, *67* 501–537.
(52) Shavitt, I. *Int. J. Quantum Chem.* **1977**, *S11*, 131–148.
(53) (a) Roos, B. O.; Siegbahn, P. E. M. In *Methods of Electronic Structure Theory*; Schaefer, H. F., III, Ed.; Plenum Press: New York, 1977. (b) Roos, B. O. In *Ab Initio Methods in Quantum Chemistry-II*, Prigogine, I.; Rice, S.; Lawley, K. P., Eds.; *Adv. Chem. Phys.* **1987**, *69*, 399–445.
(54) Huron, B.; Rancurel, P.; Malrieu, J.-P. *J. Chem. Phys.* **1973**, *58*, 5745–5759.
(55) Evangelisti, S.; Daudey, J.-P.; Malrieu, J.-P. *Chem. Phys.* **1983**, *75*, 91–102.
(56) Pulay, P. In *Ab Initio Methods in Quantum Chemistry-II*; Prigogine, I.; Rice, S.; Lawley, K. P., Eds.; *Adv. Chem. Phys.* **1987**, *67*, 241–286.
(57) Fournier, R.; Andzelm, J.; Salahub, D. R. *J. Chem. Phys.* **1989**, *90*, 6371–6377.
(58) Fournier, R. *J. Chem. Phys.* **1990**, *92*, 5422–5429.
(59) Schlegel, H. B. In *Ab Initio Methods in Quantum Chemistry-I*; Prigogine, I.; Rice, S., Lawley, K. P., Eds.; *Adv. Chem. Phys.* **1987**, *67*, 249–286.
(60) Chelikowsky, J. R.; Chou, M. Y. *Phys. Rev. B* **1988**, *37*, 6504–6507.
(61) Forner, W.; Seel, M. *J. Chem. Phys.* **1987**, *87*, 443–450.
(62) Boustani, I. Pewestorf, W.; Fantucci, P.; Bonačič-Koutecký, V.; Koutecký, J. *Phys. Rev. B* **1987**, *B35*, 9437–9450.
(63) Raghavachari, K.; Haddon, R. C.; Binkley, J. S. *Chem. Phys. Lett.* **1985**, *122*, 219–224.
(64) Parrinello, M. In *Modern Techniques in Computational Chemistry*; Clementi, E., Ed.; Escom Science: Leiden, 1990.
(65) Car, R.; Parrinello, M. *Phys. Rev. Lett.* **1985**, *55*, 2471–2474.
(66) Kirkpatrick, S.; Gelatt, G. D., Jr.; Vecchi, M. P. *Science* **1983**, *220*, 671–679.
(67) Remler, D. K.; Madden, P. A. *Mol. Phys.* **1990**, *70*, 921–966 and references therein.
(68) Murrel, J. N.; Carter, S.; Farantos, S. C.; Huxley, P.; Varandas, A. J. C. *Molecular Potential Energy Functions*; John Wiley: New York, 1984.
(69) Johnson, B. F. G.; Woolley, R. G. *J. Chem. Soc., Chem. Commun.* **1987**, 634–636.
(70) Knight, W. D.; Clemenger, K.; De Heer, W. A.; Saunders, W. A.; Chou, M. Y.; Cohen, M. L. *Phys. Rev. Lett.* **1984**, *52*, 2141–2143.
(71) Cohen, M. L.; Chou, M. Y.; Knight, W. D.; De Heer, W. A. *J. Phys. Chem.* **1987**, *91*, 3141–3149.
(72) Ekardt, W. *Phys. Rev. B* **1984**, *29*, 1558–1564.
(73) Clemenger, K. *Phys. Rev. B* **1985**, *32*, 1359–1362.
(74) Iniguez, M. P.; Lopez, M. J.; Alonso, J. A.; Soler, J. M. *Z. Phys. D* **1989**, *11*, 163–174.
(75) Woods, R.; Saxon, D. *Phys. Rev.* **1954**, *93*, 577.
(76) Björnholm, S.; Borggreen, J.; Echt, O.; Hansen, K.; Pedersen, J.; Rasmussen, H. D. *Phys. Rev. Lett.* **1990**, *13*, 1627–1630.
(77) Martin, T. P.; Bergmann, T.; Göhlich, H.; Lange, T. *Chem. Phys. Lett.* **1990**, *172*, 209–213.
(78) Göhlich, H.; Lange, T.; Bergmann, T.; Martin, T. P. *Phys. Rev. Lett.* **1990**, *65*, 748–751.
(79) Katakuse, I.; Ichihara, T.; Fujita, Y.; Matsuo, T.; Sakurai, T.; Matsuda, H. *Int. J. Mass Spectrom. Ion Processes* **1985**, *67*, 229–236.
(80) Lin, Z.; Slee, T.; Mingos, D. M. P. *Chem. Phys.* **1990**, *142*, 321–334.
(81) Quinn, C. *An Introduction to the quantum chemistry of solids*; Clarendon: Oxford, 1973.
(82) Kittel, C. *Introduction to Solid State Physics*; Wiley: New York, 1986.
(83) Kittel, C. *Quantentheorie der Festkörper*; Oldenburg: München, 1970.
(84) Korringa, J. *Physica's Grav.* **1947**, *13*, 392–400.
(85) Kohn, W.; Rostocker, N. *Phys. Rev.* **1954**, *94*, 1111–1120.
(86) Mattuck, R. D. *A Guide to Feynman Diagrams in the Many-Body Problem*; Cassels, J. M., Ed.; McGraw-Hill: New York, 1967.
(87) Schiff, L. I. *Quantum Mechanics*, 2nd ed.; McGraw-Hill Book Co.: New York, 1955.
(88) Linderberg, J.; Ohrn, Y. *Propagators in Quantum Chemistry*; Academic Press: New York, 1973.
(89) Fetter, A.; Walecka, J. *Quantum theory of many-particle systems*; McGraw-Hill: New York, 1971.
(90) Pariser, R. *J. Chem. Phys.* **1956**, *24*, 250–268.
(91) Rowe, D. J. *Rev. Mod. Phys.* **1968**, *40*, 153–166.
(92) Rowe, D. J. *Nucl. Phys.* **1966**, *80*, 209–222.
(93) Puska, M. J.; Nieminen, R. M.; Manninen, M. *Phys. Rev. B* **1985**, *31*, 3486–3495.
(94) Ekardt, W. *Phys. Rev. B* **1985**, *31*, 6360–6370.
(95) Zangwill, A.; Soven, P. *Phys. Rev. A.* **1980**, *21*, 1561–1572.
(96) Ekardt, W. *Phys. Rev. B* **1985**, *32*, 1961–1970.
(97) Ekardt, W.; Penzar, Z. *Phys. Rev. B* **1988**, *38*, 4273–4276.
(98) Nilsson, S. G.; Mat.-Phys. redd. K.Dan. Videsnk. Selsk. **1951**, *16*, 29.
(99) Ishii, Y.; Ohnishi, S.; Sugano, S. *Phys. Rev. B.* **1986**, *33*, 5271–5279.
(100) Membrado, M.; Pacheco, A. F.; Sanudo, J. *Phys. Rev. B* **1990**, *41*, 5643–5647.
(101) Baladron, C.; Iniguez, M. P.; Alonso, J. A. *Z. Phys. B* **1985**, *59*, 187–191.
(102) Manninen, M. *Solid State Commun.* **1986**, *59*, 281–284.
(103) Abarenkov, I. V.; Heine, V. *Phil. Mag.* **1965**, *12*, 529.
(104) Asheroti, N. W. *Phys. Lett.* **1966**, *23A*, 48.
(105) Atkins, P. W. *Molecular Quantum Mechanics*; Oxford University Press: New York, 1983.
(106) Koutecký, J.; Scheuch, C. *Int. J. Quantum Chem.* **1990**, *37*, 373–387.
(107) Haken, H. Quantenfeldtheorie des Festkörpers, B. G. Teubner, Stuttgart, 1973.
(108) Clar, E. *Aromatische Kohlenwasserstoffe*, 2nd ed.; Springer-Verlag: Berlin, 1952.
(109) Blaise, P.; Spiegelmann, F.; Maynau, D.; Malrieu, J. P. *Phys. Rev. B* **1990**, *41*, 5566–5577.
(110) Igel-Mann, G.; Wedig, U.; Fuentealba, P.; Stoll, H. *J. Chem. Phys.* **1986**, *84*, 5007–5012.
(111) Jena, P.; Khanna, S. N.; Rao, B. K. In *Microclusters*; Sugano, S.; Nishina, Y.; Ohnishi, S. Eds., Springer-Verlag: Heidelberg, 1987; pp 47–53.
(112) Jena, P.; Rao, B. K.; Nieminen, R. M. *Solid State Commun.* **1986**, *59*, 509–512.
(113) Fantucci, P.; Koutecký, J.; Pacchioni, G. *J. Chem. Phys.* **1984**, *88*, 325–328.
(114) Khanna, S. N.; Rao, B. K.; Jena, P.; Martins, J. L. *NATO ASI Ser., Ser. B* **1987**, *158*, 435–438.
(115) Lepetit, M. B.; Oujia, B.; Malrieu, J. P.; Maynau, D. *Phys. Rev. A* **1989**, *39*, 3274–3288.
(116) Maynau, D.; Malrieu, J. P. *J. Chem. Phys.* **1988**, *88*, 3163–3173.
(117) McAdon, M. H.; Goddard, W. A., III.; *Phys. Rev. Lett.* **1985**, *55*, 2563–2566.
(118) McAdon, M. H.; Goddard, W. A., III.; *J. Non-Cryst. Solids* **1985**, *75*, 149–159.
(119) Rao, B. K.; Jena, P.; Shillady, D. D. *Phys. Rev. B* **1984**, *30*, 7293–7296.
(120) Rao, B. K.; Jena, P. *Phys. Rev. B* **1985**, *32*, 2058–2069.
(121) Rao, B. K.; Jena, P. *J. Phys. F* **1986**, *16*, 461–472.
(122) Rao, B. K.; Jena, P. *Ultramicroscopy* **1986**, *20*, 51–54.
(123) Rao, B. K.; Jena, P.; Manninen, M.; Nieminen, R. M. *Phys. Rev. Lett.* **1987**, *58*, 1188–1191.
(124) Rao, B. K.; Khanna, S. N.; Jena, P. *Z. Phys. D: At., Mol.*

Clusters **1986**, *3*, 219–222.
(125) (a) Rao, B. K.; Khanna, S. N.; Jena, P. *NATO ASI Ser., Ser. B* **1987**, *158*, 369–382. (b) Rao, B. K.; Khanna, S. N.; Jena, P. *Solid State Commun.* **1985**, *56*, 731–734.
(126) Rao, B. K.; Khanna, S. N.; Jena, P. *Chem. Phys. Lett.* **1985**, *124*, 202–204.
(127) Ray, A. K. *J. Phys. B* **1986**, *19*, 1253–1259.
(128) Ray, A. K.; Fry, J. L.; Myles, C. W. *J. Phys. B* **1985**, *18*, 381–386.
(129) Shillady, D. D.; Rao, B. K.; Jena, P. *NATO ASI Ser., Ser. B* **1987**, *158*, 493–498.
(130) Spiegelmann, F.; Blaise, P.; Malrieu, J. P.; Maynau, D. *Z. Phys. D: At., Mol. Clusters* **1989**, *12*, 341–346.
(131) Pavolini, D.; Spiegelmann, F. *J. Chem. Phys.* **1987**, *87*, 2854–2862.
(132) Rao, B. K.; Jena, P.; Manninen, M. *Phys. Rev. B* **1990**, *32*, 477–479.
(133) Boustani, I.; Koutecký, J. *J. Chem. Phys.* **1988**, *88*, 5657–5662.
(134) Koutecký, J.; Boustani, I.; Bonačić-Koutecký, V. *Int. J. Quant. Chem.* **1990**, *38*, 149–161.
(135) Bonačić-Koutecký, V.; Fantucci, P.; Koutecký, J. *J. Mol. Struct. (THEOCHEM)* **1988**, *166*, 221–228.
(136) Cocchini, F.; Upton, T. H.; Andreoni, W. *J. Chem. Phys.* **1988**, *88*, 6068–6077.
(137) Hall, R. W. *J. Chem. Phys.* **1990**, *93*, 8211–8219.
(138) Ray, A. K. *Solid State Commun.* **1989**, *71*, 311–316.
(139) Ray, A. K. *Solid State Commun.* **1989**, *72*, 1051–1056.
(140) Spiegelmann, F.; Pavolini, D. *J. Chem. Phys.* **1988**, *89*, 4954–4964.
(141) Bréchignac, C.; Cahuzac, Ph.; Roux, J.-Ph.; Pavolini, D.; Spiegelmann, F. *J. Chem. Phys.* **1987**, *87*, 5694–5699.
(142) Bonačić-Koutecký, V.; Fantucci, P.; Koutecký, J. *Phys. Rev. B* **1988**, *B37*, 4369–4374.
(143) Bonačić-Koutecký, V.; Boutstani, I.; Guest, M. F.; Koutecký, J. *J. Chem. Phys.* **1988**, *89*, 4861–4866.
(144) Bonačić-Koutecký, V.; Blase, A.; Bravo-Pérez, G.; Fantucci, P.; Koutecký, J. To be published.
(145) Fantucci, P.; Polezzo, S.; Bonačić-Koutecký, V.; Koutecký, J. *Z. Phys. D: At., Mol. and Clusters* **1989**, *13*, 355–361.
(146) Müller, W.; Flesch, J.; Meyer, W. *J. Chem. Phys.* **1984**, *80*, 3297–3310.
(147) Müller, W.; Meyer, W. *J. Chem. Phys.* **1984**, *80*, 3311–3320.
(148) Jeung, G. H.; Malrieu, J. P.; Daudey, J. P. *J. Chem. Phys.* **1982**, *77*, 3571–3577.
(149) Beckmann, H.-O.; Koutecký, J.; Bonačić-Koutecký, V. *J. Chem. Phys.* **1980**, *73*, 5182–5190.
(150) Gatti, C.; Fantucci, P.; Pacchioni, G. *Theor. Chim. Acta* **1987**, *72*, 433–458.
(151) Moullet, I.; Martins, J. L.; Reuse, F.; Buttet, J. *Z. Phys. D: At., Mol. Clusters* **1989**, *12*, 353–356.
(152) Moullet, I.; Martins, J. L.; Reuse, F.; Buttet, J. *Phys. Rev. B* **1990**, *19*, 31–36.
(153) Moullet, I.; Martins, J. L.; Reuse, F.; Buttet, J. *Phys. Rev. Lett.* **1990**, *65*, 476–479.
(154) Martins, J. L.; Buttet, J.; Car, R. *Phys. Rev. B* **1985**, *31*, 1804–1816.
(155) (a) Ballone, P.; Andreoni, W.; Car, R.; Parrinello, M. *Phys. Rev. Lett.* **1988**, *60*, 271–278. (b) Andreoni, W.; Pastore, G. *Phys. Rev. B* **1990**, *41*, 10243–10246. (c) Jones, R. O.; Hohl, D. *Chem. Phys.* **1990**, *92*, 6710–6721 and references therein. (d) For a recent review, see: Andreoni, W. *Z. Phys. D* **1991**, *19*, 31–36.
(156) Ballone, P.; Andreoni, W.; Car, R.; Parrinello, M. *Europhys. Lett.* **1989**, *8*, 73–78.
(157) Röthlisberger, U.; Andreoni, W. *J. Chem. Phys.* **1991**, *94*, 8129–8151.
(158) Bonačić-Koutecký, V.; Pittner, J.; Scheuch, C.; Fantucci, P.; Koutecký, J., to be published.
(159) Fantucci, P.; Bonačić-Koutecký, V.; Koutecký, to be published.
(160) Garland, D. A.; Lindsay, D. M. *J. Chem. Phys.* **1984**, *80*, 4761–4766.
(161) Pacchioni, G.; Koutecký, J. *J. Chem. Phys.* **1989**, *81*, 3588–3593.
(162) Bonačić-Koutecký, V.; Fantucci, P.; Koutecký, J. *J. Chem. Phys.* **1990**, *93*, 3802–3825.
(163) (a) Lindsay, D. M.; Wang, Y.; George, T. F. *J. Chem. Phys.* **1987**, *86*, 3500–3511. (b) Lindsay, D. M.; Wang, Y.; George, T. F. *J. Chem. Phys.*, in press.
(164) Koutecký, J.; Bonačić-Koutecký, V.; Boustani, I.; Fantucci, P.; Pewestorf, W. In *Large Finite Systems*; Jortner, Y., Pullman, A., Pullman, B., Eds.; Reidel: Dordrecht, 1987; pp 303–317.
(165) Koutecký, J.; Bonačić-Koutecký, V.; Boustani, I.; Fantucci, P. In *Elemental and Molecular Clusters*; Benedek, G., Martin, T. P., Pacchioni, G.; Eds.; Springer-Verlag: Berlin, 1987; pp 214–227.
(166) The geometry of Na_{20} has been investigated by using ECP–CVC procedure mainly in connection with the absorption spectra and will be discussed in section IV.
(167) (a) Bréchignac, C.; Cahuzac, Ph.; Roux, J. P. In *Elemental and Molecular Clusters*; Benedek, G., Martin, T. P., Pacchioni, G., Eds.; Springer-Verlag: Berlin, 1987; pp 254–262. (b) Bréchignac, C.; Cahuzac, Ph. *Laser Chem.* **1986**, *5*, 321–337.
(168) Bréchignac, C.; Cahuzac, Ph.; Pflaum, R.; Roux, J.-Ph. *J. Chem. Phys.* **1988**, *88*, 3732–3735.
(169) Bréchignac, C.; Cahuzac, Ph.; Roux, J.-Ph. *Chem. Phys. Lett.* **1986**, *127*, 445–451.
(170) Bréchignac, C.; Cahuzac, Ph.; Roux, J.-Ph. *J. Chem. Phys.* **1987**, *87*, 229–238.
(171) Bréchignac, C.; Cahuzac, Ph.; Roux, J.-Ph. *J. Chem. Phys.* **1988**, *88*, 3022–3027.
(172) Bréchignac, C.; Cahuzac, Ph.; Leygnier, J.; Pflaum, R.; Roux, J.-Ph.; Weiner, *J. Z. Phys. D: At., Mol. Clusters* **1989**, *12*, 199–203.
(173) Bréchignac, C.; Cahuzac, Ph.; Leygnier, J.; Weiner, J. *J. Chem. Phys.* **1989**, *90*, 1492–1498.
(174) Bréchignac, C.; Cahuzac, Ph.; Carlier, F.; De Frutos, M. *Phys. Rev. Lett.* **1990**, *64*, 2893–2896.
(175) Lee, T.; Rendell, A. P.; Taylor, P. R. *J. Chem. Phys.* **1990**, *92*, 489–495.
(176) Marino, M. M.; Ermler, W. C. *J. Chem. Phys.* **1987**, *86*, 6283–6294.
(177) Rohlfing, C. M.; Binkley, J. S. *Chem. Phys. Lett.* **1987**, *134*, 110–114.
(178) Ross, R. B.; Ermler, W. C.; Pitzer, R. M.; Kern, C. W. *Chem. Phys. Lett.* **1987**, *134*, 115–120.
(179) (a) Ermler, W. C.; Ross, R. B.; Kern, C. W.; Pitzer, R. M.; Winter, N. W. *J. Phys. Chem.* **1988**, *92*, 3042–3046. (b) Ross, R. B.; Kern, C. W.; Pitzer, R. M.; Ermler, W. C.; Winter, N. W. *J. Phys. Chem.* **1990**, *94*, 7771–7774. (c) Ross, R. B.; Ermler, W. C.; Luana, V.; Pitzer, R. M.; Kern, C. W. *Int. J. Quantum Chem.* **1990**, *24S*, 225–240.
(180) Pettersson, L. G. M.; Bauschlicher, C. W., Jr. *Chem. Phys. Lett.* **1986**, *130*, 111–114.
(181) Rao, B. K.; Khanna, S. N.; Jena, P. *Phys. Rev. B* **1987**, *36*, 953–960.
(182) Reuse, F.; Khanna, S. N.; De Coulon, V.; Buttet, J. *Phys. Rev. B* **1989**, *39*, 12911–12914.
(183) See ref 176. Another example of LSD low-spin ground state has been reported in refs 154 and 157 for icosahedral Na_{13}, while high-spin ground state has been found for Li_{13} employing HF–CI calculations (cf. ref 161).
(184) Pewestorf, W.; Bonačić-Koutecký, V.; Koutecký, J. *J. Chem. Phys.* **1988**, *89*, 5794–5802.
(185) Fantucci, P.; Bonačić-Koutecký, V.; Pewestorf, W.; Koutecký, J. *Quantum Chemistry: Basic Aspects-Actual Trends*, Elsevier Publ. Co.: 1989; Vol. 62, pp 449–459.
(186) Fantucci, P.; Bonačić-Koutecký, V.; Pewestorf, W.; Koutecký, J. *J. Chem. Phys.* **1989**, *91*, 4229–4241.
(187) Rao, B. K.; Jena, P. *Int. J. Quantum Chem. Symp.* **1988**, *22*, 287–296.
(188) Rao, B. K.; Jena, P. *Phys. Rev. B* **1988**, *37*, 2867–2873.
(189) Zhang, S. B.; Cohen, M. L.; Chou, M. Y. *Phys. Rev. B* **1987**, *36*, 3455–3458.
(190) Walch, S. P.; Bauschlicher, C. W., Jr.; Langhoff, S. R., Jr. *J. Chem. Phys.* **1986**, *85*, 5900–5907.
(191) Akeby, H.; Panas, I.; Pettersson, L. G. M.; Siegbahn, P.; Wahlgren, U. *J. Phys. Chem.* **1990**, *94*, 5471–5477.
(192) (a) Flad, J.; Igel-Mann, G.; Preuss, H.; Stoll, H. *Surf. Sci.* **1985**, *156*, 379–385. (b) Flad, J.; Igel-Mann, G.; Preuss, H.; Stoll, H. *Chem. Phys.* **1984**, *90*, 257–269.
(193) Arratia-Perez, R.; Malli, G. L. *J. Magn. Reson.* **1987**, *73*, 134–142.
(194) Lee, Y. S.; Ermler, W. C.; Pitzer, K. S. *J. Chem. Phys.* **1980**, *73*, 360–366.
(195) Lee, Y. S.; Ermler, W. C.; Pitzer, K. S. *J. Chem. Phys.* **1979**, *70*, 288–292.
(196) Ross, R. B.; Ermler, W. C. *J. Phys. Chem.* **1985**, *89*, 5202–5206.
(197) Pyykkö, P. *Chem. Rev.* **1988**, *88*, 563–594.
(198) Arratia-Perez, R.; Malli, G. L. *J. Chem. Phys.* **1986**, *85*, 6610–6622.
(199) Bauschlicher, C. W., Jr.; Langhoff, S. R.; Partridge, H. *J. Chem. Phys.* **1990**, *93*, 8133–8137.
(200) Howard, J. A.; Sutcliffe, R.; Mile, B. *J. Phys. Chem.* **1983**, *87*, 2268–2271.
(201) Howard, J. A.; Sutcliffe, R.; Mile, B. *Surf. Sci.* **1985**, *156*, 214–227.
(202) Ozin, G. A.; Mattar, S. M.; McIntosh, D. F. *J. Am. Chem. Soc.* **1984**, *106*, 7765–7776.
(203) Balasubramanian, K.; Feng, P. *J. Phys. Chem.* **1990**, *94*, 1536–1544.
(204) Balasubramanian, K. *J. Chem. Phys.* **1988**, *89*, 5731–5738.
(205) Balasubramanian, K.; Feng, P.; Liao, M. *J. Chem. Phys.* **1989**, *91*, 3561–3569.
(206) Balasubramanian, K.; Das, K. K. *J. Phys. Chem.* **1990**, *94*, 8379–8380.
(207) Whiteside, R. A. Ph.D. Thesis, Carnegie Mellon University, Pittsburg, PA, 1981.

(208) Hanley, L.; Whitten, J. L.; Anderson, S. L. *J. Phys. Chem.* **1988**, *92*, 5803–5812.
(209) Pellegatti, A.; Marinelli, F.; Roche, M.; Maynau, D.; Malrieu, J. P. *J. Phys.* **1987**, *48*, 29–43.
(210) Pellegatti, A.; Marinelli, F.; Roche, M.; Maynau, D.; Malrieu, J. P. *J. Phys. C* **1987**, *20*, 5141–5147.
(211) Boustani, I.; Li, Y.; Bonačič-Koutecký, V.; Koutecký, J., to be published.
(212) Pettersson, L. G. M.; Bauschlicher, C. W., Jr.; Halicioglu, T. *J. Chem. Phys.* **1987**, *87*, 2205–2213.
(213) (a) Raghavachari, K.; Binkley, J. S. *J. Chem. Phys.* **1987**, *87*, 2191–2197. (b) Raghavachari, K.; Binkley, J. S. *NATO ASI Ser., Ser. B* **1987**, *158*, 317–322.
(214) Martin, L. M. L.; Francois, J. P.; Gijbels, R. *J. Chem. Phys.* **1991**, 3753–3761.
(215) Ramirez-Solis, A.; Novaro, O.; Ruiz, M. E. *Phys. Rev. B* **1987**, *35*, 4082–4084.
(216) Kappes, M. M.; Schär, M.; Röthlisberger, U.; Yeretzian, C.; Schumacher, E. *Chem. Phys. Lett.* **1988**, *143*, 251–258.
(217) (a) Brêchignac, C.; Cahuzac, Ph.; Carlier, F.; Leygnier, J. *Phys. Rev. Lett.* **1989**, *63*, 1368–1371. (b) Brêchignac, C.; Cahuzac, Ph.; Carlier, F.; De Frutos, M.; Leygnier, J. *J. Chem. Soc., Faraday Trans.* **1990**, *86*, 2525–2531.
(218) Brêchignac, C.; Cahuzac, Ph. *Z. Phys. D: At., Mol. Clusters* **1986**, *3*, 121–129.
(219) Durand, G. *J. Chem. Phys.* **1989**, *91*, 6225–6237.
(220) Durand, G.; Daudey, J. P.; Malrieu, J. P. *Theor. Chim. Acta* **1988**, *74*, 299–309.
(221) Knight, W. D.; De Heer, W. A.; Saunders, W. A. *Lect. Notes Phys.* **1987**, *269*, 15–24.
(222) Saito, S.; Ohnishi, S. *NATO ASI Ser., Ser. B* **1987**, *158*, 115–119.
(223) Kappes, M. M.; Kunz, R.; Schumacher, E. *Chem. Phys. Lett.* **1982**, *91*, 413–418.
(224) Kappes, M. M.; Radi, P.; Schär, M.; Yeretzian, C.; Schumacher, E. *Z. Phys. D: At., Mol. Clusters* **1986**, *3*, 115–119.
(225) Kappes, M. M.; Schär, M.; Yeretzian, C.; Heiz, U.; Vayloyan, A.; Schumacher, E. *NATO ASI Ser., Ser. B* **1987**, *158*, 145–149.
(226) Schriver, K. E.; Persson, J. L.; Honea, E. C.; Whetten, R. L. *Phys. Rev. Lett.* **1990**, *64*, 2539–2542.
(227) Knight, W. D.; Clemenger, K.; De Heer, W. A.; Saunders, W. A. *Phys. Rev. B* **1985**, *31*, 2539–2540.
(228) Manninen, M. *Phys. Rev. B* **1986**, *34*, 6886–6894.
(229) Stampfli, P.; Bennemann, K. H. *NATO ASI Ser., Ser. B* **1987**, *158*, 473–478.
(230) Fantucci, P.; Polezzo, S.; Bonačič-Koutecký, V.; Koutecký, L.; Guest, F., to be published.
(231) Durand, G.; Daudey, J. P.; Malrieu, J. P. *J. Phys.* **1986**, *47*, 1335–1346.
(232) Bauschlicher, C. W., Jr.; Langhoff, S. R.; Partridge, H.; Walch, S. P. *J. Chem. Phys.* **1987**, *86*, 5603–5612.
(233) Durand, G.; Daudey, J. P.; Malrieu, J. P. *Lect. Notes Phys.* **1987**, 127–134.
(234) Malrieu, J. P.; Maynau, D. *Few-Body Syst. Suppl.* **1987**, *2*, 323–330.
(235) Blaise, P.; Malrieu, J. P.; Maynau, D.; Oujia, B. *THEOCHEM* **1988**, *169*, 469–486.
(236) Blaise, P.; Malrieu, J. P.; Maynau, D. *Surf. Sci.* **1989**, *221*, 513–533.
(237) Malrieu, J. P. *NATO ASI Ser., Ser. B* **1987**, *158*, 383–393.
(238) Bader, R. F. W.; Nguyen-Dang, T. T. *Adv. Quantum Chem.* **1981**, *14*, 63–124.
(239) Bader, R. F. W.; Nguyen-Dang, T. T.; Tal, Y. *Rep. Prog. Phys.* **1981**, *44*, 893–948.
(240) Bader, R. F. W.; Essen, H. *J. Chem. Phys.* **1984**, *80*, 1943–1960.
(241) Upton, T. H. *J. Chem. Phys.* **1987**, *86*, 7054–7064.
(242) Upton, T. H. *Phys. Rev. Lett.* **1986**, *56*, 2168–2171.
(243) Baladron, C.; Lopez, J. M.; Iniguez, M. P.; Alonso, J. A. *Z. Phys. D: At., Mol. Clusters* **1989**, *11*, 323–326.
(244) Iniguez, M. P.; Balbas, L. C.; Alonso, J. A. *NATO ASI Ser., Ser. B* **1987**, *158*, 263–267.
(245) Iniguez, M. P.; Alonso, J. A.; Aller, M. A.; Balbas, L. C. *Phys. Rev. B* **1986**, *34*, 2152–2157.
(246) Lopez, M. J.; Iniguez, M. P.; Alonso, J. A. *Phys. Rev. B* **1990**, *41*, 5636–5642.
(247) Saito, S.; Cohen, M. L. *Phys. Rev. B* **1988**, *38*, 1123–1130.
(248) Saito, S.; Cohen, M. L. *Z. Phys. D: At., Mol. Clusters* **1989**, *12*, 205–208.
(249) Saito, S.; Ohnishi, S. *Phys. Rev. Lett.* **1987**, *59*, 190–193.
(250) Sheng, P.; Chou, M. Y.; Cohen, M. L. *Phys. Rev. B* **1986**, *34*, 732–739.
(251) Baladron, C.; Alonso, J. A. *Phys. Lett. A* **1989**, *140*, 67–71.
(252) Baladron, C.; Alonso, J. A.; Iniguez, M. P. *J. Phys. F* **1987**, *17*, L197–L200.
(253) Robles, J.; Iniguez, M. P.; Alonso, J. A.; Mananes, Z. *Z. Phys. D: At., Mol. Clusters* **1989**, *13*, 269–275.
(254) Rubio, A.; Balbas, L. C.; Vega, A. *Z. Phys. D: At., Mol. Clusters* **1989**, *12*, 209–211.
(255) Balbas, L. C.; Rubio, A.; Alonso, J. A.; Borstel, G. *Chem. Phys.* **1988**, *120*, 239–247.
(256) Kappes, M. M.; Schär, M.; Radi, P.; Schumacher, E. *J. Chem. Phys.* **1986**, *84*, 1863–1875.
(257) De Heer, W. A.; Milani, P.; Chatelain, A. *Phys. Rev. Lett.* **1989**, *63*, 2834–2836.
(258) Moskovits, M. *Metal Clusters*; Moskovits, M., Eds.; Wiley: New York, 1986.
(259) Garland, D. A.; Lindsay, D. M. *J. Chem. Phys.* **1983**, *78*, 2813–2816.
(260) Gole, J.; Green, G.; Pace, S.; Preuss, D. *J. Chem. Phys.* **1982**, *76*, 2247–2266.
(261) Crumley, W.; Hayden, J.; Gole, J. *J. Chem. Phys.* **1986**, *84*, 5250–5261.
(262) Rohlfing, E.; Valentini, J. *Chem. Phys. Lett.* **1986**, *126*, 113–118.
(263) Herrmann, A.; Leutwyler, S.; Schumacher, E.; Wöste, L. *Helv. Chem. Acta* **1978**, *61*, 453–487.
(264) (a) Broyer, M.; Delacretaz, G.; Labastie, P.; Wolf, J. P.; Wöste, L. *Phys. Rev. Lett.* **1986**, *57*, 1851–1854. (b) Delacretaz, G.; Grant, E. R.; Whetten, R. L. Wöste, L.; Zwanziger, J. W. *Phys. Rev. Lett.* **1986**, *24*, 2598–2601. (c) Broyer, M.; Delacretaz, G.; Ni, G.-Q.; Wolf, J. P.; Wöste, L. *Chem. Phys. Lett.* **1988**, *145*, 232–236. (d) Broyer, M.; Delacretaz, G.; Ni, G.-Q.; Wolf, J. P.; Wöste, L. *J. Chem. Phys.* **1989**, *90*, 4620–4621.
(265) (a) Morse, M.; Hopkins, J.; Langridge-Smith, P. R. R.; Smalley, R. *J. Chem. Phys.* **1983**, *79*, 5316–5328. (b) Morse, M. D. *Chem. Phys. Lett.* **1987**, *133*, 8–13.
(266) Cheng, P.; Duncan, M. *Chem. Phys. Lett.* **1988**, *152*, 341–346.
(267) Fu, Z.; Lemire, G.; Hanrick, Y.; Taylor, S.; Shui, J.; Morse, M. D. *J. Chem. Phys.* **1988**, *88*, 3524–3531.
(268) Wolf, J.-P.; Delacretaz, G.; Wöste, L. *Phys. Rev. Lett.* **1989**, *63*, 1946–1949.
(269) Leopold, D. G.; Lineberger, K. *J. Chem. Phys.* **1986**, *85*, 51–55.
(270) Leopold, D. G.; Ho, J.; Lineberger, W. C. *J. Chem. Phys.* **1987**, *86*, 1715–1726.
(271) Ho, J.; Ervin, K. M.; Lineberger, W. C. *J. Chem. Phys.* **1990**, *93*, 6987–7002.
(272) Pettiette, C. L.; Yang, S. H.; Craycraft, M. J.; Conceicao, J.; Laaksonen, R. T.; Cheshnovsky, O.; Smalley, R. E. *J. Chem. Phys.* **1988**, *88*, 5377–5382.
(273) Ganteför, G.; Meiwes-Broer, K. H.; Lutz, H. O. *Phys. Rev. A* **1988**, *37*, 2716–2718.
(274) Ganteför, G.; Gausa, M.; Meiwes-Broer, K.-H.; Lutz, H. *Z. Phys. D: At., Mol. Clusters* **1988**, *9*, 253–261.
(275) Begemann, W.; Hector, R.; Liu, Y. Y.; Tiggesbaumker, J.; Meiwes-Broer, K. H.; Lutz, H. O. *Z. Phys. D: At., Mol. Clusters* **1989**, *12*, 229–233.
(276) McHugh, K. M.; Eaton, J. G.; Lee, G. H.; Sarkas, H. W.; Kidder, L. H.; Snodgrass, J. T.; Manaa, M. R.; Bowen, K. H. *J. Chem. Phys.* **1989**, *91*, 3792–3793.
(277) De Heer, W. A.; Selby, K.; Kresin, V.; Masui, J.; Vollmer, M.; Chatelain, A.; Knight, W. D. *Phys. Rev. Lett.* **1987**, *59*, 1805–1808.
(278) Brêchignac, C.; Cahuzac, Ph.; Carlier, F.; Leygnier, *J. Chem. Phys. Lett.* **1989**, *164*, 433–437.
(279) Wang, C.; Pollack, S.; Kappes, M. M. *Chem. Phys. Lett.* **1990**, *166*, 26–31.
(280) Wang, C.; Pollack, S.; Cameron, D.; Kappes, M. M. *J. Chem. Phys.* **1990**, *93*, 3787–3801.
(281) Jarrold, M.; Creegan, K. *Chem. Phys. Lett.* **1990**, *166*, 116–122.
(282) Fallgren, H.; Martin, T. P. *Chem. Phys. Lett.* **1990**, *168*, 233–238.
(283) Broyer, M.; Chevaleyre, J.; Dugourd, Ph.; Wolf, J.-P.; Wöste, L. *Phys. Rev. A* **1990**, *42*, 6954–6957.
(284) Yang, S. H.; Pettiette, C. L.; Conceicao, J.; Cheshnovsky, O.; Smalley, R. E. *Chem. Phys. Lett.* **1987**, *139*, 233–238.
(285) Ganteför, G.; Gausa, M.; Meiwes-Broer, K. H.; Lutz, H. O. *J. Chem. Soc., Faraday Trans.* **1990**, *86*, 2483–2488.
(286) Ganteför, G.; Gausa, M.; Meiwes-Broer, K. H.; Lutz, H. O. *Faraday Discuss. Chem. Soc.* **1988**, *86*, 197–208.
(287) Chesnovsky, O.; Taylor, K. J.; Conceicao, J.; Smalley, R. E. *Phys. Rev. Lett.* **1990**, *64*, 1785–1788.
(288) Raghavachari, K.; Rohlfing, C. M. *J. Chem. Phys.* **1991**, *94*, 3670–3678.
(289) Larsson, S.; Volosov, A.; Rosén, A. *Chem. Phys. Lett.* **1987**, *137*, 501–504.
(290) Rosén, A.; Wastberg, B. *J. Am. Chem. Soc.* **1988**, *110*, 8701–8703.
(291) Lüthi, P.; Almlöf, J. *Chem. Phys. Lett.* **1987**, *135*, 357–360.
(292) Raghavachari, K. *Chem. Phys. Lett.* **1990**, *171*, 259–253.
(293) Bauschlicher, C. W., Jr.; Langhoff, S. R.; Taylor, P. R. *J. Chem. Phys.* **1988**, *88*, 1041–1045.
(294) Bauschlicher, C. W., Jr. *Chem. Phys. Lett.* **1989**, *156*, 91–94.
(295) Bonačič-Koutecký, V.; Fantucci, P.; Koutecký, J. *J. Chem. Phys.* **1989**, *91*, 3794–3795.
(296) Selby, K.; Vollmer, M.; Masui, J.; Kresin, V.; De Heer, W. A.; Knight, W. D. *Z. Phys. D: At., Mol. Clusters* **1989**, *12*, 477–479.
(297) Selby, K.; Vollmer, M.; Masui, J.; Kresin, V.; De Heer, W. A.; Knight, W. D. *Phys. Rev. B* **1989**, *40*, 5417–5427.

(298) Selby, K.; Kresin, V.; Masui, J.; Vollmer, M.; de Heer, W.; Scheidemann, A.; Knight, W. D. *Phys. Rev. B.* **1991**, *43*, 4565–4578.
(299) Blanc, J.; Broyer, M.; Chevaleyre, J.; Dugourd, Ph.; Kuhling, H.; Labastie, P.; Ulbricht, M.; Wolf, J.-P.; Wöste, L. *Z. Phys. D: At., Mol. Clusters*, in press.
(300) Blanc, J.; Bonačić-Koutecký, V.; Broyer, M.; Chevaleyre, J.; Dugourd, Ph.; Koutecký, J.; Scheuch, C.; Wolf, J. P.; Wöste, L. *J. Chem. Phys.*, in press.
(301) Dugourd, Ph.; Blanc, J.; Bonačić-Koutecký, V.; Broyer, M.; Chevaleyre, J.; Koutecký, J.; Pittner, J.; Wolf, J. P.; Wöste, L. To be published.
(302) Wang, C.; Pollack, S.; Hunter, J.; Alameddin, G.; Hoover, T.; Cameron, D.; Liu, S.; Kappes, M. M. *Zeitschrift f. Physik D*, **1991**, *19*, 13–17.
(303) Bonačić-Koutecký, V.; Fantucci, P.; Koutecký, J. *Chem. Phys. Lett.* **1988**, *146*, 518–523.
(304) Bonačić-Koutecký, V.; Fantucci, P.; Koutecký, J. *Chem. Phys. Lett.* **1990**, *166*, 32–38.
(305) Bonačić-Koutecký, V.; Kappes, M. M.; Fantucci, P.; Koutecký, J. *Chem. Phys. Lett.* **1990**, *170*, 26–34.
(306) Bonačić-Koutecký, V.; Gaus, J.; Guest, M. F.; Koutecký, J. To be published.
(307) Bonačić-Koutecký, V.; Gaus, J.; Fantucci, P.; Koutecký, J. *Z. Phys. D: At., Mol. Clusters* **1991**, in press.
(308) Pollack, S.; Wang, C.; Kappes, M. M. *J. Chem. Phys.* **1991**, *94*, 2496–2501.
(309) Brêchignac, C.; Cohuzoc, Ph.; Carlier, F.; De Frutos, M.; Leygnier, J. *Zeitschrift f. Physik D* **1991**, *19*, 1–6.
(310) Bruna, P.; Peyerimhoff, S. *Adv. Chem. Phys.* (Prigogine, I., Rice, S., Lawley, K., Eds.) **1987**, *67*, 1–97.
(311) Michl, J.; Bonačić-Koutecký, V. *Electronic aspects of organic photochemistry*; John Wiley & Sons: New York, 1990.
(312) Das, K. K.; Balasubramanian, K. *Chem. Phys. Lett.* **1991**, *176*, 571–574.
(313) Balasubramanian, K.; Feng, P. Y.; Liao, M. Z. *J. Chem. Phys.* **1989**, *91*, 3561–3570.
(314) Pacchioni, G.; Koutecký, J. *J. Chem. Phys.* **1988**, *88*, 1066–1073.
(315) Magers, D.; Harrison, R.; Bartlett, R. *J. Chem. Phys.* **1986**, *84*, 3284–3290.
(316) Balasubramanian, K. *J. Chem. Phys.* **1986**, *85*, 3401–3406.
(317) Balasubramanian, K. *Chem. Phys. Lett.* **1987**, *135*, 283–287.
(318) Werner, H.-J. *Adv. Chem. Phys.* (Prigogine, I., Rice, S., Lawley, K., Eds.) **1987**, *69*, 1–62.
(319) Partridge, H.; Bauschlicher, C. W., Jr.; Langhoff, S. R. *Chem. Phys. Lett.* **1990**, *175*, 531–535.
(320) Guest, M. F.; Kendrick, J. Daresbury Lab. Report, No. CCP 1/86, 1986, unpublished.
(321) Herrmann, A.; Hoffmann, M.; Leutwyler, S.; Schumacher, E.; Wöste, L. *Chem. Phys. Lett.* **1979**, *62*, 216–222.
(322) Gerber, W.; Schumacher, E. *J. Chem. Phys.* **1979**, *69*, 1692–1703.
(323) Gerber, W. Ph.D. Thesis, Bern, 1980.
(324) Lindsay, D. M.; Thompson, G. A. *J. Chem. Phys.* **1982**, *77*, 1114–1117.
(325) Walch, S.; Laskowski, B. *J. Chem. Phys.* **1986**, *84*, 2734–2743.
(326) Zwanziger, J. W.; Whetten, R.; Grant, E. R. *J. Phys. Chem.* **1986**, *90*, 3289–3301.
(327) Pollack, S.; Wang, C. R. C.; Dahlseid, T.; Kappes, M. M. To be published.
(328) Gatti, C.; Polezzo, S.; Fantucci, P.; Bonačić-Koutecký, V.; Koutecký, J. To be published.
(329) Wang, C. R. C.; Pollack, S.; Hunter, J.; Alameddin, G.; Hoover, T.; Kappes, M. M. To be published.
(330) Pacheco, J. M.; Broglia, R. A. *Phys. Rev. Lett.* **1989**, *62*, 1400–1402.
(331) Ekardt, W.; Penzar, Z. *Phys. Rev. B* **1991**, *43*, 1322–1340.
(332) Yannouleas, C.; Broglia, R. To be published.
(333) Gatti, C.; Polezzo, S.; Fantucci, P. *Chem. Phys. Lett.* **1990**, *75*, 645–654.
(334) Fantucci, P.; Polezzo, S.; Bonačić-Koutecký, V.; Koutecký, J. *J. Chem. Phys.* **1990**, *92*, 6645–6654.
(335) Notice that D_{2d} structure of Li_8 transforms into the T_d structure via geometries of lower symmetry without passing through a barrier.
(336) Bauschlicher, C. W., Jr.; Langhoff, S. R.; Partridge, H. *J. Chem. Phys.* **1989**, *91*, 2412–2419.
(337) Shibuya, T.; Yoshitani, M. *Chem. Phys. Lett.* **1987**, *137*, 13–16.
(338) (a) Basch, H. *J. Am. Chem. Soc.* **1981**, *103*, 4657–4663. (b) Walch, S. P. *J. Chem. Phys.* **1987**, *87*, 6776–6778.
(339) LaiHing, K.; Cheng, P. Y.; Duncan, M. A. *Z. Phys. D: At., Mol. Clusters* **1989**, *13*, 161–169.
(340) Ekardt, W. *Phys. Rev. Lett.* **1984**, *52*, 1925–1928.
(341) Beck, D. E. *NATO ASI Ser. B* **1987**, *158*, 395–400.
(342) (a) Yannouleas, C.; Broglia, R. A.; Brack, M.; Bortignon, P. F. *Phys. Rev. Lett.* **1989**, *63*, 255–258. (b) Yannouleas, C.; Pacheco, J. M.; Broglia, R. A. *Phys. Rev. B* **1990**, *41*, 6088–6091.
(343) Reinhardt, P.-G.; Brack, M.; Genzken, O. *Phys. Rev. A* **1990**, *41*, 5568–5582.
(344) Yannouleas, C.; Broglia, R. To be published.
(345) Bernath, M.; Yannouleas, C.; Broglia, R. A. To be published.
(346) Bertsch, G. F.; Tomanek, D. *Phys. Rev. B* **1989**, *40*, 2749–2751.
(347) Pacheco, J. M.; Broglia, R. A.; Mottelson, B. R. To be published.